Regulation of airway smooth muscle contraction by PGE_2

A thesis submitted to the
School of Health and Science,
Dundalk Institute of Technology

For the degree of **Doctor of Philosophy**

By

Leanna M Morgan B.Sc (Hons)

April 2022

Under the supervision of **Prof. Gerard Sergeant** &
co-supervision of **Dr. Eamonn Bradley**

Declaration

We, the undersigned declare that this thesis entitled ‘Regulation of airway smooth muscle contraction by PGE_2’ is entirely the author’s own work and has not been taken from the work of others, except as cited and acknowledged within the text.

The thesis has been prepared according to the regulations of Dundalk Institute of Technology and has not been submitted in whole or in part for an award in this or any other institution.

Author Name: Leanna Morgan

Author Signature:

Date: 17/05/2022

Supervisor Name: Prof. Gerard Sergeant

Supervisor Signature:

Date:17/05/2022

Table of Contents

Acknowledgements

Firstly, I would like to express my sincere gratitude to my supervisor, Prof. Gerard Sergeant, for your guidance and invaluable advice throughout this project, and more importantly thank you for your unwavering support during the last four years. I truly appreciate the time, patience and enthusiasm that you devoted to me and this project. I would also like to thank Prof. Keith Thornbury and Prof. Mark Hollywood for their valuable advice and suggestions throughout this project.

I am forever grateful to our post docs, Eamonn, Roddy and Caoimhin. Thank you for the time (and patience), you devoted to training me on the techniques used in this study but also thank you for the memories, you made my time in the SMRC so enjoyable. A special mention to Eamonn as my co-supervisor for his continuous assistance and advice. I will be forever thankful to Niki, for the hours he spent synthesising on behalf of this project but more importantly for the time he spent making me laugh, you were the highlight of my time here. To Billie, thank you for all your technical support, kindness and friendship throughout the years.

I would like to thank the colleagues I have worked alongside, especially the five BREATH girls, who have shared every moment of this journey with me, thank you for the support, memories and friendship. A special mention, to the now Dr. Ruth Matthews, from undergrad to postgrad you've been my greatest support and best friend, I could not have done it without you by my side.

I am deeply grateful and forever thankful to my family, my mam, dad, brothers and sisters for their unrelenting confidence in me and their unconditional love and support throughout these four years. Thank you all for your patience and for never being shy about how proud you are of me.

Finally, my deepest thank you to my boyfriend and best friend, Tiff. You've travelled every step of this journey with me, you've held my hand through the triumphs and tribulations of the last four years, always ready to celebrate, encourage or reassure when required and I sincerely thank you for it. I will never find the words to cover my gratitude to you for your unequivocal love and support, not only during this project, but always and so, I dedicate this thesis to you.

Glossary

Abbreviations

AA	Arachidonic acid
AC	Adenylyl cyclase
ACh	Acetylcholine
Akt kinase	Protein kinase B
ASM	Airway smooth muscle
ASMCs	Airway smooth muscle cells
ATP	Adenosine triphosphate
BK channels	Large conductance calcium-activated potassium channels
°C	Degrees Celsius
bp	Base pair
Ca^{2+}	Calcium ions
cADPR	Cyclic adenosine diphosphate ribose
CaM	Calmodulin
cAMP	Cyclic adenosine monophosphate
CCh	Carbachol
cDNA	Complimentary DNA
cGMP	Cyclic guanosine monophosphate
CHO	Chinese hamster ovary
CICR	Calcium-induced calcium release
CO_2	Carbon dioxide
COPD	Chronic obstructive pulmonary disease
CPI-17	C kinase-potentiated phosphatase inhibitor-17
CRC	Calcium-release channel
DAG	1, 2-diacylglycerol
DMSO	Dimethyl sulfoxide
DNA	Deoxyribonucleic acid
dNTPs	Deoxynucleotide triphosphates
dsDNA	Double-stranded DNA
EC_{50}	Half-maximal excitatory concentration

EDTA	Ethylenediamine tetraacetic acid
EFS	Electrical field stimulation
E_k	Potassium equilibrium
EMCCD	Electron multiplying charge coupled device
EP	Prostanoid E
EPAC	Exchange protein activated by cAMP
ERKs	Extracellular signal-regulated kinases
FKBP	FK506-binding protein
FPS	Frames per second
GOI	Genes of interest
GPCRs	G protein-coupled receptors
hBSMCs	Human bronchial smooth muscle cells
Hz	Hertz
IbTx	Iberiotoxin
IC_{50}	Half-maximal inhibitory concentration
IFN-γ	Interferon γ
IL	Interleukin
I_{max}	Maximum inhibition
IP_3	Inositol-1, 4, 5-triphosphate
K^+	Potassium
MCh	Methacholine
Mins	Minutes
ml	Millilitre
MLCK	Myosin light chain kinase
MLCP	Myosin light chain phosphatase
MLD	Micro lens disc
μM	Micromolar
mM	Millimolar
mN	Millinewton
mRNA	Messenger ribonucleic acid
MRs	Muscarinic receptors
ms	Millisecond
MYPT1	Myosin phosphatase target subunit 1

n	Sample number
N	Animal Number
NANC	Non-adrenergic non-cholinergic
NCX	Sodium calcium exchanger
nM	Nanomolar
NO	Nitric oxide
O_2	Oxygen
PARs	Protease-activated receptors
PGD_2	Prostaglandin D_2
PGE_2	Prostaglandin E_2
$PGF_{2\alpha}$	Prostaglandin F2alpha
PGH_2	Prostaglandin H_2
PGI_2	Prostacyclin
PHD	Pinhole disc
PI3K	Phosphatidylinositol 3-kinase
PIP_2	Phosphatidylinositol 4,5-bisphosphate
PKA	Protein kinase A
PKG	Protein kinase G
PLC	Phospholipase C
PMCA	Plasma membrane calcium-ATPase
PP1c1δ	Catalytic type 1 subunit
qPCR	Real-time quantitative PCR
rMLC	Regulatory myosin light chain
RNase	Ribonuclease
RT-PCR	Reverse transcriptase-polymerase chain reaction
RyRs	Ryanodine receptors
s	Second
SCaMPER	Sphingolipid calcium-release-mediating protein for the endoplasmic reticulum
S.E.M	Standard error of the mean
SDCLM	Spinning disc confocal laser microscope
SERCA	Sarco/endoplasmic reticulum Ca^{2+}-ATPase
siRNA	Small interfering RNAs

SM	Smooth muscle
SMC	Smooth muscle cell
SOC	Store-operated channel
SR	Sarcoplasmic reticulum
STIM 1	Stromal interacting molecule 1
STOCs	Spontaneous transient outward currents
TAE	Tris,acetic acid EDTA buffer
TNF-α	Tumour necrosis factor α
TRP	Transient receptor potential
TRPC1	TRP canonical 1
TRPV1	TRP vanilloid 1
TTX	Tetrodotoxin
TxA_2	Thromboxane A_2
VDCCs	Voltage dependent calcium channels
VIP	Vasoactive intestinal peptide
WT	Wild-type
α	Alpha
β	Beta
Δ	Delta
γ	Gamma
007-AM	8-pCPT-2-O-Me-cAMP-AM
6-MB-cAMP	N^6-monobutyryl-cyclic adenosine monophosphate

Abstract

Protease-activated receptor 2 (PAR2) is the most abundant PAR in the human lung and is expressed in bronchial epithelium and smooth muscle. There are conflicting reports on the precise role of PAR2 in the airways and studies have shown it can induce both bronchoconstriction and bronchodilation effects. While PAR2 is present on airway smooth muscle cells, it has been suggested that the inhibitory effects of PAR2 in the airways could be mediated via endogenous prostanoids. Prostaglandin E_2 (PGE_2) is the most abundantly produced prostanoid in the body and exerts its biological effects through activation of four prostanoid E receptors (EPRs). Activation of EP1 and EP3Rs promotes airway inflammation and cough, whereas EP2 and EP4Rs induce potent bronchodilation (Aso *et al*. 2013; Sastre and del Pozo 2012; Tilley *et al.* 2003), however, the precise cellular mechanisms underlying the effects of PGE_2 in airway smooth muscle have not been fully elucidated. The aims of this study were to: 1) investigate the mechanisms underlying PAR2 mediated relaxations in murine airway smooth muscle; 2) identify the EP receptor subtype responsible for the inhibitory effects of PGE_2 in murine airway smooth muscle; 3) examine the underlying cellular processes and possible role of K^+ channels in PGE_2-induced relaxations of airway smooth muscle and 4) investigate if PGE_2 affected calcium signalling in isolated airway smooth muscle cells.

Isometric tension recordings were obtained from murine bronchial rings and intracellular calcium measurements were recorded from isolated airway smooth muscle cells using confocal microscopy. Transcriptional expression of EPR subtypes in whole bronchial tissue and isolated airway smooth muscle cells was investigated using RT-PCR and RT-quantification was determined using qPCR. The key findings of this study were: 1) PAR2 activation elicited potent relaxation of bronchial rings pre-contracted with EFS and the cholinergic agonist CCh (1μM) via release of endogenous PGE_2; 2) Exogenous application of PGE_2 relaxed bronchial rings in a concentration-dependent manner; 3) The inhibitory effects of PGE_2 were reduced in the presence of an EP2R antagonist but not an EP4R antagonist; 4) PGE_2-induced inhibition of EFS-evoked contractions were also reduced by an EP2R antagonist, but not an EP4R antagonist, however

inhibitory effects of the EP4R antagonist were unmasked when it was applied in the presence of the EP2R antagonist; 5) PGE_2-induced relaxations of CCh and EFS-evoked contractions were reduced in the presence of the BK channel blocker, iberiotoxin but not by the K_v7 channel blocker, XE-991; 6) PGE_2 reduced the frequency and amplitude of CCh-induced calcium oscillations in isolated murine airway smooth muscle cells; 7) These effects were mimicked by the EP2R agonist, (*R*)-Butaprost, the AC activator, forskolin, the exchange protein activated by cAMP (EPAC) activator, 007-AM, the PKA activator, 6-MB-cAMP, and were partially reduced by the PKA inhibitor, Rp-8-CPT-cAMP; 8) CCh-induced calcium oscillations were inhibited by the IP_3R inhibitor, 2-APB, the RyR inhibitor, tetracaine and, to a lesser extent, removal of calcium from the extracellular solution; 9) Caffeine-induced calcium transients in isolated airway smooth muscle cells were not affected by addition of PGE_2; 10) All EPR subtypes were expressed in whole bronchial tissue, but EP4R was not detected in isolated airway smooth muscle cells.

Taken together, these data suggest a role for EP2Rs in PGE_2-induced inhibition of cholinergic responses in murine airway smooth muscle. These effects may involve activation of BK channels and inhibition of calcium oscillations through upregulation of PKA, and possibly EPAC, to inhibit IP_3R evoked calcium release.

Publications

Abstracts related to this thesis were communicated in different national and international scientific meetings:

1. LM Morgan, MA Hollywood, KD Thornbury, LP McGarvey and GP Sergeant. (2018). Prostaglandin E_2 inhibits calcium oscillations in murine airway smooth muscle cells. *Irish Journal of Medical Science*, 187(8), pp. 283. Irish Thoracic Society Meeting, Belfast, Antrim, Northern Ireland.

2. LM Morgan, E Bradley, MA Hollywood, KD, Thornbury, LP McGarvey and GP Sergeant. (2019). Role of large conductance Ca^{2+}-activated K^+ channels in PGE_2-induced relaxations of murine airway smooth muscle. The FASEB Science Research Conference on Smooth Muscle, West Palm Beach, Florida, USA.

3. LM Morgan, E Bradley, MA Hollywood, KD Thornbury, LP McGarvey and GP Sergeant. (2019). PGE_2-induced relaxations of murine airway smooth muscle involve activation of large-conductance Ca^{2+}-activated K^+ channels. Irish Journal of Medical Science, 188(10), pp. 274. Irish Thoracic Society Meeting, Galway, Ireland.

1. Literature Review

1.1 The respiratory system

The respiratory system spans from the nasal orifices to the periphery of the lungs and is comprised of two components; the upper and lower respiratory tracts (Ward *et al*. 2010; Underwood 2004). The upper respiratory tract consists of the nose, pharynx and larynx, while the lower respiratory tract contains the trachea, bronchi and lungs (Ward *et al*. 2010). The lower respiratory tract commences with the trachea which then bifurcates into the right and left primary bronchi, ultimately leading into the right and left lungs. Structurally, the human lungs are divided into lobes, with the right containing three lobes while the left consists of two, in order to facilitate the positioning of the heart (Mader 2007). The lungs are permeated by a vast number of blood vessels, lymphatics and nerves (see *Figure 1.1*).

Primary bronchi divide repeatedly with each subsequent branching containing less cartilage and an increased volume of smooth muscle (Spence and Mason 1992). Once a width of 1 mm is reached these air passages are referred to as bronchioles, which can be categorised into terminal and respiratory bronchioles (Ward *et al*. 2010; Marieb 2001). Terminal bronchioles lead to respiratory bronchioles, which possess alveoli and participate in gas exchange. Respiratory bronchioles may also direct air into alveolar ducts and alveolar sacs, which are the main site of gaseous exchange in the lungs (Ward *et al*. 2010; Underwood 2004).

The respiratory tract is lined with epithelial cells including ciliated columnar epithelial cells and non-ciliated epithelial cells. Non-ciliated epithelial cells are primarily present in the alveoli and alveolar ducts (Ward *et al.* 2010; Marieb 2001). In addition, the human airways contain goblet or mucous cells which secrete mucus to trap foreign objects entering the airways as well as basal and clara cells which act as primary stem cells giving rise to ciliated and mucous cells. Clara cells are also believed to secrete bronchiolar surfactant, which decreases surface tension and participates in lung immunity (Ward *et al.* 2010; Knight and Holgate 2003).

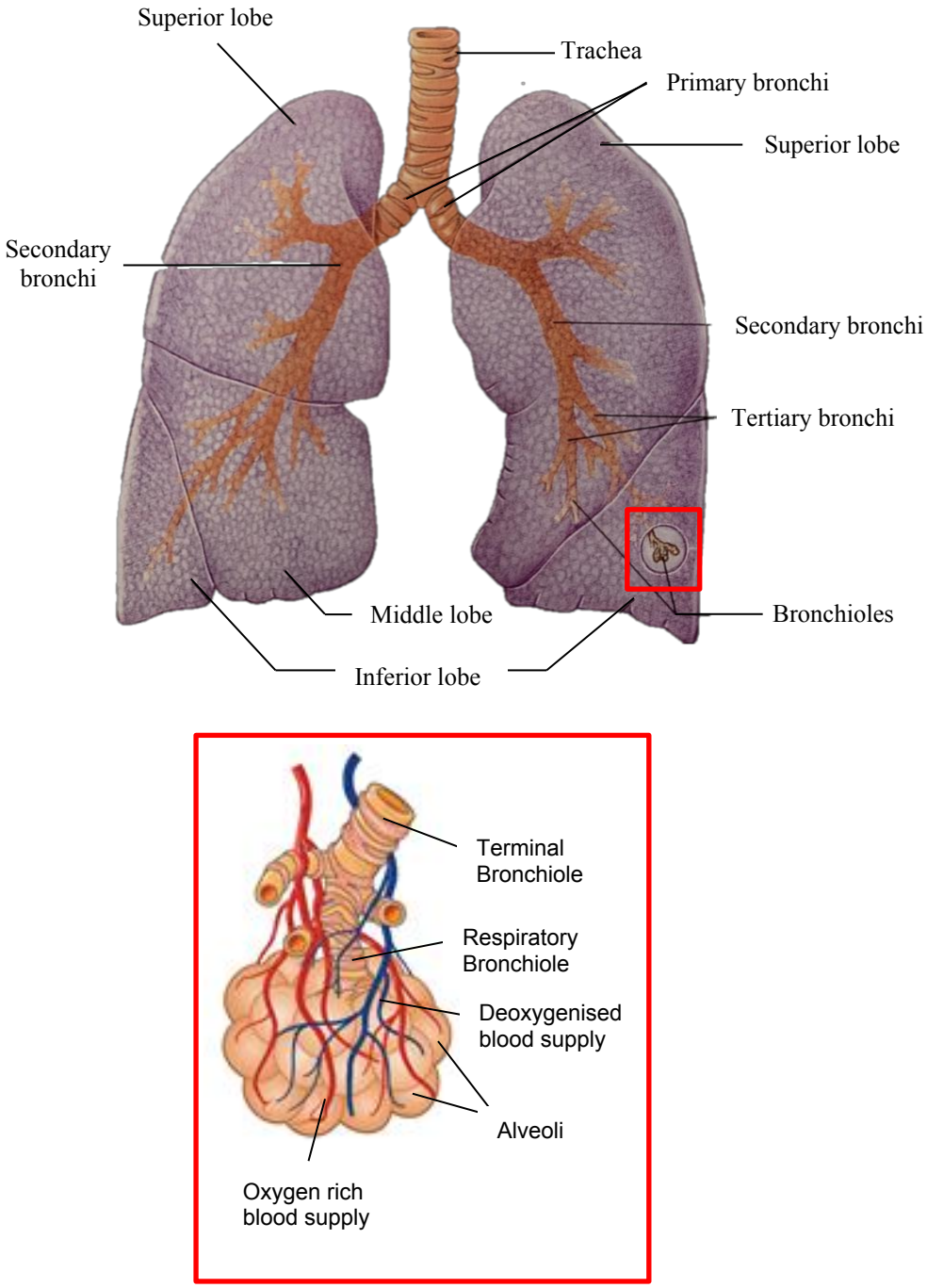

Figure 1.1 Diagram of the anatomy of the respiratory tract (adapted from Nursing Times 2018; Spence and Mason 1992).

1.2 Smooth muscle

Muscle tissues are generally divided into two basic categories, striated muscle which includes skeletal and cardiac muscle and non-striated or smooth muscle such as airway, uterine, vascular and gastrointestinal (Kuo and Ehrlich 2015). These two muscle categories differ in both structure and function. Striated muscle can be characterised by its striped appearance produced by the longitudinal arrangement of alternating actomyosin fibres (Kuo and Ehrlich 2015; Craig and Padrón 2004). Regular striations are absent in smooth muscle and therefore give the muscle a 'smooth' appearance (Gabella 1984). Another defining feature of smooth muscle, and arguably the most important element which separates it from striated muscle, is the ability of smooth muscle to be contracted and controlled autonomously (Hafen and Burns 2020; Sanders 2008; Craig and Padrón 2004; Gabella 1984). Striated muscle is associated with rapid, precisely controlled movements whereas smooth muscle is specialised for slow and sustained contraction. Smooth muscle, in comparison to skeletal or cardiac muscle, is fatigue resistant due to its minimal consumption of adenosine triphosphate (ATP) thus, allowing for prolonged contraction (Craig and Padrón 2004; Gabella 1984; Paul *et al.* 1976). Depending on location smooth muscle contractility can be controlled by the autonomic nervous system, pacemaker cells, hormones as well as autocrine/paracrine stimuli (Kuo and Ehlrich 2015; Canning 2006; Sanders *et al.* 2006; Mizuma *et al.* 2001).

1.2.1 Smooth muscle contraction

The activation mechanisms that regulate smooth muscle cell (SMC) contraction are dependent upon the SMC location and function (Berridge 2008). Contraction of SMCs can occur by electromechanical or pharmacomechanical (receptor) coupling (Kirschstein *et al.* 2009; Shabir *et al.* 2004; McFadzean and Gibson 2002; Somlyo and Himpens 1989). Electromechanical coupling is dependent upon depolarisation of membrane potential to initiate calcium influx across the plasma membrane through voltage-dependent calcium channels (VDCCs). In contrast, pharmacomechanical coupling occurs independently of membrane potential and results in an increase in intracellular calcium levels in response to stimuli such as acetylcholine (ACh) and noradrenaline binding to

postjunctional receptors on SMCs (Kirschstein *et al.* 2009; McFadzean and Gibson 2002; Itoh 1991; Coburn and Baron 1990; Somlyo and Himpins 1989). The primary receptors involved in agonist-induced calcium increase are G_q protein-coupled receptors. Stimulation of G_q protein-coupled receptors results in activation of phospholipase C (PLC) and hydrolysis of phosphatidylinositol 4,5-bisphosphate (PIP_2) to the potent second messengers: inositol 1, 4, 5-triphosphate (IP_3) and 1, 2-diacylglycerol (DAG). Binding of IP_3 to IP_3 receptors (IP_3Rs) located on the cytosolic surface of the sarcoplasmic reticulum (SR) results in calcium release from the SR into the cytosol. This increase in cytosolic calcium can induce further calcium release from the SR via ryanodine receptors (RyRs) in a phenomenon known as calcium-induced calcium release (CICR). DAG is mainly involved in calcium sensitisation which enables smooth muscle to sustain a contraction once the initial calcium transient has diminished. Through activation of protein kinase C (PKC), DAG can stimulate a range of downstream targets including myosin light-chain kinase (MLCK) which will enhance and maintain contraction (Kuo and Ehlrich 2015; Steinburg 2008).

Once intracellular calcium concentration is increased, by either electromechanical or pharmacomechanical coupling, calcium binds to calmodulin (CaM) creating a calcium-CaM complex. Smooth muscle contraction is regulated by the antagonistic actions of MLCK and myosin light-chain phosphatase (MLCP) to phosphorylate and dephosphorylate regulatory myosin light-chain (rMLC). MLCP is comprised of a catalytic type 1 subunit (PPc1δ), a regulatory subunit, myosin phosphatase target subunit 1 (MYPT1) and an accessory 20-KDa subunit (M20) with undetermined function (Joo and Yamanda 2014). The catalytic activity and specificity of PPc1δ towards phosphorylated rMLC is regulated by MYPT1. MYPT1 contains a number of phosphorylation sites that can down or upregulate MLCP activity (Alvarez-Santos *et al.* 2020). Activation of MLCK by the calcium-CaM complex phosphorylates the 20kDa light chain of myosin (LC_{20}) resulting in active rMLC. Phosphorylated rMLC then interacts with adjacent actin filaments to form cross-bridges between actin and myosin, the two fundamental effector proteins that drive contraction (Hill-Eubanks *et al.* 2011; Sanderson *et al.* 2008; Gunst and Tang 2000; Kamm and Stull 1985). This process is dependent upon energy released from ATP by myosin ATPase activity, which drives the

interaction between myosin heads and actin to initiate cross-bridge cycling, generating tension (Hafen and Burns 2020; Webb 2003). Although, contraction is increased by cytosolic calcium, and subsequent phosphorylation of rMLC, a number of studies have shown that phosphorylation of rMLC is transient, suggesting that persistent activation of rMLC is not necessary for maintenance of tonic contraction. It has been proposed that sustained contraction of smooth muscle involves formation of 'latch-bridges' following dephosphorylation of myosin cross-bridges. Latch-bridges generate unaltered force in comparison to cross-bridges, but have a slow rate of dissociation of myosin heads from actin filaments, thus allowing for prolonged contraction with minimal ATP expenditure (Murphy and Rembold 2005; Dillon *et al.* 1981).

Smooth muscle contraction is regulated by a range of calcium-sensitisation mechanisms that enable calcium-independent processes to sustain contraction once the initial calcium transient has diminished (Kuo and Ehlrich 2015; Somylo and Somylo 1994). These processes include, G protein-mediated inhibition of MLCP by rho-kinase, via phosphorylation of MYPT1, to prevent the dephosphorylation of active rMLC (Puetz *et al.* 2009; Kimura *et al.* 1996) and DAG-activated PKC which can phosphorylate C kinase-potentiated phosphatase inhibitor-17 (CPI-17) to downregulate MLCP thereby, promoting cell contraction (Kuo and Ehlrich 2015; Steinburg 2008). In addition, PKC can modulate smooth muscle contraction via activation of L-type calcium channels thus, increasing calcium influx and elevating intracellular calcium concentration (Raifman *et al*. 2017; Hirota *et al.* 2007; Webb 2003).

1.2.2 Smooth muscle relaxation

Smooth muscle relaxation occurs following the removal of the contractile stimulus or as a result of direct inhibition of the contractile mechanism (Webb 2003). As intracellular calcium drives smooth muscle contraction conversely, a reduction in cytosolic calcium concentration can induce relaxation. According to Bootman (2012), in smooth muscle, calcium is generally maintained at a resting intracellular concentration of ~100nM, an extracellular concentration of 2-4mM and a concentration of ~400μM in the SR. The intracellular calcium concentration can be reduced via a number of processes including removal of calcium from the cytosol to the extracellular space via the plasma membrane calcium-ATPase

(PMCA) pump and the sodium/calcium exchanger (NCX). Calcium can also be sequestered into intracellular calcium stores by the SR/ER calcium-ATPase (SERCA) pump. The PMCA pump employs ATP as a driving force to rapidly extrude calcium from the intracellular milieu to the extracellular space, against its concentration gradient (Yu and Rasenick 2012; Wray and Burdyga 2010). The NCX uses the energy residing from the sodium gradient across the plasma membrane to expel calcium against its electrochemical gradient. This exchange removes one calcium ion in exchange for influx of three sodium ions (Hirota *et al.* 2007). A reduction in cytosolic calcium concentration leads to dissociation of calcium from CaM, thus inactivating MLCK and preventing contraction (Kuo and Ehlrich 2015; Webb 2003; Horowitz *et al.* 1996). Smooth muscle relaxation can also occur via activation of MLCP which dephosphorylates active rMLC (Horowitz *et al.* 1996). In addition, calcium levels can be affected by a number of calcium-binding proteins namely, calretinin and calbindin which are present within the cytosol to serve as calcium buffers when intracellular calcium concentration rises (Wray and Burdyga 2010).

The pathways that regulate smooth muscle relaxation are modulated by second messengers such as cyclic adenosine monophosphate (cAMP) and cyclic guanosine monophosphate (cGMP) following activation of G_s protein-coupled receptors or upregulation of nitric oxide (NO), respectively (Nitsche *et al*. 2018; Kuo and Ehlrich 2015). These second messengers mediate their effects through cAMP-dependent protein kinase A (PKA) and cGMP-dependent protein kinase G (PKG) pathways. Both PKA and PKG can directly modulate the contractile process in a number of ways including: 1) phosphorylation and subsequent activation of calcium pumps to remove cytosolic calcium; 2) downregulation of GTPase RhoA which reduces the sensitivity of the contractile apparatus by inhibition of MLCK and reduction in actin polymerisation 3) phosphorylation of BK channels to induce membrane hyperpolarisation and subsequent inhibition of VDCCs and 4) PKG can directly inhibit MLCK thus, terminating rMLC phosphorylation (Kuo and Ehlrich 2015; Zhang *et al*. 2010; Fukao *et al.* 1999; Kume *et al.* 1994).

1.2.3 Airway smooth muscle

Historically, the importance of airway smooth muscle (ASM) in health and disease was extensively debated with some studies describing ASM as a mere degenerate remnant that served no modern function (Seow and Fredberg 2001). However, there is now agreement among a plethora of studies which indicates that ASM serves a number of critical functions including, airway contractility, expulsion of foreign objects and regulation of airway calibre (Yan *et al.* 2018; Mitzner 2004; James and Carroll 2000). Despite historic views regarding the physiological role of ASM, the correlation between ASM dysfunction and development of airway related diseases is irrefutable (Yan *et al.* 2018; Jones *et al.* 2016; Pascoe *et al.* 2012; Hogg *et al.* 2004; James and Carroll 2000). ASM is the main effector in contractile responses to various stimuli in the airways and therefore, its dysfunction is associated with chronic bronchoconstriction, a prominent feature of airway diseases (Bara *et al.* 2010). ASM-related bronchoconstriction is modulated by airway remodelling and inflammation, both of which are features of airway diseases including asthma and chronic obstructive pulmonary disease (COPD, Jones *et al.* 2016; Rodriguez-Roisin 2005; Hogg *et al.* 2004). Airway remodelling involves both increased volume and size of airway smooth muscle cells (ASMCs) in the walls of the airway, referred to as hyperplasia and hypertrophy. The level of airway remodelling in ASM correlates with COPD severity (Panettieri *et al.* 2008; Hogg *et al.* 2004; Benayoun *et al.* 2003; Ebina *et al.* 1993). Additionally, ASMCs can facilitate inflammatory responses, including secretion of a number of pro-inflammatory mediators such as, Interleukin 17 (IL-17) and tumour necrosis factor α (TNFα), thus, contributing to the global airway inflammation observed in both COPD and asthma (Damera *et al.* 2009; Johnson and Knox 1997).

1.2.4 Airway smooth muscle contraction

In contrast to most smooth muscle types, L-type calcium channel blockers elicit only modest effects on ASM contraction. Instead, it is widely accepted that ASM contraction is primarily regulated by release of calcium from intracellular calcium stores (Jude *et al.* 2008; Pelaia *et al.* 2008; Sanderson *et al.* 2008). Exposure of ASM to contractile agonists produces a biphasic increase in intracellular calcium concentration which is distinguished by an initial rapid

elevation in calcium, followed by a decline to a sustained calcium concentration above basal level (Sims *et al*. 1996; Murray *et al*. 1991; Shieh 1991). A number of studies have shown that the sustained calcium response elicited by ASM is mediated by propagating rhythmical, regenerative increases and decreases in calcium, known as calcium oscillations or waves, rather than a static increase in intracellular calcium levels (Prakash *et al.* 2000; Prakash *et al.* 1997; Liu and Farley 1996; Sims *et al.* 1996). Studies have shown that the contractile state of ASMCs directly correlates with the frequency of agonist-induced calcium oscillations within SMCs. Roux *et al*. (1997) showed that in rat tracheal SMCs the initial components of muscarinic receptor-induced calcium oscillations were not affected by removal of external calcium or application of the VDCC blocker verapamil. However, they were inhibited by the endoplasmic calcium-ATPase blocker, thapsigargan, suggesting that this activity was reliant on calcium release from intracellular stores and did not involve calcium influx via VDCCs. Prakash *et al.* (1997) demonstrated that calcium oscillations in porcine tracheal SMCs could be initiated in the absence of extracellular calcium, but were not sustained, possibly due to depletion of intracellular calcium stores.

1.3 Calcium signalling in the airways

1.3.1 The sarcoplasmic reticulum

ASMC contraction is primarily mediated via calcium release from the SR. Within ASMCs, the SR is an extensive system of tubules, vesicles and cisternae and is regarded as the primary calcium reserve (Hill-Eubanks 2011; Wray and Burdyga 2010). Therefore, refilling and maintenance of calcium levels within the SR is a critical component for ASMC function. Cytosolic calcium can be rapidly transported into the SR via the actions of the SR/ER calcium ATPase (SERCA) pump at the expense of ATP. There are three known mammalian isoforms of SERCA (SERCA1, 2 & 3) and SERCA2 is the subtype present in smooth muscle (Berchtold *et al.* 2000; Baba-Aissa *et al.* 1996).

SERCA pump activity is regulated by pH, calcium concentration and modulatory proteins, such as phospholamban (Wray and Burdyga 2010). Non-phosphorylated phospholamban binds to the SERCA pump and, through direct protein-protein interactions, reduces its calcium affinity, inhibiting calcium influx.

Phosphorylation of phospholamban activates the SERCA pump enhancing cytosolic calcium removal into the SR. This has been suggested as a potential downstream target for a number of calcium modulators including, PKA activation following stimulation of β-adrenoreceptors (Hirota *et al.* 2005). McGraw *et al.* (2006) using DNA microarrays and western blots found that phospholamban transcripts and protein were substantially reduced in the airways of transgenic mice overexpressing β_2-adrenergic receptors. In addition, these mice were less responsive to methacholine, suggesting that β-adrenoreceptor agonists could downregulate phospholamban in ASMCs and reduce airway hyperreactivity. In contrast, phosphorylation of phospholamban by PKA in cardiac myocytes facilitates rapid transport of cytosolic calcium into the SR, ensuring sufficient store filling necessary to produce the next contraction (Engelhardt *et al*. 2004; Sato *et al.* 2001).

The calcium storage capacity of the SR is augmented by the intraluminal calcium-binding proteins calsequestrin and calreticulin which bind to calcium with a high capacity and low affinity. Calsequestrin is primarily found in striated muscle, however, its expression has been noted in a number of smooth muscles including the stomach (Volpe *et al.* 1994; Raeymaekers *et al.* 1993), vas deferens (Volpe *et al.* 1994; Villa *et al.* 1993), ileum (Raeymaekers *et al.* 1993), aorta (Volpe *et al.* 1994) and trachea (Raeymarkers *et al.* 1993). Camacho and Lechleiter (1995) reported that overexpression of calreticulin inhibited IP_3R-evoked calcium oscillations suggesting that it may couple to IP_3Rs in *Xenopus* oocytes. However, Villa *et al.* (1993) found that calreticulin does not display discrete distribution within the SR in vas deferens smooth muscle. It has been suggested that greater than 50% of calcium within the SR is bound to calreticulin (Nakamura *et al.* 2001). In addition to its role in calcium storage in the SR, calreticulin mediates additional functions including chaperoning SR proteins and modulating transcription factors within the nucleus (Holaska *et al.* 2001).

Following store depletion, replenishment of the SR involves re-uptake of calcium. However, due to the inevitable loss of some calcium from the cytoplasm into the extracellular milieu, sustained calcium responses require additional calcium influx. Calcium sensors within the SR initiate store-operated calcium entry (SOCE). As the name suggests, SOCE involves the activation of store-

operated channels on the plasma membrane giving rise to the calcium release-activated calcium current (I_{crac}, Yu and Rasenick 2012; Putney and Bird 2008; Ay *et al.* 2004; Hoth and Penner 1992). In ASM, it has been suggested that Orai1, a member of the Orai family of proteins, and stromal interacting molecule 1 (STIM1) are responsible for SOCE activity (Liao *et al.* 2008; Peel *et al.* 2008; Peel *et al.* 2006). STIM1 is a calcium-binding membrane protein present on the SR that acts as a calcium sensor, monitoring intraluminal calcium content (Liou *et al.* 2005; Zhang *et al.* 2005). Following SR depletion, STIM 1 aggregates with other STIM1 proteins to form punctate structures within the SR proximal to the plasma membrane where they interact with Orai1 proteins on the plasma membrane to facilitate SOCE (Peel *et al.* 2008; Liou *et al.* 2005). In human ASMCs, knockdown of STIM1 by small interfering RNAs (siRNAs) significantly reduced SOCE in response to store depletion by histamine (Peel *et al.* 2006). In addition, Peel *et al.* (2008) demonstrated that siRNA knockdown of ORAI1 mRNA and protein resulted in a reduced inward current with I_{crac} characteristics in cultured human ASMCs.

Calcium efflux from the SR, in response to various stimuli, occurs via activation of two main multigene families of intracellular calcium-release channels (CRCs): IP_3R and RyR channels. A third CRC has also been observed, sphingolipid calcium-release-mediating protein for the endoplasmic reticulum or SCaMPER. It is believed that SCaMPER releases calcium from the SR following activation by increased levels of sphingolipid, however, the properties of this channel have not been as thoroughly investigated as IP_3R and RyR channels (Mao *et al.* 1996).

1.3.2 IP_3Rs in airway smooth muscle

IP_3Rs are transmembrane tetrameric structures, which form large-conductance calcium-permeable channels within intracellular membranes, predominately those of the SR. Opening of the central pore is stimulated by binding of IP_3 to the four IP_3R subunits, which initiates a conformational change within the cytoplasmic domain. It has been hypothesised that this conformational shift facilitates calcium binding, which then initiates pore opening (Alzayady *et al.* 2016; Seo *et al.* 2012; Taylor and Tovey 2010; Bezprozvanny *et al.* 1991). Three IP_3R subtypes have been identified (IP_3R1, 2 and 3). IP_3Rs are extensively

expressed in smooth muscle, however expression levels of each subtype varies depending upon tissue type and species (Wray and Burdyga 2010). Song *et al.* (2009) demonstrated that all three IP_3R subtypes were present in mouse ASM using western blots. However, Morel *et al.* (2003), found that rat portal vein expressed $IP_3R1\&2$ whereas, $IP_3R1\&3$ were expressed in rat uterine smooth muscle. This contrasts to human uterine smooth muscle, where all three IP_3Rs were identified (Morgan *et al.* 1996). A plethora of evidence exists for the role of IP_3Rs in the airways, however, precise detail of the expression and functional role of each subtype in ASM of a number of species are limited (Zhang *et al.* 2021; Xu *et al.* 2018; Li *et al.* 2011; Sanderson *et al.* 2008; Hirota *et al.* 2007).

IP_3 is produced at the plasma membrane following activation of PLC by agonist-receptor interactions. PLC initiates the cleavage of membrane bound PIP_2 to liberate IP_3 into the cytoplasm where it can bind to and activate IP_3Rs. In addition, IP_3Rs are also regulated by cytosolic calcium concentration, which enables calcium release by IP_3Rs to further modulate calcium release from neighbouring IP_3Rs (Iino 2000; Patel *et al.* 1999). Kaftan *et al.* (1997) demonstrated that, under physiological conditions, submicromolar ($<1\mu M$) concentrations of intracellular calcium were sufficient to activate IP_3Rs in the presence of IP_3 in canine cerebellar SR vesicles. In contrast, high levels of intracellular calcium can inhibit opening of IP_3R1 (Sanderson *et al.* 2008; Foskett *et al.* 2007; Hirota *et al.* 2007; Bezprozvanny *et al.* 1991). Bezprozvanny *et al.* (1991) demonstrated that increasing concentrations of calcium (10nM to 250nM) increased IP_3R1 activity in endoplasmic reticulum vesicles from canine cerebellum. However, at concentrations above 250nM channel activity was reduced. Similarly, Mak *et al.* (1998) found that increasing calcium concentrations augmented opening of *Xenopus* IP_3R1, but that channel inhibition was only recorded at calcium concentrations $>10\mu M$. In contrast, Ramos-Franco *et al.* (2000) reported that increasing the calcium concentration elicited no inhibitory effects on rat IP_3R2 activity, even at relatively high calcium concentrations ($400\mu M$). Hagar *et al.* (1998) demonstrated similar findings in planar lipid bilayers expressing IP_3R3. The bimodal relationship between IP_3R1 opening and calcium has been proposed as a mechanism for the generation of propagating calcium waves observed in ASMCs (Sanderson *et al.* 2008; Thomas *et al*. 1996).

IP_3R activation is modulated by a number of protein kinases and regulatory proteins (Bai and Sanderson 2006; Komalavilas and Lincoln 1996). Attenuation of IP_3R signalling by cAMP and its downstream mediators has been widely reported in ASMCs (Dale *et al*. 2018; Bai and Sanderson 2006; Tolloczko *et al*. 1997). Bai and Sanderson (2006) reported that calcium release induced by repetitive flash-photolysis of caged-IP_3 was decreased following pre-treatment with the AC activator, forskolin in mouse lung slices. Similarly, Dale *et al.* (2018) demonstrated that IP_3R-dependent calcium release induced by histamine in cultured human ASMCs was reduced by the β-adrenoreceptor agonist, isoproterenol. In 2014, Morgan *et al.* (2014) established that the inhibitory effects of β_2-adrenoreceptor activation on calcium signals in cultured human ASMCs were mediated via PKA. Taken together, these data suggest that attenuation of IP_3R signalling contributes to PKA-mediated bronchodilation.

Augmented IP_3R expression in ASMCs has been linked to enhanced calcium mobilisation, airway remodelling and hyperresponsiveness, which are common markers of asthma (Matsuzaki *et al.* 2011). For example, IP_3-5-phosphatase, an enzyme that degrades IP_3, was downregulated in asthmatic rat models, suggesting a role for increased IP_3 concentration in asthma. Cytokines, such as IL-4, -5 and -13, are prominent influences in asthma. Kellner *et al.* (2008) reported that the expression of IP_3Rs, RyRs and SERCA2 in human ASMCs were upregulated in response to incubation with IL-13 and that enhanced IP_3R-dependent calcium transients in response to ACh were also observed in these cells (Kellner *et al.* 2008).

1.3.3 RyRs in airway smooth muscle

RyRs are large membrane-spanning tetrameric ion channels comprised of a cytosolic N-terminal region, containing calcium and regulatory protein binding sites, and a short SR-luminal carboxy-terminus (Lanner *et al*. 2010; Samso and Wagenknecht 1998). In mammals, three distinct RyR isoforms have been identified (RyR1, 2 and 3, Sutko *et al.* 1997; Hakamata *et al.* 1992; Nakai *et al.* 1990; Zorzato *et al.* 1990). RyR1 and RyR2 are primarily expressed in skeletal and cardiac muscle, respectively (Rossi and Sorrento 2002; Nakai *et al*. 1990; Zorzato *et al*. 1990). RyR3 is the most widely expressed subtype and is found in

a variety of tissue types (Lanner *et al*. 2010; Giannini *et al.* 1995; Ottini *et al*. 1996). The expression of RyRs in ASM is species dependent. For example, in human ASM only RyR3 was detected, whereas RyR1&2 were found in rat ASM and all three subtypes were identified in mouse ASM (Du *et al.* 2006; Du *et al.* 2005; Hyvelin *et al.* 2000). Du *et al.* (2005) used immunofluorescence to show that RyR1 and RyR3 were distributed at specific locations within mouse ASMCs. RyR1 was primarily expressed on the periphery of the cell near the plasma membrane, whereas RyR3 appeared to localise to the perinuclear region. In the same study, expression of RyR2 was confirmed using RT-PCR, however, it was not detected in immunofluorescent studies. This discrepancy was attributed to a lack of efficacy of the RyR2 antibodies available (Du *et al.* 2005). RyR1 and/or RyR2 deficient mice are non-viable suggesting a critical role for these subtypes in physiology and development (Takeshima *et al.* 1998; Takeshima *et al.* 1994). In contrast, RyR3 knockout mice are viable and display minor, if any, differences in comparison to WT (Ji *et al*. 2004; Löhn *et al.* 2001; Takeshima *et al*. 1996). In addition, Du and colleagues reported that contractions of mouse bronchi induced by low concentrations of CCh (<1μM) were primarily mediated by RyR2 whereas, contractions induced by higher concentrations were mediated via RyR1, as these responses were sensitive to the RyR1 blocker, dantrolene (Du *et al.* 2005).

CICR is the primary activation mechanism of RyRs. RyRs also display inhibition at high intracellular calcium levels. Previous studies have indicated that RyR1 and RyR2 are activated by sub/low micromolar calcium concentrations and are inactivated within the high micromolar/millimolar range (Meissner 2004; Coronado *et al.* 1994). RyR3 displays the lowest calcium sensitivity of the three subtypes and has been suggested to act as a high-threshold release channel (Takeshima *et al.* 1996). In addition to calcium, RyRs are also modulated by the intracellular messenger cyclic adenosine diphosphate ribose (cADPR). cADPR allosterically activates RyRs at low cytosolic calcium concentrations, although it's unclear if the effects of cADPR occur directly, or indirectly via effects on the FK506-binding protein (FKBP, Wang *et al.* 2004). A role for cADPR has been reported in agonist-induced calcium responses in ASM. Prakash *et al.* (1998) found that addition of cADPR to porcine SMCs failed to evoke calcium oscillations, but increased the frequency of ACh-induced calcium oscillations. In the same study addition of the cADPR antagonist, 8-amino-cADPR, inhibited

ACh-evoked calcium oscillations. Similar effects were also reported by White *et al.* (2003) in porcine ASMCs. These studies suggest that ACh-induced calcium oscillations in ASM are dependent on cADPR, possibly by activation of RyRs. Consistent with this idea are findings from Bergner and Sanderson (2002), which showed that ACh-evoked calcium oscillations in mouse lung slices were abolished by the RyR inhibitor, ryanodine. Similarly, Prakash *et al.* (1997) demonstrated that ACh-induced calcium oscillations were reduced in the presence of ryanodine in porcine tracheal SMCs. However, other studies have reported no effects of ryanodine on agonist-induced calcium oscillations in ASM. Ressmeyer *et al.* (2010) found that ryanodine had no discernible effects on histamine-evoked calcium oscillations in cultured human ASMCs and Bai *et al.* (2009) observed no effect of ryanodine on methacholine (MCh)-induced calcium responses in mouse ASMCs. This discrepancy may be attributable to the ryanodine concentration employed, as studies which reported inhibitory effects of ryanodine used a concentration of 100μM whereas those which reported that ryanodine was ineffective employed ryanodine at a concentration of 50μM.

RyR-evoked calcium release can also contribute to ASM relaxation through the generation of calcium sparks (Lifshitz *et al.* 2011; Du *et al.* 2005; ZhuGe *et al*. 2004; Bergner and Sanderson 2002). Calcium sparks, which are defined as “local intracellular calcium transients, caused by coordinated opening of a cluster of ryanodine-sensitive calcium release channels in the sarcoplasmic reticulum” – Jagger *et al.* (2000) are observed in a number of smooth muscle types including ASM (Lifshitz *et al.* 2011; Jagger *et al.* 2000; Sieck *et al.* 1997; Janssen and Sims 1994; Hisada *et al*. 1990). In ASMCs, calcium sparks activate proximal large-conductance calcium-activated potassium (BK) channels giving rise to spontaneous transient outward currents (STOCs), subsequently hyperpolarising the membrane and initiating muscle relaxation (Hill and Eubanks 2011; Lifshitz *et al.* 2011; Jagger *et al.* 2000; Nelson *et al.* 1995). Using dual immunocytochemistry, Lifshitz *et al.* (2011) found that RyR1 and RyR2, but not RyR3, were co-localised in clusters around BK channels on the plasma membrane of mouse ASMCs. In addition, ZhuGe *et al*. (1998) reported that calcium sparks generated by RyRs activated both BK channel-mediated outward currents and opposed inward calcium-activated chloride currents, suggesting that RyRs may also modulate chloride channels in ASMCs. This indicates a potential

regulatory role for RyRs on membrane potential, whereby calcium sparks induce BK currents at positive potentials and chloride currents at more negative potentials (Bao *et al.* 2008; ZhuGe *et al*. 1998).

1.4 Potassium channels

Potassium (K^+) conductance across the plasma membrane is a key regulator of membrane potential (Wang 2014; Valverde *et al.* 2011). There are four distinct categories of mammalian K^+ channels: 1) voltage-gated K^+ channels; 2) calcium-activated K^+ channels; 3) inward rectifier K^+ channels and 4) tandem pore domain "leak" K^+ channels (Valverde *et al.* 2011; Yost 1999). Activation of K^+ channels in ASM hyperpolarises the membrane potential thus contributing to ASM relaxation (Valverde *et al.* 2011). Various agonists, including prostaglandin E_2 (PGE_2), induce smooth muscle relaxation via activation of K^+ channels (Zhu *et al.* 2002; Kotlikoff 1993).

1.4.1 Large-conductance calcium-activated potassium channels

BK channels are extensively distributed on the surface of SMCs and play an important role in regulating smooth muscle tone (Tao *et al.* 2016; Kyle and Braun 2014; Wang 2014; Salkoff *et al.* 2006; Kotlikoff 1993). Single channel BK currents have been recorded using the patch-clamp technique in ASMCs of a variety of species including, mouse, guinea pig, horse, pig and human (Bradley *et al.* 2018; Snetkov *et al.* 1996; Wang and Kotlikoff 1996; Murray *et al.* 1991; Saunders and Farley 1991). BK channels are gated by both membrane potential and/or intracellular Ca^{2+} levels (Jackson 2017; Kyle and Braun 2014; Magleby 2003; Tomita and Kume 1994). Activation of BK channels initiates pore opening and K^+ efflux, resulting in a hyperpolarisation of membrane potential (Wang 2014; Tomita and Kume 1994; Nelson *et al.* 1990). Intracellular second messengers also regulate BK channel activity, either directly through interaction with the channel or indirectly by affecting the intracellular calcium concentration (Wang 2014). PKA-induced modulation of BK channels has been observed in the smooth muscle of porcine and mouse trachea and guinea pig basilar artery cells (Zhou *et al.* 2010; Song and Simard 1995; Kume *et al.* 1994) and PKG is responsible for BK channel phosphorylation in human, bovine and porcine

coronary arteries (Zhu *et al.* 2002; White *et al.* 2000). PKA and PKG modulate BK channel open probability via direct phosphorylation of the BK channel alpha subunit at serine 869 and serine 1072, respectively (Tian *et al.* 2001; Fukao *et al.* 1999).

1.4.2 K_v7 channels

K_v7 voltage-gated K^+ channels, are members of the K_v superfamily, and are encoded by five genes (KCNQ 1-5) to produce $K_v7.1$-$K_v7.5$ channels. Unlike other voltage-gated K^+ channels, K_v7 channels activate at very negative voltages and regulate resting membrane potential in a variety of excitable cells (Brueggemann *et al.* 2018; Haick *et al.* 2017; Brueggemann *et al.* 2012). All five subtypes have been detected in human, guinea pig and mouse ASM (Evseev *et al.* 2013; Brueggemann *et al.* 2012). K_v7 channels mediate neuronal 'M currents', which are important regulators of excitability in response to activation of muscarinic receptors (Lechner *et al.* 2003; Robbins *et al.* 1993).

K_v7 channel activity has been reported as critical to maintaining the relaxed state in human airways (Brueggemann *et al.* 2012). In addition, Brueggemann *et al.* (2012) demonstrated that application of bronchoconstrictor agonists methacholine and histamine, suppressed K_v7 currents in guinea pig ASMCs. K_v7 channel activators are effective bronchodilators, suggesting a possible role for K_v7 channel agonists as a novel therapy for constrictive airway diseases (Brueggemann *et al.* 2014).

1.5 Airway innervation

Parasympathetic cholinergic innervation is the primary neuronal pathway that controls tone in human ASM (Kistemaker and Prakash 2019; Van der Velden and Hulsmann 1999; Belvisi *et al.* 1996). Acetylcholine (ACh) released from cholinergic parasympathetic nerves can act post-junctionally on ASMC M3 muscarinic receptors (M_3Rs) to induce contraction, or pre-junctionally on M_2Rs to inhibit ACh release in a negative feedback loop (Kistemaker and Prakash 2019; Van der Velden and Hulsmann 1999; Spicuzza *et al.* 1998). Sympathetic innervation is sparse in human ASM, however, β_2 -adrenoceptors are abundant on ASMCs and activation of these receptors causes bronchodilation (Ward *et al*.

2010; Van der Velden and Hulsmann 1999). Additionally, the airways are also supplied by non-adrenergic non-cholinergic (NANC) nerves. NANC nerves, can be inhibitory through the release of nitric oxide (NO) / vasoactive intestinal peptide (VIP) or excitatory via release of substance P and neurokinins (Kristemaker and Prakash 2019; Van der Velden and Hulsmann 1999; Widdicombe 1998; Foda *et al.* 1995).

1.6 Muscarinic receptors

To date, five mammalian muscarinic receptor (MR) subtypes have been identified and subsequently cloned (M_1R – M_5R, Buels and Fryer 2012; Fryer and Jacoby 1998; Bonner *et al.* 1987). MRs are extensively distributed throughout the human body, mediating a number of diverse physiological functions (Abrams *et al.* 2006). All MR subtypes are G protein-coupled receptors, comprising seven transmembrane domains linked by alternating intracellular and extracellular domains (Hulme *et al.* 1991). M_1, M_3 and M_5 receptors are $G_{q/11}$ protein-coupled receptors that predominantly activate PLC resulting in upregulation of inositol IP_3 and DAG. M_2 and M_4 receptors are $G_{i/o}$-coupled receptors which inhibit AC activation and reduce intracellular cAMP levels (Buels and Fryer 2012; Burford and Nahorski 1996).

ASMCs express both M_2 and M_3Rs, although M_2Rs outnumber M_3Rs by a ratio of 4:1 (Gosens *et al.* 2006). However, functional studies have proposed that M_3Rs are predominantly responsible for ACh-induced ASM contraction (Ikeda *et al.* 2012, Gosens *et al.* 2006). As M_2Rs are coupled to G_i protein-coupled receptors and therefore impede AC production, they are believed to play an indirect role in regulation of ASM contraction, by off-setting AC-induced relaxation (Buels and Fryer 2012; Roffel *et al.* 1990; Barnes *et al.* 1988). MRs are also present on human airway submucosal glands (M_1 and M_3Rs) and airway epithelium (M_3R) (Mak *et al.* 1992; Mak and Barnes 1990). Pre-junctional M_2Rs act as a negative feedback to inhibit ACh release, whereby ACh released from nerves activates the M_2Rs, inhibiting further release of ACh (Fryer *et al.* 2006; Fryer and Jacoby 1998; Minette and Barnes 1988).

Dysregulation of MRs has been implicated in a number of airway diseases. Decreased function of pre-junctional M_2Rs on parasympathetic nerves has been

linked with asthma-related hypersensitivity, whereby the M_2R negative feedback mechanism fails, resulting in excessive ACh release from nerves (Beuls and Fryer 2012; Haddad *et al.* 1996). Allergen-induced attenuation of M_2R function has been attributed to the secretion of major basic protein from eosinophils, which functions as an allosteric M_2R antagonist (Coulson and Fryer 2003). Additionally, decreased function of M_2Rs on nerves supplying the submucosal glands has been linked with increased ACh release and a subsequent increase in mucous secretion evident in a number of airway diseases (Gosens *et al.* 2006; Ramnarine *et al.* 1996).

1.7 Protease-activated receptors

Protease-activated receptors (PARs) are a family of G protein-coupled receptors, that are activated via extracellular proteolytic activity (Kawabata and Kawao 2005, Chambers *et al*. 2001; Lan *et al*. 2001). The PAR family is capable of stimulating diverse and complex intracellular signalling pathways and is involved in a range of critical physiological and pathological processes (Jin *et al*. 2016). Four distinct PARs have been identified (PAR1-4). Activation of these receptors is dependent on proteolytic cleavage within the extracellular amino-terminal domain, exposing a new N-terminus that acts as a 'tethered-ligand' to irreversibly self-activate the receptor (Pera and Penn 2016; Soh *et al*. 2010; Chambers *et al*. 2001; Lan *et al*. 2001). PARs express distinct cleavage sites for thrombin (PAR1, 3 and 4) and trypsin/tryptase (PAR2 and 4) (Ossovskaya and Bunnet 2004; Xu *et al*. 1998; Vu *et al*. 1991).

PARs have been detected in the majority of human tissues, including heart, bladder and lung (D'Andrea *et al*. 2003; Xu *et al*. 1998; Nystedt *et al*. 1994). Despite the irreversible nature of PAR activation, the subsequent signalling cascade is rapidly discontinued, in a process known as desensitisation (Soh *et al*. 2010). The mechanisms responsible for PAR desensitisation are not fully clear, however upregulation of phosphorylating subunits and subsequent receptor internalisation is believed to be involved. Once internalised, G protein-coupled receptors are relocated to recycling endosomes where they are dephosphorylated and returned to the cell surface or transferred to lysosomes and degraded (Ricks and Trejo 2009). The redistribution of uncleaved PARs from

the intracellular matrix to the cell surface replenishes PAR distribution which is essential for cell resensitisation (Bohm *et al*. 1996; Hein *et al*. 1994).

Several studies have suggested a critical role for phosphorylation in the desensitisation of PARs. For example, overexpression of G protein-coupled kinases 3 & 5 initiated increased PAR1 phosphorylation, which significantly reduced receptor signalling (Ishii *et al*.1994). In addition, Paing *et al*. (2002) demonstrated a role for β-arrestins 1 & 2 in the desensitisation of PAR1 in both wild-type (WT) and phosphorylation-defective mutants, suggesting that β-arrestin-dependent desensitisation of PAR1 does not involve phosphorylation and internalisation. In general, β-arrestins bind to activated G protein-coupled receptors, initiating receptor uncoupling from G proteins, enabling receptor internalisation. β-Arrestins 1 and 2 have also been linked to PAR2 desensitisation. However, unlike PAR1, phosphorylation-defective PAR2 mutants failed to recruit β-arrestin 1 or 2 and subsequent receptor desensitisation was significantly impaired in comparison to WT (Stalheim *et al*. 2005; Dery *et al*. 1999). In addition, studies have also demonstrated a role for PKC in PAR2 desensitisation and internalisation. For example, Bohm *et al*. (1996) found that pharmacological inhibitors of PKC augmented PAR2-mediated elevation of intracellular calcium levels in rat kidney epithelial cells. The mechanisms underlying PAR3 and 4 desensitisation remain largely unknown. PAR4 is believed to undergo internalisation, however the process behind this is poorly understood (Soh *et al*. 2010).

1.7.1 PAR2

PAR2 is the most abundant PAR in the human lung and is expressed in bronchial epithelium, smooth muscle and a number of immune cells, including mast cells, macrophages and neutrophils (Roche *et al*. 2003: D'Andrea *et al*. 2000; Howells *et al*. 1997). It also couples to a number of G proteins including, $G_{q/11}$, $G_{i/o}$ and $G_{12/13}$, therefore it is perhaps unsurprising that PAR2 activation can induce diverse, and often conflicting, responses (Geppetti and Trevisani 2003; Miotto *et al*. 2002; Lan *et al*. 2001). Evidence is available to support a role for PAR2 in both pro-inflammatory and bronchoprotective responses in the airways (Ossovskaya and Bunnet 2004; Geppetti and Trevisani 2003; Chambers *et al*.

2001; Cocks *et al*. 1999). Like all PARs, activation of PAR2 is mediated via the cleavage of the N terminal tail to expose a 'tethered-ligand' which irreversibly self-activates the receptor. PAR2 expresses specific cleavage sites for endogenously released trypsin and tryptase. In addition, peptides such as 2-furoyl-LIGRLO-amide (fLIGRLO) that correspond to the sequence of the 'tethered-ligand', exposed following proteolytic cleavage, are also utilised to activate PAR2 (Maruyama *et al.* 2017; Hollenburg *et al.* 2008) see *Figure 1.2*. Hollenburg *et al.* (2008) demonstrated that fLIGRLO exhibited superior binding affinity to PAR2 in comparison to previously available peptides such as SLIGRL-NH_2. Additionally, Hollenburg and colleagues demonstrated that the scrambled peptide 2-furoyl-OLRGIL-NH_2 failed to activate PAR2. In contrast to proteolytic cleavage, activation via exogenous peptides does not irreversibly activate the receptor (Maruyama *et al.* 2017; Pera and Penn 2016; Soh *et al.* 2010).

Several lines of evidence support a role for PAR2 in the generation of airway disease via enhanced inflammation and bronchoconstriction. For example, the proteases involved in PAR2 stimulation, trypsin and mast cell tryptase, are historically linked to inflammatory diseases such as arthritis and asthma (Kawabata and Kawao 2005; Schmidlin *et al*. 2001; Rice *et al*. 1998). Schmidlin *et al*. (2001) reported that addition of trypsin, tryptase and a PAR2-stimulating peptide induced contraction of isolated human bronchi and calcium mobilisation in cultured human ASMCs and Chambers *et al*. (2001) demonstrated that PAR2 activation elicited a small contraction in isolated human ASM. PAR2 is also upregulated in bronchial blood vessels and epithelium of asthmatics (Miotto *et al*. 2002; Knight *et al*. 2001) and *in vivo* studies of ovalbumin-sensitised mice, found that administration of a PAR2 agonist enhanced leucocyte infiltration into bronchoalveolar lavage and augmented airway hyperreactivity to inhaled methacholine (Schmidlin *et al*. 2002).

In contrast, a number of studies have presented evidence for an inhibitory role for PAR2 in the airways via release of endogenous prostanoids, primarily PGE_2, from epithelial cells (Asokananthan *et al*. 2002; Chambers *et al*. 2001; Lan *et al*. 2001; Cocks *et al*. 1999). Lan *et al*. (2001) found that PAR2 agonists reduced the amplitude of CCh-evoked contractions of isolated mouse trachea and similar results were obtained by Cocks and Moffat (2001) in isolated mouse bronchi. These inhibitory effects were attributed to release of PGE_2 as they were

blocked by the COX 1/2 inhibitor, indomethacin and the mixed DP/EP1/EP2 receptor antagonist AH6809. Further investigation, utilising an enzyme immunoassay, confirmed that PGE_2 concentration in the organ bath was increased following PAR2 stimulation (Lan *et al*. 2001). Additionally, Chambers *et al*. (2001) found that denuding the epithelium of isolated human ASM and addition of indomethacin augmented PAR2-induced contractions, suggesting a protective role of epithelial PAR2 receptors via prostanoid production in human ASM. Therefore, the role of PAR2 in the airways is complex and requires further investigation.

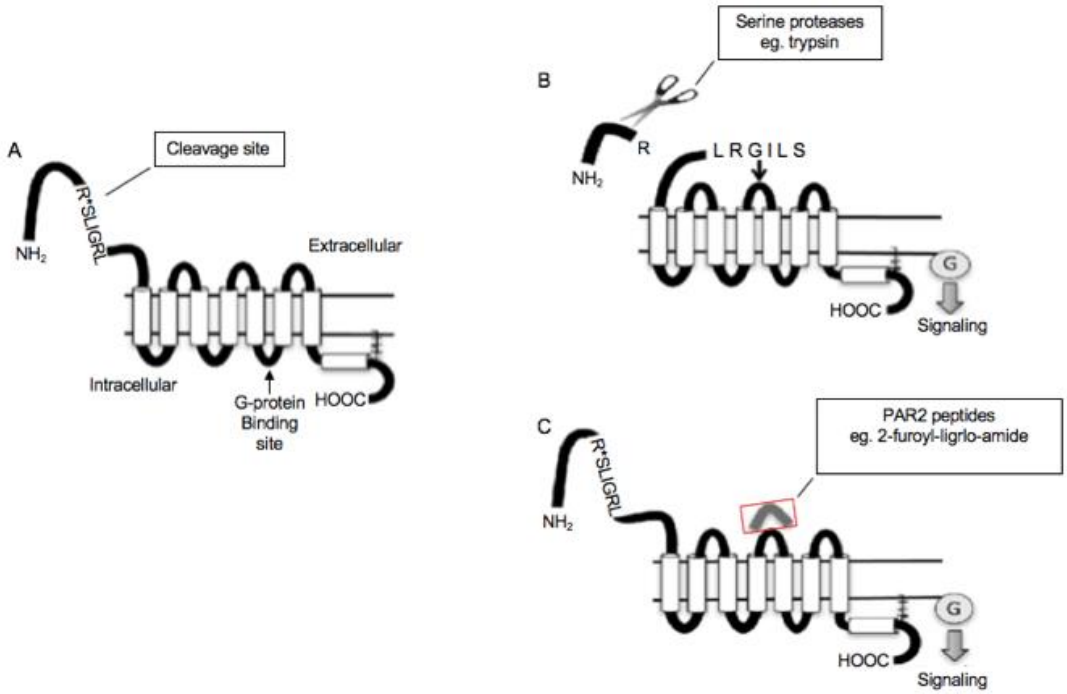

Figure 1.2 Summary of PAR2 activation by cleavage of the N terminus via endogenous proteases (A&B) and the stimulation of PAR2 by exogenously added peptides such as fLIGRLO (C, adapted from Maruyama *et al.* 2017).

1.8 Prostaglandin E_2

Prostaglandins were first discovered by Goldblatt and von Euler in the 1930s (von Euler 1936; Goldblatt 1933). PGE_2 is a metabolite of the precursor arachidonic acid (AA), as are prostacyclin (PGI_2), prostaglandin F2alpha ($PGF_{2\alpha}$), prostaglandin D_2 (PGD_2) and thromboxane A_2 (TxA_2) (Smyth *et al.* 2009). However, PGE_2 is the most abundantly produced prostanoid in the body (Sastre and del Pozo 2012). Production of PGE_2 is fundamentally reliant on three enzymatic reactions: 1) production of AA through interaction of phospholipase A_2 with membrane glycerophospholipids; 2) conversion of AA to PGH_2, an unstable intermediate prostanoid by cyclooxygenase (COX) enzymes and 3) synthesis of PGE_2 from prostaglandin H_2 (PGH_2) via prostaglandin E synthase (Claar *et al.* 2015; Sastre and del Pozo 2012; Vancheri *et al*. 2004).

PGE_2 is functionally versatile and mediates a variety of biological processes including, pain, cough, airway inflammation and bronchodilation (Lebender *et al.* 2018; Claar *et al*. 2015; Konya *et al.* 2013). The first study which highlighted an inhibitory effect of PGE_2 in ASM was published by Piper and Vane (1969). The diverse range of cellular processes initiated by PGE_2 are attributable to the existence of four prostanoid E receptors, EP 1, 2, 3 and 4 which initiate distinct signalling pathways (Claar *et al*. 2015; Benyahia *et al*. 2012; Tilley *et al.* 2003; Sheller *et al*. 2000), see *Figure 1.3*.

In addition to acting as a potent bronchodilator, PGE_2 has also been shown to reduce airway inflammation. Pro-inflammatory stimuli, including bradykinin, ACh and cytokines such as IL-1β, TNF-α and interferon γ (IFN-γ), stimulate ASMCs to produce PGE_2, which inhibits mast-cell mediator release and eosinophil chemotaxis to reduce further inflammation (Johnson and Knox 1997). Moreover, PGE_2 has also been found to potentiate the differentiation and function of regulatory T cells, which limits immune responses, therefore, preventing hyperresponsiveness observed in airway diseases such as asthma (Baratelli *et al.* 2005). Inhaled PGE_2 also reduced the levels of the pro-inflammatory mediators, eosinophils and PGD_2 in the airways of allergen-challenged asthmatic patients (Hartert *et al.* 2000; Gauvreau *et al.* 1999).

In human airways, PGE_2 is produced by a variety of cell types including, epithelium, macrophages, lymphocytes, alveolar cells and smooth muscle cells (Mastalerz *et al.* 2008; Johnson and Knox 1997). However, during an immune response, epithelial cells, infiltrating inflammatory cells and fibroblasts are the major sources of PGE_2 production. An imbalance in cellular production of PGE_2 and/or inadequate cellular response to PGE_2 has been implicated in a number of conditions including aspirin-induced asthma, which is associated with inhibition of COX-1 and subsequent decrease in PGE_2 production (Kalinski 2012; Mastalerz *et al.* 2008; Tai *et al.* 2002).

1.9 Prostanoid E receptors

1.9.1 EP1 receptors

EP1Rs are not as widely distributed as the other prostanoid E receptors, and are found primarily in the kidney and lungs (Lebender *et al*. 2018). EP1R expression has been demonstrated in mouse, guinea pig and rat ASM (Safholm *et al*. 2013; McGraw *et al.* 2006), but not in human ASMCs (Clarke *et al*. 2005; Yano *et al*. 2002, Mori *et al*. 2011). EP1Rs are G_q-coupled receptors, thus activation of EP1Rs initiates an increase in intracellular calcium via activation of the PLC/IP_3 pathway, resulting in smooth muscle contraction (Lebender *et al*. 2018). Coleman *et al*. (1994) found that EP1R activation induced calcium release from intracellular stores by an IP_3-independent mechanism and Katoh *et al*. (1995) stated that EP1R responses in Chinese hamster ovary (CHO) were partially mediated via an influx of extracellular calcium. Additionally, McGraw *et al*. (2006) reported that EP1R activation augmented desensitisation of β_2-ARs, whereby the selective EP1R agonist, 17-phenyltrinor-PGE_2 decreased the concentration of cAMP produced by β_2-adrenoceptor activation. This suggests that multiple mechanisms can be evoked following EP1R activation, dependent upon tissue and species type.

1.9.2 EP2 receptors

EP2Rs are abundantly expressed in a variety of tissues, most prominently the brain, lung and ovaries (Fitzpatrick *et al*. 2014; Ganesh 2014; Konya *et al.* 2013). The role of EP2Rs in human ASM is complex and evidence suggests that the bronchodilator effects of PGE_2 are primarily mediated by activation of EP4Rs, rather than EP2Rs. For example, Buckley *et al.* (2011) reported that the selective EP4R agonist ONO-AE1-329, but not the EP2R agonist ONO-AE1-259-01, relaxed human airways contracted with CCh and Benyahia *et al.* (2012) showed that PGE_2-induced relaxations of ASM were reduced by the EP4R antagonist GW627368X. Nevertheless, there is also evidence which supports an important role for EP2Rs in relaxation of human ASM. For example, Marsh *et al.* (2020) showed that inhibition of vagal nerve-induced bronchoconstriction by the TRPA1 agonist AITC, was prevented by the EP2R antagonist PF-04418948. Similarly, constriction of human airways in response to activation of mast cells was enhanced by PF-04418948, consistent with an inhibitory role for EP2Rs in ASM. Activation of EP2Rs in human ASMC also results in inhibition of histamine-evoked calcium signals. Therefore, it is evident that EP2Rs play an important physiological role in human ASM. EP2Rs are responsible for the relaxant effects of PGE_2 in mouse, guinea pig and monkey ASM (Buckley *et al*. 2011; Tilley *et al*. 2003; Fortner *et al*. 2001; Sheller *et al*. 2000). EP2Rs are G_s protein-coupled receptors that mediate cellular signalling via activation of AC and subsequent increase in cAMP levels (Aso *et al*. 2013; Sastre and del Pozo 2012; Vancheri *et al*. 2004) see *Figure 1.3*. Upregulation of intracellular cAMP activates PKA, and possibly exchange protein directly activated by cAMP (EPAC, Lebender *et al*. 2018) to induce smooth muscle relaxation. PKA is believed to induce relaxation via phosphorylation of calcium ATPases (to remove cytosolic calcium), downregulation of MLCK and phosphorylation of BK channels (Kuo and Ehrlich 2015; Morgan *et al*. 2014; Wooldridge *et al.* 2004; Frank *et al.* 2003). Roscioni *et al*. (2011) showed that EPAC mediated its effects through downregulation of RhoA and activation of Rac1, resulting in inhibition of MLCK. Activation of both PKA and EPAC signalling pathways induces ASM relaxation and bronchodilation (Zhu *et al*. 2002; Konya *et al.* 2013; Lebender *et al.* 2018), however, the exact mechanisms underlying these effects are unclear.

EP2Rs also play a role in immune/inflammatory responses and are present on various immune cells including eosinophils, mast cells, T cells, macrophages and neutrophils (Corrigan *et al*. 2012; Sturm *et al*. 2008). Corrigan *et al*. (2012) demonstrated a deficiency of EP2Rs and an increased presence of immune cells in the mucosa of patients with certain forms of asthma. Additionally, EP2R activation has been implicated in the inhibition of airway cell migration through phosphorylation of heat shock protein 20 and depolymerisation of actin stress fibres. This suggests a possible role for EP2Rs in attenuating airway remodelling observed in asthmatic patients (Aso *et al*. 2013).

1.9.3 EP3 receptors

Unlike the other prostanoid E receptors, the EP3R has multiple isoforms (Coleman *et al*. 1994; Irie *et al*. 1993). These isoforms are generated by alternative splice variants of the C-terminal tail (Hatae *et al.* 2002). Currently, eight different isoforms have been identified in human tissue, however, there is some discrepancy regarding the nomenclature of the EP3R isoforms. According to Kotani *et al*. (2000) eight isoforms are present in human tissue ($EP3_{I\text{-}VI}$, $EP3_e$ and $EP3_f$). Three isoforms have been identified in mouse tissue, $EP3_\alpha$, $EP3_\beta$ and $EP3_\gamma$ (Hatae *et al.* 2002). The various isoforms are capable of mediating diverse intracellular second messengers, due to their ability to couple with G_i, G_s or G_q proteins, respectively (Schlemper *et al.* 2005; Tilley *et al.* 2003).

In human and mouse airway tissue, EP3Rs are believed to be located on airway parasympathetic nerves (Israel and Regan 2009; Maher *et al*. 2009; Chung 2005; Tilley *et al*. 2003). EP3Rs when coupled to G_i-proteins and mediate their effects through inhibition of adenylate cyclase and subsequent reduction in intracellular cAMP levels (Hatae *et al.* 2002). Gauvreau *et al.* (1999) found that pre-treatment of atopic asthmatics with PGE_2 induced cough in a number of patients. EP3Rs were implicated as the prostanoid receptor responsible for this effect, due to their ability to activate sensory nerves (Buckley *et al.* 2011; Maher *et al.* 2009). Activation of EP3Rs has also been shown to be a potent promoter of ASMC migration in humans (Aso *et al.* 2013). In contrast, Schlemper *et al.* (2005) described a role for EP3Rs in bradykinin-induced relaxation of epithelium-intact guinea pig trachea. They found that ‘cross-talk’ between PGE_2 and

bradykinin via EP3R activation resulted in significant synergistic relaxation, demonstrating a bronchoprotective role for EP3Rs in the airways of some species.

1.9.4 EP4 receptors

EP4Rs are widely distributed throughout the body, with mRNA expression observed in almost all mouse tissue types (Narumiya *et al.* 1999). Similar to EP2Rs, EP4Rs are G_s protein-coupled receptors that predominately mediate cellular signalling through upregulation of intracellular cAMP and subsequent activation of PKA (Aso *et al.* 2013; Srivastava *et al.* 2013; Kalinski 2012; Regan 2003; Tilley *et al.* 2003) see *Figure 1.3*. Like EP2Rs, EP4Rs are capable of inhibiting ASMC migration via phosphorylation of heat shock protein 20 and depolymerisation of actin stress fibres (Aso *et al.* 2013). In human airway EP4Rs are responsible for the bronchoprotective/relaxant effects of PGE_2 (Benyahia *et al*. 2012; Buckley *et al.* 2011).

Although, EP2 and EP4Rs share similarities in pharmacology, they are structurally quite different, sharing only 38% homology in amino acid identity in the transmembrane domain (Regan 2003). Another distinguishing feature is the length of the C-terminal sequence; EP2Rs possess a short C-terminal sequence in comparison to EP4Rs (Breyer *et al.* 2001). EP4Rs also exhibit short-term PGE_2-induced desensitisation and internalisation, an effect not associated with EP2Rs (Desai *et al.* 2000; Nishigaki *et al.* 1996). In addition to the cAMP/PKA pathway, EP4Rs can activate phosphatidylinositol 3-kinase (PI3K) resulting in the phosphorylation of extracellular signal-regulated kinases (ERKs) (Fujino *et al.* 2003; Fujino *et al.* 2002). Activation of this pathway results in upregulation of protein kinase B (Akt kinase) which plays a crucial role in regulating cell migration/proliferation, apoptosis and transcription.

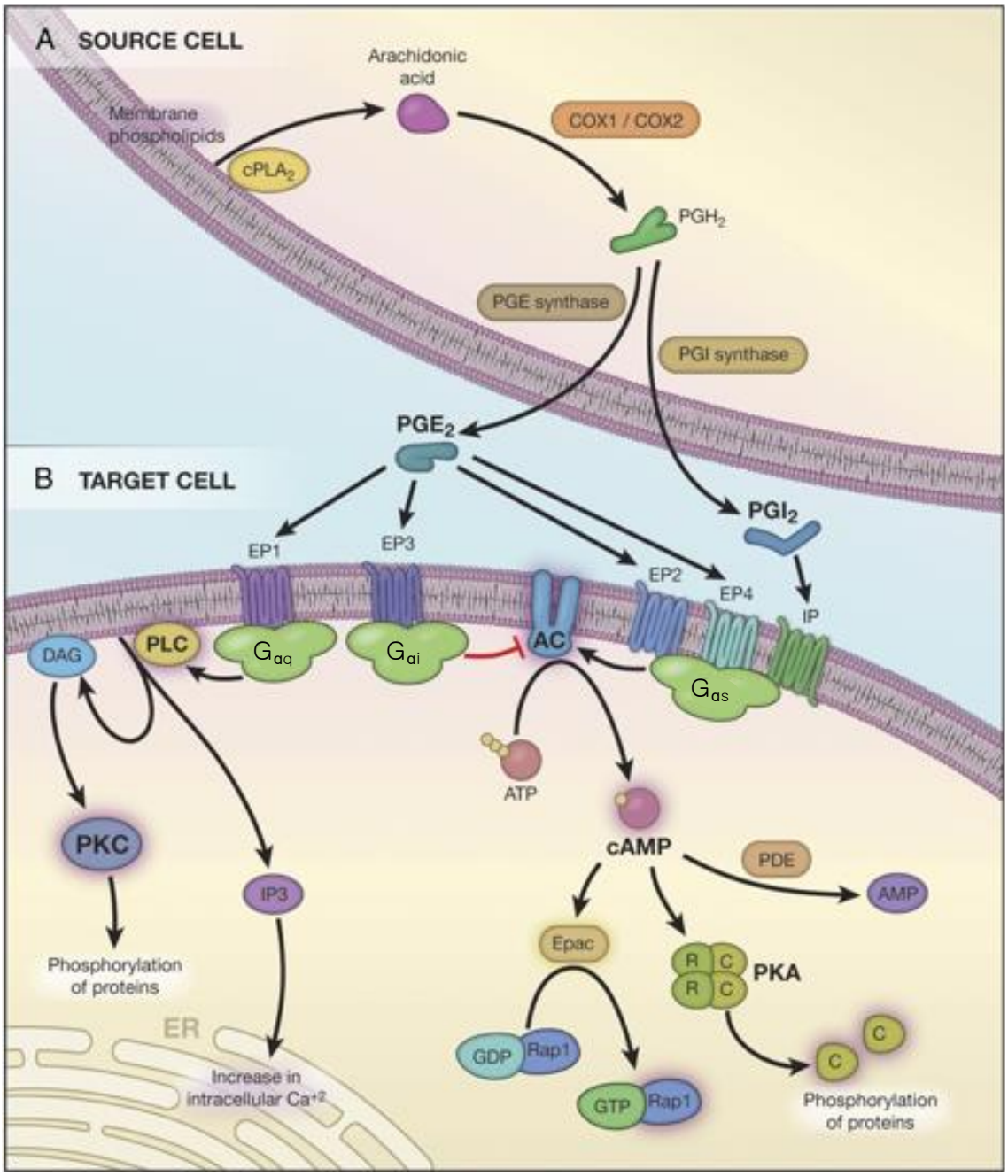

Figure 1.3 Summary of prostanoid synthesis, receptors and signalling pathways (adapted from Zaslona and Peters-Golden 2015).

1.10 Aims of this study

Activation of PAR2 can elicit bronchodilation through production of endogenous prostanoids, such as PGE_2 (Sastre and del Pozo 2012; Chambers *et al*. 2001). Previous studies have shown that PGE_2 acts as a potent bronchodilator via stimulation of EP2 or EP4Rs, however the majority of these studies were performed on tracheal smooth muscle and not the smaller airways which are the major site of airflow limitation in diseases such as COPD (Yanai *et al*. 1992). The relaxant effect of PGE_2 is believed to occur via activation of AC, an increase in cAMP levels and activation of PKA and possibly EPAC. However, the exact cellular mechanisms underlying the inhibitory effects of PGE_2 in ASM are still unclear. The aims of this project were as follows:

- Investigate the mechanisms underlying PAR2-mediated bronchodilation of mouse ASM.

- Identify the EPRs responsible for PGE_2-induced relaxation of mouse bronchial rings.

- Examine the role of K^+ channels in PGE_2-induced relaxation of mouse bronchial rings.

- Investigate if PGE_2 affects calcium signalling in isolated ASMCs.

2. Materials and Methods

2.1 Tissue preparation

Male and female C57BL/6 wild-type (WT) mice, aged between 12-16 weeks, were euthanised with intraperitoneal pentobarbital. This was carried out by a qualified laboratory animal technician, in accordance with EU Directive 2010/63/EU and approved by the Dundalk Institute of Technology Animal Care and Use Committee. Environmental conditions within the animal facility were controlled using a closed-circuit system with temperature ranging between 18-20°C and humidity maintained at a constant of 50%.

The airways were extracted, immersed in Krebs' solution and pinned out on a Sylgard base Petri dish. Surrounding connective tissue, blood vessels and fat were removed by fine dissection to expose the bronchi. The adjoining lobes were removed, isolating the primary bronchi. Each bronchus was cut into two sections, creating four bronchial rings of approximately 2-3mm in length.

2.2 Isometric tension recordings

Individual bronchial rings were secured between two 'S'-shaped hooks and suspended in water-jacketed organ baths containing Krebs' solution maintained at 37°C and bubbled with 95% O_2 - 5% CO_2. The bronchial rings were mounted between two platinum electrodes (5mm length, 2.5mm apart) for point stimulation and adjusted to a tension of approximately 5mN. Tissues were equilibrated for a period of 60 minutes before experimentation began. Tissue responses were recorded in real time using a multi-channel Myobath system (*Figure 2.1*) and data were obtained using LabsScribe3 software. EFS was delivered via platinum electrodes connected to a MultiSyim system-D330 stimulator (Digitimer Ltd, England). The EFS protocol consisted of a 1 second pulse (frequency 2Hz) with a ten second interval between pulses and a pulse width of 0.3ms. This frequency was chosen as autonomic nerves have been shown to discharge at low frequencies (0.4-12Hz) (Widdicombe, 1966). In addition, this protocol yielded robust contractions that were not maximal and therefore allowed drug-mediated increases in contraction amplitude to be observed.

Isometric tension recordings were analysed using LabScribe software. EFS-induced contractions were analysed by obtaining an average of 5 responses to EFS under control conditions and during addition of drugs. Agonist-generated contractions were analysed using two methods; the mean integrated tension response was obtained by placing cursors at the beginning and end of a stimulus period measuring either, (A) the integral of the total area under the trace from the baseline, or (B) the peak amplitude of the contraction.

2.3 Isolation of mouse airway smooth muscle cells

Mouse ASMCs were isolated enzymatically using 1mg/ml of papain (Worthington), 1mg/ml bovine serum albumin (BSA; Sigma), 1mg/ml dithioerythritol (DTE; Sigma) and 1mg/ml collagenase (type II; Sigma). Tissue dissection (Section 2.1) was performed in ice cold calcium-free solution. Isolated bronchi (Section 2.1) were finely chopped into fragments and placed in a 35mm Nunclon dish containing calcium-free solution, for 15-20 minutes at 4°C. Calcium-free solution was utilised throughout this protocol to ensure that the ASMCs were relaxed during the digestion process. Tissue fragments were then transferred to a 1.5ml Eppendorf for enzymatic cell dispersion, which was completed in two steps. Firstly, tissue fragments were incubated in the primary dispersal medium comprised of papain, BSA and DTE dissolved in calcium-free solution for 35 minutes at 37°C. The suspension was then washed thoroughly with calcium-free solution before the incubation in the second dispersal medium containing collagenase and BSA dissolved in calcium-free solution. This incubation was performed for 10 minutes at 37°C. After 10 minutes, the tissue was thoroughly rinsed again and allowed to rest on ice for 15 minutes. ASMCs were released from the tissue fragments by gentle trituration with three glass pipettes of decreasing diameter. Isolated cells were stored in a solution containing 100μM calcium at 4°C and were utilised within 8 hours.

2.4 Collection of isolated ASMCs for RNA extraction

Freshly isolated mouse ASMCs were deposited in a 35mm Nunclon dish and placed on a Nikon inverted microscope within a standard patch clamp apparatus. Throughout collection, cells were maintained at 37°C with continuously perfused Hanks' solution. Cells were identified as ASMCs based upon their elongated spindle shape. Large diameter pipettes, approximately 100μm tip diameter, were produced using a Flaming/Brown micropipette puller (Sutter Instruments Co., USA). The pipette was prefilled with Hanks' solution and attached to the electrode holder of the patch clamp set up. Following identification of a SMC, the pipette tip was maneuvered adjacent to the selected cell using a micromanipulator (Burleigh). Negative pressure was applied through the pipette to force the single ASMC into the pipette. The pipette was then removed and each individual ASMC was expelled into an RNase-free Eppendorf pre-filled with lysis buffer by applying positive pressure. The collected ASMCs were then used immediately for RNA extraction. Each sample contained approximately 15 ASMCs.

2.5 Calcium imaging

Isolated ASMC suspension (3ml) was added to 2ml of 100μM calcium chloride made in calcium-free Hanks' in a WillCo-dish® glass bottom dish (35x10mm), before being mounted on the stage of a Nikon Eclipse T*i* microscope and allowed settle at room temperature for 40 minutes. Cells were incubated with 0.5μM Fluo-4AM (Molecular Probes) in a dark environment for 7 minutes prior to experimentation.

After incubation with Fluo-4AM, cells were continuously perfused with Hanks' solution maintained at 37°C. Furthermore, cells under examination were continuously superfused via a custom-built close delivery system. This gravity-fed system was comprised of multiple reservoirs (syringe bodies, containing pharmacological agents added to Hanks' solution). A three-way tap at the bottom of the syringe body permitted the opening and closing of specific reservoirs. Silicon tubing was attached to the individual three-way taps which extended into

a manifold with an outlet consisting of a glass micropipette, with a tip diameter of 200μm. This micropipette was placed approximately 300μm from the cell under examination.

Calcium events in isolated ASMC were recorded using a Nipkow spinning disk confocal microscope. Unlike conventional microscopy, which applies a single point source to scan the specimen of interest, confocal microscopy consists of a spinning pinhole aperture at the light source focusing only a single beam of light onto the specimen. The reverting light rays pass through a detector pinhole aperture and are accumulated by a photomultiplier that converts the light signal to an electrical signal that can be recorded (*Figure 2.2*). This detector pinhole is located at the exact site where returning light rays are focused, therefore, only permitting light proximal to the focal plane to be detected, excluding unwanted light rays, thus producing a sharper image with increased resolution.

In this study, a spinning disk confocal laser microscope (SDCLM) was utilised. Cells were imaged using an iXon 887 electron multiplying charge coupled device (EMCCD) camera (Andor Technology, Belfast; 512 x 512 pixels, pixel size 16 x 16μM), coupled to a dual Nipkow Spinning Disk (CSU21, Yokogawa, Japan), inclusive of a pinhole disk (PHD) attached to a micro lens disk (MLD). The MLD contains 20,000 micro lenses co-aligned to corresponding pinholes in the PHD, which focus light directly onto the pinholes as the disk revolves at high speed (*Figure 2.3*). Consequently, the emission of light reaches the specimen at multiple points simultaneously, resulting in improved light transmission, minimal light damage to the specimen and enhanced image clarity.

A Krypton-argon laser (ILE400, Melles Griot, UK) was utilised at 488nm to excite the Fluo-4AM and the resulting fluorescent emissions were detected at >510nm. Experiments were completed using a x60 objective lens (Nikon eclipse Ti2, 1.4/NA). Images were captured at a frame rate of 15 frames per second (pixel size 0.266 x 0.266μM).

2.5.1 Image analysis

Image recordings were performed on a desktop PC using Andor iQ software (Andor, Belfast). Files were saved as a stack of TIFF (tagged image file

format) images. Individual recording files were analysed using ImageJ software (version 1.48, National Institute of Health, MD, USA) for *post-hoc* analysis. The initial analysis step involved subtraction of the background fluorescence, achieved by subtracting the mean fluorescence of a null frame from each frame to obtain 'F'. A pseudolinescan image was produced by drawing a fluctuating single line within the cell and applying the 'reslice' function in ImageJ. This function displays the pixel intensity as a succession of lines, each representing a single frame from the movie stack. These are then arranged vertically, left to right so that the vertical axis of the line-scan represents the length of the cell (μm) and horizontal axis displays time (seconds). This allows for the spatial and temporal aspects of the calcium events to be viewed. The minimum or basal fluorescence measured between oscillations was defined as 'F_0'. F/F_0 plots were derived from the entire *post-hoc* linescan and plots of the intensity were performed in Excel. The amplitude of calcium events was determined from the intensity profile by measuring the difference in basal calcium levels between events to peak fluorescence, shown as $\Delta F/F_0$.

2.6 RNA extraction

2.6.1 Whole mouse bronchial tissue

Bronchi from two WT mice of the same age were isolated (Section 2.1) and pooled as a single RNA sample to generate sufficient RNA for PCR analysis. RNA yield from pooled bronchi typically ranged between 300-400ng/μl. Bronchial tissue was flash frozen in liquid nitrogen and ground up using a chilled (-80°C) mortar and pestle. The pulverised tissue was immediately transferred to a ribonuclease (RNase) free 1.5ml Eppendorf tube containing 1ml Trizol™. To aid homogenisation, the Trizol™ tissue sample was triturated initially through an 18-gauge needle, and then a 21-gauge needle. The sample was then allowed to incubate at room temperature for 5 minutes. Chloroform (200μl) was added to the Trizol™/tissue sample, vortexed and incubated at room temperature for 3 minutes. It was then centrifuged at 4°C for 15 minutes in order to separate into layers the protein, DNA and RNA components of the tissue. The upper aqueous layer containing RNA was isolated into a clean RNase free Eppendorf and 500μl

of isopropanol was added to assist RNA precipitation. Following vortexing and a 10-minute incubation at room temperature the sample was centrifuged at 4°C for 10 minutes. Subsequently, an RNA pellet was produced. The pellet was isolated by discarding the supernatant and washing with the addition of 1ml of 75% ethanol. Further centrifugation at 4°C, yielded an RNA pellet that was allowed to air dry. The pellet was then re-suspended in RNase-free water and stored at -80°C until further use.

2.6.2 Isolated airway smooth muscle cells

RNA was extracted from ASMCs using the RNeasy Micro Kit (Qiagen) as per the manufacturer's instructions. This included, lysing the ASMCs using β-mercaptoethanol buffer solution, which contained an RNA carrier followed by vortexing for 30 seconds. Ethanol was then added to the RNA lysate and the sample transferred to a provided RNeasy MiniElute Spin Column. This was followed by a series of reagent additions and centrifugation steps including a DNase treatment. The final step involved elution of the RNA from the spin column membrane into RNase-free water. The eluted RNA was stored at -80°C until further required.

2.7 Reverse transcriptase-polymerase chain reaction (RT-PCR)

2.7.1 Complimentary DNA synthesis

Complimentary DNA (cDNA) is double-stranded DNA synthesised from RNA using the enzyme reverse transcriptase. cDNA was produced from RNA samples using the Superscript II RNase-H reverse transcriptase kit (Invitrogen). Random hexamers (200μg/μl) were used to transcribe 5-10μl of RNA sample. The applied protocol involved an initial incubation at 25°C for 10 minutes, then Superscript activation at 42°C for 50 minutes, followed by an inactivation step at 70°C for 15 minutes. The synthesised cDNA was then stored at -20°C until further use.

2.7.2 PCR

PCR is a technique used to amplify cDNA fragments for the detection of target genes of interest (GOI). When the target GOI is present within the cDNA sequence, PCR will exponentially amplify the specified DNA sequence resulting in the production of millions of copies of the particular DNA fragment. This involves the use of *Taq* polymerase, a thermostable DNA polymerase, that possesses the ability to synthesise complimentary DNA strands from an existing template at high temperatures (70-80°C). To perform the PCR, 2X Amplitaq Gold PCR mastermix (Applied Biosystems) was utilised, as it contains the necessary components needed to complete PCR (including, a thermolabile DNA polymerase, deoxynucleotide triphosphates (dNTPs) and a buffer solution). PCR reactions also require the use of sense and anti-sense primers for the GOI as well as the appropriate cDNA template. Prior to the examination of single ASMC cDNA for GOI, control RT-PCR were conducted to ensure cDNA contained ASMCs by the presence of *Myh11* (smooth muscle myosin) as well as to check for RNA expression of contaminating cells such as *Uchl1* (neuronal cells), *P4ha1* (fibroblasts) and *Cpa3* (mast cells). Only cDNA which was negative for contaminating cells and positive for smooth muscle myosin were utilised to test for GOI.

A typical RT-PCR reaction mix consisted of the following:

Reagent	Volume (μl)
2X Amplitaq Gold	12.5
PCR grade water	8.5
Sense primer (10μM)	1
Anti-sense primer (10μM)	1
Template cDNA	2
Total	25

Table 2.1 PCR reaction reagents

RT-PCR reactions were performed in a Techne TC-512 thermal cycler, which was pre-programmed with the protocol demonstrated in Table 2.2. Following the RT-PCR protocol PCR products were stored at 4°C until further use.

Step		Temperature (°C)	Time (min)
1	Initial Denaturation	95	5
2	Denaturation	95	0.5
	Annealing	57	0.5
	Extension	72	0.5
	X 40 cycles		
3	Final Extension	72	7

Table 2.2 Thermal steps used in PCR amplification

2.7.3 Further PCR amplification

An additional PCR amplification consisting of 20 cycles was on occasion required for the visualisation of amplicons from cDNA synthesised from ASMCs. This was due to the low concentration of cDNA yielded during cDNA synthesis of single cells. When further PCR amplification was necessary, the steps followed in Section 2.7.2 were repeated however, the PCR product from the first PCR amplification was used in place of the cDNA template. Additionally, the non-template control reaction from the original PCR reaction was also subjected to a second amplification cycle, as a control.

2.8 Agarose gel electrophoresis and gel imaging

Agarose gel electrophoresis was employed to separate the DNA fragments obtained from the PCR based on their size. Agarose gel forms a porous matrix when solidified that permits strands of DNA to migrate, predominately based on their size, through the matrix when an electric field is

applied. As DNA is polyanionic, it will migrate towards the anode through the porous matrix with smaller strands progressing quicker than larger strands. Thus, resolution and separation of the DNA fragments is achieved.

In the present study, a 2% agarose gel was utilised. This was prepared by dissolving Ultra-Pure agarose (Invitrogen, 2.0g) in 1x Tris-Acetic acid-EDTA or TAE (Sigma Aldrich, 100ml) buffer. The mixture was heated in the microwave until boiling point was reached and the agarose dissolved. This suspension was allowed to cool for approximately 5 minutes, or until the temperature fell below 55°C, before the addition 1x SYBR Safe DNA gel stain (Invitrogen). SYBR Safe DNA gel stain, is a nucleic acid staining agent that permits the visualisation of resolved DNA under the excitation of UV light. The suspension was poured carefully to prevent bubbles into an electrophoresis-casting tray, and a comb inserted before the gel solidified. Following solidification the comb was removed leaving negative indentations, or wells, in the gel, enabling the PCR products to be loaded. The gel was submerged in 1x TAE buffer in an electrophoresis chamber (Scie-Plas, UK) and the samples loaded. 10μl of PCR product was added to 2μl of 6x DNA loading buffer prior to loading. 2μl of a 100-base pair (bp) DNA ladder (Thermo Scientific) was also added to 2μl of 6x DNA and loaded in a parallel lane to the PCR sample to compare the relative size of the amplicons obtained. Gel electrophoresis was performed at 80V for approximately 90 minutes.

The resulting gel was transferred to an INGENIUS gel documentation system (Syngene Bio Imaging) and positioned onto the glass plate of a UV-transilluminator (312nm). The UV light exposure activates SYBR Safe bound to the DNA fragments allowing the migration of the DNA in the form of bands to be visualised. The focus and zoom were adjusted appropriately, and a digital image of the gel was taken and stored electronically.

2.9 Primer design

Primers were designed in-house using NCBI primer design software. The primers shown in Table 2.3 were designed with the following parameters: the length of each primer varied between 19-21bp; the predicted amplicon size

ranged from 96-266bp; the melting temperature for each primer ranged from 61-63°C and the GC content ranged between 52-63%. Primers were designed to span exon-exon boundaries where possible. Primers were synthesised by Invitrogen and stored at -20°C. The sequence of the primers utilised in this study and the expected amplicon size are listed in Table 2.3.

Primer name	Genbank ID	Sequence (5'-3')	Size (bp)
Ptger1 FWD	NM_013641.3	GGGCTTAACCTGAGCCTAGC	100
Ptger1 REV		GTGATGTGCCATTATCGCCTG	
Ptger2 FWD	NM_008964.4	GGAGGACTGCAAGAGTCGTC	96
Ptger2 REV		GCGATGAGATTCCCCAGAACC	
Ptger3 FWD	NM_011196	CCGGAGCACTCTGCTGAAG	219
Ptger3 REV		CCCCACTAAGTCGGTGAGC	
Ptger4 FWD	NM_001136079.2	CTTGTTGGTAAGCCCGGTGA	114
Ptger4 REV		AGACCCGACAGACCGAAGAA	
Myh11 FWD	NM_013607.2	TACAAGGAGCAGGCAGAA	218
Myh11 REV		GCTCACTGCGAAGTTTCCT	
Uchl1 FWD	NM_011670.2	GGAGATTAACCCCGAGATGC	252
Uchl1 REV		CAGGAGTTTCCGATGGTCTG	
Cpa3 FWD	NM_007753.2	AGGCTCTTCCTTAGACTGGG	226
Cpa3 REV		GACTCCACCAAGCATTGAT	
P4ha1 FWD	NM_011030.2	GGAGCCTTGGAGACGGTA	266
P4ha1 REV		TCGCTCATATAGAACAGCCAC	
Actb FWD	**NM_007393.3**	**CTAGGCACCAGGGTGTG**	**205**
Actb REV		**GTGAGCAGCACAGGGT**	

Table 2.3 List of primer sequence (5'-3') and amplicon size used in this study (Primers highlighted in bold were utilised for qPCR studies only).

2.10 Real-time quantitative PCR

Real-time quantitative PCR (qPCR) was utilised to measure the relative transcriptional expression of selected GOI in mouse bronchus. Real-time qPCR amplifies amplicons in a similar manner to PCR and the protocol utilised was identical to the thermal protocol described in Table 2.2. In contrast to regular PCR, qPCR simultaneously quantifies the specific DNA sequence by measuring the intensity of fluorescence emitted during each cycle. This is achieved by the addition of SYBR Green (Applied Biosystems) which binds to double-stranded DNA (dsDNA) with high specificity. SYBR green absorbs light at 488nm and emits light at 522nm when bound to dsDNA, therefore fluorescence emitted is proportional to the amount of dsDNA present.

Initially, the efficiency of each primer pair was calculated by constructing a standard curve from amplicons obtained from a number of serial dilutions of template cDNA. Standard curves for each individual primer were attained from mouse brain cDNA used at concentrations of 1:10, 1:20, 1:100, 1:200. Primer efficiency was calculated from each standard curve using Quantica computer software. Each primer had an efficiency value within the 90 -110% range required for accurate qPCR results. To ensure that the observed fluorescence was amplicon-based, melting curve analysis was performed on each reaction. This entailed ramping the temperature from 70°C to 90°C to melt the dsDNA (Techne-Quantica real-time thermal cycler). The presence of a single peak indicated that one PCR product was produced during the reaction. The presence of additional peaks indicated that non-specific binding or primer dimer had occurred. Only reactions containing a single peak were utilised for further analysis.

Actb (β-actin) was used as a reference housekeeping gene and a subsequent standard curve was produced, against which the standard curve of the GOI was compared. All samples were performed in triplicate and a non-template control (NTC) was included for each primer set.

2.11 Statistical analysis

Each experiment consisted of a number of experimental runs (n) and was performed on a number of different animals (N). The minimum N number used was 3 and the minimum experimental runs (n) conducted was 6. Statistical analysis was performed using GraphPad Prism 7.0 to calculate IC/EC_{50} and to calculate statistical significance (*p<0.05, **p<0.01, ***p<0.001, ****p<0.0001). Statistical analysis was performed using Student's t-test (paired), one-way analysis of variance (ANOVA) or two-way ANOVA. Bonferroni multiple comparison test was used for ANOVA. Summary data is presented as the mean ± standard error of the mean (S.E.M). For analysis of concentration-effect data, a dose-response construct (log [agonist] vs. response) was employed to determine the IC/EC_{50} values.

2.12 Solutions and drugs

Concentrations within parentheses are mM, unless stated otherwise.

2.12.1 Solutions

Calcium-free solution (cell isolation)

MSG (80), NaCl (55), KCl (6), glucose (10), $MgCl_2.6H_2O$ (2), Hepes (10).
Solution pH was adjusted to 7.3 using concentrated NaOH solution (3M).

Calcium-free solution (superfusate)

NaCl (125), KCl (5.4), glucose (10), sucrose (2.9), $NaHCO_3$ (4.2), KH_2PO_4 (0.4), Na_2HPO_4 (0.3), $MgCl_2.6H_2O$ (2.3), EGTA (5.0), $MgSO_4.7H_2O$ (0.4), Hepes (10).
Solution pH was adjusted to 7.4 using concentrated NaOH solution (3M).

Hanks' solution

NaCl (125), KCl (5.4), glucose (10), sucrose (2.9), $NaHCO_3$ (4.2), KH_2PO_4 (0.4), Na_2HPO_4 (0.3), $MgCl_2.6H_2O$ (0.5), $CaCl_2.2H_2O$ (1.8), $MgSO_4.7H_2O$ (0.4), Hepes (10).
Solution pH was adjusted to 7.4 using concentrated NaOH solution (3M).

Krebs' solution

NaCl (120), KCl (5.9), $NaHCO_3$ (25), glucose (5.5), NaH_2PO_4 (1.2), $MgCl_2$ (1.2), $CaCl_2$ (2.5).

Solution was continuously bubbled with 95% O_2 and 5% CO_2 to maintain a pH of 7.4.

High K^+ solution

NaCl (65.8), KCl (60), $NaHCO_3$ (25), glucose (5.5), NaH_2PO_4 (1.2), $MgCl_2$ (1.2), $CaCl_2$ (2.5).

Solution was continuously bubbled with 95% O_2 and 5% CO_2 to maintain a pH of 7.4.

2.12.2 Drugs

Drugs utilised were made up in distilled water, ethanol or dimethyl sulfoxide (DMSO) depending on their stated solubility characteristics. Stock solutions of each drug were aliquoted and stored as per manufacturer's instructions. Serial dilutions of stock solutions were performed daily when lower concentrations were necessary. Drug concentrations were selected using published literature as detailed below (*section 2.12.3)*.

Name	**Supplier**	**Action**	**Vehicle**
ω-conotoxin	ABCAM	N-type calcium channel blocker	Water
2-Aminoethoxydiphenylborane (2-APB)	Sigma Aldrich	IP_3R inhibitor	Ethanol
6-MB-cAMP	BioLog	PKA activator	Water
8-pCPT-2-O-Me-cAMP-AM (007-AM)	BioLog/*	EPAC activator	DMSO
Atropine	Sigma Aldrich	MR antagonist	Water
Caffeine	Sigma Aldrich	RyR activator	Hanks' solution

Carbachol (CCh)	Sigma Aldrich	Cholinergic agonist	Water
Compound X	*	BK channel opener	DMSO
fLIGRLO	*	PAR2 agonist	Water
fOLRGIL	*	Scrambled PAR2 peptide	Water
Fluo-4AM	Molecular Probes	Fluorescent calcium indicator	DMSO
Forskolin	ABCAM	AC activator	Ethanol
Iberiotoxin (IbTx)	SMARTOX	BK channel inhibitor	Water
Indomethacin	ABCAM	COX 1/2 inhibitor	Ethanol
ONO-AE3-208	Tocris	EP4R antagonist	DMSO
Indomethacin	ABCAM	COX 1/2 inhibitor	Ethanol
ONO-AE3-208	Tocris	EP4R antagonist	DMSO
PF-04418948	Sigma Aldrich	EP2R antagonist	DMSO
Prostaglandin E_2	Sigma Aldrich	EPR agonist	Ethanol
(*R*)-Butaprost	Sigma Aldrich	EP2R agonist	Ethanol
Rp-8-CPT-cAMPS	BioLog	PKA inhibitor	Water
SC-19220	Sigma Aldrich	EP1R antagonist	DMSO
Tetracaine	Sigma Aldrich	RyR inhibitor	Water
Tetrodotoxin (TTX)	Alomone Labs	Sodium channel inhibitor	Water
XE-991	Tocris	K_V7 channel blocker	DMSO

*Synthesised in-house by Dr. Nicholas Mullins at DkIT.

2.12.3 Drug concentration justifications

ω-conotoxin (300nM)

Tanaka *et al.* (1999) demonstrated that 1μM ω-conotoxin effectively abolished lower frequency EFS-evoked contractions (2-32Hz) in rat mesenteric artery. In the current study, the effect of ω-conotoxin was examined on 4Hz EFS-induced relaxations and therefore, a concentration of 300nM was determined to be sufficient for the current study.

007-AM (10μM)

007-AM has been utilised as an EPAC activator at a range of concentrations from 1-10μM throughout the literature (Fong *et al.* 2019; Humphries *et al.* 2017; Stott *et al.* 2016; Ponsioen *et al.* 2009).

2-APB (100μM)

2-APB is widely used throughout the literature as an IP_3R inhibitor at concentrations of 100μM (Griffin *et al.* 2016, Drumm *et al.* 2015, Kyle *et al.* 2013). In addition, Bai *et al.* (2009) reported that 100μM 2-APB was sufficient to inhibit calcium signals induced by 200nM MCh in murine airway lung slices, therefore 100μM 2-APB was utilised in the current study.

Atropine (1μM)

Atropine is used widely throughout the literature at a concentration of 1μM as a muscarinic receptor antagonist (Han *et al.* 2019; Janssen *et al.* 2004; Széll *et al.* 2000; Shigemoto and Ohmori 1991; Ullman *et al.* 1991).

Caffeine (10mM)

Caffeine was used at a sub-maximal threshold concentration of 10mM to ensure sufficient sensitization of RyRs (Griffin *et al.* 2016; Drumm *et al.* 2015; Kong *et al.* 2008).

Compound X (3μM)

Bradley *et al.* (2016) demonstrated consistent inhibitory effects of 3μM Compound X on contractions induced by U46619 in mouse bronchial rings.

fLIGRLO (1μM)

McGuire (2004) found that 1μM fLIGRLO elicited maximal inhibitory effects on pre-contracted rat aorta and murine femoral arteries, therefore a concentration of 1μM fLIGRLO was utilised throughout this study.

Iberiotoxin (300nM)

Iberiotoxin (300nM) is used throughout the literature as a selective BK channel inhibitor (Hannigan *et al.* 2016; Kyle *et al.* 2013).

Indomethacin (10μM)

Indomethacin is used throughout the literature at concentrations ranging from 1μM to 10μM (Lan *et al.* 2001; Schmidlin *et al.* 2001; Cocks *et al.* 1999; Ullman *et al* 1988). Hwang *et al.* 2004 found that concentrations of <4μM indomethacin prevented PGE_2 synthesis for a maximum of 2 hours in C6 glioma cells. Therefore, to ensure that endogenous PGE_2 was not released during experimentation maximal concentrations of 10μM indomethacin were chosen for this study.

ONO-AE3-208 (20nM)

According to manufacturer guidelines, ONO-AE3-208 is a selective EP4R antagonist with a K_i of 1.3nM for EP4Rs and 30nM for EP2Rs. Therefore, ONO-AE3-208 was utilised at 20nM to achieve maximal inhibition of EP4Rs while remaining specificity.

PF-04418948 (100nM)

PF-04418948 has a reported IC_{50} of 16nM and a 2000-fold selectivity for EP2Rs over any other EPR according to manufacturer's documentation. PF-04418948 is frequently used at concentrations greater than 1μM (Zhang *et al.* 2019; Birrell *et al.* 2013). However, in the current study the inhibitory effects of selective EP2R

agonist (R)-Butaprost on CCh-evoked contractions were effectively reduced in the presence of 100nM PF-04418948, therefore 100nM was utilised throughout this study.

Rp-8-CPT-cAMPs (100μM)

Rp-8-CPT-cAMPs is utilised throughout the literature at concentrations up to 1mM (Morgan *et al.* 2014; Roscioni *et al.* 2009; Spicuzza *et al.* 2001). Roscioni *et al.* (2009) found that concentrations of 100μM Rp-8-CPT-cAMPs had no discernable effects on the inhibitory effects of 007-AM on MCh-evoked contractions and therefore, was a specific inhibitor of PKA at this concentration.

SC-19220 (10μM)

SC-19220 has an IC_{50} of 6.7μM according to manufacturer's guidelines and is utilised throughout the literature as a selective EP1R antagonist at concentrations of 10μM (Chan and Mashimo 2013; Jadhav *et al.* 2009)

Tetracaine (100μM)

In smooth muscle, tetracaine in concentrations greater than 50μM is known to inhibit calcium release from ryanodine sensitive stores (Chernov and Jagger 2002; Hyvelin *et al.* 2000). To ensure complete inhibition of RyRs, 100μM tetracaine was utilised in the current study.

Tetrodotoxin (100nM)

According to manufacturer guidelines, tetrodotoxin is a potent and selective inhibitor of voltage gated sodium channels Na_v 1.6, 1.1, 1.3, 1.4, 1.2 and 1.7, with IC_{50} values ranging from 2.3-36nM. In the current study 100nM was sufficient to abolish EFS-evoked contractions in murine bronchial rings.

XE-991 (10μM)

Evseev *et al.* (2013) demonstrated that 10μM XE-991 abolished K_V7 currents in mouse ASMCs. Therefore, 10μM XE-991 was selected to inhibit K_V7 channels in this study.

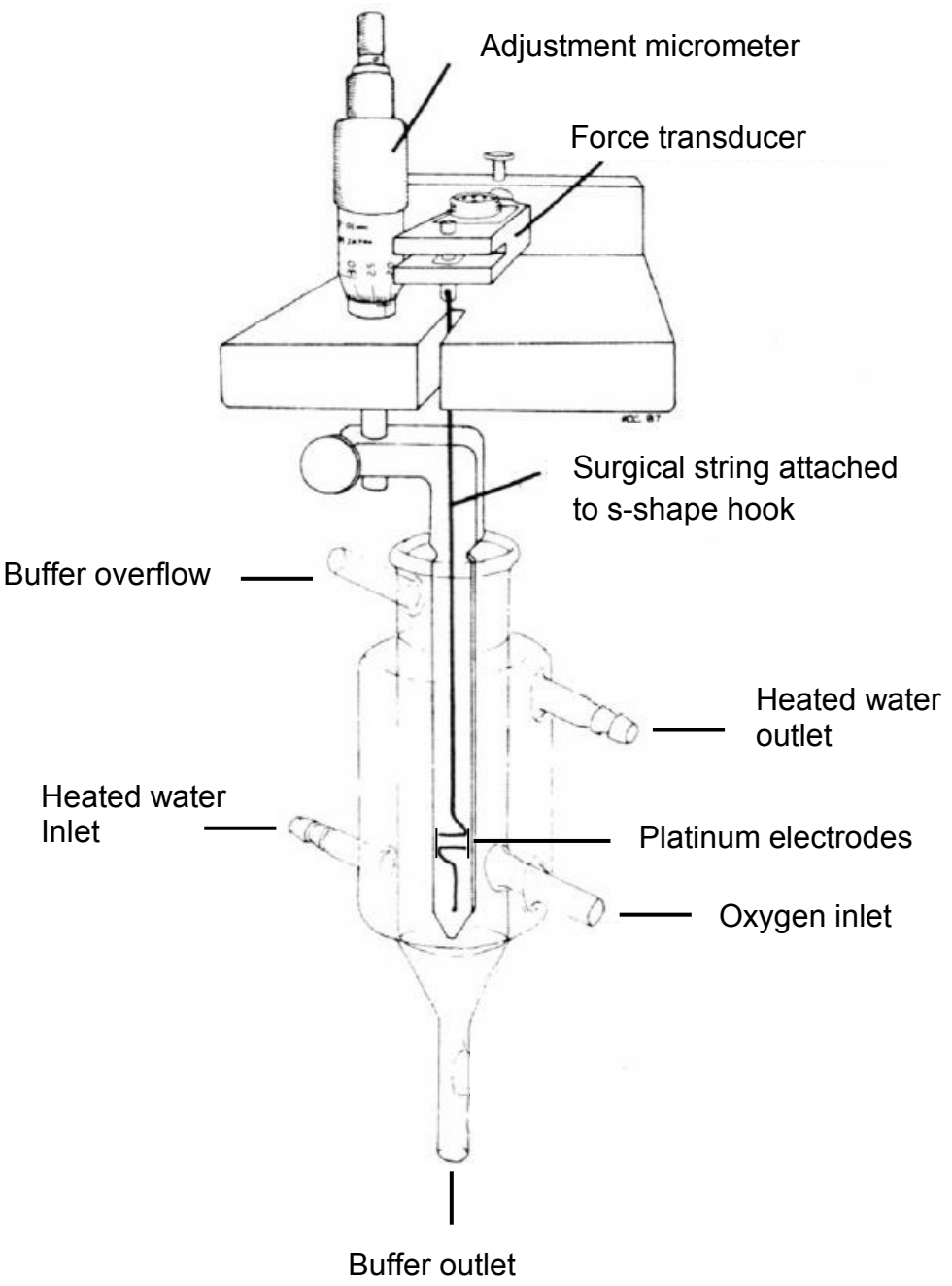

Figure 2.1. Representative image of a tension myobath system. The bronchus tissue was suspended between two s-shaped hooks and submerged in an organ bath containing Krebs' solution bubbled with 95% O_2: 5% CO_2. Two platinum electrodes allow for point stimulation of the tissue sample (Image adapted from Angus and Wright, 2000).

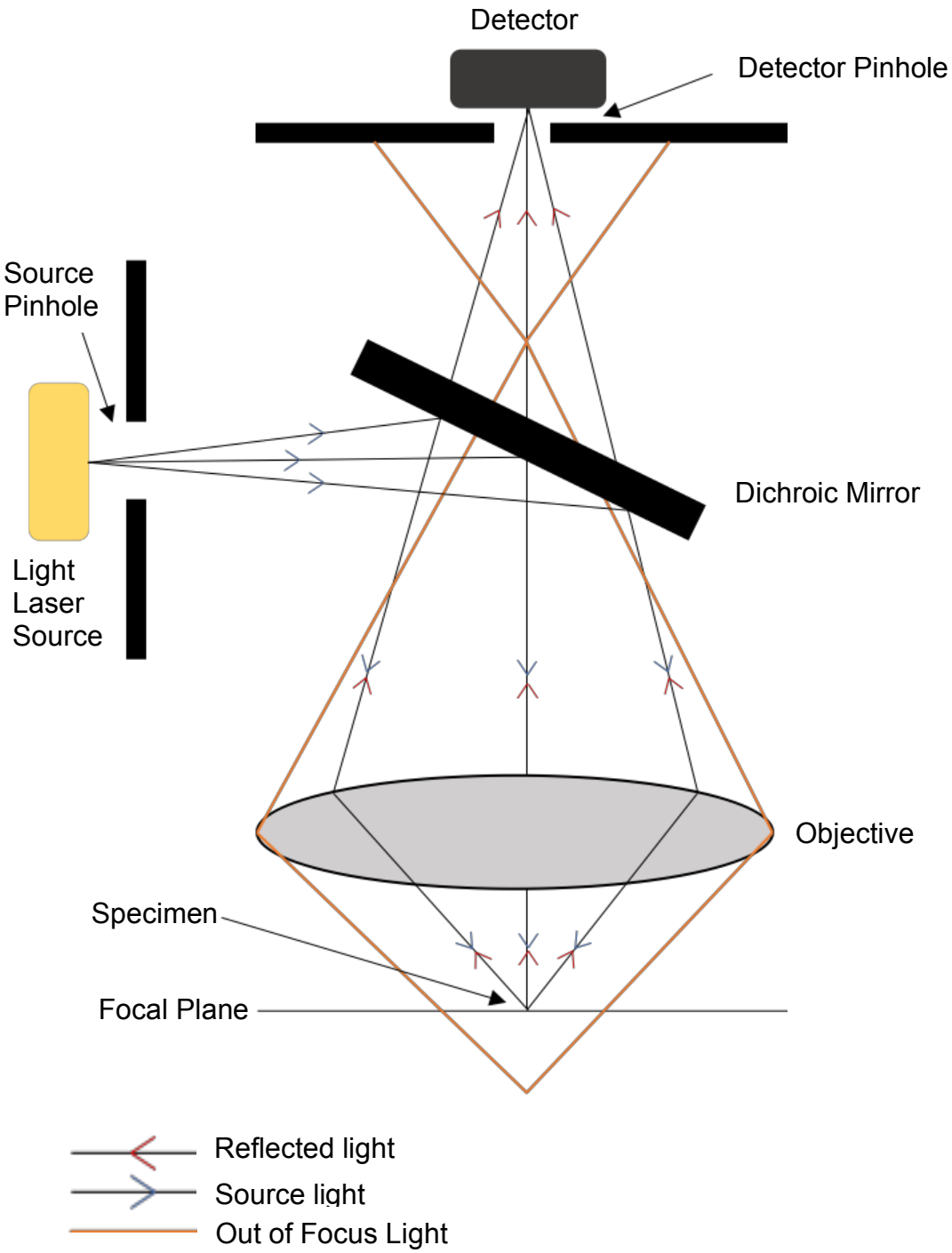

Figure 2.2. Simplified light paths of a confocal microscope

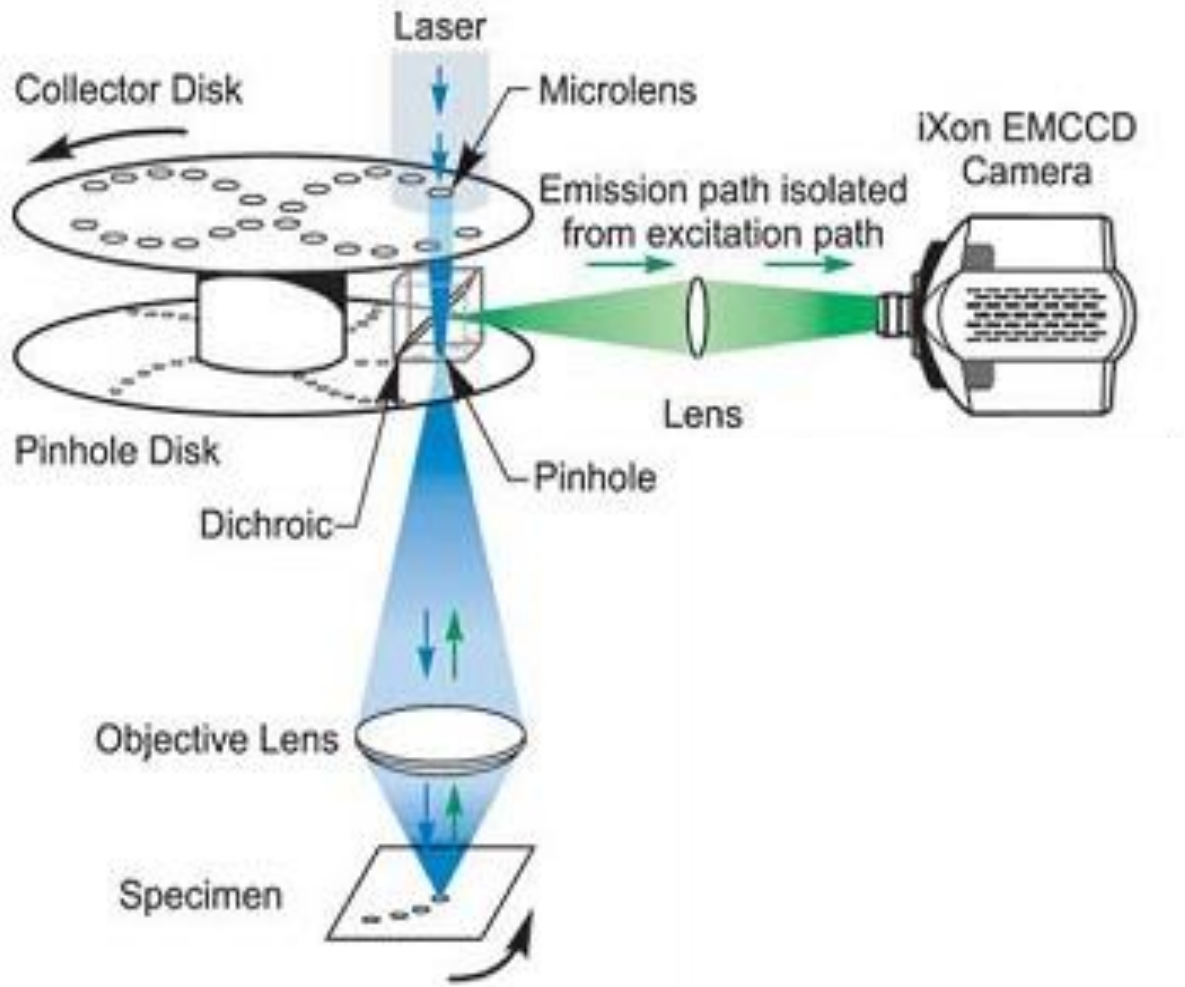

Figure 2.3. Representative image of the Nipkow spinning disk and micro lens array (image from Andor Oxford Instruments).

3. Characterisation of PAR2-mediated relaxation of mouse ASM

3.1 Introduction

PARs are a distinct family of G protein-coupled receptors, consisting of four members (PAR 1-4, Kawabata and Kawao 2005; Lan *et al.* 2001). PARs are self-activated by tethered peptide ligands that become exposed following proteolytic cleavage of the N-terminus of the receptors (Asokananthan *et al*. 2002; Chambers *et al.* 2001; Schmidlin *et al.* 2001). PAR1,3 & 4 express distinct cleavage sites for thrombin, while PAR2 & 4 possess cleavage sites for trypsin/tryptase (Ossovskaya and Bunnet 2004; Xu *et al.* 1998; Vu *et al.* 1991). Expression of one or more PARs has been detected in the majority of human tissues including heart, bladder and lung (D'Andrea *et al.* 2003; Xu *et al.* 1998; Nystedt *et al.* 1994) and PAR2 has been detected in bronchial epithelium and smooth muscle of a number of species, including human and mouse (Kawabata and Kawao 2005; Asokananthan *et al*. 2002; Schmidlin *et al.* 2002; D'Andrea *et al.* 1998).

PAR2 stimulation has been linked to airway hyperresponsiveness, inflammation and ASMC proliferation, which may contribute to respiratory diseases such as asthma (Kawabata and Kawao 2005, Chambers *et al*. 2001). Chambers *et al.* (2001) demonstrated that PAR2 activation elicited a small contraction in isolated human ASM. However, other studies have demonstrated an inhibitory role for PAR2 in the airways, via release of endogenous prostanoids, primarily PGE_2, from epithelial cells (Asokananthan *et al*. 2002; Chambers *et al*. 2001; Lan *et al.* 2001; Cocks *et al.* 1999). For example, PAR2 agonists have been shown to reduce the amplitude of CCh-evoked contractions in isolated mouse trachea. These effects were thought to involve release of PGE_2 as they were blocked by indomethacin, as well as the mixed DP/EP1/EP2 receptor antagonist AH6809. In addition, an enzyme immunoassay confirmed that PGE_2 concentration in the organ bath increased following PAR2 stimulation (Lan *et al.* 2001). Taken together, these findings suggest that the effects of PAR2 activation in ASM are complex and require further investigation.

The aim of this chapter was to characterise the mechanism responsible for PAR2-mediated relaxation of mouse primary bronchus.

3.2 Results

3.2.1 Effect of the PAR2 agonist, fLIGRLO on CCh-induced contractions of mouse bronchial rings

Lan *et al.* (2001) reported that activation of PAR2 elicited bronchodilation in mouse trachea. However, Chambers *et al.* (2001) found that stimulation of PAR2 elicited a small contraction in isolated human ASM, demonstrating diverse functions of PAR2 in the airways. In light of this, experiments were performed to determine if the PAR2 agonist, 2-furoyl-LIGRLO-amide (fLIGRLO) affected contractions induced by the cholinergic agonist, carbachol (CCh). fLIGRLO activates PAR2, by mimicking the 'tethered-ligand' which, following proteolytic cleavage, is exposed and self-activates the receptor (Maruyama *et al.* 2017; Pera and Penn 2016; Soh *et al.* 2010). *Figures 3.1A, B & C* are representative tension recordings illustrating that the amplitude of CCh-evoked contractions were significantly reduced by application of 1μM fLIGRLO, and that these inhibitory responses were reproducible. Therefore, these experiments serve as time-controls for other experiments which examined the effects of selected drugs on these responses. *Figure 3.1D* shows a summary bar chart for the above time-control experiment. Repeated applications of fLIGRLO elicited similar inhibitory results with responses ranging from an initial 62% reduction in amplitude (from 4.0 ± 0.53 to 1.5 ± 0.29mN) to a 75% reduction on the third application (from 4.4 ± 0.62 to 1.1 ± 0.35mN, ANOVA, $p<0.05$, n=6, N=5). These data show that activation of PAR2 inhibits CCh-evoked contractions of mouse ASM.

Control experiments were next performed using the scrambled peptide, fOLRGIL to verify that the specific fLIGRLO peptide sequence, rather than the amino acid composition, was required to activate the PAR2. *Figures 3.2A&B* are representative tension recordings showing the effect of fLIGRLO (*Figure 3.2A*) versus fOLRGIL (*Figure 3.2B*) on CCh-evoked contractions of ASM. The summary bar charts in *Figure 3.2C&D* show that fLIGRLO significantly reduced the amplitude of CCh-evoked contractions by 73%, from 4.4 ± 0.62 to 1.2 ± 0.35mN (*Figure3.2C*, paired t-test, $p<0.01$,) whereas, fOLRGIL reduced the response by 27%, from 4.4 ± 0.62 to 3.2 ± 0.41mN (*Figure3.2D,* paired t-test, $p>0.05$, n=7, N=6). These data demonstrate that fLIGRLO induced a much

greater response than the scrambled version fOLRGIL, suggesting that the effects of fLIGRLO were consistent with an action on PAR2.

3.2.2 The role of prostanoids in the inhibitory effects of the PAR2 agonist, fLIGRLO on CCh-induced contractions of mouse bronchial rings

In order to examine if the inhibitory effects of fLIGRLO were dependent on release of endogenous prostanoids we examined if fLIGRLO responses were affected by the COX 1/2 inhibitor, indomethacin (10μM). Indomethacin, prevents synthesis of endogenous prostaglandins as COX enzymes are essential for the conversion of precursor AA to prostanoid intermediates (Claar *et al*. 2015; Sastre and del Pozo 2012; Vancheri *et al*. 2004). *Figures 3.3A&B* are representative tension recordings showing the effect of 1μM fLIGRLO before (*Figure 3.3A*) and during the presence of indomethacin (*Figure 3.3B*). The summary bar chart in *Figure 3.3C* shows that 1μM fLIGRLO significantly reduced the mean amplitude of CCh-evoked contractions by 74% from 3.7 ± 0.4 to 0.7 ± 0.2mN (paired t-test, $p<0.001$). In the presence of indomethacin fLIGRLO failed to inhibit the CCh response (4.2 ± 0.66 to 4.3 ± 0.67mN, *Figure 3.3D,* paired t-test, $p>0.05$, n=7, N=4). These data suggest that fLIGRLO-induced relaxations are mediated via the production of endogenous prostanoids.

PGE_2 is the most abundantly released prostanoid in the body (Sastre and del Pozo 2012) and mediates its relaxant effect on ASM through activation of EP2 and/or EP4Rs, depending on species (Tilley *et al.* 2003). To investigate if the fLIGRLO responses involved activation of EP2Rs we examined if they were affected by the selective EP2R antagonist, PF-04418948 (100nM). *Figures 3.4A&B* are representative tension recordings showing the effect of 1μM fLIGRLO before (*Figure 3.4A*) and during the presence of PF-04418948 (*Figure 3.4B*). It is evident from these experiments that fLIGRLO-induced relaxations were abolished in the presence of PF-04418948. The summary bar chart shown in *Figure 3.4C*, shows that 1μM fLIGRLO significantly reduced the amplitude of CCh responses by 66% from 3.8 ± 0.69 to 1.3 ± 0.32mN (paired t-test, $p<0.01$), whereas, in the presence of PF-04418948 only a 4% reduction was observed (from 4.6 ± 0.64 to 4.4 ± 0.58mN, *Figure 3.6D,* paired t-test, $p>0.05$, n=6, N=4).

These data suggest that activation of EP2Rs are likely responsible for the fLIGRLO-induced inhibition of CCh responses in mouse ASM.

3.2.3 Effect of the BK channel blocker, iberiotoxin (300nM) on effects of the PAR2 agonist, fLIGRLO on CCh-evoked contractions of mouse bronchial tissue

EP2Rs are G_s protein-coupled receptors that activate adenylate cyclase resulting in an increase in cytosolic cAMP levels. Increases in cAMP levels, initiates activation of PKA, and possibly EPAC, to induce ASM relaxation (Aso *et al.* 2013; Billington *et al.* 2013). Zhu *et al.* (2002) found that PGE_2-induced relaxation of human coronary artery smooth muscle involved activation of BK channels. Therefore, we next investigated if fLIGRLO-induced relaxations of mouse ASM were affected by blockade of BK channels using the potent BK channel blocker, iberiotoxin (IbTx). Representative tension recordings showing the effects of 1μM fLIGRLO before and in the presence of IbTx (300nM) are shown in *Figures 3.5A* and *3.5B*, respectively. The summary bar charts in *Figures 3.5C&D* show that fLIGRLO decreased the amplitude of CCh-induced contractions under control conditions by 78%, from 4.1 ± 0.5 to 0.89 ± 0.13mN (*Figure 3.5C*, paired t-test, $p<0.001$) compared to 58% in the presence of IbTx (from 3.8 ± 0.4 to 1.6 ± 0.1mN, *Figure 3.5D*, paired t-test, $p<0.001$, n=8, N=4). These data demonstrate that PAR2-induced relaxation of ASM is reduced when BK channels are blocked.

3.2.4 Effect of the muscarinic receptor antagonist, atropine and neurotoxin, tetrodotoxin on EFS-evoked contractions of mouse bronchial rings

EFS-induced contractions are mediated by release of ACh from parasympathetic nerves in the airways (Spicuzza *et al.* 1998). Experiments were performed to examine the effect of nerve-evoked contractions of ASM. Contractions were evoked using EFS at a frequency of 2Hz (1 second duration) at 10 second intervals. To confirm that contractions induced by this protocol resulted from activation of cholinergic nerves, control experiments examining the effect of atropine and TTX were performed. *Figure 3.6A* is a representative tension recording showing that application of the muscarinic receptor antagonist, atropine (1μM) abolished EFS-evoked contractions in mouse ASM. *Figure 3.6B*

shows the recording indicated by the red box in panel A on an expanded timescale. The summary bar chart in *Figure 3.6C* plots the mean amplitude of EFS responses in control and in the presence of atropine. Atropine abolished the responses in every experiment (paired t-test, $p<0.05$, n=6, N=6). *Figure 3.7A* is a representative tension recording showing the effect of the potent neurotoxin, tetrodotoxin (TTX) on EFS-induced contractions of mouse bronchial rings. It is clear that TTX, abolished EFS-evoked contractions in mouse ASM. The summary bar chart in *Figure 3.7B*, shows that TTX inhibited the mean amplitude of EFS responses from 1.7 ± 0.5 to 0.001 ± 0.0004mN (paired t-test, $p<0.05$, n=7, N=6). These data confirm that the EFS responses elicited by this protocol were mediated by activation of cholinergic nerves.

3.2.5 Effect of the PAR2 agonist, fLIGRLO on EFS-evoked contractions of mouse bronchial rings

The above data show that activation of PAR2 with fLIGRLO inhibits contractile responses of ASM induced by the cholinergic agonist, CCh. Therefore we next investigated if similar results were observed on contractions induced by stimulation of cholinergic nerves. *Figures 3.8A*, *B & C* are representative tension recordings illustrating that EFS-induced contractions (frequency 2Hz, 1 second duration and 10 seconds interval) were significantly reduced by 1μM fLIGRLO and that these inhibitory responses were reproducible. *Figure 3.8D* shows a summary bar chart for the above time-control experiment. Repeated applications of fLIGRLO produced similar inhibitory results, ranging from 100% inhibition in response to the first application (from 1.07 ± 0.29 to 0 ± 0) to 88% inhibition on the second application (from 1.3 ± 0.28 to 0.16 ± 0.12mN, ANOVA, $p<0.05$, n=6, N=5).

Experiments were next performed to investigate if the inhibitory effect of fLIGRLO on EFS responses was abolished by indomethacin. *Figures 3.9A&B* are representative tension recordings showing the effect of 1μM fLIGRLO before (*Figure 3.9A*) and during the presence of indomethacin (*Figure 3.9B*). fLIGRLO (1μM) significantly reduced the mean amplitude of EFS responses under control conditions by 93% from 0.75 ± 0.15 to 0.05 ± 0.04mN (*Figure 3.9C,* paired t-test, $p<0.01$) compared to 7% in the presence of indomethacin from 1.4 ± 0.19 to 1.3

± 0.2mN (*Figure 3.9D,* paired t-test, p>0.05, n=7, N=4). These data suggest that inhibition of EFS-evoked contractions of ASM by the PAR2 agonist, fLIGRLO require production of endogenous prostanoids.

To test if the inhibitory effects of fLIGRLO on EFS-evoked contractions involved activation of EP2Rs, as was the case for CCh responses, the effects of fLIGRLO were repeated in the presence of PF-04418948. *Figure 3.10A&B* are representative tension recordings showing the effect of 1μM fLIGRLO before (*Figure 3.10A*) and in the presence of PF-04418948 (*Figure 3.10B*). *Figure 3.10C* shows that in control conditions fLIGRLO reduced EFS-evoked contractions by 85% from 1.1 ± 0.22 to 0.16 ± 0.08mN (paired t-test, p<0.0001). However, in the presence of PF-04418948 (*Figure 3.10D*), a reduction of only 24% was obtained following application of fLIGRLO (from 1.7 ± 0.24 to 1.3 ± 0.24mN, paired t-test, p<0.001, n=15, N=14).

Interestingly, a small inhibitory response to fLIGRLO remained in the presence of PF-04418948 suggesting that activation of EP2Rs did not account for the full effect of fLIGRLO. PGE_2 can also inhibit contraction of ASM via activation of EP4Rs (Buckley *et al.* 2011), therefore, we next examined if the fLIGRLO response was affected by the selective EP4R antagonist ONO-AE3-208 (20nM). *Figure 3.11 A&B* are representative tension recordings showing the effects of fLIGRLO on EFS-evoked contractions, before (*Figure 3.11A*) and during the presence of ONO-AE3-208 (*Figure 3.11B*). Summary bar charts shown in Figures *3.11C&D*, show that ONO-AE3-208 did not inhibit fLIGRLO-induced relaxations, with a reduction of 87% from 1.5 ± 0.55 to 0.2 ± 0.13mN (*Figure 3.11C,* paired t-test, p<0.05) in control conditions, compared to 96% 1.2 ± 0.49 to 0.05 ± 0.04mN in the presence of the selective EP4R antagonist (*Figure 3.11D*, paired t-test, p<0.05, n=6, N=6). These data suggest that inhibition of EFS-evoked contractions by fLIGRLO does not involve activation of EP4Rs. However, when ONO-AE3-208 was applied in the continuous presence of PF-04418948 the remaining contraction was greatly reduced. *Figures 3.12A&B* are representative tension recordings showing the effects of fLIGRLO before (*Figure 3.12A*) and during the presence of the selective EP2R antagonist PF-04418948 (100nM, *Figure 3.12B*). As previously shown, PF-04418948 significantly reduced fLIGRLO-induced relaxations, leaving a small residual response. Addition of selective EP4R antagonist, ONO-AE3-208 (20nM), in the continued presence of

PF-04418948 further inhibited the residual effects of fLIGRLO (*Figure 3.12C*). The summary bar charts in *Figures 3.12 D,E&F* show that fLIGRLO (1μM) significantly reduced the mean amplitude of EFS responses under control conditions by 82% from 1.3 ± 0.39 to 0.24 ± 0.15mN (*Figure 3.12D*, paired t-test, $p<0.01$). In the presence of PF-04418948 this effect was reduced to 15% (from 2 ± 0.41 to 1.7 ± 0.37mN, *Figure 3.12E*, paired t-test, $p<0.01$) and the inhibitory effect of fLIGRLO was reduced further, to 5% (from 1.9 ± 0.4 to 1.8 ± 0.4mN), when ONO-AE3-208 was also added (*Figure 3.12F*, paired t-test, $p<0.05$, n=8, N=8). These data highlight that PAR2 receptor-induced inhibition of EFS responses in ASM primarily involves EP2Rs and, to a lesser extent, EP4Rs, but that this effect was only apparent when EP2Rs were already blocked.

3.2.6 Effect of the BK channel blocker, iberiotoxin (300nM) on PAR2 agonist, fLIGRLO on EFS-evoked responses of mouse bronchial tissue

We next examined if fLIGRLO-induced inhibition of EFS-evoked contractions were affected by blockade of BK channels using IbTx. *Figures 3.13A&B* are representative tension recordings showing the effect of 1μM fLIGRLO before (*Figure 3.13A*) and during the presence of IbTx (300nM, *Figure 3.13B*). It was noticeable that IbTx affected both the amplitude and the duration of the inhibitory effect of fLIGRLO, therefore, we measured the amplitude of EFS responses when fLIGRLO had its maximal effect and during the final minute of its application. The summary bar charts in *Figures 3.13C&E*, show that under control conditions 1μM fLIGRLO maximally reduced the amplitude of EFS-evoked contractions by 96% (from 1.3 ± 0.3 to 0.05 ± 0.05mN, *Figure 3.13C*, paired t-test, $p<0.01$) and that this effect was sustained over 3 minutes, such that contractions were reduced by 92% during the final minute of its application (from from 1.3 ± 0.3 to 0.11 ± 0.08mN, *Figure 3.13E*, paired t-test, $p<0.05$). However, in the presence of IbTx a maximal inhibitory response of only 64% was observed (from 1.4 ± 0.24 to 0.47 ± 0.16mN, *Figure 3.13D,* paired t-test, $p<0.05$) and only a 30% reduction was observed during the final minute of fLIGRLO application (from 1.4 ± 0.24 to 0.98 ± 0.22mN, *Figure 3.13F*, paired t-test, $p>0.05$, n=6, N=5). These data indicate that inhibition of nerve-evoked contractions by activation of PAR2 is greatly reduced by blockade of BK channels.

3.2.7 Effect of the PAR2 activator, fLIGRLO and PGE_2 on high K^+-induced contractions

The above data suggests that activation of PAR2 induces relaxation of ASM via activation of EP2Rs and that this effect is reduced when BK channels are blocked. Therefore, it is possible that activation of EP2Rs leads to opening of BK channels, which is likely to hyperpolarise ASMCs and reduce calcium entry via VDCCs. An increase of potassium in the extracellular medium from 6mM to 60mM would shift the potassium equilibrium potential (E_k) more positively (in the range of ~-20mV, assuming an internal K^+ concentration of 140mM) which is within the window current range for L-type calcium channels (-50mV to -10mV). Therefore, we examined if contractions induced by an increase in external K^+ concentration (60mM), to directly induce calcium influx via VDCCs, were affected by PGE_2 and fLIGRLO. Janssen *et al.* (2004) demonstrated that contractions evoked by high concentrations of extracellular K^+ were reduced by atropine in porcine ASM, suggesting that some of this effect was mediated by release of ACh. Therefore, atropine was present throughout these experiments to prevent contractions arising from release of ACh. *Figures 3.14A&B* are representative tension recordings showing the effect of PGE_2 (10nM, *Figure 3.14A*) and the PAR2 agonist, fLIGRLO (1μM, *Figure 3.14B*) on high K^+-induced contractions of mouse ASM. The summary bar charts (*Figure 3.14C&D*) show that PGE_2 reduced the amplitude of high K^+-induced contractions (sustained response) by 55% from 1.3 ± 0.39 to 0.58 ± 0.2mN (*Figure 3.14C*, paired t-test, $p<0.05$, n=7, N=4). fLIGRLO reduced the amplitude of high K^+-induced contractions by 22%, from 0.73 ± 0.28 to 0.57 ± 0.24mN (*Figure 3.14D*, paired t-test, $p<0.05$, n=6, N=4). These data suggest that fLIGRLO and PGE_2 can inhibit ASM contractility via additional mechanisms besides activation of BK channels.

3.2.8 Effect of 4Hz EFS on CCh-evoked contractions in mouse ASM

Thus far the data suggest that activation of PAR2 can inhibit cholinergic nerve mediated contractions of ASM by inducing release of PGE_2 which acts on EP2Rs. Experiments were next performed to assess the effect of EFS on ASM preparations that were pre-contracted with CCh. *Figures 3.15A&B* are representative tension recordings demonstrating that 4Hz EFS induced

relaxation of bronchial rings that were pre-contracted with 1μM CCh (10 second duration) and that this effect was not affected by application of TTX. *Figures 3.15C&D* are summary bar charts which show that 4Hz EFS reduced the amplitude of CCh-induced contractions by 57% from 4.6 ± 0.50 to 2.0 ± 0.63mN (*Figure 3.15C*, paired t-test, $p<0.01$) compared to 76% in the presence of TTX (4.5 ± 0.4 to 1.1 ± 0.28mN, *Figure 3.15D*, paired t-test, $p<0.001$, n=6, N=6) in the presence of TTX. Rattay (1999) suggested that EFS may induce neurotransmitter release by direct effects on the nerve terminal in the absence of an action potential across the axon. However, we found that the inhibitory effects of 4Hz EFS were not affected by the blockade of the VDCC responsible for neurotransmitter release, N-type calcium channels. *Figures 3.16A&B* are representative tension recordings showing that 4Hz EFS-induced relaxations were not reduced by the N-type calcium channel blocker, ω-conotoxin (300nM). *Figures 3.16C&D* are summary bar charts showing that under control conditions 4Hz EFS reduced the amplitude of CCh-evoked contractions by 70% from 4.7 ± 0.34 to 1.4 ± 0.32mN (*Figure 3.16C*, paired t-test, $p<0.001$), no discernible effects were observed in ω-conotoxin (74% reduction from 4.6 ± 0.42 to 1.2 ± 0.38mN, *Figure 3.16D*, paired t-test, $p<0.0001$, n=6, N=6). These data indicate that 4Hz EFS does not modulate inhibitory effects through the activation of nerves.

Figures 3.17A&B are representative tension recordings showing that EFS-evoked relaxations of ASM were reduced by indomethacin, suggesting that this response relied on release of endogenous prostanoids. *Figures 3.17C&D* are summary bar charts showing that under control conditions 4Hz EFS reduced the amplitude of CCh-evoked contractions by 43% from 5.1 ± 1.2 to 2.9 ± 1.4mN (*Figure 3.17C*, paired t-test, $p<0.01$), compared to 18% in the presence of indomethacin (from 5.6 ± 1.1 to 4.6 ± 1.2mN, *Figure 3.17D*, paired t-test, $p>0.05$, n=7, N=5). These data suggest that EFS-induced inhibition of CCh responses were dependent on the production of endogenous prostanoids.

This effect was examined further by testing if EFS-induced relaxations involved activation of EP2Rs. *Figures 3.18A&B* are representative tension recordings showing the effect of 4Hz EFS before (*Figure 3.18A*) and during the presence of PF-04418948 (*Figure 3.18B*). It is evident from this experiment that the EFS-induced relaxations were significantly reduced in the presence of PF-04418948. The summary bar chart shown in *Figure 3.18C*, shows that 4Hz nerve-

stimulation significantly reduced the amplitude of CCh responses by 70% (from 4.6 ± 0.73 to 1.4 ± 0.3mN (paired t-test, p<0.001), whereas, in the presence of PF-04418948 a reduction of only 12% was observed (from 5.2 ± 0.78 to 4.6 ± 0.61mN, *Figure 3.18D,* paired t-test, p<0.05, n=10, N=5). These data suggest EFS inhibited CCh-induced contractions of ASM via release of PGE_2 acting on EP2Rs. It is unclear which cells are responding to EFS to release PGE_2, however since these responses were resistant to TTX and ω-conotoxin it seems unlikely that activation of nerves were involved in this response.

To examine this effect in more detail we examined if 4Hz EFS-evoked responses were also reduced by the blockade of BK channels. Representative tension recordings showing the effects of EFS-evoked relaxations before and in the presence of IbTx (300nM) are shown in *Figures 3.19A* and *3.19B* respectively. The summary bar charts in *Figures 3.19C&D* show that 4 Hz EFS reduced CCh-induced responses by 57% from 4.4 ± 0.86 to 1.9 ± 0.72mN (*Figure 3.19C*, paired t-test, p<0.001). In the presence of IbTx this effect was reduced to 35%, from 4.3 ± 0.79 to 2.8 ± 0.74mN (*Figure 3.19D*, paired t-test, p<0.05, n=7, N=5). These data suggest that EFS-evoked relaxation were partly reduced by blockade of BK channels.

3.2.9 Effect of the PAR2 activator, fLIGRLO on CCh-evoked calcium oscillations of mouse ASMCs

PAR2 is expressed on bronchial epithelium, smooth muscle and a variety of immune cells including mast cells and macrophages, all of which can produce PGE_2 (Mastalerz *et al.* 2008; D'Andrea *et al*. 2000; Roche *et al*. 2003; Howells *et al*. 1997; Johnson and Knox 1997). To examine if the inhibitory actions associated with PAR2 activation were due to direct effects on ASMCs, we examined the effect of fLIGRLO (1μM) on CCh-evoked calcium oscillations in freshly isolated mouse AMSCs. *Figure 3.20A* is a representative pseudolinescan demonstrating the effect of the PAR2 agonist, fLIGRLO (1μM) on calcium oscillations induced by 1μM CCh. The corresponding intensity profile plot is displayed in *Figure 3.20B*. Activation of PAR2 had no discernible effects on CCh-evoked calcium oscillations. Overall, in 6 cells the mean frequency of calcium oscillations was not significantly reduced from 16 ± 5.5 min^{-1} under control

conditions. to 16 ± 4.6 min^{-1} in fLIGRLO (*Figure 3.20C,* paired t-test, p>0.05). Oscillation amplitude was also not affected by fLIGRLO from 1.5 ± 0.32 to 1.4 ± 0.3 $\Delta F/F_0$ (*Figure 3.20D,* paired t-test, p>0.05, n=6, N=5). These data suggest that the inhibitory effects on CCh responses in ASM elicited by PAR2 activation were not mediated via direct inhibition of calcium oscillations in ASMCs.

* The contribution of Dr. Eamonn Bradley to *Figures 3.15* and *3.16* is greatly appreciated.

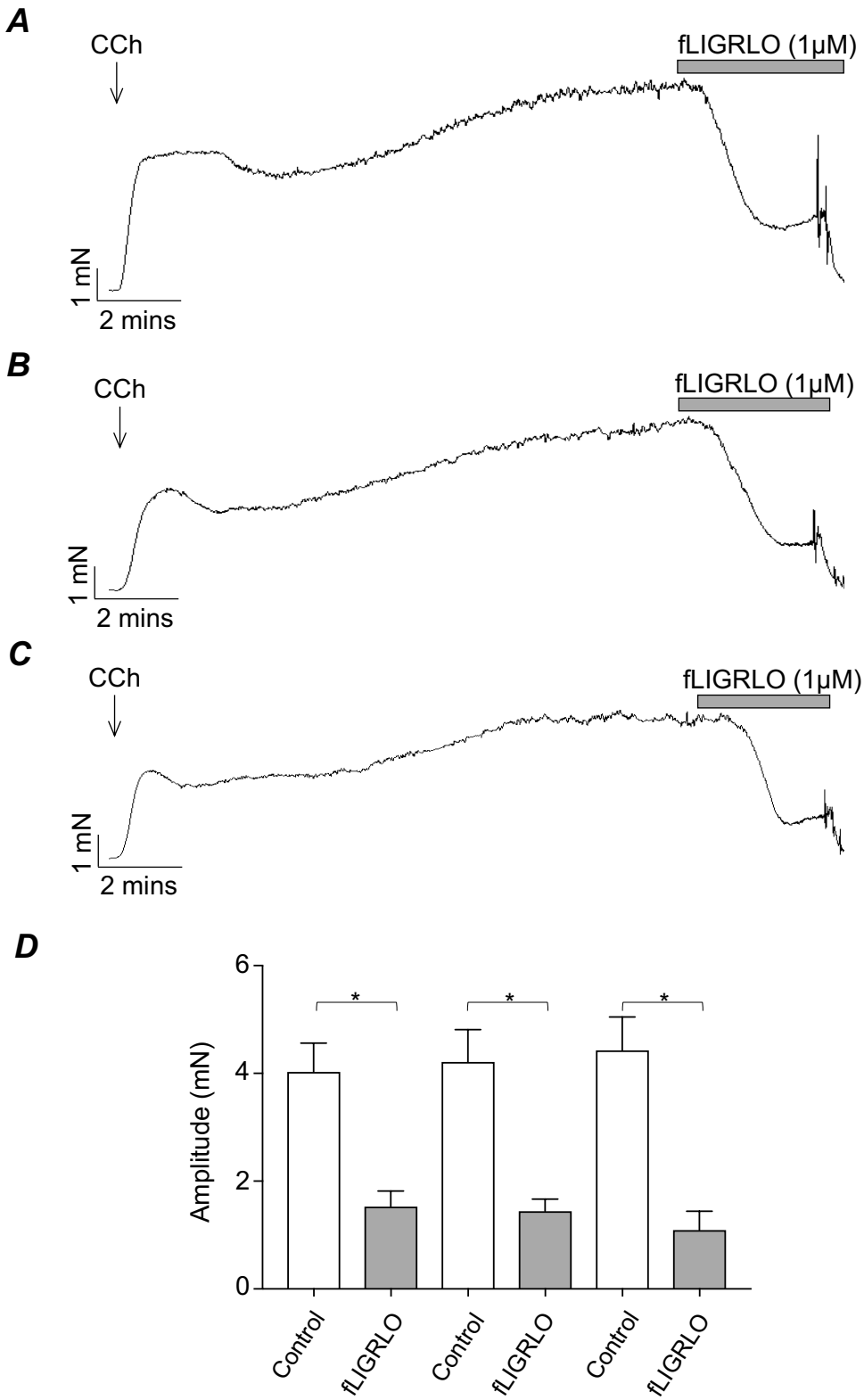

Figure 3.1. ***Effect of consecutive applications of fLIGRLO on CCh-induced contractions of mouse bronchial rings***. **A, B** & **C** are representative tension recordings made from the same preparation showing the effect of fLIGRLO (1μM) with twenty minute intervals on CCh-evoked contractions (1μM). ***D*** summary bar charts showing the mean amplitude of three consecutive additions of fLIGRLO compared with control (n=6, N=5, *p<0.05, ANOVA).

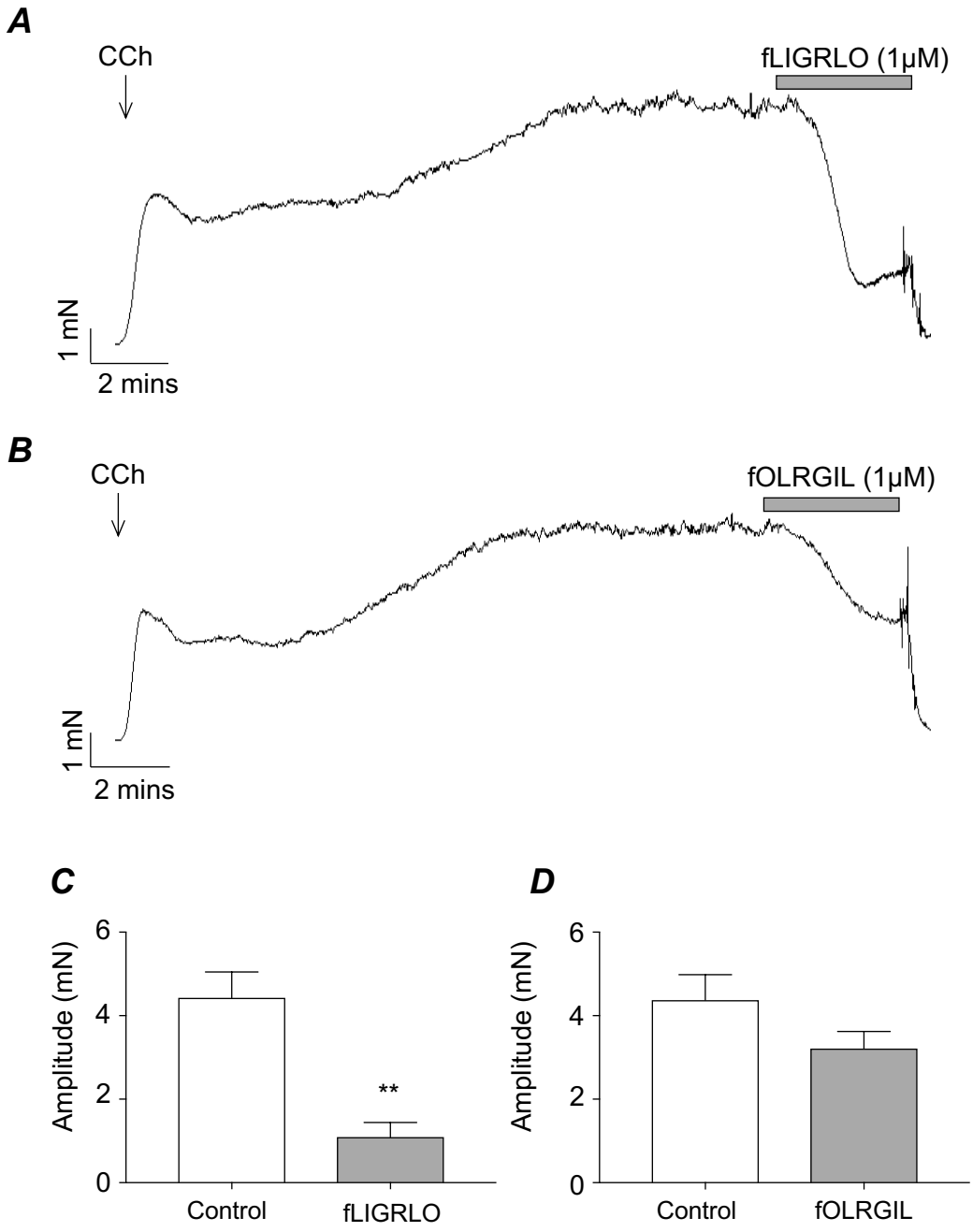

Figure 3.2. ***The inhibitory effects of fLIGRLO versus the scrambled peptide, fOLRGIL on CCh-evoked contractions of mouse bronchial rings.*** (**A**) Representative tension recordings exhibiting the effect of fLIGRLO (1μM) on CCh-evoked contractions (1μM) and (**B**) the effect of the scrambled peptide, fOLRGIL (1μM). (**C** & **D**) Summary bar charts showing the inhibitory effects of fLIGRLO (**C**, n=7, N=6, **p<0.01, paired t-test) and (**D**) the scrambled peptide, fLORGIL.

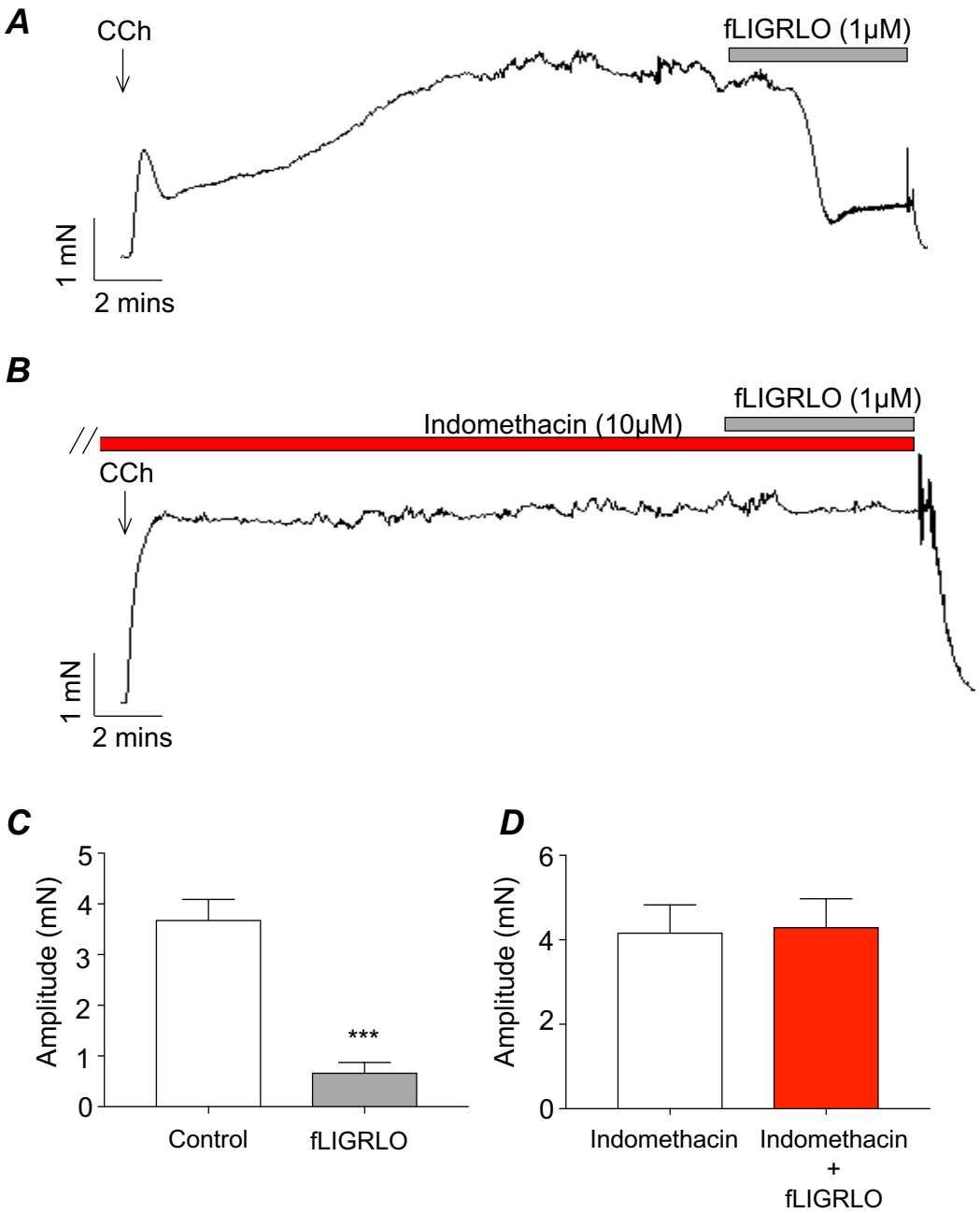

Figure 3.3. ***Effect of the COX 1/2 inhibitor, indomethacin on fLIGRLO-induced inhibition of CCh-induced contractions of mouse bronchial rings.*** (**A** & **B**) Representative tension recordings exhibiting the effect of fLIGRLO (1μM) on CCh-evoked contractions (1μM) in the absence (**A**) and presence of indomethacin (10μM, **B**). (**C** & **D**) Summary bar charts showing mean amplitude of relaxation induced by fLIGRLO in control conditions (**C**, n=7, N= 4, ***p<0.001, paired t-test) and following incubation with 10μM indomethacin (**D**).

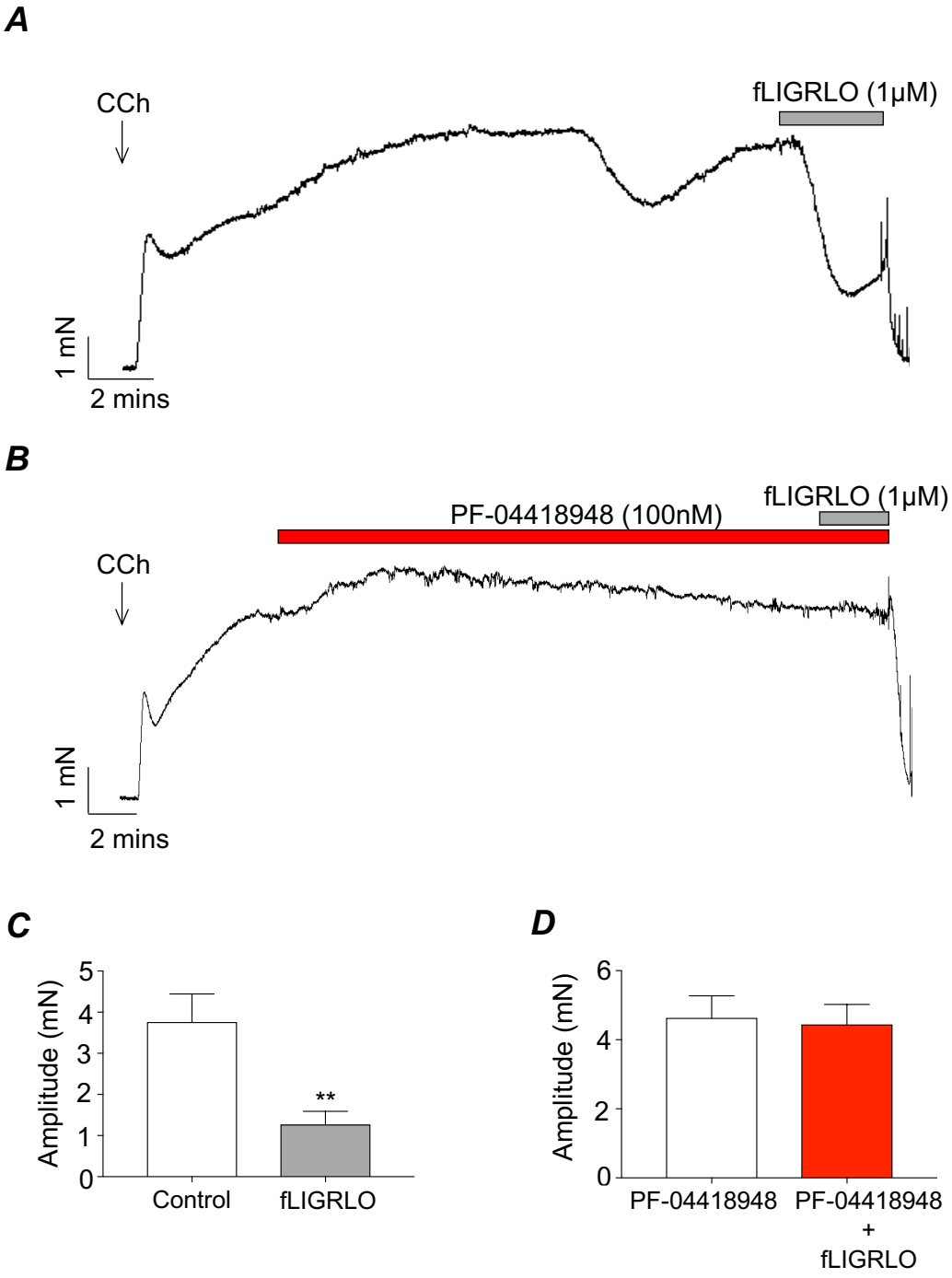

Figure 3.4. ***Effect of the EP_2 receptor antagonist, PF-04418948 on fLIGRLO-induced inhibition of CCh-induced contractions of mouse bronchial rings.*** (**A** & **B**) Representative tension recordings showing the effects of fLIGRLO (1μM) before (A) and during the presence of PF-04418948 (100nM, **B**). (**C** & **D**) Summary bar charts from 6 similar experiments showing the effect of fLIGRLO (1μM) on CCh-induced contractions under control conditions (**C**, n=6, N=4, **p<0.01, paired t-test) and in the presence of PF-04418948 (**D**).

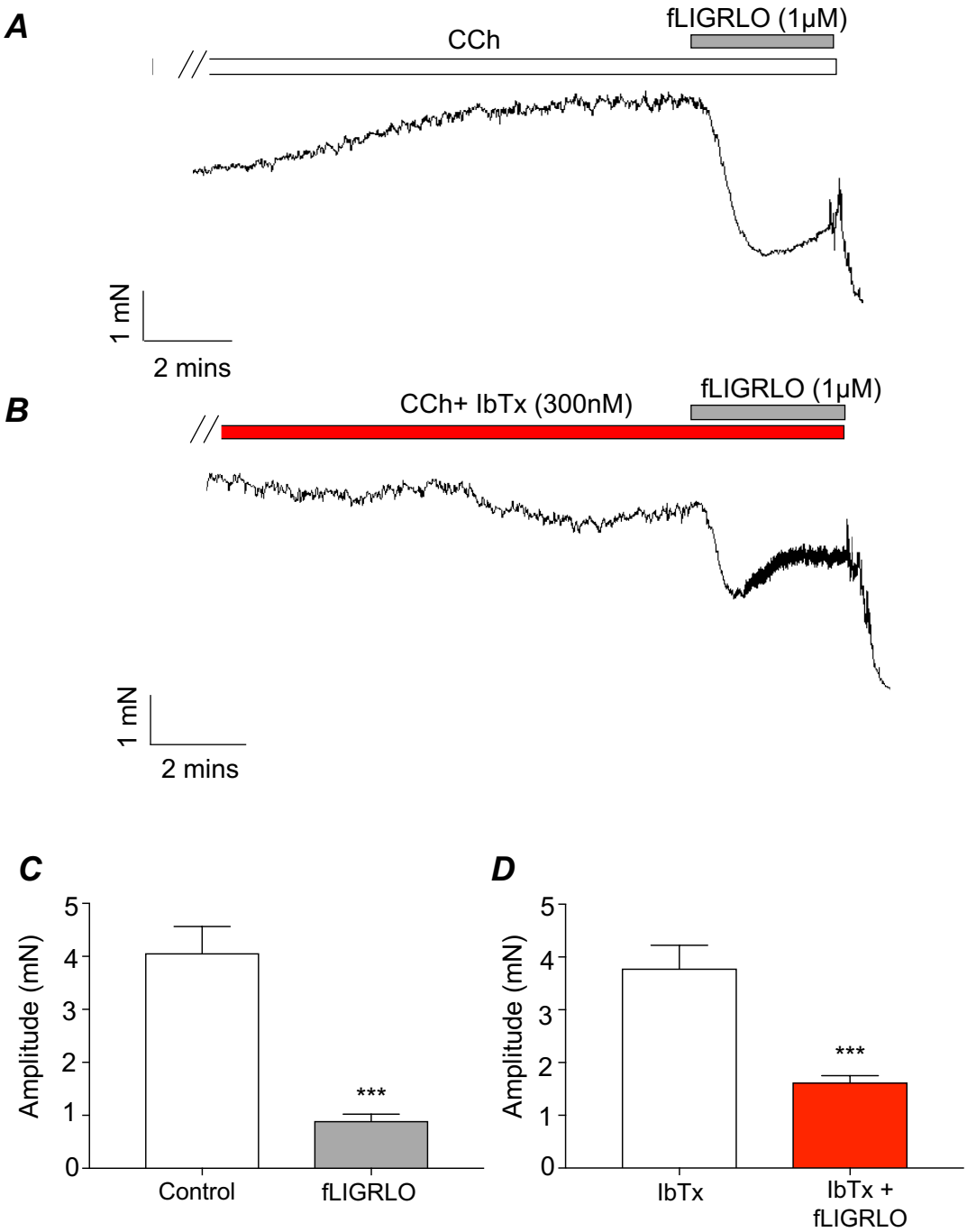

Figure 3.5. ***Effect of the BK channel blocker, iberiotoxin on fLIGRLO-induced relaxations of mouse bronchial rings.*** (**A** & **B**) Representative tension recordings exhibiting the effect of fLIGRLO (1μM) on CCh-evoked contractions in the absence (**A**) and presence of iberiotoxin (300nM, **B**). (**C** & **D**) Summary bar charts from 8 similar experiments showing the maximum response of fLIGRLO (1μM) on CCh-induced contractions in control (**C**) and in the presence of iberiotoxin (**D,** n=8, N=4, ***p<0.001, paired t-test).

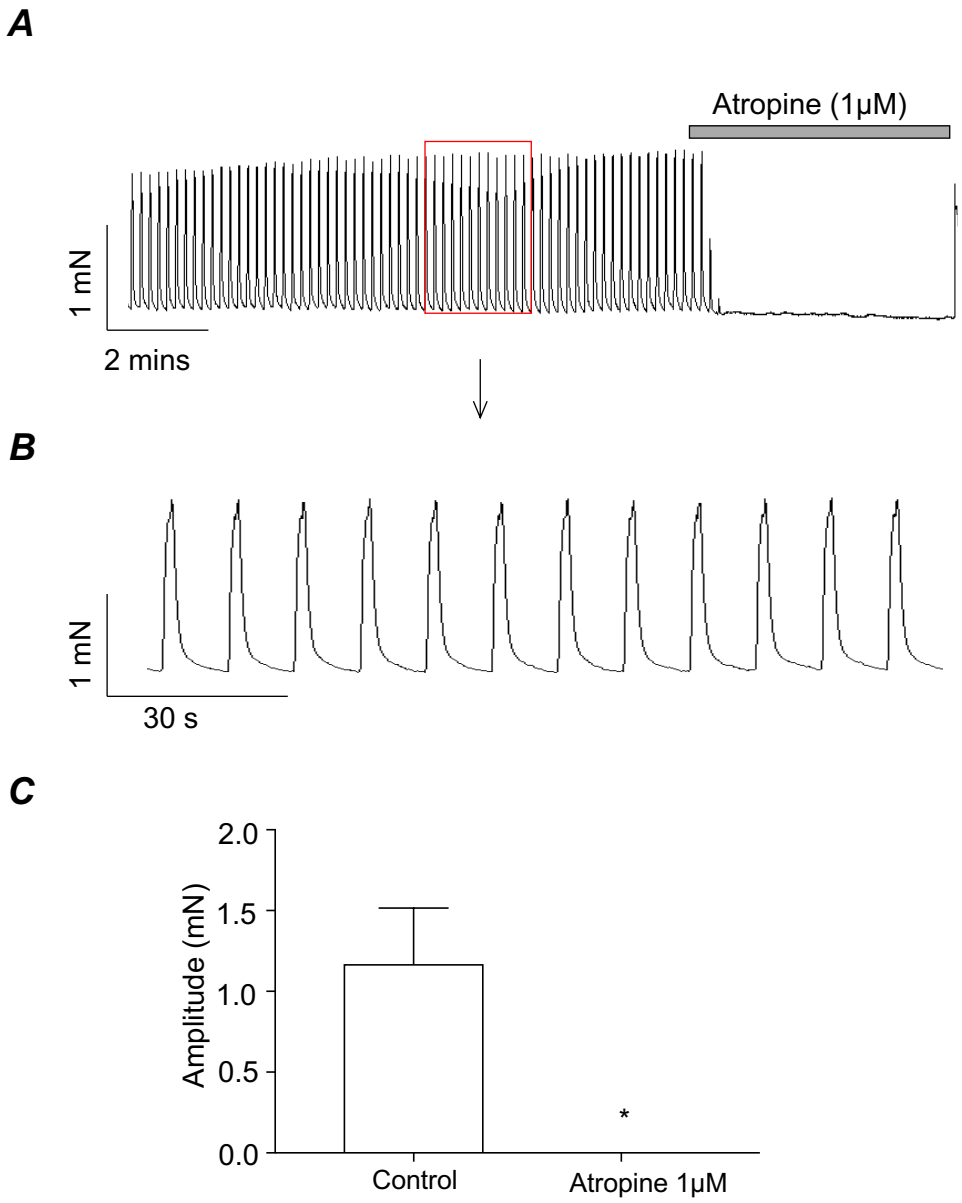

Figure 3.6. ***Atropine abolished EFS-evoked contractions of mouse bronchial rings.*** (**A**) Representative isometric tension recording showing the effect of the muscarinic antagonist, atropine (1μM) on EFS-evoked contractions (2 Hz) of mouse bronchial rings. (**B**) shows the section of recording highlighted within the red box in panel A on an expanded timescale. (**C**) Summary bar chart plotting the mean amplitude of contraction in control conditions and in atropine (n=6, N=6, *p<0.05, paired t-test).

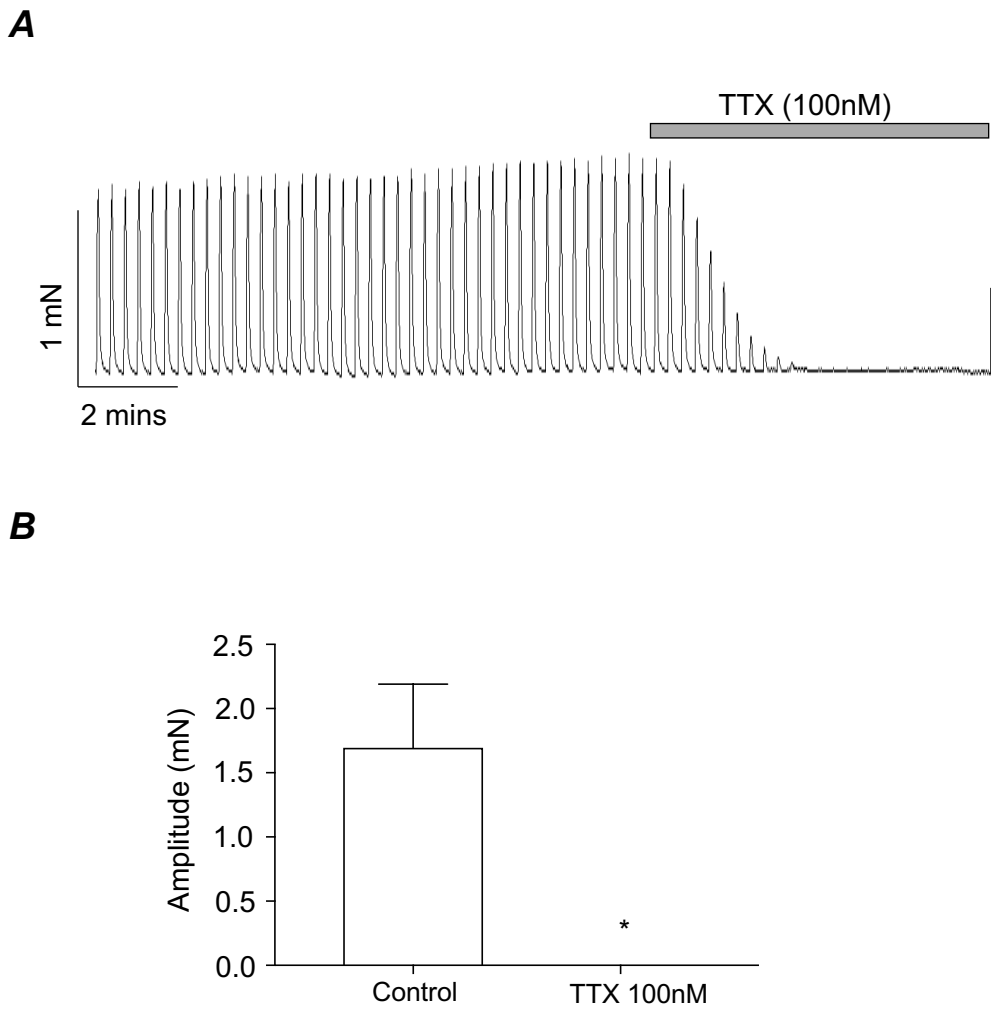

Figure 3.7. ***TTX abolished EFS-evoked contractions of mouse bronchial rings.*** (**A**) Representative isometric tension recording showing the effect of the neurotoxin, TTX (100nM) on EFS-evoked cholinergic contractions (2Hz). (**C**) Summary bar chart plotting the mean amplitude of contraction before and after the addition of TTX (n=7, N=6, *p<0.05, paired t-test).

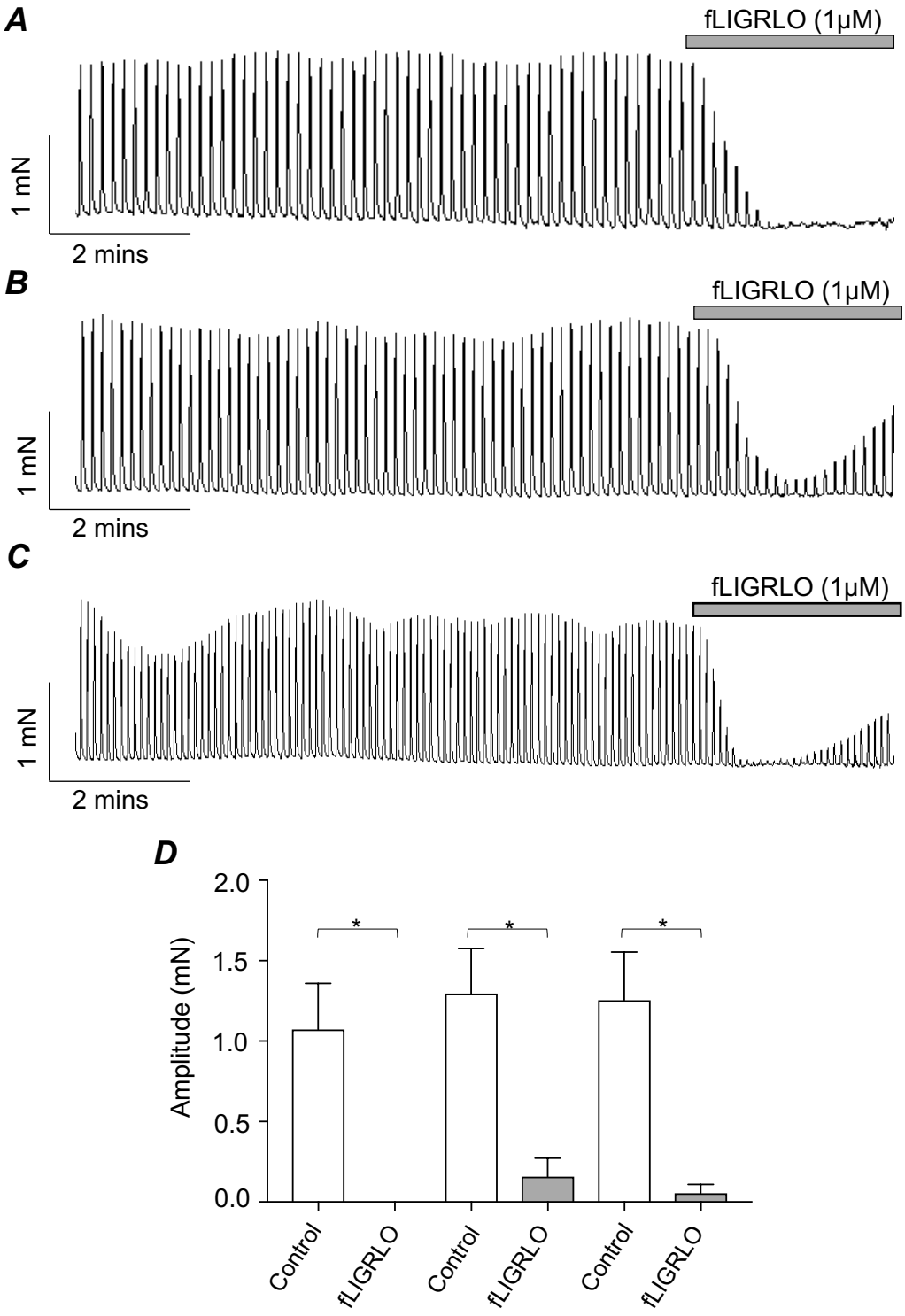

Figure 3.8. ***Effect of consecutive applications of fLIGRLO on nerve-stimulated contractions of mouse bronchial rings.*** (**A, B** & **C**) Representative tension recordings exhibiting the effect of consecutive additions of fLIGRLO (1μM) on EFS-evoked contractions (2Hz). (**D**) Summary bar charts showing the mean amplitude of contraction induced by three consecutive additions of fLIGRLO compared with control (n=6, N=5, *p<0.05, ANOVA).

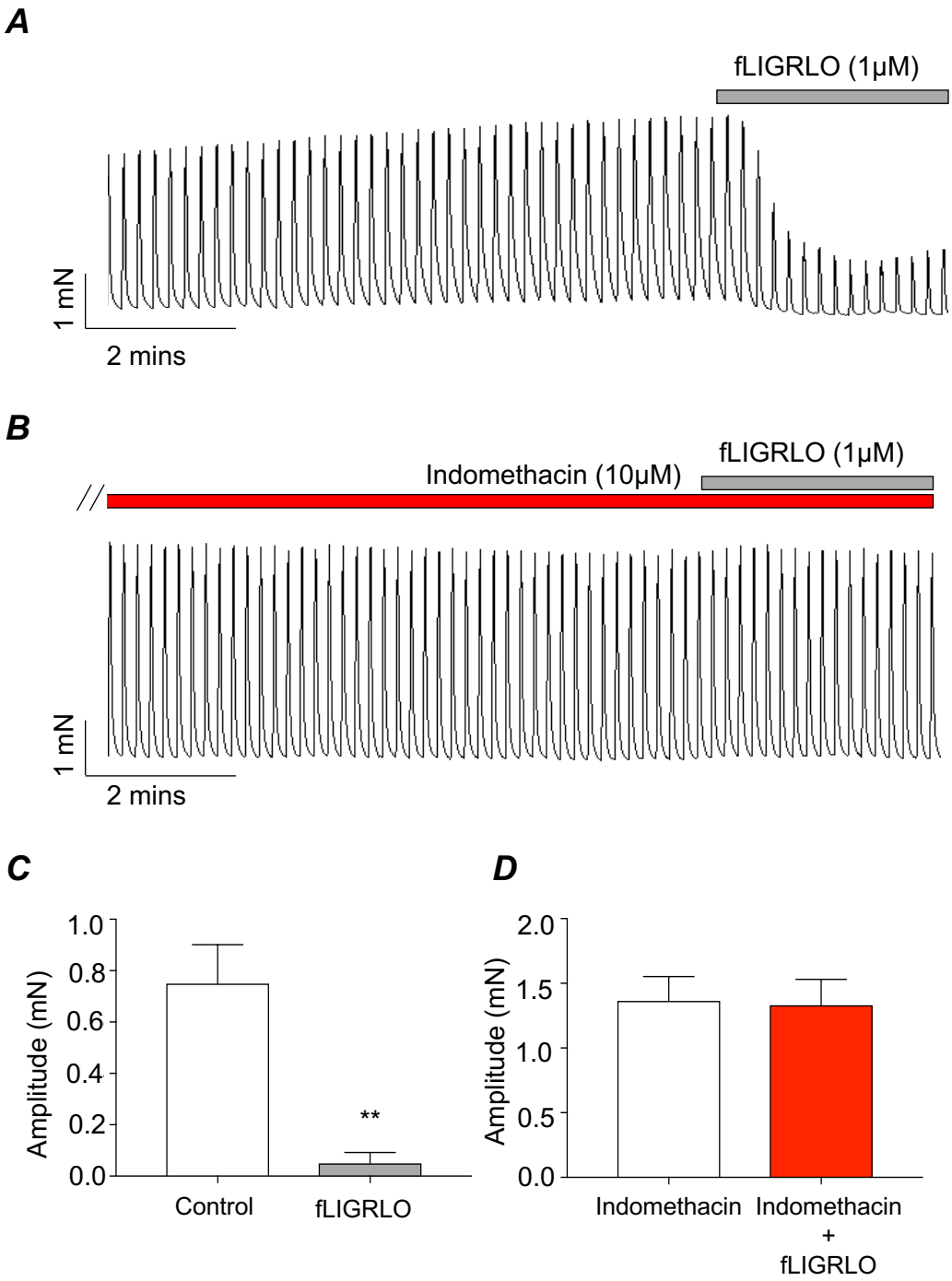

Figure 3.9. ***Effect of the COX 1/2 inhibitor, indomethacin on fLIGRLO-induced relaxations on nerve-stimulated contractions of mouse bronchial rings.*** (**A** & **B**) Representative tension recordings exhibiting the effect of fLIGRLO (1μM) on EFS-evoked contractions (2Hz) in the absence (**A**) and presence of indomethacin (10μM, **B**). (**C & D**) Summary bar charts showing mean amplitude in control conditions (**C**, n=7, N=4, **p<0.01, paired t-test) and following incubation with 10μM indomethacin (**D**).

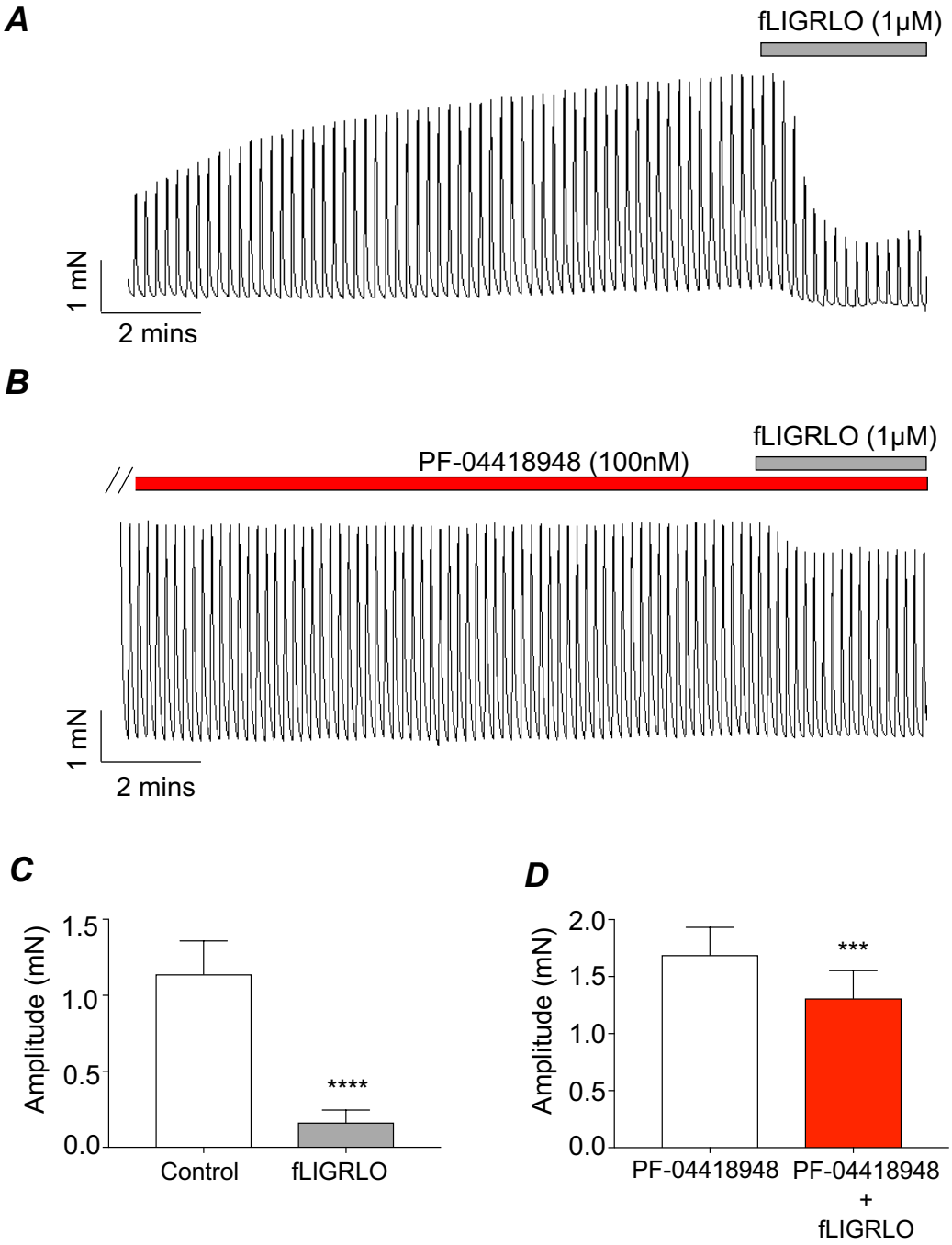

Figure 3.10. ***Effect of the EP2R antagonist, PF-04418948 on fLIGRLO-induced inhibition of 2 Hz EFS-evoked contractions of mouse bronchi.*** (**A** & **B**) Representative tension recordings showing the effects of fLIGRLO (1μM) before (**A**) and during the presence of PF-04418948 (100nM, **B**). Summary bar charts (n=15, N=14) showing the effect of fLIGRLO (1μM) on mean amplitude in control (**C**) and in the presence of PF-04418948 (**D**, 100nM, ***p<0.001, ****p<0.0001, paired t-test).

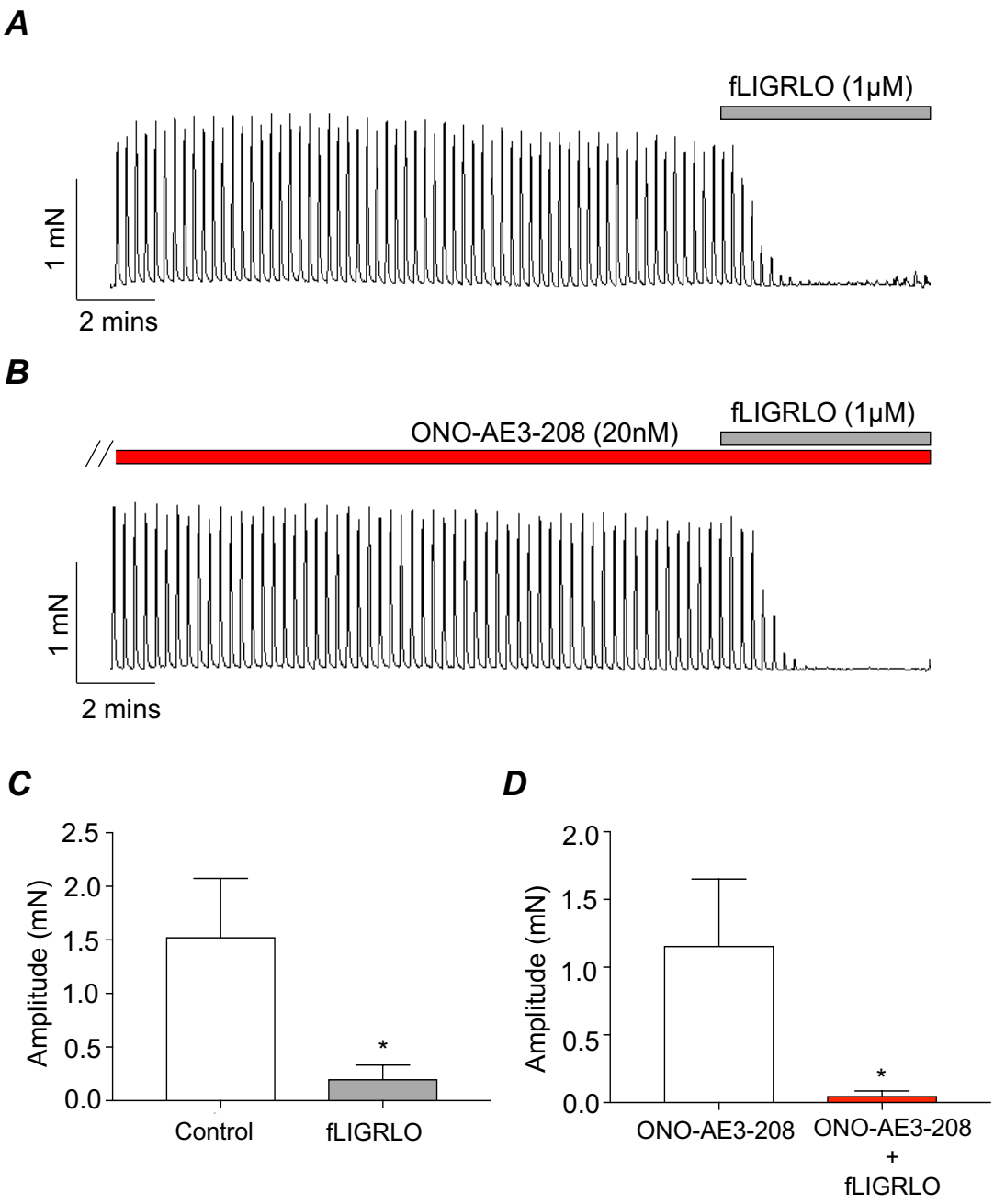

Figure 3.11. ***Effect of the EP4 receptor antagonist, ONO-AE3-208 on fLIGRLO-induced relaxations on 2Hz EFS-evoked contractions of mouse bronchial rings.*** (**A**-**B**) Representative tension recordings showing the effects of fLIGRLO (1μM) before (**A**) and in the presence of ONO-AE3-208 (20nM, **B**). (**C** & **D**) Summary bar charts for fLIGRLO under control conditions (**C**) and in the presence of ONO-AE3-208 (**D**) (n=6, N=6, *p<0.05, paired t test).

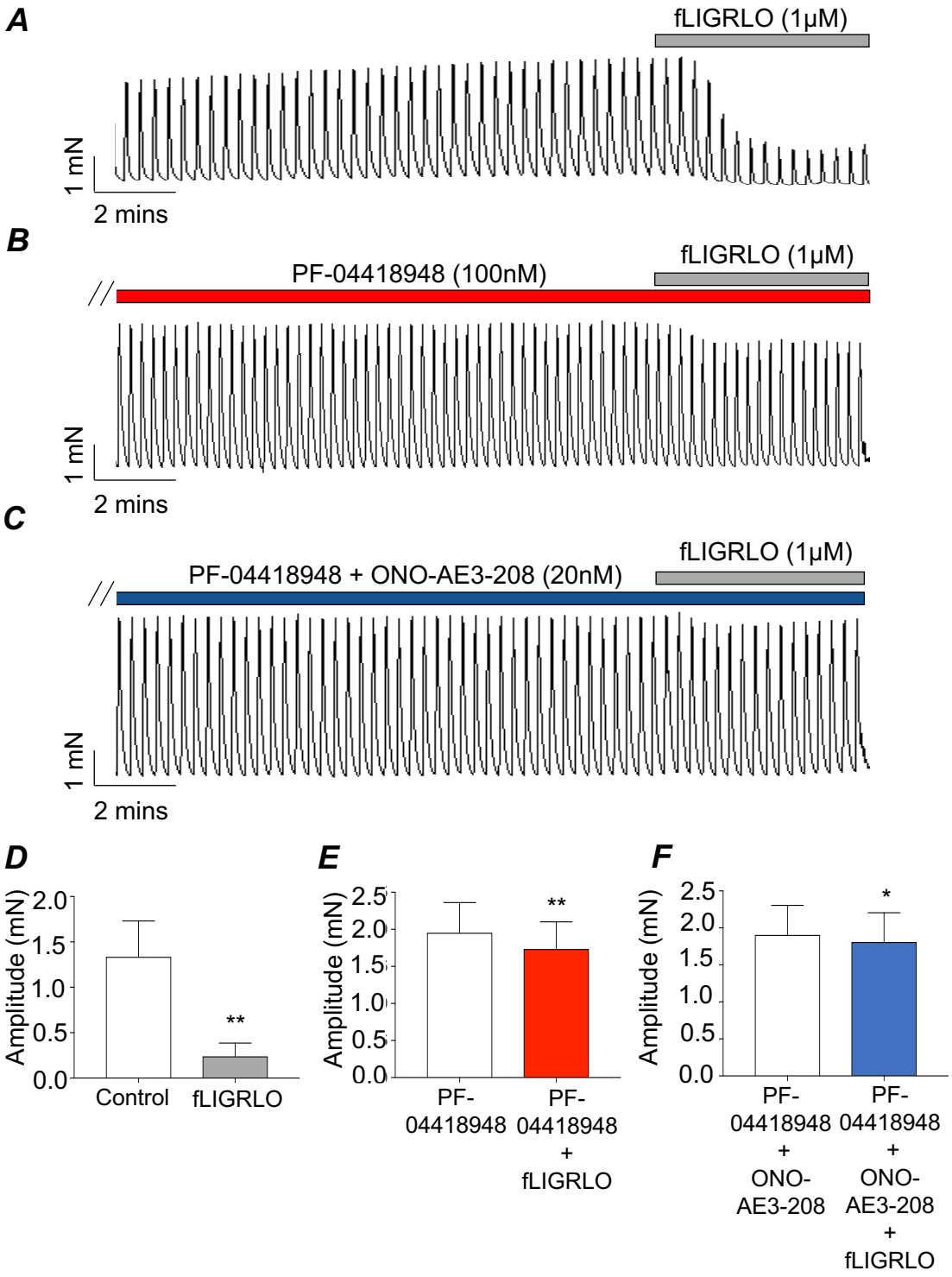

Figure 3.12. ***Effect of the EP2R antagonist, PF-04418948 plus the EP4R antagonist, ONO-AE3-208 on fLIGRLO-induced inhibition of EFS-evoked contractions of mouse bronchi.*** (**A**-**C**) Representative tension recordings showing the effects of fLIGRLO (1μM) before (**A**), during the presence of PF-04418948 (100nM, **B**) and PF-04418948 plus ONO-AE3-208 (20nM, **C**). Summary bar charts (n=8, N=8) showing the effect of fLIGRLO on mean amplitude in control (**D**), in the presence of PF-04418948 (**E**) and PF-04418948 plus ONO-AE3-208 (**F,** *p<0.05, **p<0.01, paired t-test).

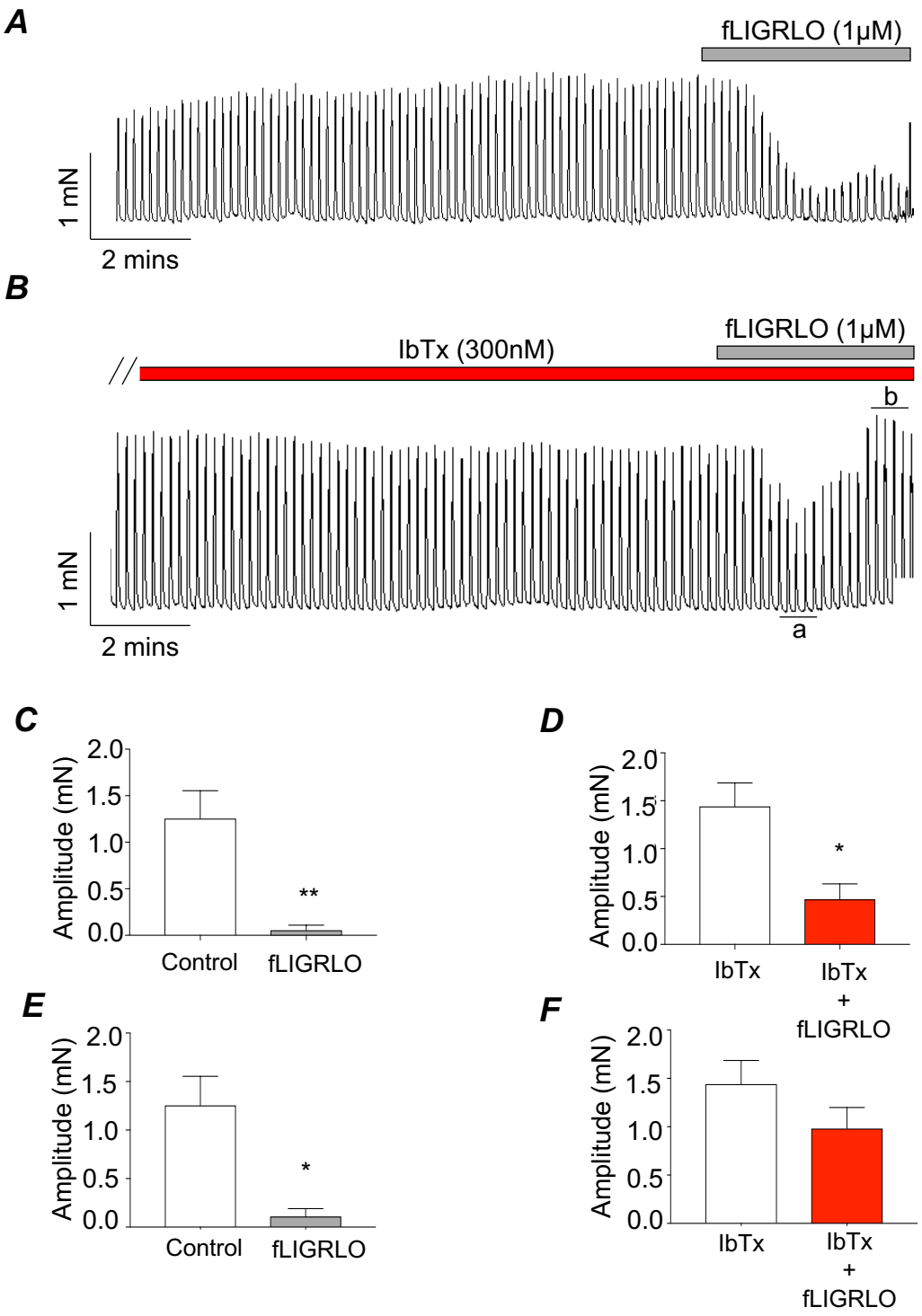

Figure 3.13. ***Effect of the BK channel blocker, iberiotoxin on fLIGRLO-induced inhibition of nerve-stimulated contractions of mouse bronchial rings.*** (**A** & **B**) Representative tension recordings showing the effect of 1μM fLIGRLO on EFS-evoked contractions in the absence (**A**), presence of IbTx (300nM, **B**). (**C** & **D**) Summary bar charts showing the maximum relaxation (**a**) elicited by fLIGRLO (1μM) in control (**C**) and in the presence of IbTx (**D**). (**E** & **F**) Summary bar charts showing the effect of fLIGRLO (1μM) on the mean amplitude during the final 5 pulses (**b**) in control (**E**) and in the presence of IbTx (**F**) (n=6, N=5, *p<0.05, **p<0.01, paired t-test).

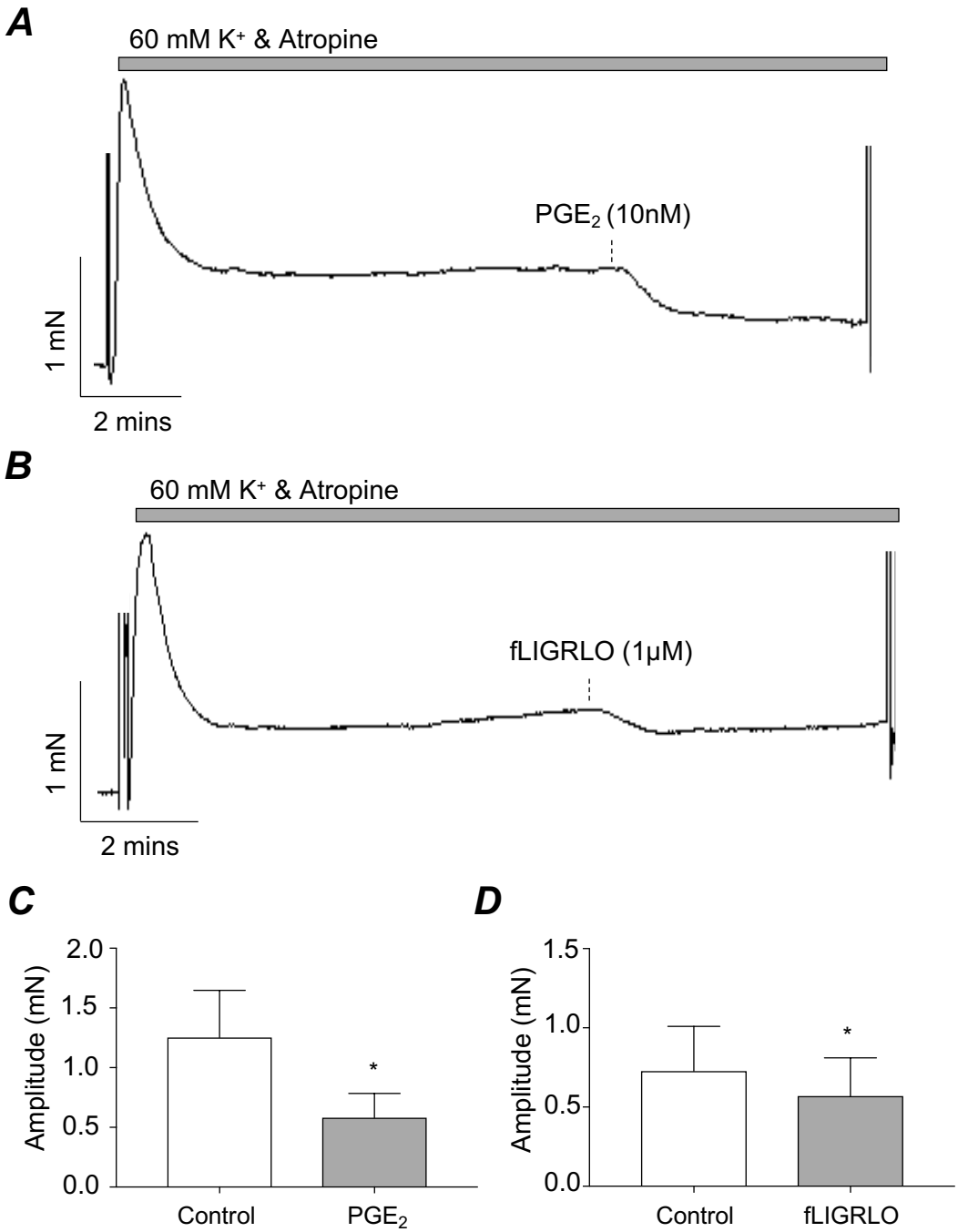

Figure 3.14. ***Effect of PGE_2 and the PAR2 agonist, fLIGRLO on high K^+-evoked contractions of mouse bronchial rings.*** (**A** & **B**) Representative tension recordings showing effects of PGE_2 (**A**) and fLIGRLO (**B**) on contractions induced by 60mM K^+. (**C** & **D**) Summary bar charts showing the effect of PGE_2 (**C**, n=7, N=4) and fLIGRLO (**D**, n=6, N=4) on high K^+-induced contractions (*$p<0.05$, paired t-test).

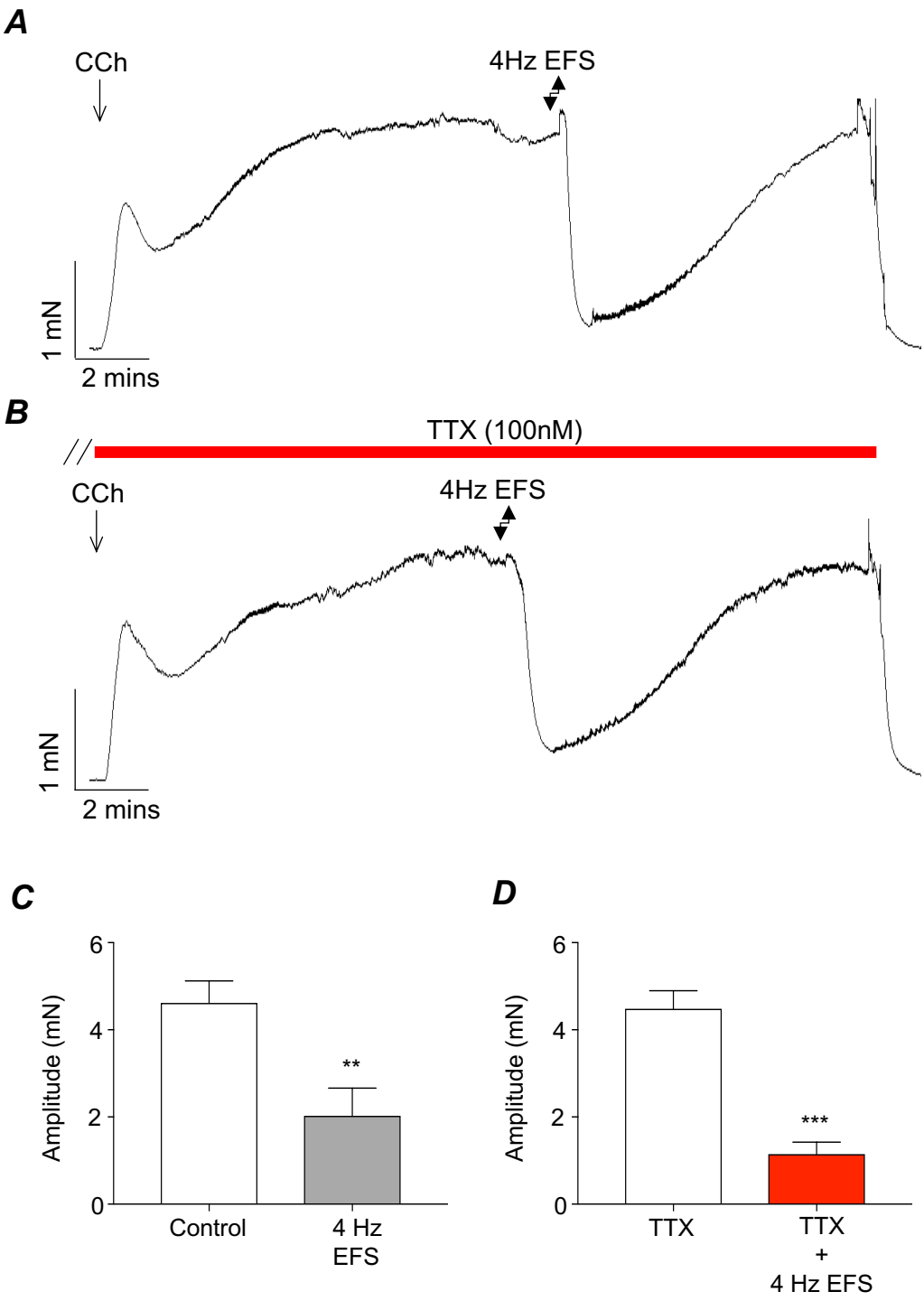

Figure 3.15. ***Effect of the neurotoxin, TTX on (4Hz) EFS-induced relaxations of mouse bronchial rings, pre-contracted with CCh.*** (**A** & **B**) Representative tension recordings showing the effects of 4Hz EFS-stimulated relaxations before (**A**) and in the presence of TTX (100nM), **B**). (**C** & **D**) Summary bar charts showing amplitude of CCh-evoked contractions before and during 4Hz EFS, in the absence of TTX (**C**) and in the presence of TTX (**D**) (n=6, N=6, **p<0.01, ***p<0.001, paired t-test).

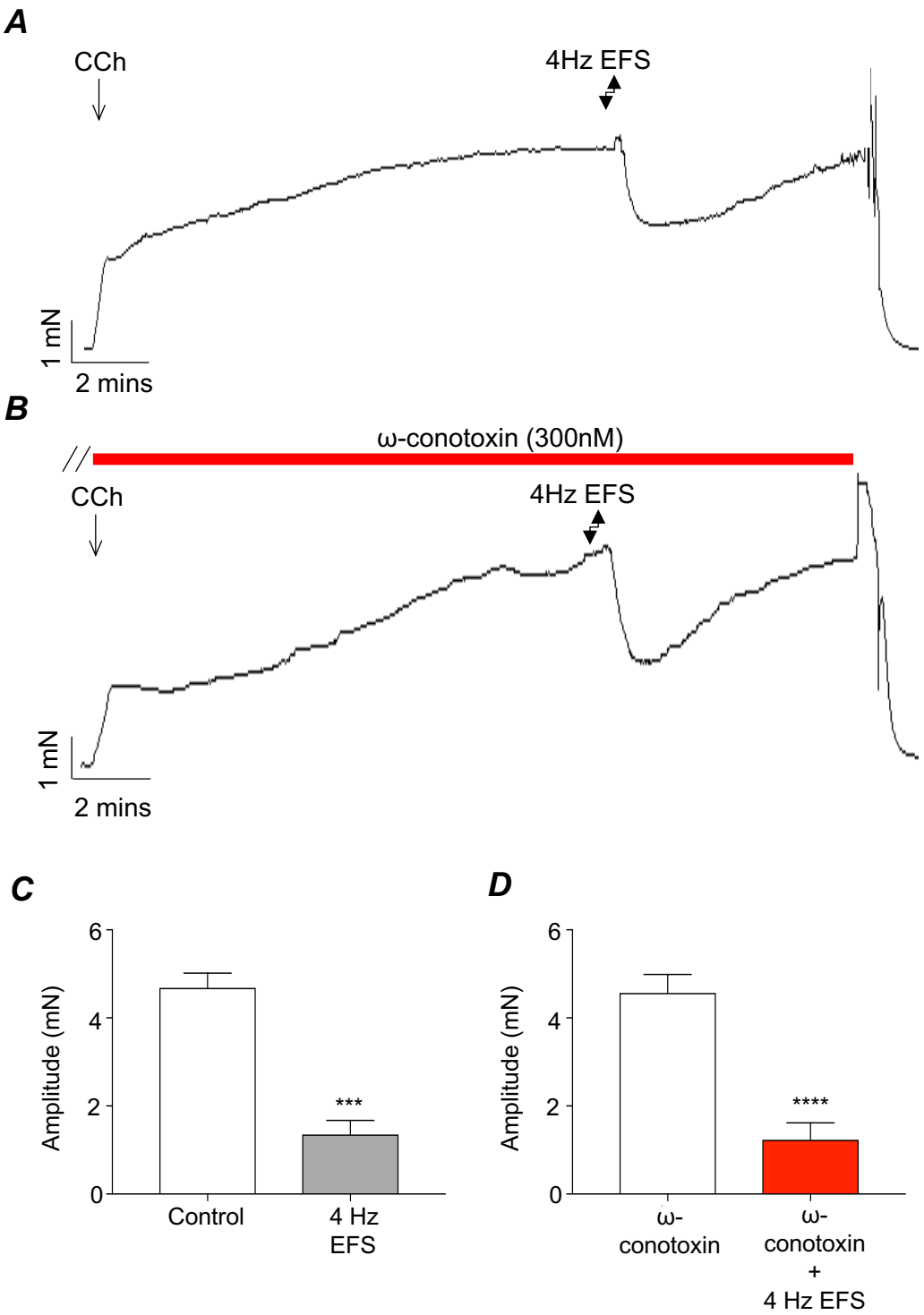

Figure 3.16. ***Effect of the N-type calcium channel blocker, ω-conotoxin on EFS-induced relaxations of mouse bronchial rings, pre-contracted with CCh.*** (**A** & **B**) Representative tension recordings showing the effects of 4Hz EFS before (**A**) and in the presence of ω-conotoxin (300nM, **B**). (**C** & **D**) Summary bar charts showing the effect of 4Hz EFS on CCh-evoked contraction amplitude in control (**C**) and in the presence of ω-conotoxin (**D**) (n=6, N=6, ***p<0.001, ****p<0.0001, paired t-test).

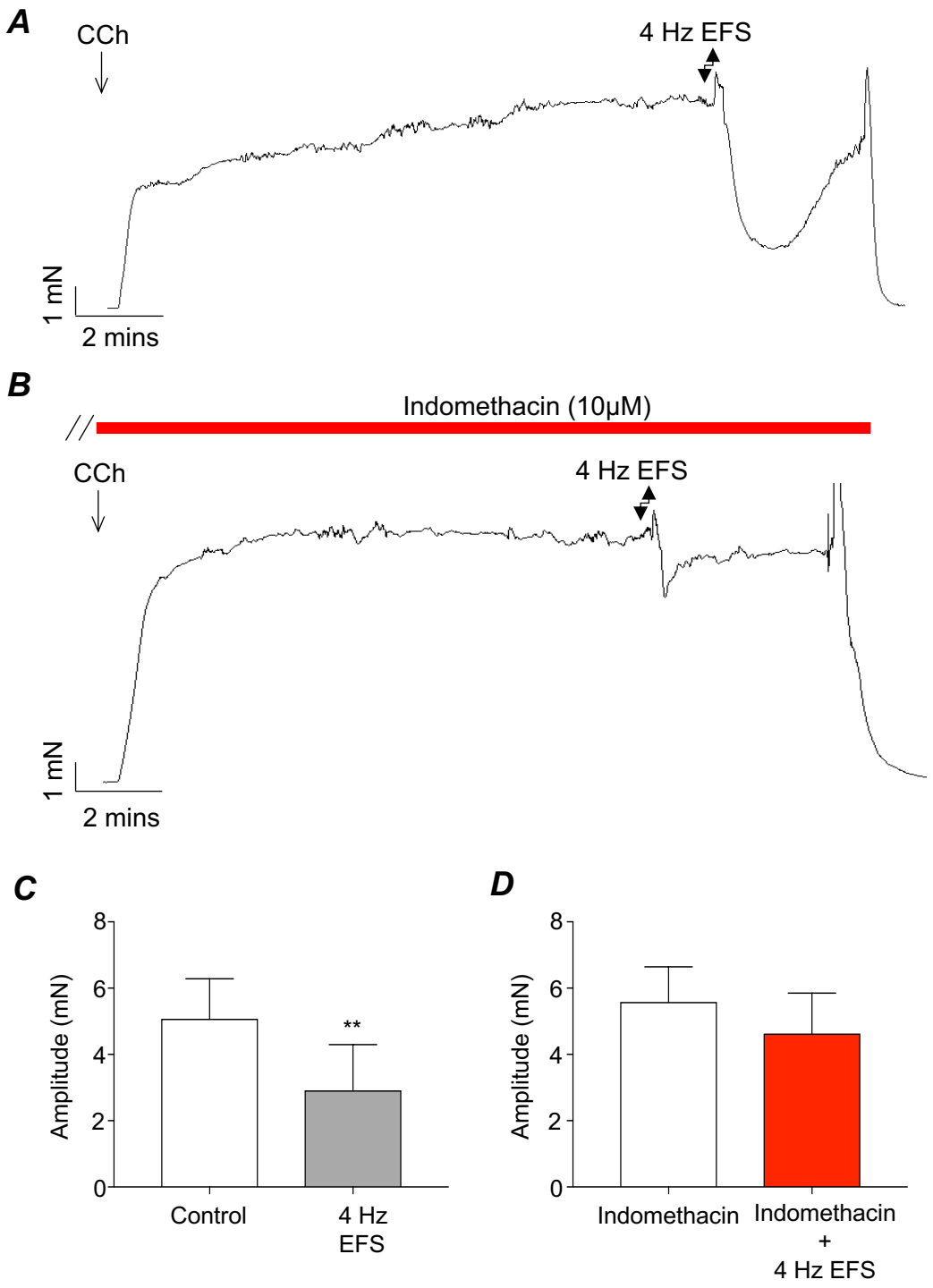

Figure 3.17. ***Effect of the COX 1/2 inhibitor, indomethacin on (4Hz) EFS-induced relaxations of mouse bronchial rings, pre-contracted with CCh.*** (**A** & **B**) Representative tension recordings showing the effects of 4Hz EFS-stimulated relaxations before (**A**) and in the presence of indomethacin(10μM), **B**). (**C** & **D**) Summary bar charts showing amplitude of CCh-evoked contractions before and during 4Hz EFS, in the absence of indomethacin (**C**, n=7, N=5, **p<0.01, paired t-test) and in the presence of indomethacin (**D**).

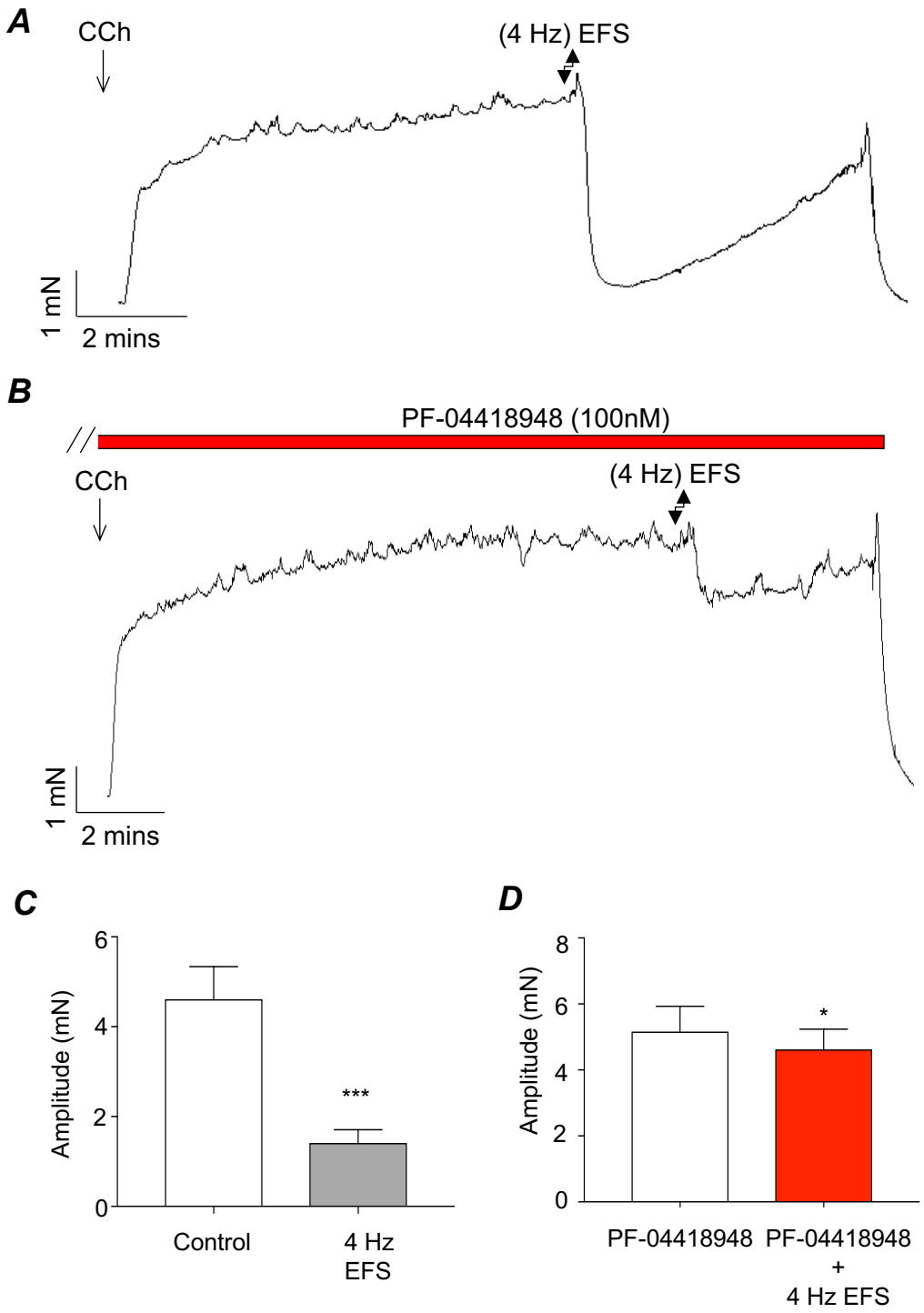

Figure 3.18. ***Effect of the EP2R antagonist, PF-04418948 on EFS-induced relaxations of mouse bronchial rings, pre-contracted with CCh.*** (**A** & **B**) Representative tension recordings showing the effects of 4 Hz EFS before (**A**) and in the presence of PF-04418948 (100nM, **B**). (**C** & **D**) Summary bar charts showing the effect of 4Hz EFS on CCh-evoked contraction amplitude in control (**C**) and in the presence of PF-04418948 (**D**) (n=10, N=5, *p<0.05, ***p<0.001, paired t-test).

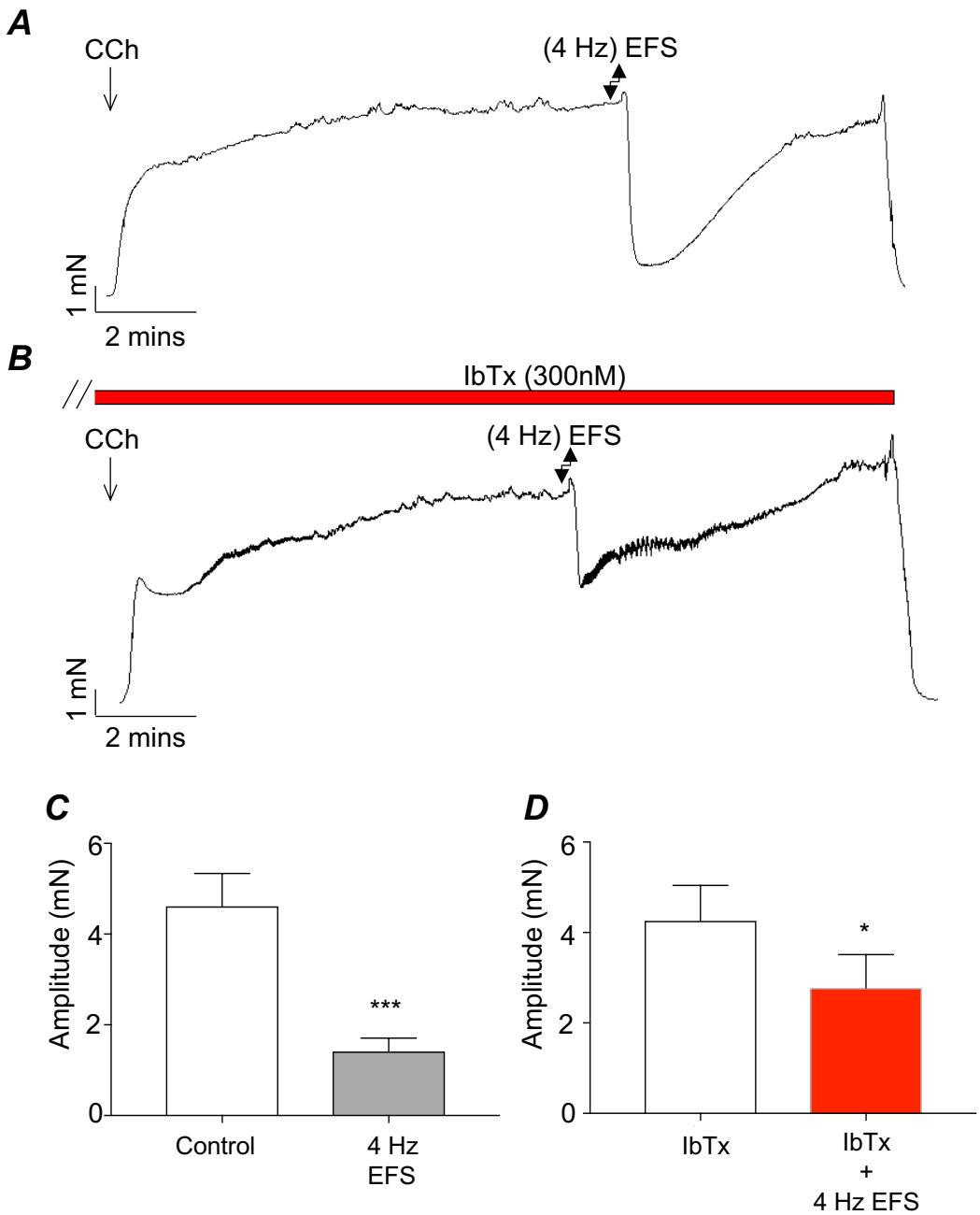

Figure 3.19. ***Effect of the BK channel inhibitor, IbTx on (4 Hz) EFS-induced relaxations on CCh-evoked contractions of mouse bronchial rings.*** (**A** & **B**) Representative tension recordings showing the effects of 4 Hz EFS before (**A**) and in the presence of IbTx (300nM, **B**). (**C** & **D**) Summary bar charts showing amplitude of CCh-evoked contractions before and during 4Hz EFS, in the absence of IbTx (**C**) and in the presence of IbTx (**D**) (n=7, N=5, ***p<0.001, *p<0.05, paired t-test).

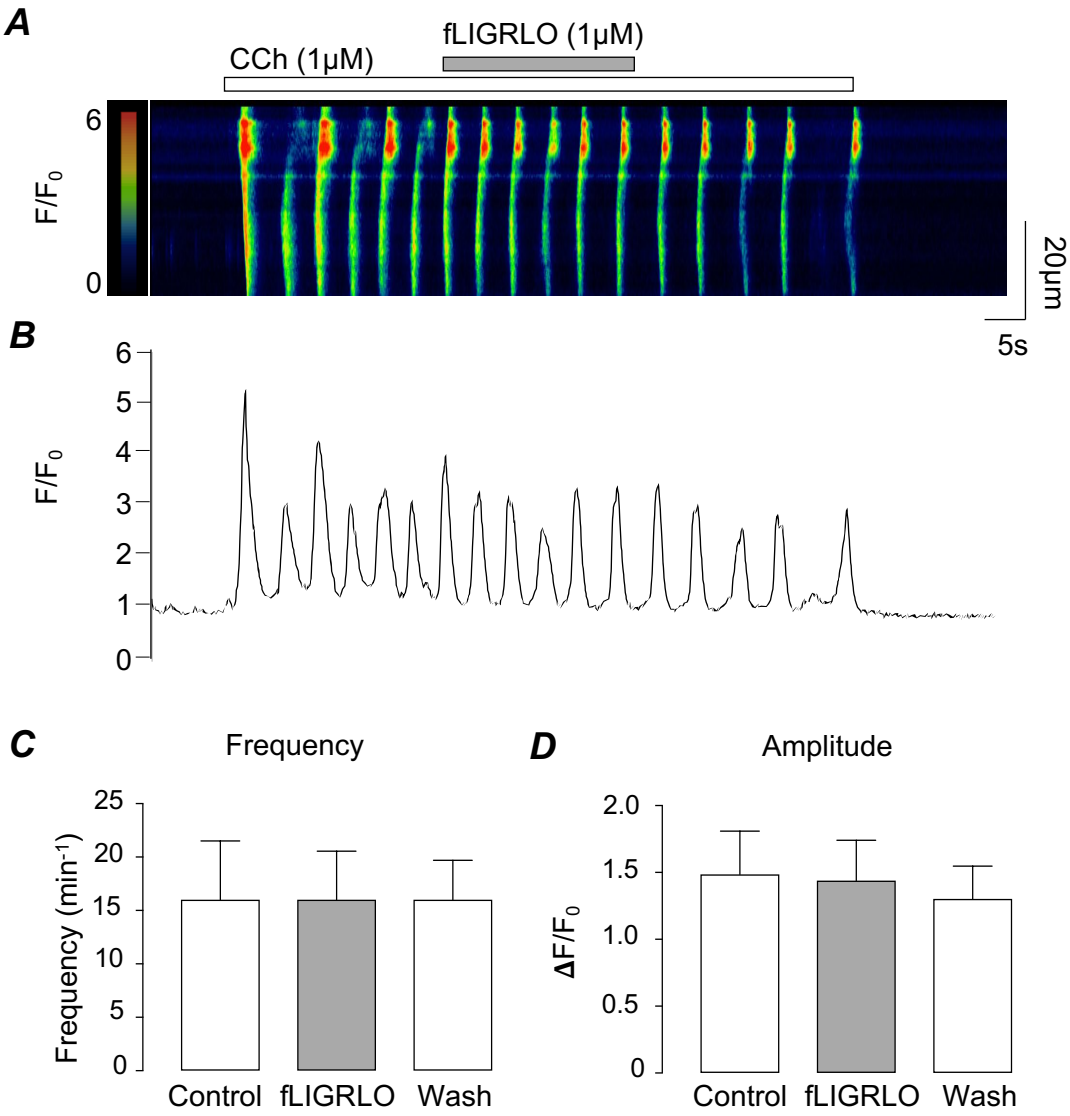

Figure 3.20. ***The PAR2 agonist, fLIGRLO did not affect CCh-induced calcium oscillations in freshly isolated ASMCs.*** (**A**) Representative pseudolinescan image showing the effects of the PAR2 agonist, fLIGRLO (1μM) on CCh (1μM)-induced calcium oscillations in a freshly isolated ASMC, and (**B**) the correlating intensity profile plot. Summary bar charts from 6 similar experiments showing effects on mean calcium oscillation frequency (**C**) and amplitude (**D**) in the presence of fLIGRLO (n=6, N=5, paired t-test, p>0.05).

3.3 Discussion

The key findings of this chapter were that: 1) activation of PAR2 receptors by, fLIGRLO inhibited both EFS and CCh-evoked contractions of mouse ASM; 2) fLIGRLO-induced inhibition of EFS and CCh-induced contractions were abolished by the COX 1/2 blocker, indomethacin and a selective EP2R antagonist, PF-04418948; 3) The EP4R antagonist, ONO-AE3-208 did not reduce the effect of fLIGRLO on CCh or EFS responses, but produced a small inhibitory effect when applied in the presence of PF-04418948; 4) fLIGRLO-induced inhibition of CCh and EFS responses were reduced in the presence of the BK channel blocker, IbTx; 5) EFS of ASM preparations pre-contracted with CCh, induced relaxations that were inhibited by indomethacin, PF-04418948 and IbTx; 6) fLIGRLO had no effect on CCh-evoked calcium oscillations in freshly isolated mouse ASMCs.

PAR2 receptors are expressed throughout the lung and can couple to a number of different G protein-coupled receptors leading to contraction or relaxation (Geppetti and Trevisani 2003; Roche *et al*. 2003: Miotto *et al*. 2002; D'Andrea *et al*. 2000; Howells *et al*. 1997). The present study shows that application of the PAR2 agonist, fLIGRLO significantly reduced the amplitude of CCh-evoked contractions of mouse bronchial rings and that these effects were abolished by the COX 1/2 blocker, indomethacin. Lan *et al.* (2001) reported similar effects using an alternative PAR2 agonist, SLIGRL-NH_2, on isolated mouse trachea. As COX enzymes are essential for prostanoid synthesis, these data suggest that PAR2 mediates its effects through the production of endogenous prostanoids. Lan and colleagues attributed these inhibitory effects to the endogenous release of PGE_2 as they found that incremental addition of SLIGRL-NH_2 induced concentration-dependent increases in PGE_2 in the organ bath using an enzyme immunoassay.

PGE_2 mediates its biological effects through activation of four distinct prostanoid E receptors (EP1-4). Previous studies reported that activation of EP2&4Rs were responsible for the relaxant effects of PGE_2 on ASM and specifically EP2Rs on mouse ASM. This was confirmed in the current study as the inhibitory effects of fLIGRLO on CCh-induced contractions were abolished by the EP2R antagonist, PF-04418948. This would suggest that the inhibitory effects

of endogenous PGE_2 are primarily mediated via activation of EP2Rs in mouse ASM. PAR2 activation inhibited EFS responses to a greater degree than those reduced by CCh. Therefore, it is possible that these effects may be brought about by prejunctional effects of PGE_2. The EP4R antagonist ONO-AE3-208 had little effect on either PAR2 induced inhibition of EFS or CCh-evoked contractions. However, a small (10%) reduction was observed on EFS responses when applied with PF-04418948. Therefore, it is possible that these effects could be mediated by activation of EP4Rs on cholinergic nerves; pre-junctional effects of PGE_2 on cholinergic nerves has been described previously by Belvisi *et al.* (1996) in guinea pig trachea. However, it is important not to overstate this effect as responses to fLIGRLO may also have desensitised over this time period as seen in *Figure 3.8*. PAR2 desensitisation has been observed in a number of studies including Bohm *et al*. (1996) in intestinal epithelial cells and Cocks *et al.* (1999) in mouse, rat, guinea pig and human airways.

Our study indicates that the inhibitory effects of PAR2 activation are predominately mediated via release of PGE_2 and activation of EP2Rs, however the downstream pathway responsible for this effect remains unclear. Several studies have shown that activation of BK channels induces relaxation of ASM (Bradley *et al.* 2018; Evseev *et al.* 2013; Kume *et al.* 1992) and Zhu *et al.* (2002) demonstrated that PGE_2 stimulated BK channels and dilatated human coronary artery myocytes. However, Moss *et al.* (2015) found that PAR2 activation in rat jugular ganglia inhibited rather than activated BK channels on bronchopulmonary sensory neurons, contributing to airway hyperresponsiveness and inflammation. In the present study we found that PAR2 responses were reduced by the BK channel blocker, IbTx and that IbTx reduced both the maximal inhibitory effect of fLIGRLO and its duration of action. These effects suggest that hyperpolarisation of the membrane could be a contributing factor in PGE_2-mediated bronchodilation, however direct measurements of membrane potential would be required to confirm this. Both PGE_2 and fLIGRLO reduced the amplitude of high K^+-induced contractions, which are known to be reliant on calcium influx via L-type calcium channels. Under these conditions E_k would be expected to be ~-20mV, therefore opening of BK channels would not be expected to influence these responses. This suggests that PGE_2 can inhibit ASM contraction by other mechanisms, possibly by inhibition of L-type calcium channels as is the case in

rat melantroph cells (Tanaka *et al.* 1998) or inhibition of RhoA, as occurs in human ASM in response to prostacyclin (PGI_2, Zieba *et al.* 2011).

Another finding described in this chapter was the ability of 4Hz EFS to elicit inhibitory effects on CCh-evoked contractions. EFS manipulates the ionic extracellular environment and therefore modulates the transmembrane potential of cell types which express voltage-dependent channels including neurons (Stern *et al.* 2017; Cameron *et al.* 2013; Jackson *et al.* 2002), endothelial cells (Zhao *et al.* 2020), epithelial cells (Cohen *et al.* 2014) and smooth muscle cells (Ding *et al.* 2009; Jackson *et al.* 2002). It is believed that a stimulus with a pulse width of 0.3ms specifically activates nerves, as contractile responses mediated with this pulse width are abolished by TTX and ω-conotoxin (Smyth *et al.* 2004). However, 4Hz EFS-evoked relaxations with a pulse with of 0.3ms in the current study were not affected by the application of TTX or ω-conotoxin, suggesting that these responses were not attributable to nerve stimulation.

4Hz EFS-evoked relaxations were reduced by COX 1/2 blockade, EP2 receptor antagonism and BK channel inhibition, indicative of a role for endogenously released PGE_2 in this response. PGE_2 is synthesised by a number of cell types in the airway including, the epithelia and ASMCs (Delamere *et al.* 1994; Goldie *et al.* 1990). However, direct activation of ASMCs to release PGE_2 following EFS stimulation can be ruled out due to the short pulse width utilised (0.3ms) in the current study. Jackson *et al.* (2002) reported that a 5Hz EFS with a pulse width of 0.6ms did not initiate calcium mobilisation or tissue movement in rabbit pulmonary artery tissue but a pulse width of 5ms increased calcium concentration and movement in the same tissue, suggesting that a pulse width of <0.6ms is not sufficient to activate SMCs. Ullman *et al.* (1990) reported an epithelium-dependent gradual reduction in amplitude of contraction of ferret trachea induced by 12Hz EFS over time and that this inhibition correlated to increased PGE_2 concentration in the organ bath solution. This effect was also diminished by addition of indomethacin and was unaffected by TTX (Ullman *et al.* 1991) in a similar manner to the current study. Therefore, it is possible in the current study that 4Hz EFS may also stimulate airway epithelia to release endogenous PGE_2, however this idea would require further investigation.

PGE_2 can be released from various cells in the airways, including ASMCs (Chambers *et al.* 2003; Delamere *et al.* 1994; Farmer *et al.* 1990) but Ricciardolo

et al. (2000) and Cocks *et al.* (1999) found that removal of the epithelium abolished PAR2-induced relaxations of guinea pig bronchi and mouse bronchi. This suggests that inhibitory effects of PAR2 on ASM are most likely brought about by release of PGE_2 from epithelia, and not from SMCs themselves. Attempts to denude the epithelium in the current study were unsuccessful due to the small diameter of the primary bronchi sections utilised. Multiple attempts with a variety of techniques resulted in nonviable tissue. However, the data in the present study shows that PAR2-induced relaxations of mouse ASM were prevented by the COX 1/2 blocker, indomethacin and the EP2R antagonist PF-04418948 and were not associated with an effect on calcium oscillations in ASMCs. These data suggest that the effects of PAR2 activation on ASM contraction were likely mediated by release of PGE_2. While this would require direct measurement of PGE_2 to confirm this is the case, there is widespread agreement among several studies (Nichols *et al.* 2012; Chambers *et al.* 2003; Lan *et al.* 2001) which incorporated enzyme immunoassays, confirming that PAR2 activation results in increased PGE_2 levels. Therefore, these assays were not considered necessary in the current experiments.

In summary, this chapter highlights that inhibition of ASM contraction induced by PAR2 activation is primarily mediated by endogenously released PGE_2 in mouse ASM. Application of the COX 1/2 blocker, indomethacin and the selective EP2R antagonist, PF-04418948 abolished fLIGRLO-induced relaxations of CCh-evoked contractions. PAR2-induced relaxations were also reduced by the BK channel blocker, IbTx, suggesting a potential role of BK channel activation in the inhibitory effect of PAR2 on mouse ASM. fLIGRLO did not directly affect CCh-evoked calcium oscillations on freshly isolated ASMCs suggesting that the production of PGE_2 is not attributable to direct activation of PAR2 on the smooth muscle. 4Hz EFS also reduced CCh-evoked contractions of mouse ASM, partially through the release of endogenously released PGE_2. Taken together, these data strongly suggest an inhibitory role for endogenously released PGE_2 in mouse ASM.

4. Effect of PGE_2 on cholinergic contractions of mouse ASM.

4.1 Introduction

Findings from Chapter 3 suggest that endogenously released PGE_2 induces potent bronchodilator effects on mouse ASM. PGE_2-induced relaxations of ASM can be mediated via activation of EP2 and/or EP4Rs (Buckley *et al*. 2011; Mori *et al*. 2011; Hartney *et al*. 2006; Tilley *et al*. 2003). Both EP2 and EP4Rs are G_s-coupled receptors which mediate their effect through upregulation of AC, increased cAMP levels and subsequent activation of PKA (Aso *et al*. 2013; Sastre and del Pozo 2012; Vancheri *et al*. 2004). Previous studies suggested that EP2Rs mediate PGE_2-induced bronchodilation of mouse and guinea pig ASM, whereas EP4Rs are responsible in human and rat ASM (Benyahia *et al*. 2012; Buckley *et al*. 2011; Hartney *et al*. 2006; Sheller *et al*. 2000). However, many of these studies were performed on tracheal smooth muscle and not on the smaller airways which are the major site of constriction in diseases such as COPD (Yanai *et al.* 1992). In addition, they utilised exogenous agonists to evoke contraction rather than the more physiologically relevant neurogenic contracture. Herrerias *et al*. (2009) reported the expression of all four EP receptors in mouse lung preparations, although precise quantitative EPR expression in isolated bronchial tissue has not yet been fully elucidated.

The objective of this chapter was to determine the EPRs responsible for PGE_2-induced relaxations of mouse bronchial rings.

4.2 Results

4.2.1 Effect of PGE_2 on EFS and CCh-induced contractions of mouse bronchial rings

Experiments were performed to determine the effect of PGE_2 on contractions of mouse ASM induced by EFS, at varying frequencies (0.5 - 8Hz). EFS-induced contractions are mediated by release of ACh from parasympathetic nerves (Spicuzza *et al.* 1998). All experiments in this chapter were performed in the presence of COX-1 and 2 inhibitor, indomethacin (10μM) to prevent release of endogenous prostaglandins. *Figure 4.1A* is a representative tension recording showing that, under control conditions, EFS of mouse bronchi yielded frequency-dependent contractions, that were sustained over the one-minute stimulation period. Application of 10nM PGE_2 significantly decreased contraction amplitude at all frequencies (*Figure 4.1B*). Subsequent application of 30nM PGE_2 (*Figure 4.1C*) further reduced the amplitude of the EFS responses. *Figure 4.1D* shows summary bar charts that plot mean contraction amplitude (measured area under the curve) in the absence and presence of 10 and 30nM PGE_2, respectively. PGE_2 (10nM) reduced the amplitude of responses induced by 0.5Hz EFS by 58% (75 $\pm$ 16 to 31 $\pm$ 7 mN.s, two-way ANOVA, $p<0.01$), while those evoked by 8Hz EFS were reduced by 40% from 212 $\pm$ 47 to 127 $\pm$ 27 mN.s (ANOVA, $p<0.01$, $p<0.0001$). This suggests that 10nM PGE_2 was slightly more effective at inhibiting contractions evoked at low-frequency EFS. 30nM PGE_2 caused a greater reduction in contraction amplitude. For example, contractions evoked by 0.5Hz EFS were reduced by 80% from 75 $\pm$ 16 to 18 $\pm$ 4 mN.s (ANOVA, $p<0.001$) and those induced by 8Hz EFS responses were reduced by 72% from 212 $\pm$ 47 to 59 $\pm$ 10 mN.s (ANOVA, $p<0.001$, $p<0.0001$, n=6, N=6).

This issue was investigated further by examining the effect of PGE_2 over a range of concentrations (10pM-10nM) on EFS responses. These experiments were performed using EFS at a single frequency (2Hz) for a duration of 1 second, repeated at 10 second intervals. *Figure 4.2A* is a representative trace showing that PGE_2 elicited concentration-dependent inhibition of 2Hz-evoked contractions. It is evident from these experiments that responses induced by this EFS protocol were more sensitive to PGE_2 than the sustained contractions

(duration one minute) observed in *Figure 4.1*. *Figure 4.2C* shows a summary concentration-effect curve for PGE_2 on EFS-induced contractions (n=21, N=18). The mean IC_{50} value for PGE_2 was 1.4nM (lower and upper 95% CI; 1.2-1.6nM).

To further examine the effect of PGE_2 on cholinergic responses in ASM, we examined its effect on contractions induced by the cholinergic agonist CCh. Cumulative addition of CCh (100nM-10μM) induced concentration-dependent increases in contraction amplitude, as illustrated in the representative tension recording in *Figure 4.3A*. The effect of 30nM PGE_2 on these responses is shown in *Figure 4.3B* and summary concentration-effect curves for CCh, before, and in the presence of PGE_2 (30nM) are shown in *Figure 4.3C* (n=6, N=5). These data show that contractions induced by 100nM CCh were abolished in the presence of 30nM PGE_2. The CCh concentration-effect curve was shifted to the right in the presence of PGE_2. The EC_{50} for CCh, under control conditions, was 105nM (95% CI; 16-197nM) Vs 1.5μM (95% CI; 0.79-2.6μM) during incubation with 30nM PGE_2.

PGE_2 mediates its biological effects through activation of four prostanoid E receptors, known as, EP1, EP2, EP3 and EP4 (Buckley *et al.* 2011). Activation of EP1 and EP3Rs stimulates airway inflammation and cough, whereas EP2 and EP4Rs promote bronchodilation (Lebender *et al.* 2018). Experiments were performed to determine if PGE_2 exerts its inhibitory effect on CCh-evoked contractions of mouse ASM via activation of EP2Rs, EP4Rs, or both. *Figures 4.4A&B* are representative tension recordings showing the effect of PGE_2 before (*Figure 4.4A*) and during the presence of the selective EP2R antagonist PF-04418948 (100nM, *Figure 4.4B*). It is clear from this experiment that much higher concentrations of PGE_2 were required to induce relaxation in the presence of PF-04418948 than in control. *Figure 4.4C* shows that PF-04418948 shifted the PGE_2 concentration effect curve to the right (IC_{50} 44nM, 95% CI; 40-50nM versus 3.5μM, 95% CI; 2.8-4.3μM, n=7, N=5).

We next investigated if EP4Rs were involved in the inhibitory effects of PGE_2 on mouse ASM. Cumulative addition of PGE_2-induced concentration-dependent relaxations, under control conditions (*Figure 4.5A*). Incubation with the EP4 selective antagonist ONO-AE3-208 (20nM, *Figure 4.5B*) had no discernable effect on PGE_2 induced relaxations. However, subsequent addition

of the EP2 antagonist PF-04418948 (100nM), in the continued presence of ONO-AE3-208, substantially inhibited the effects of PGE_2 (*Figure 4.5C*). The summary concentration-effect curves shown in *Figure 4.5D* (n=7, N=5), show that PGE_2-induced relaxations were not affected by ONO-AE3-208 (IC_{50} 33nM, 95% CI; 26-41nM in ONO-AE3-208 compared to 36nM 95% CI; 28 - 46nM in control). However, in the presence of both EP4 and EP2 antagonists the PGE_2 concentration-effect curve was shifted to the right (IC_{50} to 1.5μM, 95% CI;1.2-1.9μM). These data suggest that EP2, but not EP4Rs are involved in the inhibitory effects of PGE_2 on CCh-evoked contractions of mouse ASM.

We next examined the effect of the EP2 and EP4R antagonists on PGE_2-induced inhibition of EFS-evoked contractions. PGE_2 induced a concentration-dependent inhibition of EFS-evoked contractions in mouse ASM (*Figure 4.6A*). *Figure 4.6B* is a representative tension recording showing the effect of PGE_2 during the presence of the selective EP4R antagonist ONO-AE3-208 (20nM). ONO-AE3-208 did not affect PGE_2-induced inhibition of EFS responses. However, addition of PF-04418948 (100nM) in the continued presence of ONO-AE3-208, substantially inhibited the effects of PGE_2 (*Figure 4.6C*). Summary concentration-effect curves for PGE_2 on EFS responses are shown in *Figure 4.6D.* Under control conditions PGE_2 inhibited EFS responses with an IC_{50} of 1nM (95% CI; 0.85-1.3nM, n=6, N=5) compared to 1.4nM (1.2-1.6nM) in the presence of ONO-AE3-208. In the presence of ONO-AE3-208 and PF-04418948 the IC_{50} for PGE_2 increased to 111nM (95% CI; 90-138nM). These data suggest that EP2Rs are also important for mediating the inhibitory effects of PGE_2 on EFS responses. *Figure 4.7A-C* shows results from a similar experiment, except that the order in which the EP2 and EP4R antagonists were added was reversed. Addition of PF-04418948 reduced the inhibitory effects of PGE_2 as before (*Figure 4.7A&B*, respectively). However, subsequent addition ONO-AE3-208 (20nM), in combination with PF-04418948, further reduced the amplitude of PGE_2 on EFS responses (*Figure 4.7C)*. The summary concentration-effect curves in *Figure 4.7D* show that PF-04418948 shifted the PGE_2 concentration-effect curve to the right, ie. the PGE_2 IC_{50} value increased from 1.5nM, (95% CI; 1.2-1.9nM) in control conditions to 30nM (95% CI; 23-38nM) in PF-04418948. Addition of ONO-AE3-208, in combination with PF-04418948, further increased the IC_{50},

compared to PF-04418948 alone (from 30nM to 105nM, 95% CI; 96-114nM) in the presence of both (n=8, N=8). These data highlight that, in contrast to contractions induced by CCh, PGE_2 induced inhibition of EFS responses may involve activation of both EP2 and EP4Rs. Interestingly, the effects of EP4R inhibition were only unmasked when EP2Rs were first blocked by PF-04418948, suggesting that activation of EP2Rs may be able to compensate for the effect of blocking EP4Rs.

4.2.2 Effect of the EP2R agonist (R)-Butaprost on CCh-induced and EFS-evoked contractions of ASM

The above data indicate a role for EP2Rs in PGE_2-induced relaxations of ASM. To investigate this further, we examined the effect of the selective EP2 agonist (*R*)-Butaprost on CCh (1μM) and EFS-evoked contractions. *Figure 4.8A* is a typical tension recording showing the effect of (*R*)-Butaprost (30nM-10μM) on a CCh-induced contraction. *Figure 4.8B* shows the summary concentration-effect curve of these data. The mean IC_{50} for (*R*)-Butaprost was 451nM (95% CI; 360-569nM, n=13, N=10). It is clear that EP2R selective agonist (*R*)-Butaprost significantly reduced the amplitude of CCh-evoked contractions, mimicking the effects of PGE_2, consistent with a role for EP2Rs in the PGE_2 response.

To confirm that the effects of (*R*)-Butaprost were mediated by EP2Rs we examined if its effects were blocked by the EP2R antagonist, PF-04418948. *Figures 4.9A&B* are representative tension recordings showing the effect of (*R*)-Butaprost before (*Figure 4.9A*) and during the presence of the selective EP2R antagonist PF-04418948 (100nM, *Figure 4.9B*). PF-04418948 substantially reduced the amplitude of (*R*)-Butaprost-induced relaxations. Subsequent application of ONO-AE3-208 (20nM) in the continued presence of PF-04418948 showed no additional effect in comparison to PF-04418948 alone (*Figure 4.9C*). The summary concentration-effect curves in *Figure 4.9D* shows that PF-04418948 shifted the (*R*)-Butaprost concentration-effect curve to the right. For example, the (*R*)-Butaprost IC_{50} value increased from 344nM, (95% CI; 260-456nM) in control conditions to 17μM (95% CI; 15-19μM) in PF-04418948. Addition of ONO-AE3-208, in combination with PF-04418948 showed only a

slight change in the (*R*)-Butaprost IC_{50}, increasing it to 28μM (95% CI; 23-33μM, n=7, N=7).

We next examined if EFS responses were similarly affected by (*R*)-Butaprost. Representative tension recordings showing the effect of (*R*)-Butaprost in control conditions, in the presence of PF-04418948 and during application of PF-04418948 plus ONO-AE3-208 are shown in *Figures 4.10A, 4.10B* and *4.10C*, respectively. The summary concentration-effect curves of these data are displayed in *Figure 4.10D.* Under control conditions (*R*)-Butaprost inhibited EFS responses, with an IC_{50} of 68nM (95% CI; 49-97nM) compared to 1.8μM (1.5-2.1μM) in the presence of PF-04418948. In the presence of PF-04418948 and ONO-AE3-208, the IC_{50} was 2.4μM (95% CI; 1.9-3μM, n=6, N=6). These data indicate that activation of EP2Rs inhibits PGE_2 responses in the airway. Moreover, since the EP4R antagonist ONO-AE3-208 did not affect (*R*)-Butaprost responses, it suggests that the inhibitory effects of ONO-AE3-208 on PGE_2 responses (*Figure 4.7*) are not mediated by non-selective effects on EP2Rs.

4.2.3 Expression of EPRs in mouse bronchial tissue

RT-PCR was performed to investigate the transcriptional expression of EPR genes (*Ptger1-4*) in mouse ASM. The genes for all four EPRs were detected in whole mouse bronchial tissue (*Figure 4.11A,* n=3, N=3). *Figure 4.11B* shows that *Ptger1*, *2* and *3*, but not *Ptger4* (EP4R) were detected in isolated mouse ASMCs (n=3, N=3). Predicted amplicon sizes for each EPR gene were as follows: *Ptger1* (100bp), *Ptger2* (96bp), *Ptger3* (219bp), *Ptger4* (114bp). Quantitative analysis of each EPR gene in mouse bronchus was performed by real-time qPCR, using *Actb* (β-actin) as a relative endogenous control. These data were expressed as a ratio of each individual *Ptger* gene relative to *Actb* expression (*Figure 4.11C*). The mean expression ratio relative to *Actb* for *Ptger1*, *2*, *3* and *4* were 0.024 ± 0.006, 0.007 ± 0.003, 0.004 ± 0.001, 0.005 ± 0.001, respectively (n=4, N=4).

4.2.4 Effect of EP1R selective antagonist, SC-19220 on PGE_2 relaxations on CCh-induced contractions

As shown in *Figure 4.11C*, EP1R was the most abundant EPR transcript detected in mouse ASM. Therefore, we next examined if the selective EP1R antagonist SC-19220 (10μM) affected PGE_2-induced relaxations. *Figures 4.12A&B* are representative tension recordings showing the effect of PGE_2 before (*Figure 4.12A*) and during the presence of the selective EP1R antagonist SC-19220 (*Figure 4.12B*). *Figure 4.12C* shows that SC-19220 had no discernable effects on PGE_2-mediated relaxations. The mean IC_{50} under control conditions was 30nM (95% CI; 26-35nM, n=8, N=5) compared to 32nM (95% CI; 25-40nM) in the presence of SC-19220, indicating that EP1Rs have no role in the inhibitory action of PGE_2 in mouse ASM.

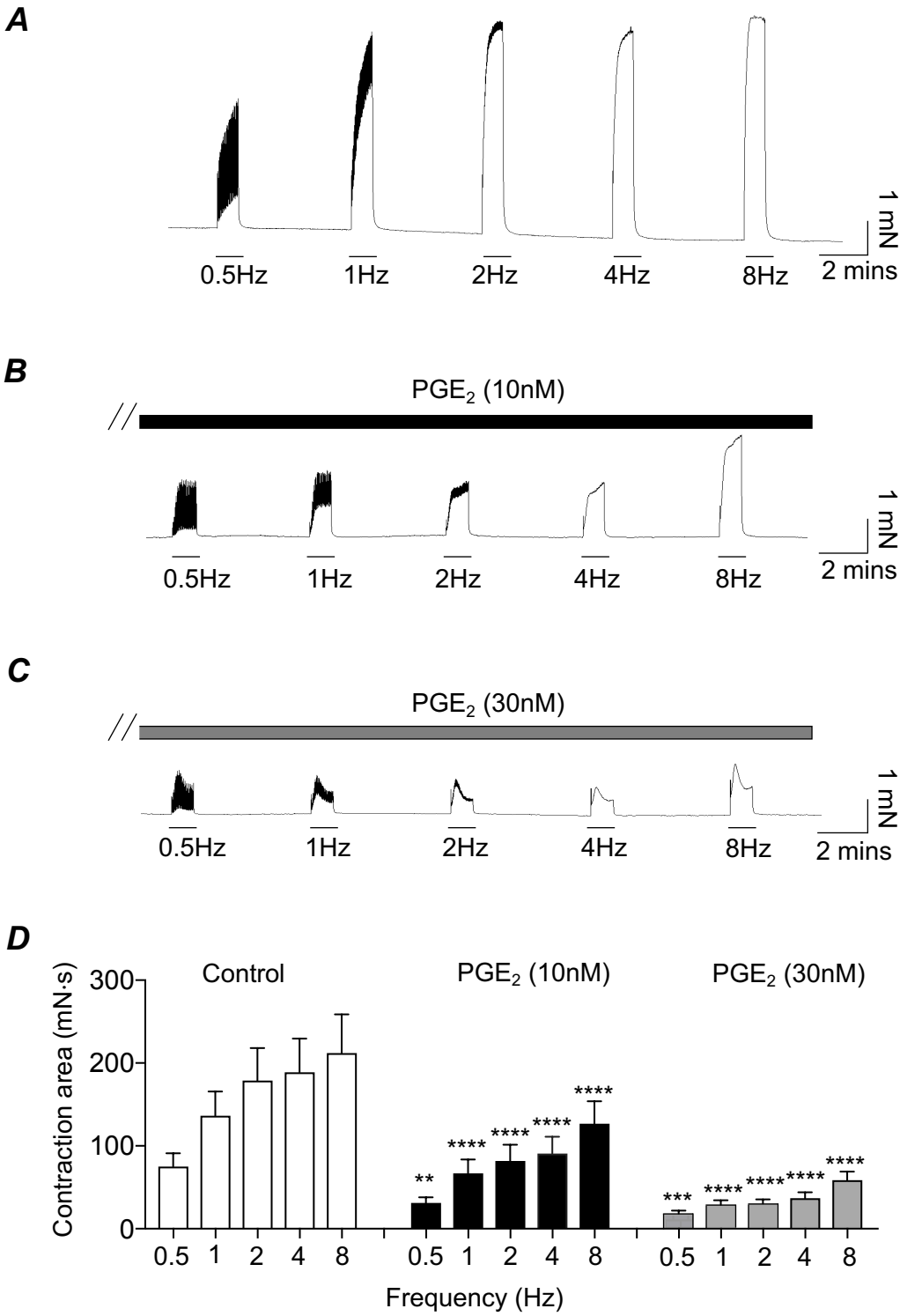

Figure 4.1*. EFS-evoked contractions of mouse bronchial rings are inhibited by PGE_2.* Representative tension recordings showing EFS-evoked contractions (0.5 – 8Hz) of ASM in control (**A**), the presence of 10nM PGE_2 (**B**) and 30nM PGE_2 (**C**). (**D**) Summary bar chart (n=6, N=6) plotting mean contraction amplitude (measured by area under the curve) in control, 10nM PGE_2 (black bars) and 30nM PGE_2 (grey bars). The responses to all frequencies were significantly reduced in 10nM PGE_2 and 30nM PGE_2 (**p<0.01, ***p<0.001, ****p<0.0001, two-way ANOVA).

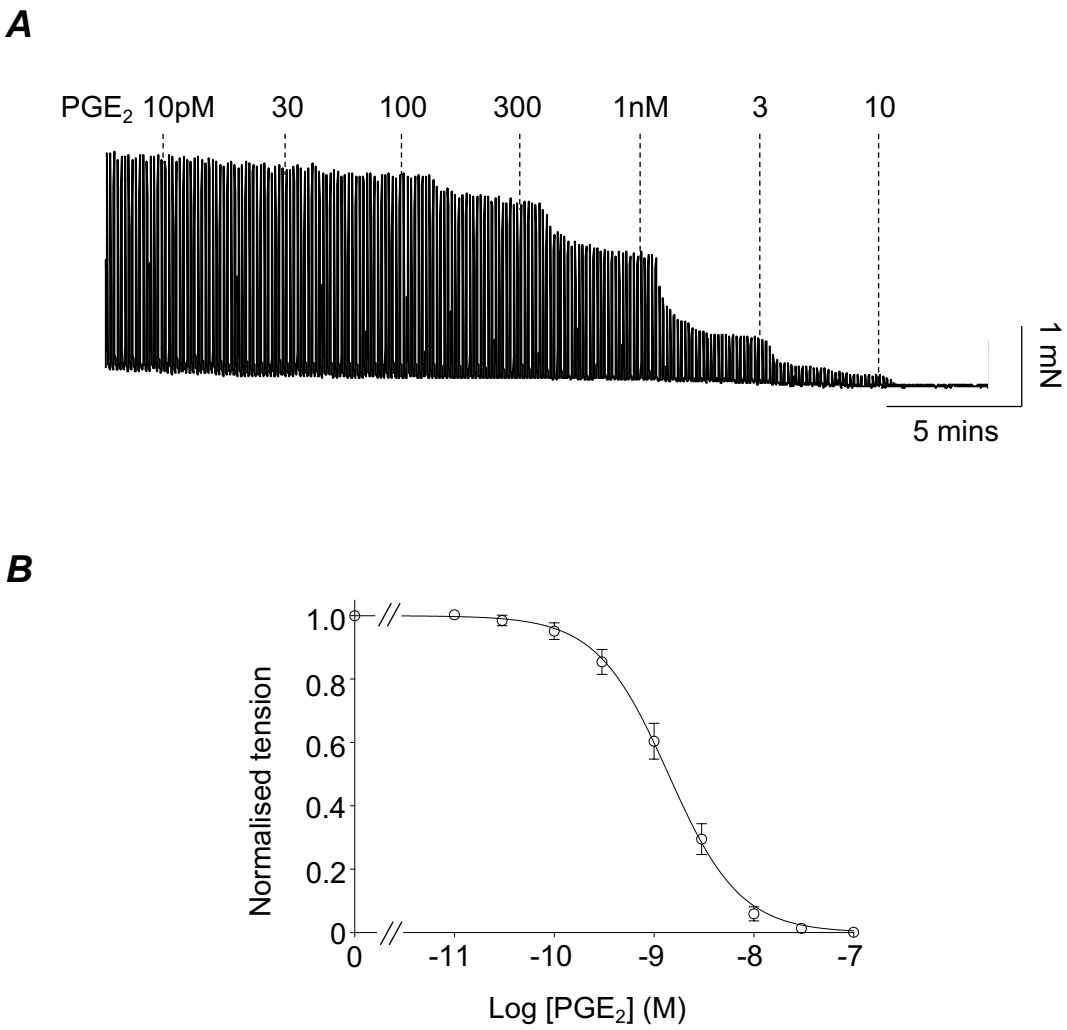

Figure 4.2. ***PGE_2 inhibits nerve-evoked contractions of mouse bronchial rings in a concentration dependent manner.*** (**A**) Representative isometric tension recording showing the effect incremental additions of PGE_2 (10pM-10nM) on EFS-evoked contractions (2Hz) of mouse bronchial rings. (**B**) Summary concentration-effect curve for PGE_2 on EFS-evoked contractions (IC_{50} = 1.4nM, n=21, N=18).

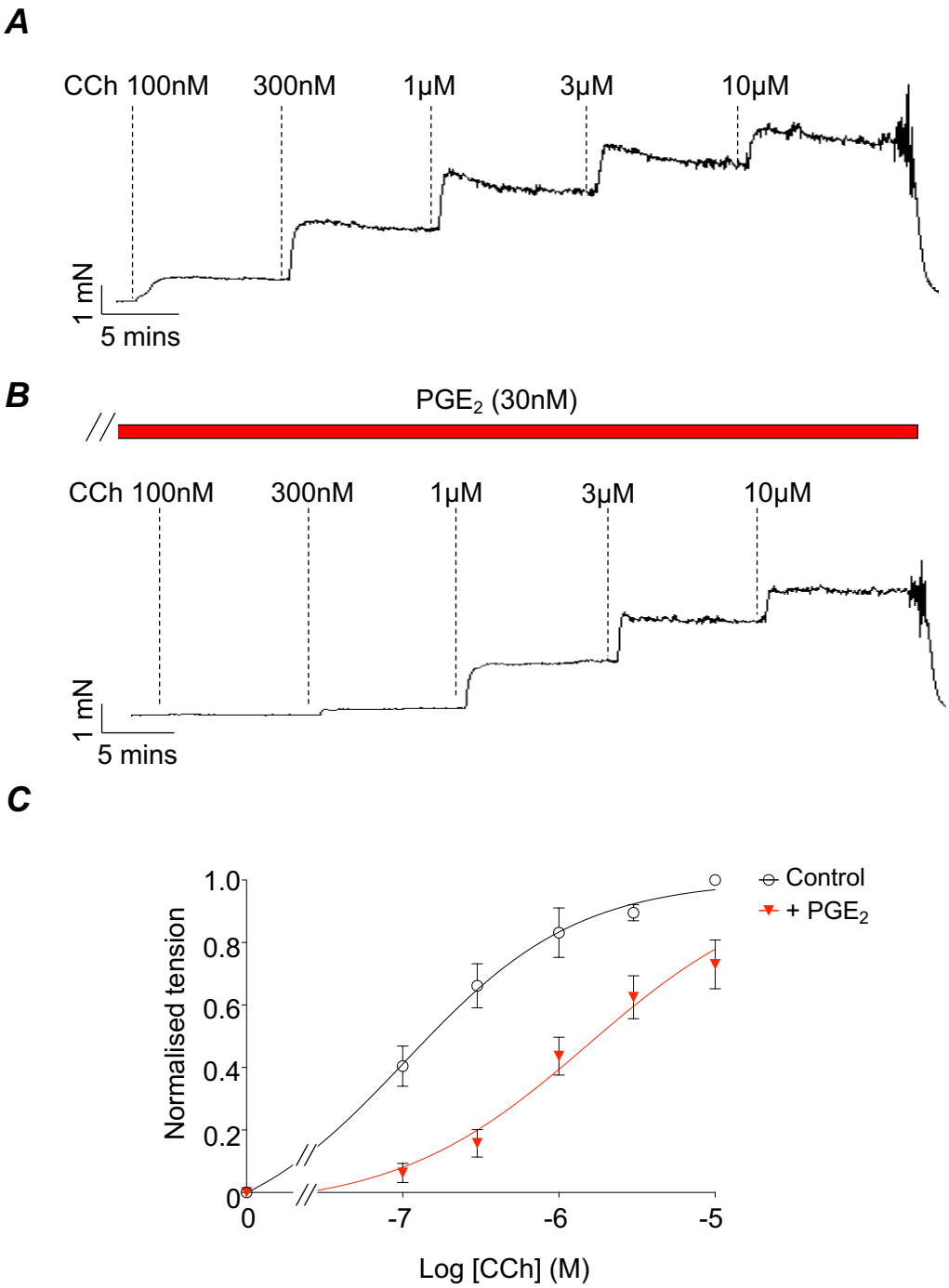

Figure 4.3. ***Effect of PGE_2 on CCh-induced contractions of mouse bronchial rings.*** Panels **A** and **B** are representative isometric tension recordings showing the effect of cumulative addition of CCh (100nM to 10μM) to ASM before (**A**) and during addition of 30nM PGE_2 (**B**). (**C**) Summary concentration-effect curves in the absence (EC_{50}=105nM) and presence of PGE_2 (EC_{50}= 1.5μM, n=6, N=5).

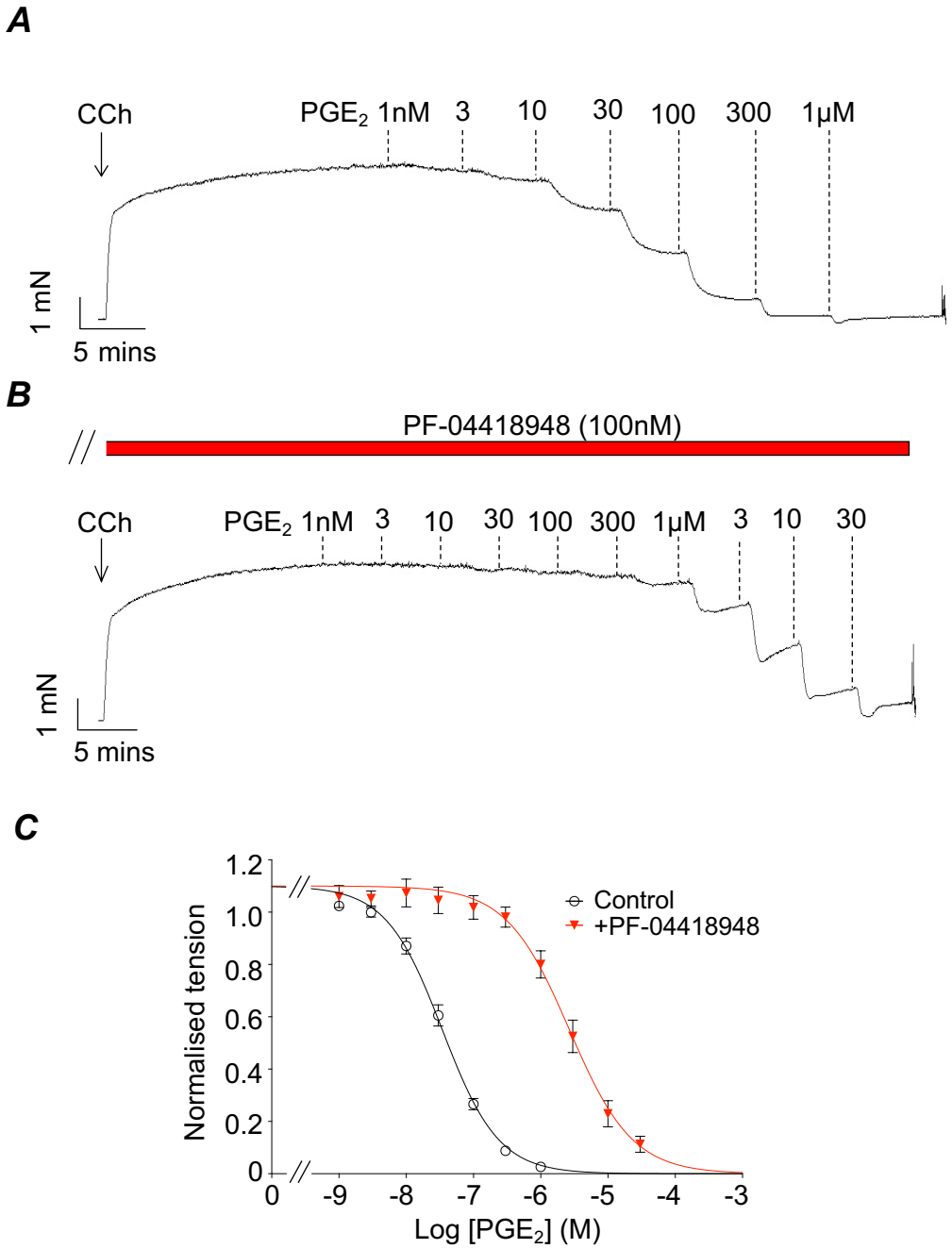

Figure 4.4. ***Effect of the EP2 receptor antagonist PF-04418948 on PGE_2-induced relaxations of mouse bronchial rings***. (**A** & **B**) Representative tension recordings showing the effect of PGE_2 (1nM – 30μM) on bronchial rings pre-contracted with 1μM CCh (***A***) and during the presence of PF-04418948 (100nM, **B**). (**C**) Summary concentration effect curves for PGE_2 in the absence (IC_{50}= 44nM) and presence of PF-04418948 (IC_{50}= 3.5μM n=7, N=5).

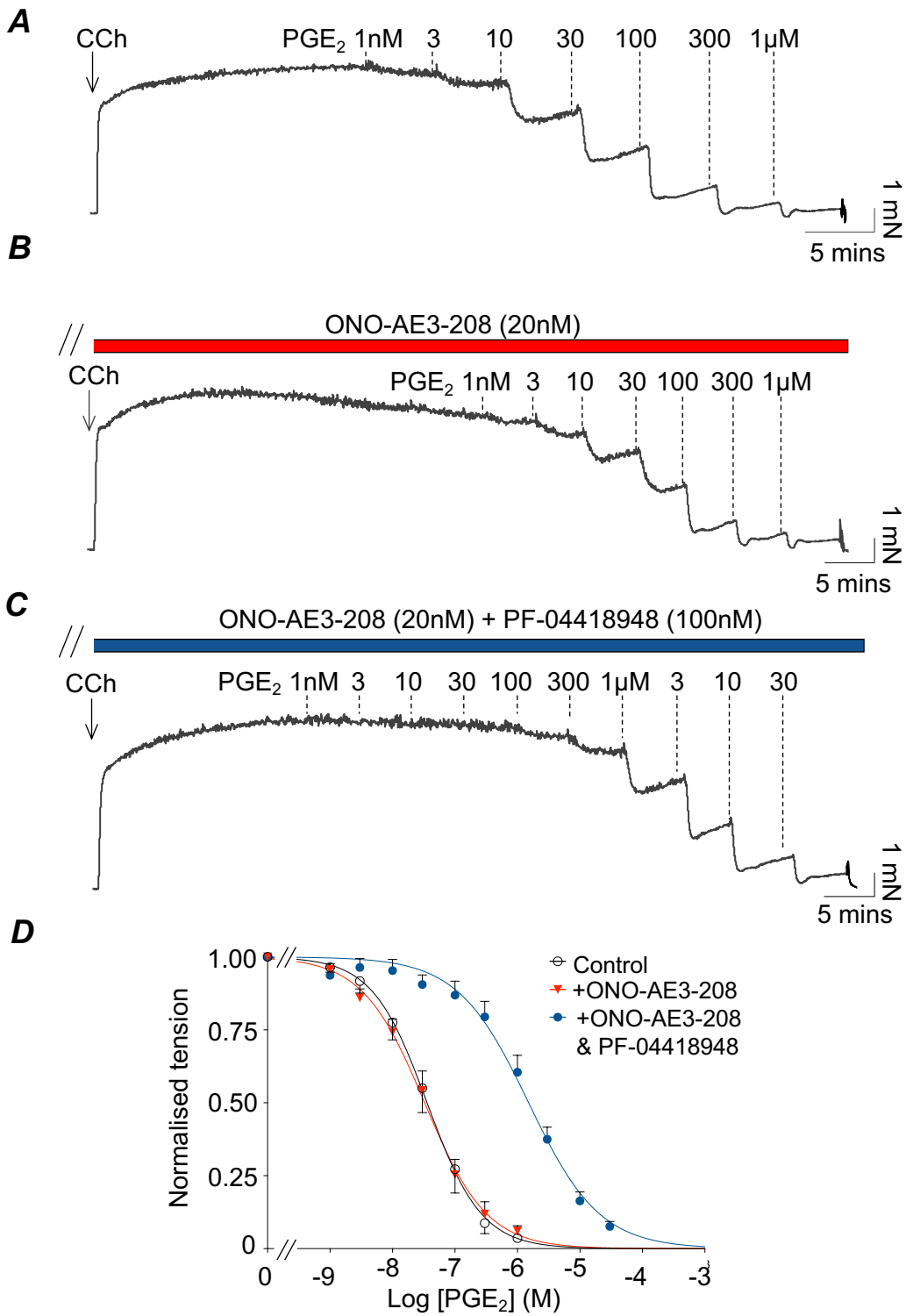

Figure 4.5. ***Effect of the EP4 receptor antagonist, ONO-AE3-208 on PGE_2-induced relaxations of mouse bronchial rings.*** (**A**-**C**) Representative tension recordings showing the effects of PGE_2 (1nM – 30μM) on CCh-evoked contractions before (**A**) and during the presence of ONO-AE3-208 (20nM, **B**) and ONO-AE3-208 plus PF-04418948 (100nM) (**C**). (**D**) Summary concentration-effect curves for PGE_2 (n=7, N=5) illustrating that the effects of PGE_2 were not affected by the EP4R antagonist ONO-AE3-208 (20nM) (IC_{50}= 36nM, compared to 33nM for controls). In contrast, addition of PF-04418948 (100nM) shifted the PGE_2 IC_{50} value to 1.5μM.

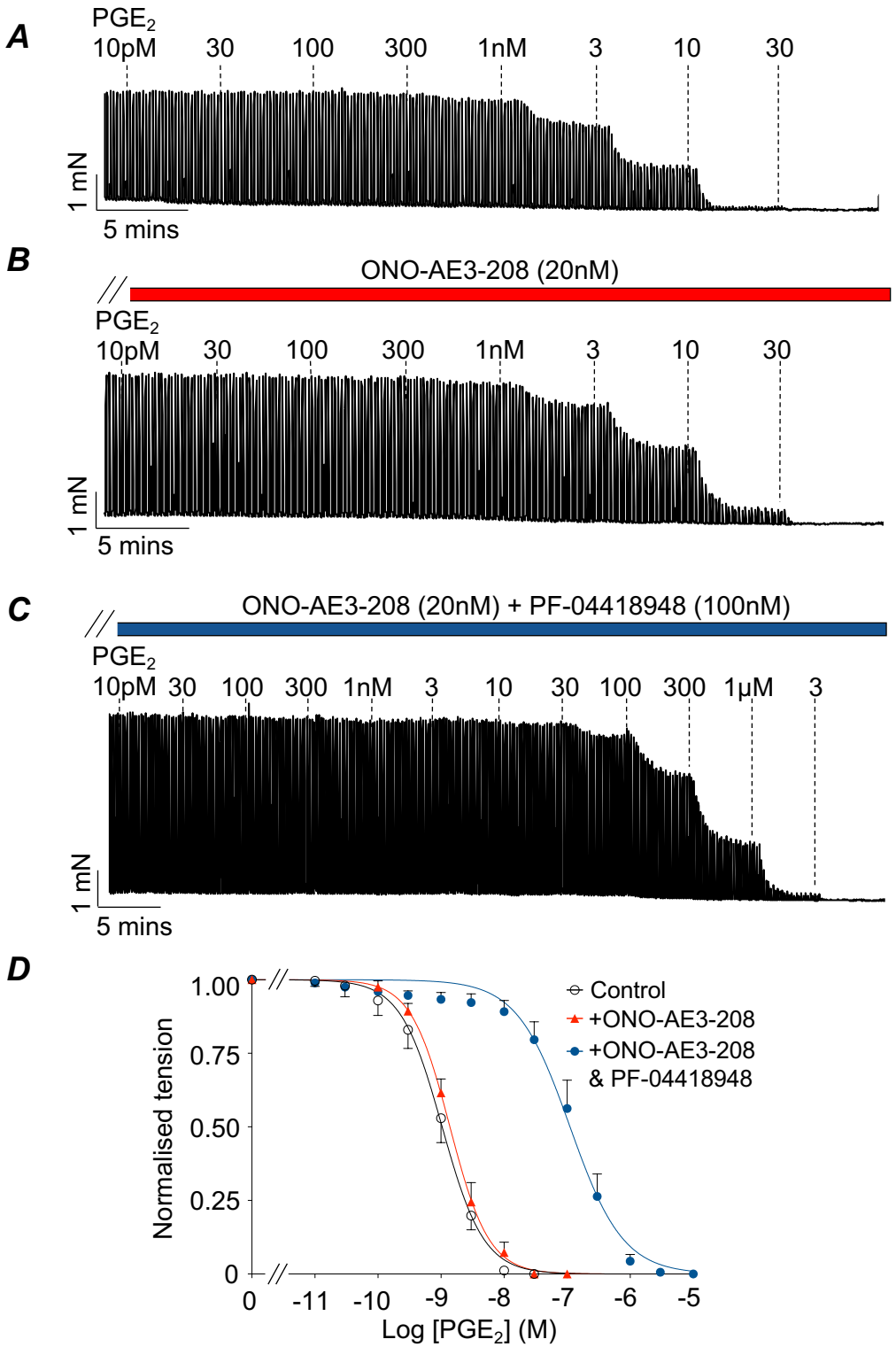

Figure 4.6. ***Effect of the EP4 receptor antagonist, ONO-AE3-208 on PGE_2-induced inhibition of EFS-evoked contractions of mouse bronchial rings.*** (**A**-**C**) Representative tension recordings showing the effects of PGE_2 (10pM – 30nM) before (**A**) and in the presence of ONO-AE3-208 (20nM, **B**) and ONO-AE3-208 plus PF-04418948 (100nM, **C**). (**D**) Summary concentration-effect curves for PGE_2 (n=6, N=5). PGE_2-induced relaxations were not affected by the EP4 receptor antagonist ONO-AE3-208 (IC_{50}= 1.4nM, compared to 1nM for controls). In contrast, addition of PF-04418948 shifted the PGE_2 IC_{50} value to 111nM.

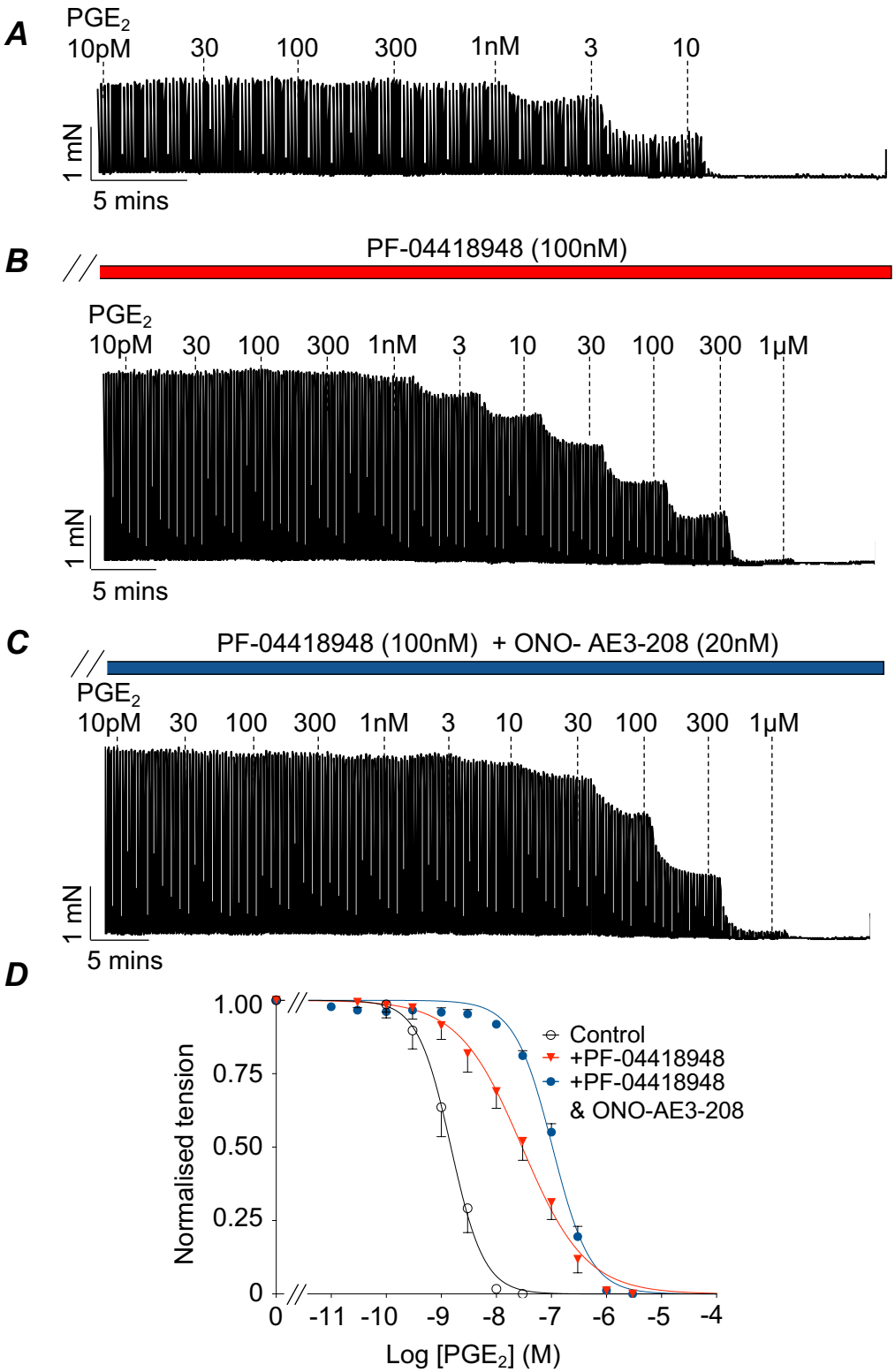

Figure 4.7. ***Effect of the EP2 receptor antagonist, PF-04418948 on PGE_2-induced inhibition of EFS-evoked contractions of mouse bronchial rings.*** (**A**-**C**) Representative tension recordings showing the effects of PGE_2 (10pM – 1µM) on EFS-evoked contractions before (**A**) and in the presence of PF-04418948 (100nM, **B**) and PF-04418948 plus ONO-AE3-208 (20nM, **C**). (**D**) Summary concentration effect curves (n=8, N=8), the presence of PF-04418948 caused a rightward shift (IC_{50}= 30nM vs. 1.5nM in control conditions) this shift was augmented by the addition of ONO-AE3-208 (IC_{50}= 105nM).

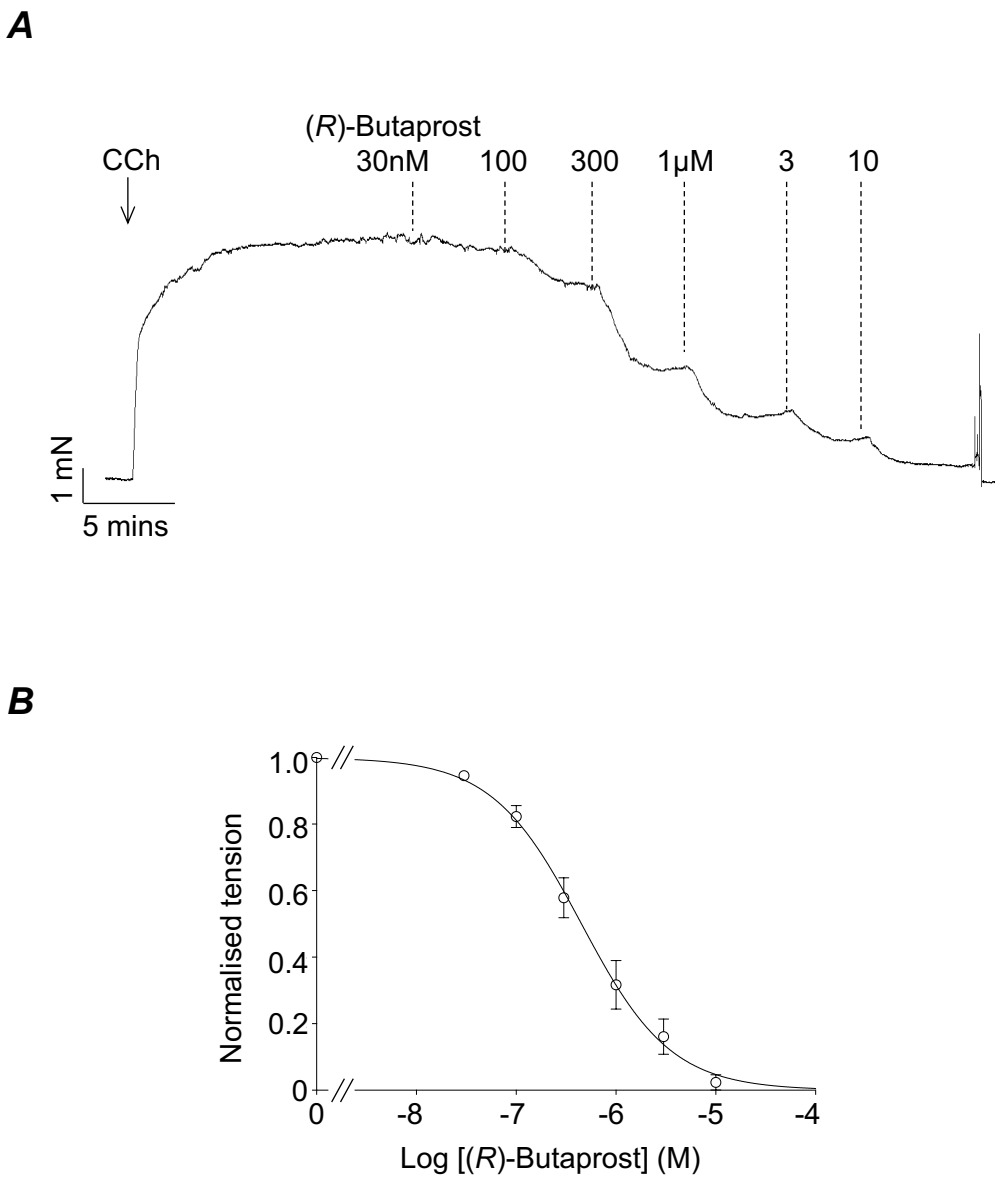

Figure 4.8. ***Effect of the selective EP2 receptor agonist (R)-Butaprost on CCh-induced contractions of mouse bronchi.*** (**A**) Representative tension recording demonstrating the effect of (*R*)-Butaprost (30nM-10μM) on a CCh-induced contraction. (**B**) Summary concentration-effect curve for (*R*)-Butaprost (n=13, N=10), illustrating the inhibitory effects of EP2R selective agonist (*R*)-Butaprost (IC_{50}= 451nM).

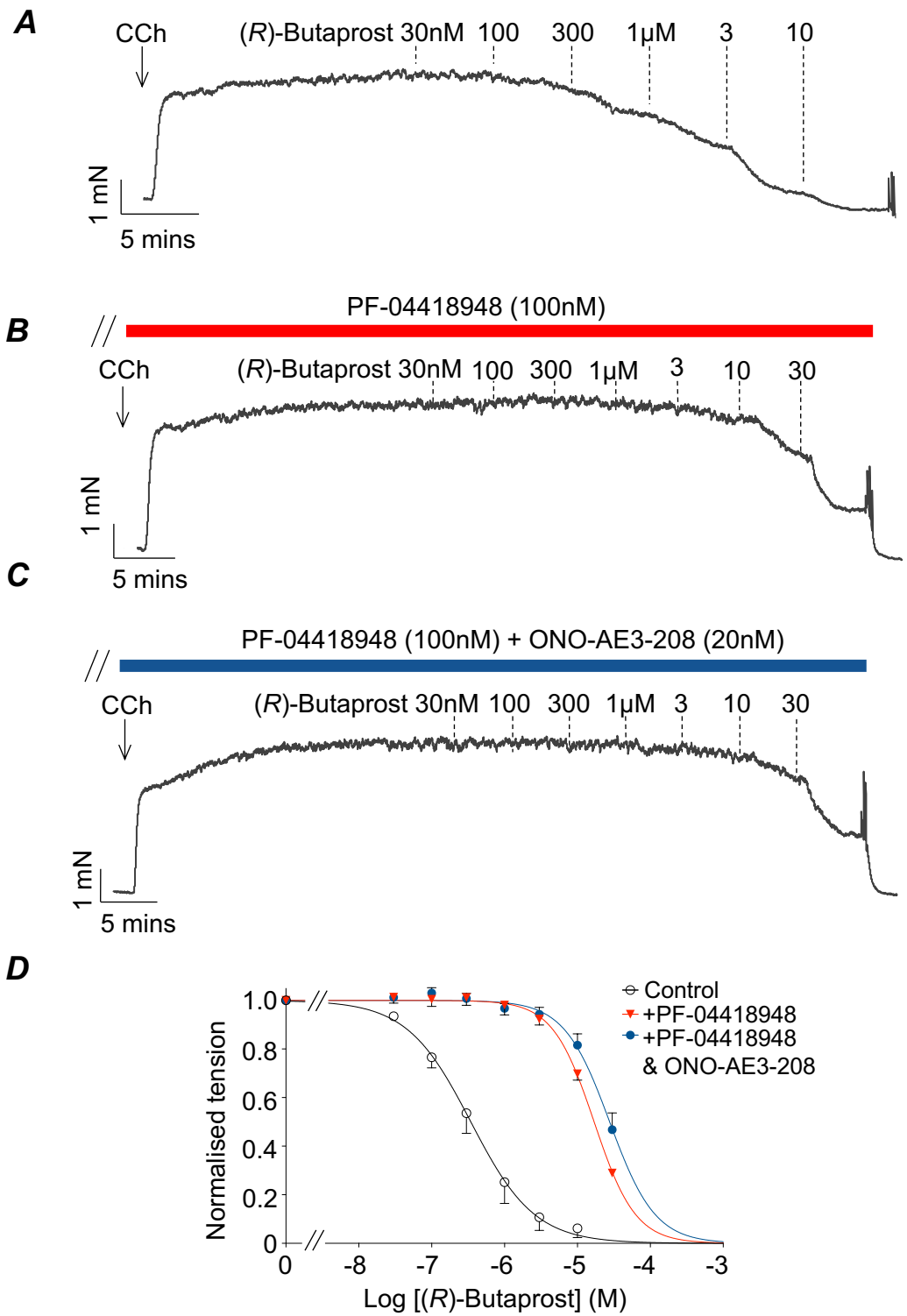

Figure 4.9. ***Effect of the EP2 receptor antagonist, PF-04418948 on (R)-Butaprost-induced inhibition of CCh-induced contractions of mouse bronchi.*** (**A**-**C**) Representative tension recordings showing the effects of (*R*)-Butaprost (30nM – 30μM) before and during the presence of PF-04418948 (100nM, **A** & **B,** respectively) and (**C**) plus ONO-AE3-208 (20nM). (**D**) Summary concentration-effect curves (n=7, N=7). PF-04418948 reduced (*R*)-Butaprost-induced relaxation (IC_{50}= 17μM vs. IC_{50}= 344nM for controls), subsequent addition of ONO-AE3-208, showed a slight change in IC_{50}, to 28μM.

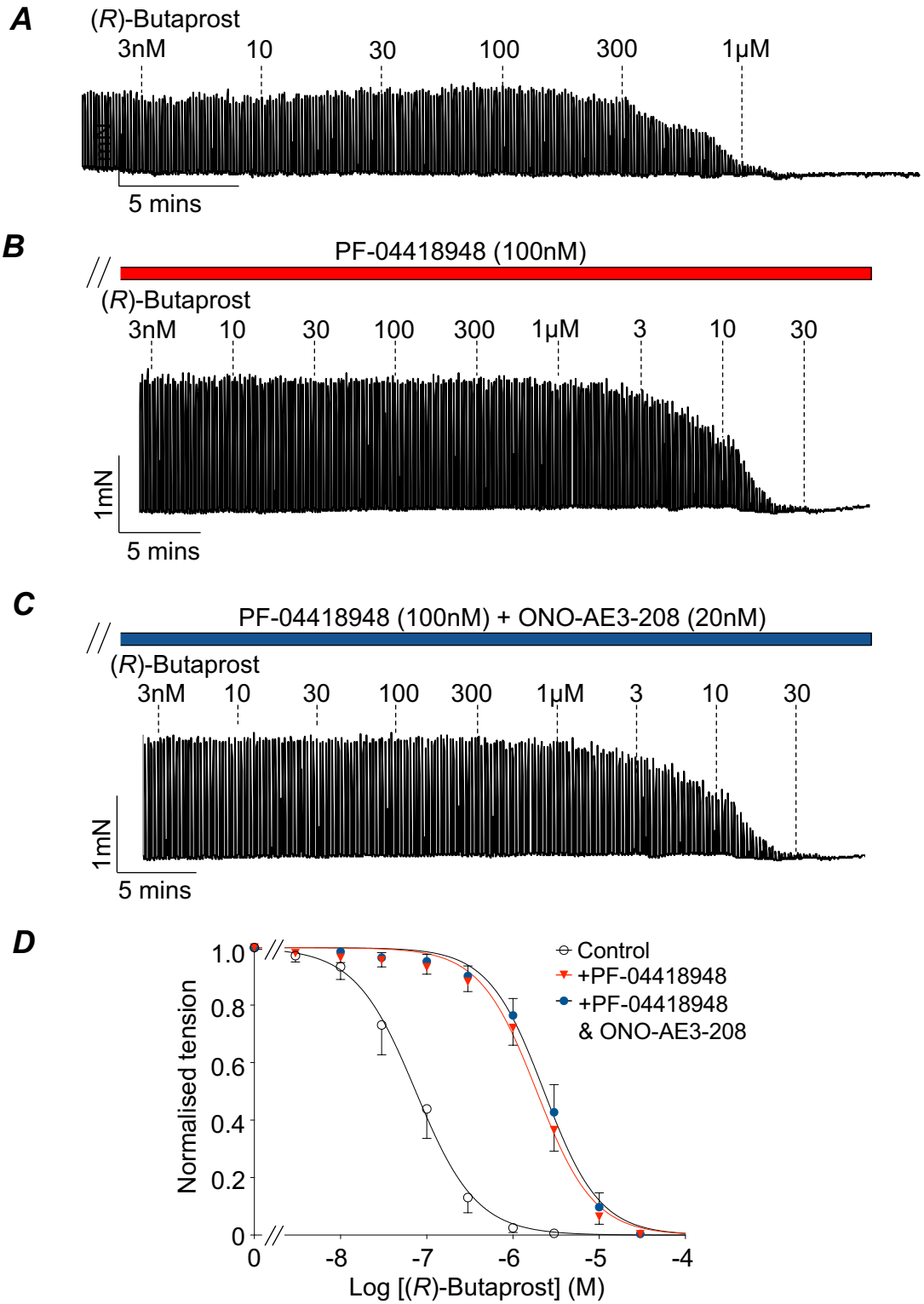

Figure 4.10. ***Effect of the EP2 receptor antagonist, PF-04418948 on (R)-Butaprost-induced inhibition of EFS-evoked contractions of mouse bronchi.*** (**A**-**C**) Representative tension recordings showing the effects of (*R*)-Butaprost (3nM – 30μM) on EFS-evoked contractions of mouse ASM before (**A**) and during the presence of 100nM PF-04418948 (**B**) and PF-04418948 plus 20nM ONO-AE3-208 (**C**). (**D**) Summary concentration effect curves (n=6, N=6). PF-04418948 caused a rightward shift (IC_{50}= 1.8μM vs. IC_{50}= 68nM for controls). ONO-AE3-208 had no discernable effects (IC_{50}= 2.4μM).

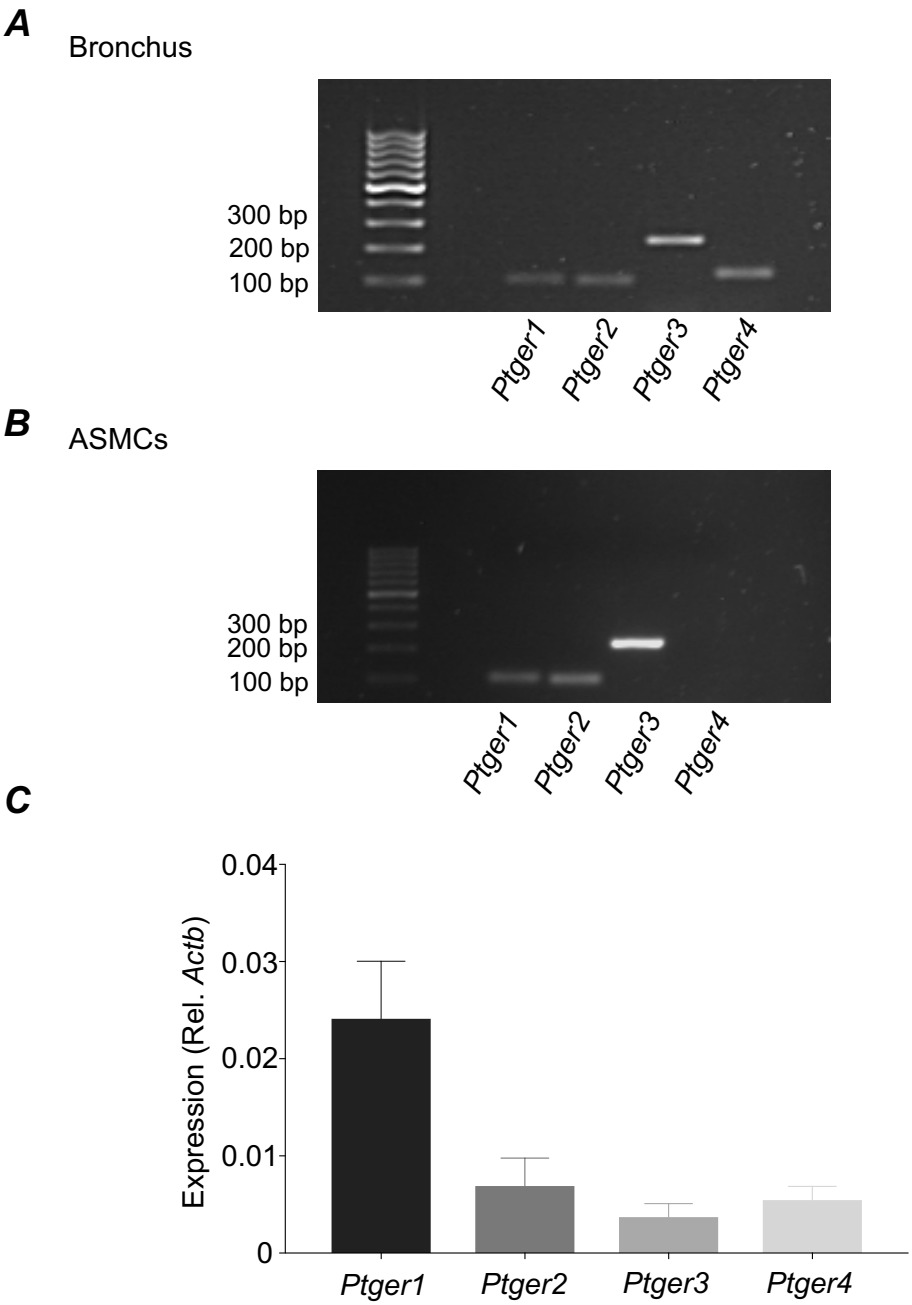

Figure 4.11. ***Expression of Ptger1-4 receptor subtypes in mouse bronchi and isolated mouse ASMCs*****.** Electrophoresis gel showing expression of the genes *Ptger1-4* which encode for the EP subtypes 1-4 in (**A**) whole bronchial tissue and (**B**) isolated ASMCs (n=3, N=3). (**C**) Quantitative RT-PCR of EPR isoforms using the same primer sets as above, normalised using *Actb* (β-actin) as a relative endogenous control (n=4, N=4).

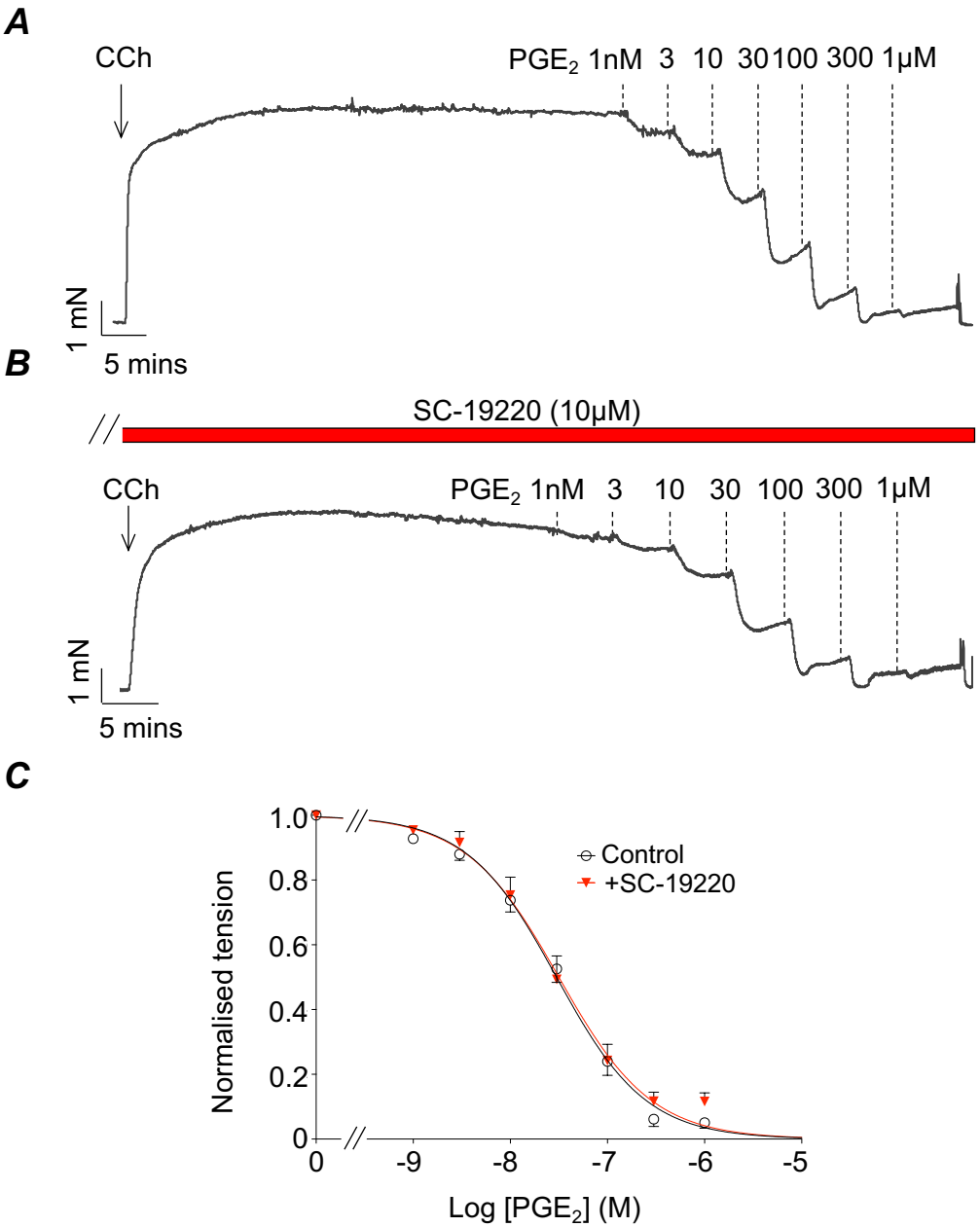

Figure 4.12. ***Effect of the EP1 receptor antagonist SC-19220 on PGE_2-induced relaxations on CCh-induced contractions of mouse bronchial rings.*** (**A** & **B**) Representative tension recordings showing the effect of PGE_2 (1nM – 1μM) on CCh-evoked contractions before (***A***) and during the presence of SC-19220 (10μM, **B**). (**C**) Summary concentration-effect curves for PGE_2 in the absence (IC_{50}= 30nM) and presence of SC-19220 (IC_{50}= 32nM n=8, N=5).

4.3 Discussion

The main findings of this chapter were that: 1) PGE_2 inhibited both EFS and CCh-induced contractions of mouse ASM in a concentration-dependent manner; 2) PGE_2-induced inhibition of CCh responses were reduced in the presence of an EP2R antagonist but not an EP4R antagonist; 3) PGE_2-induced inhibition of EFS responses was reduced by an EP2R antagonist but small inhibitory effects of the EP4R antagonist on the PGE_2 response were observed when applied in the presence of the EP2R antagonist; 4) All 4 EP receptors were expressed in mouse bronchial rings however, only EP 1, 2 and 3 were detected in isolated ASMCs.

PGE_2 mediates several biological processes including, pain, airway inflammation, cough and bronchodilation (Lebender *et al.* 2018; Konya *et al.* 2013). The diverse range of cellular functions initiated by PGE_2 are attributable to the existence of four prostanoid E receptors, EP 1, 2, 3 and 4. EPRs 1-4 instigate distinct signalling pathways which account for the diverse effects of PGE_2 (Tilley *et al.* 2003). Previous studies have reported that activation of EP2&4Rs are responsible for the relaxant effects of PGE_2 on ASM however, EP2Rs are thought to be responsible for PGE_2-induced relaxations of mouse ASM (Sheller *et al.* 2000; Tilley *et al.* 2003). This agrees with the present study which shows that PGE_2-mediated inhibition of CCh-induced contractions were significantly reduced in the presence of the selective EP2R antagonist, PF-04418948, but were unaffected by the EP4R antagonist, ONO-AE3-208. These data suggest that in mouse ASM, PGE_2-induced relaxations are primarily mediated via EP2Rs. These findings are supported by Tilley *et al*. (2003), who demonstrated a loss of bronchodilatory actions of PGE_2 in ventilated EP2 $^{-/-}$ but not EP4 $^{-/-}$ mice, pre-contracted with MCh. Similarly, Buckley *et al.* (2011), reported that PGE_2 relaxations were substantially reduced in EP2R$^{-/-}$ mouse trachea, pre-contracted with CCh, whereas they were not affected in EP4R$^{-/-}$ tracheal rings.

Application of the selective EP4R antagonist ONO-AE3-208 did not affect PGE_2-induced inhibition of neurogenic responses alone but did reduce these responses in the presence of PF-04418948, suggesting that EP4Rs may be involved in PGE_2-induced inhibition of nerve-mediated contractions of ASM.

However, as the effects of ONO-AE3-208 were only revealed when EP2Rs were inhibited, it suggests that activation of EP2Rs could compensate for the effects of PGE_2 when EP4s were blocked. Interestingly, ONO-AE3-208 did not affect PGE_2-induced inhibition of CCh responses even when PF-04418948 was present. This discrepancy between the EPRs involved in PGE_2 responses on cholinergic agonist versus EFS-induced contractions, may be attributable to pre-junctional effects of PGE_2, on EP4Rs as noted earlier in Chapter 3. In support of this idea was the finding that PGE_2 was more potent on EFS versus CCh-induced contractions (IC_{50} of 1.4nM versus 44nM). Interestingly, Belvisi *et al.* (1996), reported that PGE_2 inhibited ACh release of guinea pig trachea from cholinergic nerve terminals, consistent with the idea that PGE_2 may inhibit EFS-evoked contractions via an effect on both pre and post-junctional EPRs.

Another finding obtained in this chapter, was the greater sensitivity of EFS-evoked contractions to PGE_2 using a short pulse (1s) in comparison to longer duration stimulation (60s). It is possible that this effect is due to involvement of different cellular mechanisms at each time point and that these mechanisms have different sensitivity to PGE_2. Nerve-evoked contractions of ASM are mediated via ACh release from parasympathetic nerves and subsequent activation of M_3Rs on ASM. Activation of M_3Rs initiates the PLC signalling pathway which results in the production of IP_3 and DAG (Billington and Penn 2003). Upregulation of IP_3 initially induces calcium release from intracellular stores and then activates calcium-activated Cl^- channels causing depolarisation and therefore, opening of VDCCs (Croisier *et al.* 2013; Kotlikoff and Wang 1998; Komori *et al.* 1992). DAG activates non-selective cation channels to allow calcium to enter the cell (Unno *et al.* 2005). Komori *et al.* (1992) found that CCh responses in guinea pig ileum smooth muscle were brought about by an initial release of calcium from the SR, followed by calcium influx via VDCCs. Therefore, it is possible that responses to short pulses arise from intracellular calcium store release, whereas longer duration nerve stimulation also involve calcium influx. If so, this would suggest that PGE_2 may be more effective at inhibiting intracellular store release versus calcium influx. However, this idea requires further investigation.

Reverse-transcriptase PCR experiments demonstrated that *Ptger1*, *2*, *3* and *4* (EP1-4) were expressed in mouse bronchial rings, similar to results obtained by Herrerias *et al.* (2009), who reported the presence of all four EP

receptor genes in mouse lung preparations. Interestingly, we detected *Ptger1*, *2* and *3*, but not *Ptger4* in isolated mouse ASMCs. The absence of the *Ptger4* (EP4Rs) on mouse AMSCs correlates with the finding that the EP4R antagonist reduced PGE_2 responses on EFS, but not CCh-induced contractions. However, it cannot be ruled out that the transcriptional expression of *Ptger4* (EP4R) may be beyond the level of detection in this preparation. Real-time PCR determined that *Ptger1* (EP1) was substantially the most highly expressed EP receptor gene in mouse ASM. However, application of the selective EP1 antagonist 10μM SC-19220 showed no effect on PGE_2 relaxations of mouse bronchial rings. The lack of effect of the EP1R in mouse airway has also been described by McGraw *et al.* (2006), as selective EP1R agonists did not elicit substantial ASM contraction in mouse trachea. However, EP1R agonists were reported to augment β_2-adrenoceptor desensitisation, suggesting that activation of EP1Rs via PGE_2 may mediate a pathway that does not directly affect ASM contraction/relaxation (McGraw *et al*. 2006).

In summary, data in this chapter confirms PGE_2 as a potent bronchodilator and that these effects were primarily mediated by activation of EP2Rs and to a lesser extent, EP4Rs. Nerve-evoked contractions of ASM were more sensitive to PGE_2 than those induced by CCh, suggesting that PGE_2 could act both pre- and post-junctionally.

5. Mechanisms underlying inhibitory effects of PGE_2 on ASM

5.1 Introduction

Findings from Chapter 3 and 4 show that PGE_2-induced relaxations of mouse bronchial rings were primarily mediated via activation of EP2Rs and that relaxations induced by endogenously released PGE_2 were sensitive to BK channel blockade. However, the underlying cellular mechanisms responsible for these effects remain unclear. Activation of EP2Rs by PGE_2 is believed to increase intracellular cAMP levels to activate PKA and possibly EPAC (Taylor *et al.* 2017; Aso *et al*. 2013; Sastre and del Pozo 2012; Vancheri *et al*. 2004). PKA affects a range of cellular pathways to induce relaxation, including phosphorylation of calcium ATPases (to remove cytosolic calcium) and prevention of MLCP downregulation thereby reducing the phosphorylation of MLC and formation of actomyosin cross-bridges (Wooldridge *et al.* 2004; Frank *et al.* 2003; Kranias *et al.* 1985). Studies have also demonstrated that PKA can induce phosphorylation of BK channels (Kuo and Ehrlich 2015; Morgan *et al*. 2014) opening up another pathway by which PGE_2 and PKA could lead to ASM relaxation (Valverde *et al.* 2011). PGE_2 has been shown to induce smooth muscle relaxation via activation of K^+ channels in other smooth muscle types (Zhu *et al.* 2002; Kotlikoff 1993). Zhu *et al.* (2002) demonstrated that PGE_2 stimulated BK channel activity in human coronary artery smooth muscle cells, via activation of PKG. Therefore, the purpose of the present study was to: 1) examine if PGE_2-induced relaxations of ASM were affected by block of K^+ channels and 2) investigate the effect of PKA and EPAC activation on mouse ASM and their role in PGE_2-induced relaxations.

5.2 Results

5.2.1 Effect of the BK channel blocker, iberiotoxin (300nM) on PGE_2-induced inhibition of CCh-evoked contractions of ASM

Experiments were performed to investigate if activation of BK channels by using the BK channel opener Compound X (3μM, Ponte *et al.* 2012), inhibited contractions of ASM evoked by 1μM CCh, and if these effects were affected by the potent BK channel blocker, IbTx (300nM). The COX 1/2 inhibitor, indomethacin (10μM) was present for all experiments in this chapter to prevent release of endogenous prostaglandins. *Figures 5.1A&B* are representative tension recordings showing the effect of Compound X on CCh-induced contraction of ASM before (*Figure 5.1A*) and during the presence of IbTx (*Figure 5.1B*). The summary bar chart in *Figures 5.1C&D* shows that in control conditions Compound X reduced the amplitude of CCh-evoked contractions by 39% from 4.6 ± 0.74 to 2.8 ± 0.5mN (*Figure 5.1C*, paired t-test, $p<0.01$) and that this inhibitory effect was abolished in the presence of IbTx (4.6 ± 0.76 to 4.6 ± 0.68mN, *Figure 5.1D*, paired t-test, $p>0.05$, n=6, N=5). These data suggest that activation of BK channels can elicit bronchodilation in mouse ASM.

Zhu *et al.* (2002) showed that PGE_2-induced relaxations of human coronary artery smooth muscle were mediated via activation of BK channels. Therefore, we examined if PGE_2-induced relaxations of ASM were affected by blockade of BK channels. *Figures 5.2A&B* show the effect of cumulative application of a range of concentrations of PGE_2 (1nM - 1μM) on contractions induced by 1μM CCh before (*Figure 5.2A*) and in the presence of IbTx (*Figure 5.2B*). It is clear that the amplitude of PGE_2-induced relaxations was reduced in the presence of IbTx, compared to control. This was also evident in the summary concentration-effect curves shown in *Figure 5.2C*. Under control conditions PGE_2 abolished CCh-induced contractions at concentrations of 300nM and above. However, in IbTx 300nM PGE_2 reduced the amplitude of CCh response by approximately 70% from 5.3 ± 0.8mN to 3.7 ± 0.88mN. Higher concentrations of PGE_2 (up to 10μM) did not produce any further inhibitory effects. Overall, the mean IC_{50} for PGE_2 increased from of 22nM (95% CI; 14 - 35nM) to 34nM (23 - 50nM, n=7, N=6) in the presence of IbTx. In addition, PGE_2 had a maximum

inhibitory effect of 100% in control conditions, compared to only 70% in the presence of IbTx.

Data in Chapters 3 and 4 indicated that PGE_2-induced relaxations of ASM were predominantly mediated via activation of EP2Rs. Therefore, we next examined the effects of IbTx on relaxations induced by the selective EP2R agonist, (*R*)-Butaprost. *Figures 5.3A&B* are representative tension recordings showing the effect of (*R*)-Butaprost before (*Figure 5.3A*) and during the presence of IbTx (*Figure 5.3B*). It is clear that IbTx substantially inhibited (*R*)-Butaprost-induced relaxations. The summary concentration-effect curves displayed in *Figure 5.3C* (n=6, N=5), illustrate that addition of IbTx increased the IC_{50} from 310nM (95% CI; 245 - 390nM) under control conditions to 3.5μM (95% CI; 2.9 - 4.3μM). These data suggest that EP2R-mediated relaxation of ASM are reduced when BK channels are blocked.

EP2Rs are G_s protein-coupled receptors that mediate their inhibitory effects through the stimulation of AC. Therefore, we next examined the effect of the AC activator, forskolin. Cumulative addition of forskolin induced concentration-dependent relaxations of ASM under control conditions (*Figure 5.4A*) and these responses were only slightly reduced in the presence of IbTx (*Figure 5.4B)*. The summary concentration-effect curves in *Figure 5.4C* show that IbTx shifted the forskolin concentration-effect curve to the right. For example, the forskolin IC_{50} value increased from 1.3μM, (95% CI; 1.1 - 1.6μM) in control conditions to 3.2μM (95% CI; 2.6 - 3.9μM) in IbTx (n=7, N=7).

AC activation can lead to upregulation of both PKA and EPAC to induce inhibitory effects in ASM (Lebender *et al*. 2018; Kuo and Ehlrich 2015; Zhang *et al*. 2010). Therefore, we examined the effects of cAMP-dependent PKA and tested if these effects were reduced by blockade of BK channels. Cumulative addition of the PKA activator, N^6-monobutyryl-cyclic adenosine monophosphate (6-MB-cAMP, 10μM-1mM) induced concentration-dependent relaxations of ASM, under control conditions (*Figure 5.5A*) and these responses were diminished in the presence of IbTx (*Figure 5.5B)*. *Figure 5.5C* demonstrates that the mean IC_{50} for 6-MB-cAMP was 158μM (95% CI; 128 -195μM, n=10, N=10) under control conditions, compared to 760μM (95% CI; 0.55 - 1mM) in the presence of IbTx.

These data suggest that PKA mediated relaxations were diminished by BK channel blockade.

5.2.2 Effect of BK channel blocker iberiotoxin (300nM) on PGE_2-induced inhibition of EFS-evoked contractions of ASM

The above data suggest that EP2R-dependent relaxations of ASM are reduced by blockade of BK channels. These experiments were performed on tissues that were pre-contracted with CCh, therefore, we next tested if similar results were observed on neurogenic contractions induced by EFS. *Figures 5.6A&B* are representative tension recordings showing the effect of PGE_2, before (*Figure 5.6A*) and during the presence of the BK channel blocker, IbTx (*Figure 5.6B*) on EFS-induced responses. It was also apparent that the concentration of PGE_2 required to induce maximal inhibition increased from 10 to 100nM. It was noticeable that at concentrations of 1μM and above, a concentration-dependant increase in contraction amplitude was observed in the presence of IbTx. Under control conditions PGE_2 inhibited EFS responses with an IC_{50} of 1.3nM (95% CI; 1 - 1.5nM, n=8, N=7) compared to 3.9nM (95% CI; 3 - 4.9nM) in the presence of IbTx.

IbTx produced a similar effect on (*R*)-Butaprost-induced responses. *Figures 5.7A&B* shows the effect of the selective EP2R agonist (*R*)-Butaprost on EFS-induced contractions before (*Figure 5.7A*) and in the presence of IbTx (*Figure 5.7B*). The summary concentration-effect curves in *Figure 5.7C* show that IbTx shifted the (*R*)-Butaprost concentration-effect curve to the right. For example, the (*R*)-Butaprost IC_{50} value increased from 49nM, (95% CI; 40 - 61nM) in control conditions to 165nM (95% CI; 129 - 207nM) in IbTx (n=6, N=5). These data suggest that the inhibitory effects of PGE_2 and activation EP2Rs on nerve-evoked contractions of ASM were reduced when BK channels were blocked.

Figure 5.8 demonstrates that inhibition of BK channels produced a similar effect on forskolin-induced inhibition of EFS-evoked contractions. Cumulative addition of forskolin induced concentration-dependent relaxations of ASM, under control conditions (*Figure 5.8A*) and these responses were reduced in the presence of IbTx (*Figure 5.8B)*. *Figure 5.8C* demonstrates that the mean IC_{50} for

forskolin was 28nM (95% CI; 18 - 44μM, n=9, N=6) under control conditions, compared to 196nM (95% CI; 150 - 259nM) in the presence of IbTx.

Next, we investigated if IbTx affected responses of the selective PKA activator, 6-MB-cAMP on EFS-evoked contractions. *Figures 5.9A&B* are representative tension recordings showing the effect of 6-MB-cAMP before (*Figure 5.9A*) and during the presence of IbTx (*Figure 5.9B*). *Figure 5.9C* shows that the IC_{50} for 6-MB-cAMP was 84μM (95% CI; 57 - 140μM) under control conditions versus 101μM (95% CI; 68 - 187μM) in IbTx (n=7, N=7). However, it is clear from *Figure 5.9C* that IbTx had greater inhibitory effect on the maximal relaxation induced by of 6-MB-cAMP. For example, relaxations induced by 1mM 6-MB-cAMP were reduced by 27% from 2.2±0.4 to 1.7±0.4mN in the presence of IbTx.

5.2.3 Effect of the K_v7 channel blocker XE-991 on PGE_2-induced relaxations of ASM

The results thus far, suggest that blockade of BK channels reduces EP2R/cAMP-mediated relaxations of ASM. Brueggemann *et al.* (2012), reported that K_v7 potassium channels are involved in the bronchodilation of guinea pig and human ASMCs, therefore, we examined if blockade of K_v7 channels might also affect PGE_2-induced relaxations of ASM. *Figures 5.10A&B* are representative recordings showing the effects of PGE_2 on CCh-evoked contractions, before and during the presence of the K_v7 channel blocker, XE-991. Summary concentration-effect curves shown in *Figure 5.10C* (n=7, N=5), show that XE-991 did not affect the PGE_2 responses. The mean IC_{50} for PGE_2 was 25nM (95% CI; 14 - 42nM) under control conditions versus 17nM (95% CI; 12nM to 25nM) in the presence of XE-991 (n=7, N=5). These data suggest that inhibition of K_v7 channels does not affect PGE_2-induced relaxations of ASM.

5.2.4 Effect of PKA and EPAC modulators on airway contraction

In addition to PKA, EPAC is regarded as an important cAMP effector (Kawasaki *et al.* 1998) and Roscioni *et al.* (2011) reported that EPAC was involved in β-adrenoreceptor-mediated relaxation of guinea pig and human tracheal rings. Therefore, we examined if the EPAC activator, 8-pCPT-2-O-Me-

cAMP-AM (007-AM) inhibited CCh-induced contractions of mouse ASM. *Figures 5.11A&B* are representative tension recordings illustrating that the EPAC activator 007-AM slightly reduced the amplitude of 1μM CCh-evoked contractions of ASM, and that these effects were reproducible. *Figure 5.11D* shows a summary bar chart for 8 similar experiments showing that repeated application of 007-AM inhibited the amplitude of CCh-evoked contractions by ~15%, from 5.1 ± 0.75 to 4.4 ± 0.74 ($p<0.01$) on the first application and 5.5 ± 0.75 to 4.7 ± 0.63 on the second application respectively ($p<0.001$, n=8, N=7).

Experiments were next performed to investigate the effect of joint application of the PKA and EPAC activators 6-MB-cAMP and 007-AM. *Figure 5.12A* demonstrates that 100μM 6-MB-cAMP reduced the amplitude of CCh-evoked contractions and co-addition of 10μM 007-AM further reduced the CCh response. Summary data in *Figure 5.12* show that 6-MB-cAMP reduced the mean amplitude of CCh-evoked contractions by 40% from 4.3 ± 0.54 to 2.6 ± 0.31 and that addition of 007-AM further reduced this by 34% to a total reduction of 74% (from 4.3 ± 0.54 to 1.1 ± 0.38, *Figure 5.12C*, ANOVA, $p<0.05$). *Figure 5.12B* is a representative tension recording showing a similar experiment, except that 007-AM was added first followed by 6-MB-cAMP. Similar results were achieved such that 007-AM alone reduced the amplitude of CCh-induced contraction by 19%, but in combination with 6-MB-cAMP reduced the amplitude by 77% from 4.8 ± 0.46 to 1.1 ± 0.37 (*Figure 5.12D*, ANOVA, $p<0.05$, $p<0.01$, n=7, N=5). These data suggest that EPAC and PKA act synergistically to inhibit CCh-evoked contractions and that both PKA and EPAC can elicit bronchodilation in mouse ASM. However, it remains unclear if these modulators mediate PGE_2-induced responses.

To confirm a role for PKA, in the inhibitory effects of PGE_2 on CCh-evoked contractions, we examined if the effects of PGE_2 were reduced in the presence of the PKA antagonist 8-(4-chlorophenylthio) adenosine-3',5'-cyclic monophosphate, Rp-isomer (Rp-8-CPT-cAMPs, 100μM). The selectivity of Rp-8-CPT-cAMPS for PKA was demonstrated by Roscioni *et al.* (2011) and Morgan *et al.* (2014), as it reduced the effects induced by the PKA activator 6-Bnz-cAMP but not those induced by the EPAC activator, 007-AM, in guinea pig and human ASM. *Figures 5.13A&B* are representative tension recordings showing PGE_2-

induced relaxations in control conditions (*Figure 5.13A*) and in the presence of Rp-8-CPT-cAMPs (*Figure 5.13B*). The summary concentration-effect curves in *Figure 5.13C* show that Rp-8-CPT-cAMPs shifted the PGE_2 concentration-effect curve to the right. For example, the PGE_2 IC_{50} value increased from 34nM, (95% CI; 27 – 44nM) in control conditions to 107nM (95% CI; 78 – 146nM) in Rp-8-CPT-cAMPs (n=7, N=6). The maximum inhibitory effect of PGE_2 was also affected in the presence of Rp-8-CPT-cAMPs, from 100% in control conditions to 62% in the presence of the PKA inhibitor.

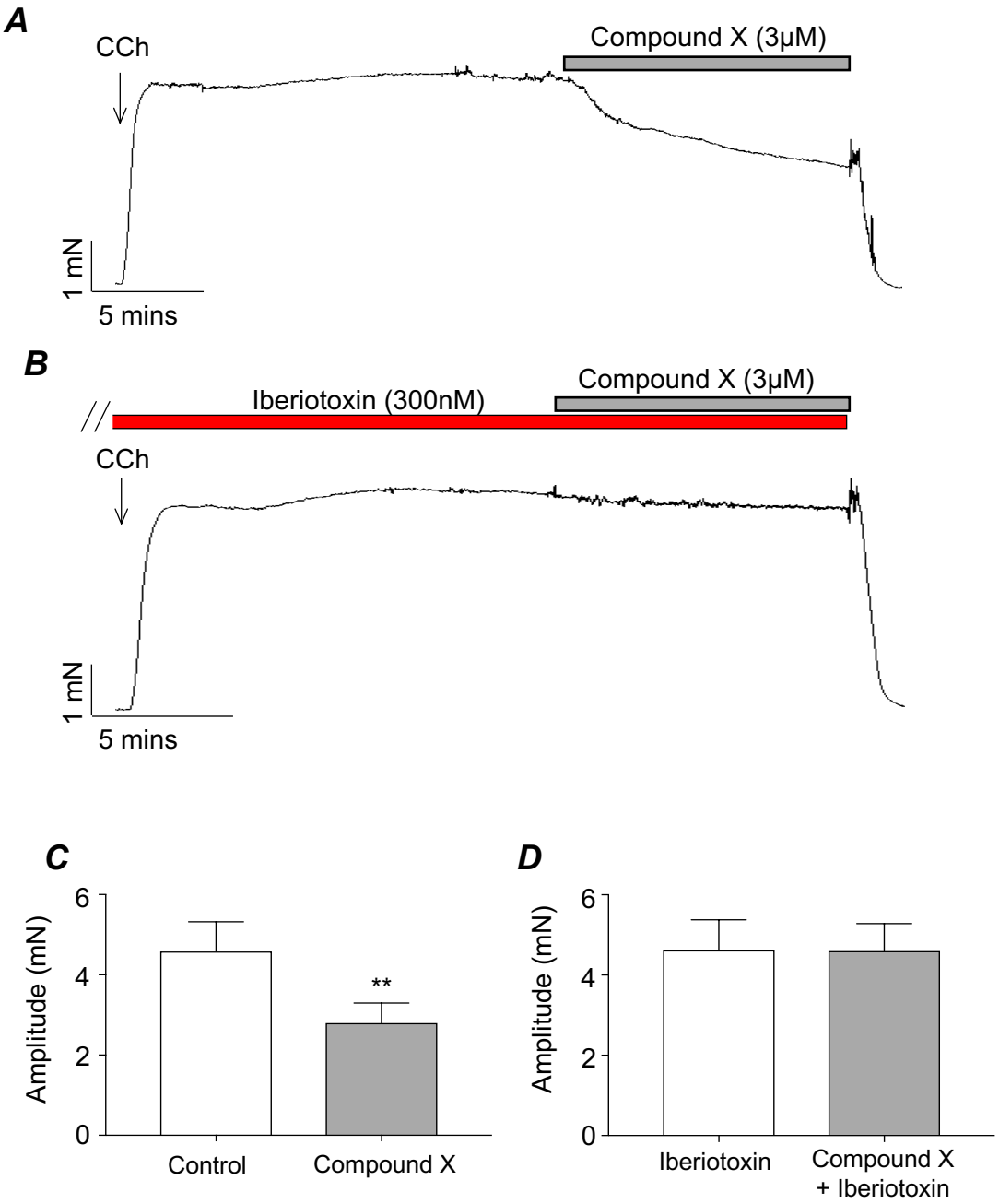

Figure 5.1. ***Effect of the BK channel blocker, iberiotoxin on Compound X-evoked relaxations of mouse bronchial rings.*** (**A** & **B**) Representative tension recordings showing the effect of the BK channel opener, Compound X (3μM) on CCh-evoked contractions in the absence (**A**) and presence of iberiotoxin (300nM, **B**). Summary bar charts plotting mean contraction amplitude from 6 similar experiments showing the effect of Compound X (3μM) on CCh-induced contractions under control conditions (**C**, n=6, N=5, **p<0.01, paired t-test) and in the presence of iberiotoxin (**D**).

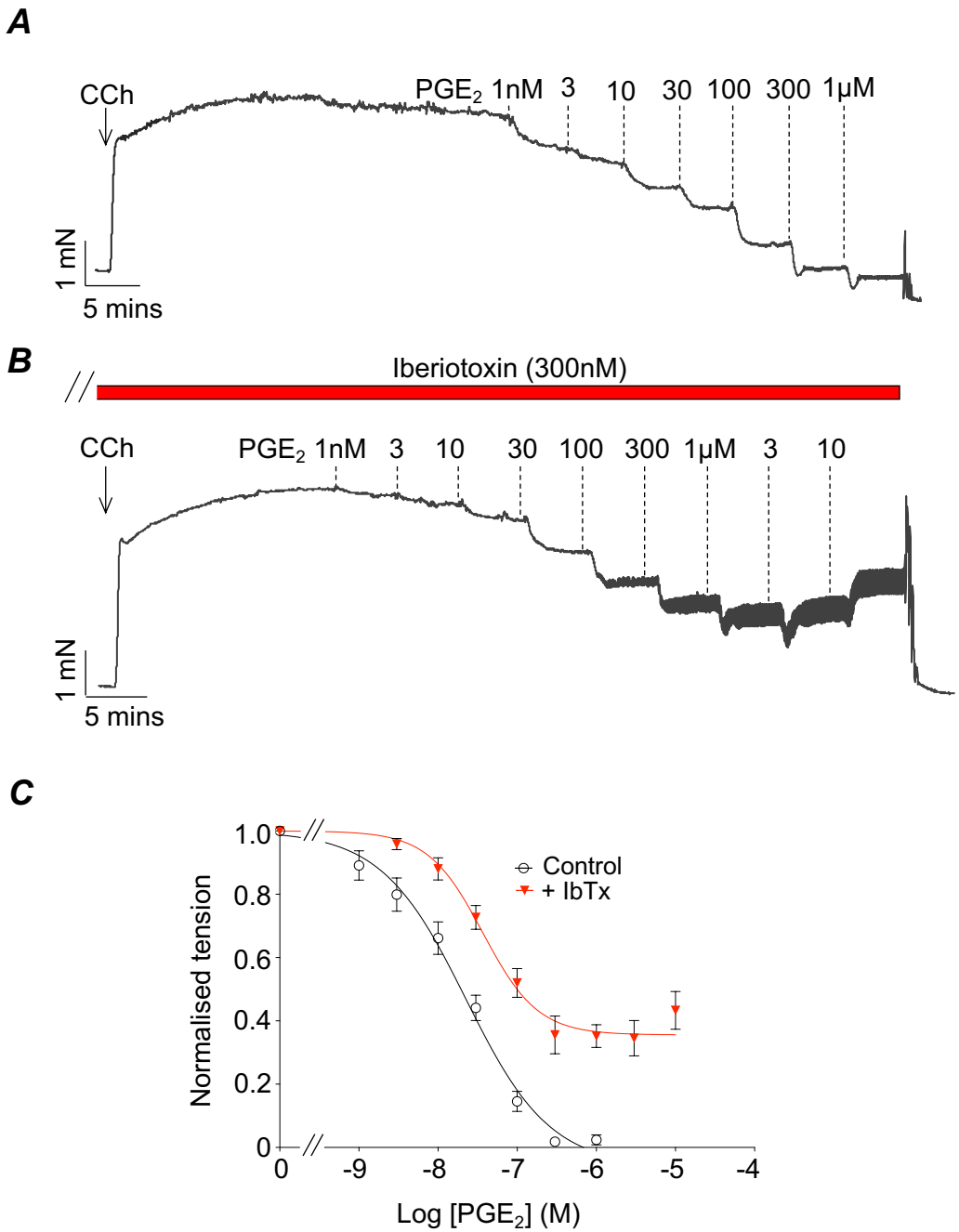

Figure 5.2. ***Effect of the BK channel blocker, iberiotoxin on PGE_2-induced relaxations of mouse bronchial rings.*** (**A** & **B**) Representative tension recordings exhibiting the effect of PGE_2 (1nM–10µM) on CCh-evoked contractions in the absence (**A**) and presence of iberiotoxin (300nM, **B**). (**C**) Summary concentration-effect curves for PGE_2 (n=7, N=6) before (IC_{50} = 22nM) and after incubation with iberiotoxin (IC_{50}= 34nM). The maximum inhibitory effect of PGE_2 in control was 100% compared to 70% in the presence of iberiotoxin.

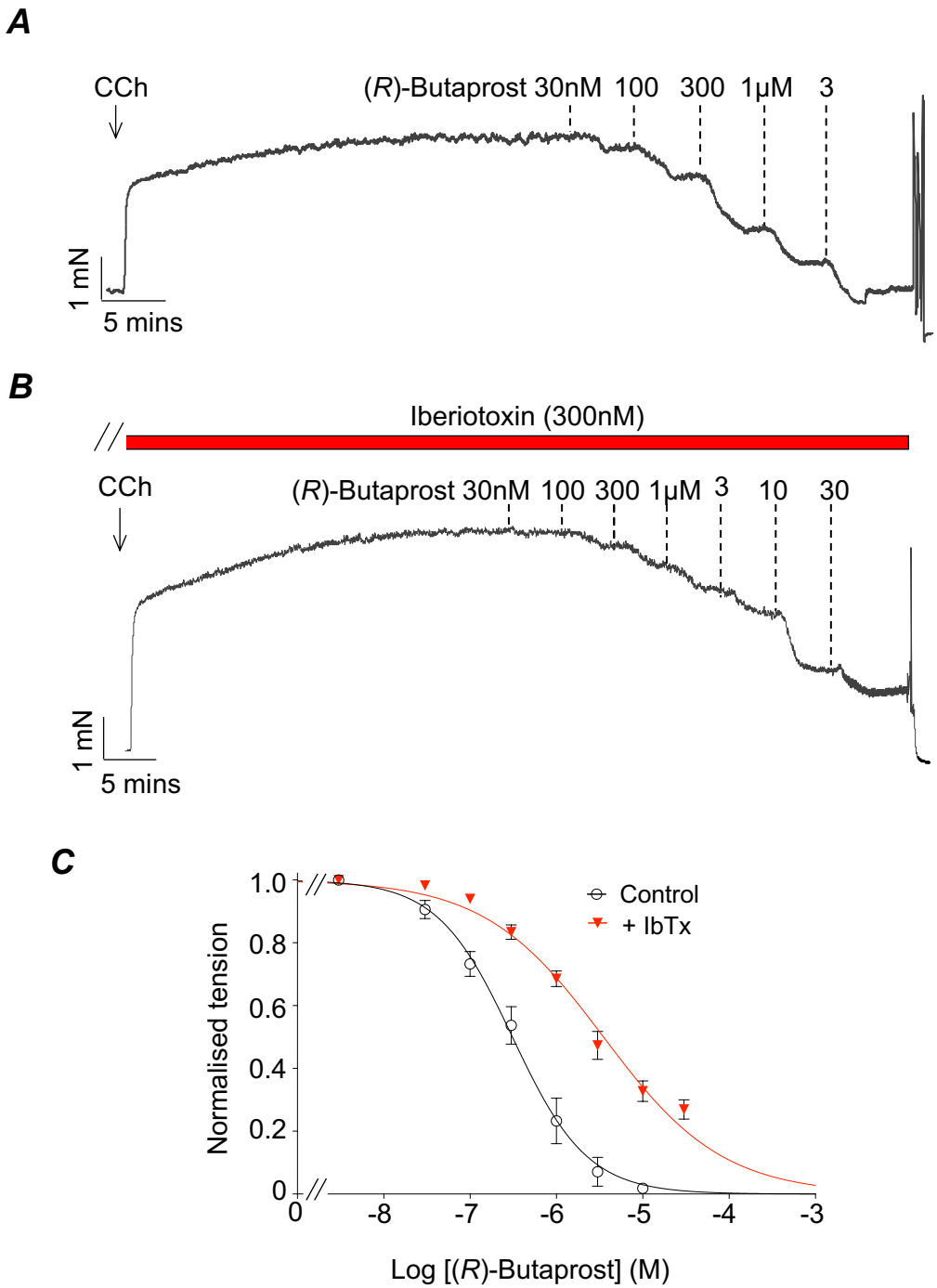

Figure 5.3. ***Effect of the BK channel blocker, iberiotoxin on relaxations of mouse bronchial rings induced by the selective EP_2 receptor agonist (R)-Butaprost***. (**A** & **B**) Representative tension recordings exhibiting the effect of (*R*)-Butaprost (30nM–30μM) on CCh-evoked contractions in the absence (**A**) and presence of iberiotoxin (300nM, **B**). (**C**) Summary concentration-effect curves for (*R*)-Butaprost (n=6, N=5) in the absence (IC_{50}= 310nM) and presence of iberiotoxin (IC_{50}= 3.5μM).

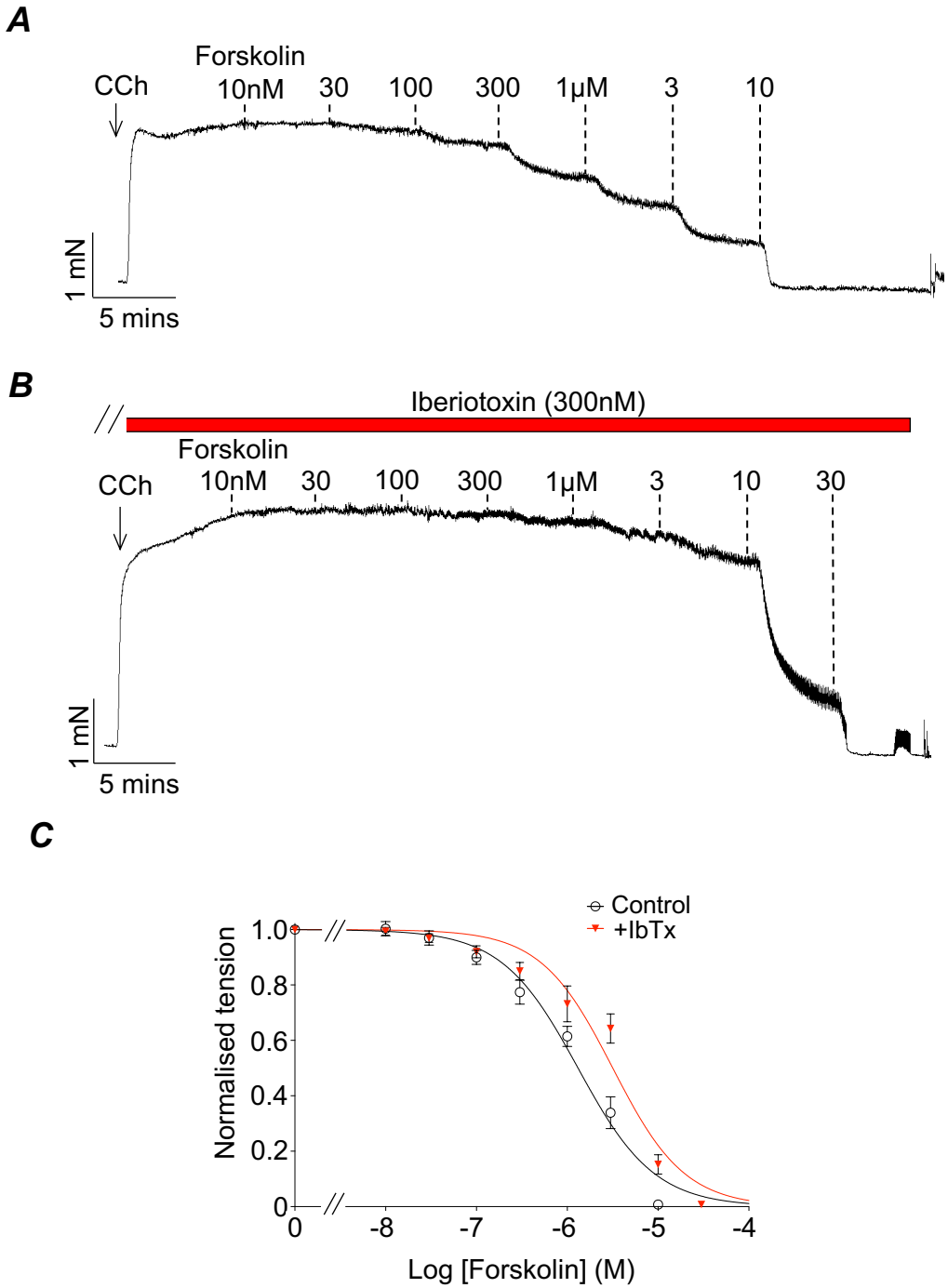

Figure 5.4. ***Effect of the BK channel blocker, iberiotoxin on forskolin-induced relaxations of mouse bronchial rings.*** (**A** & **B**) Representative tension recordings exhibiting the effect of selective AC activator forskolin (10nM–30μM) on CCh-evoked contractions in the absence (**A**) and presence of iberiotoxin (300nM, **B**). (**C**) Summary concentration-effect curves for forskolin (n=7, N=7) in the absence (IC_{50}= 1.3μM) and presence of iberiotoxin (IC_{50}= 3.2μM).

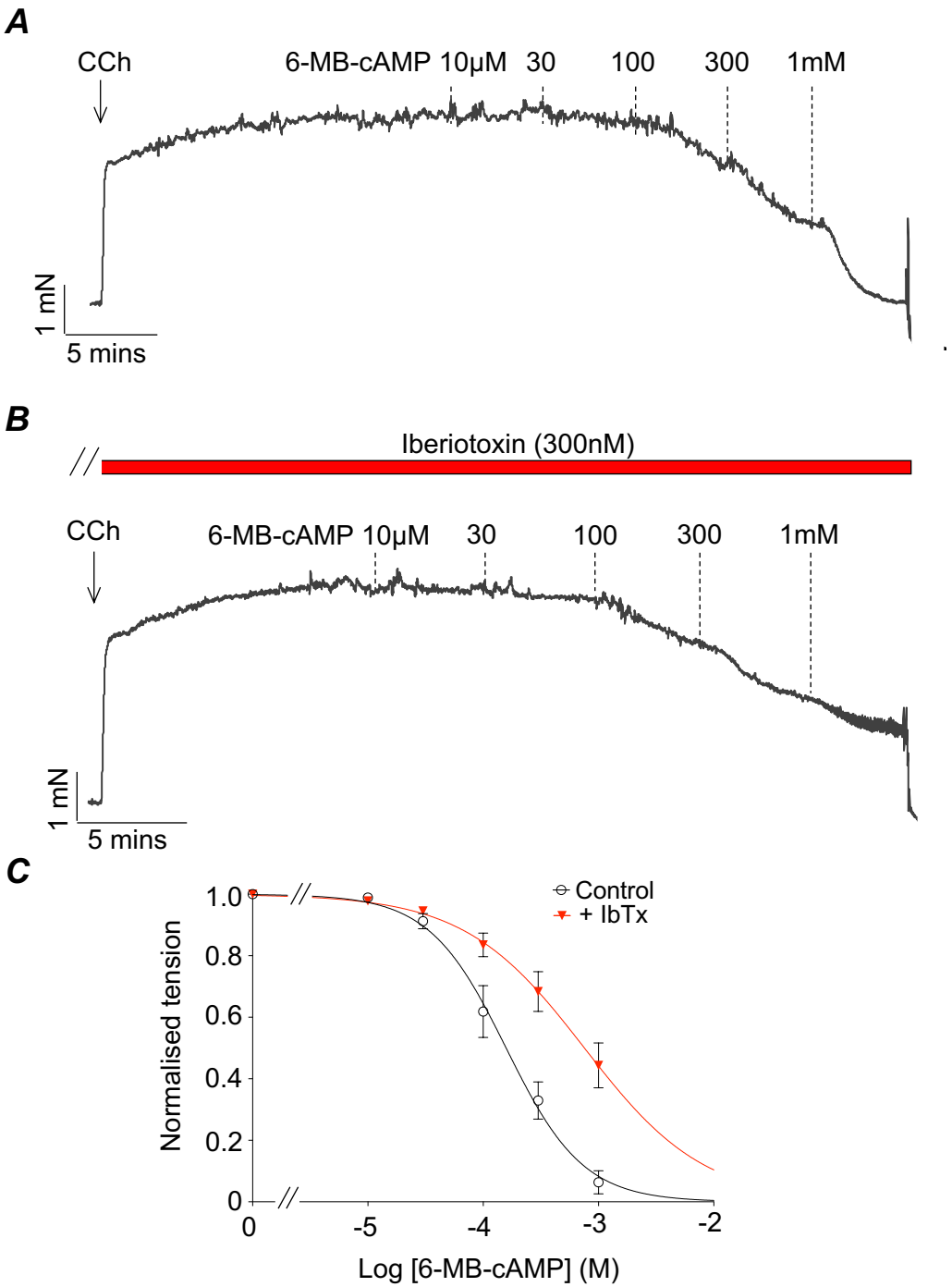

Figure 5.5. ***Effect of the BK channel blocker, iberiotoxin on 6-MB-cAMP-induced relaxations of mouse bronchial rings.*** (**A** & **B**) Representative tension recordings exhibiting the effect of the selective PKA activator, 6-MB-cAMP (10µM–1mM) on CCh-evoked contractions of ASM in the absence (**A**) and presence of iberiotoxin (300nM, **B**). (**C**) Summary concentration-effect curves for 6-MB-cAMP (n=10, N=10) in the absence (IC_{50}= 158µM) and presence of iberiotoxin (IC_{50}= 760µM).

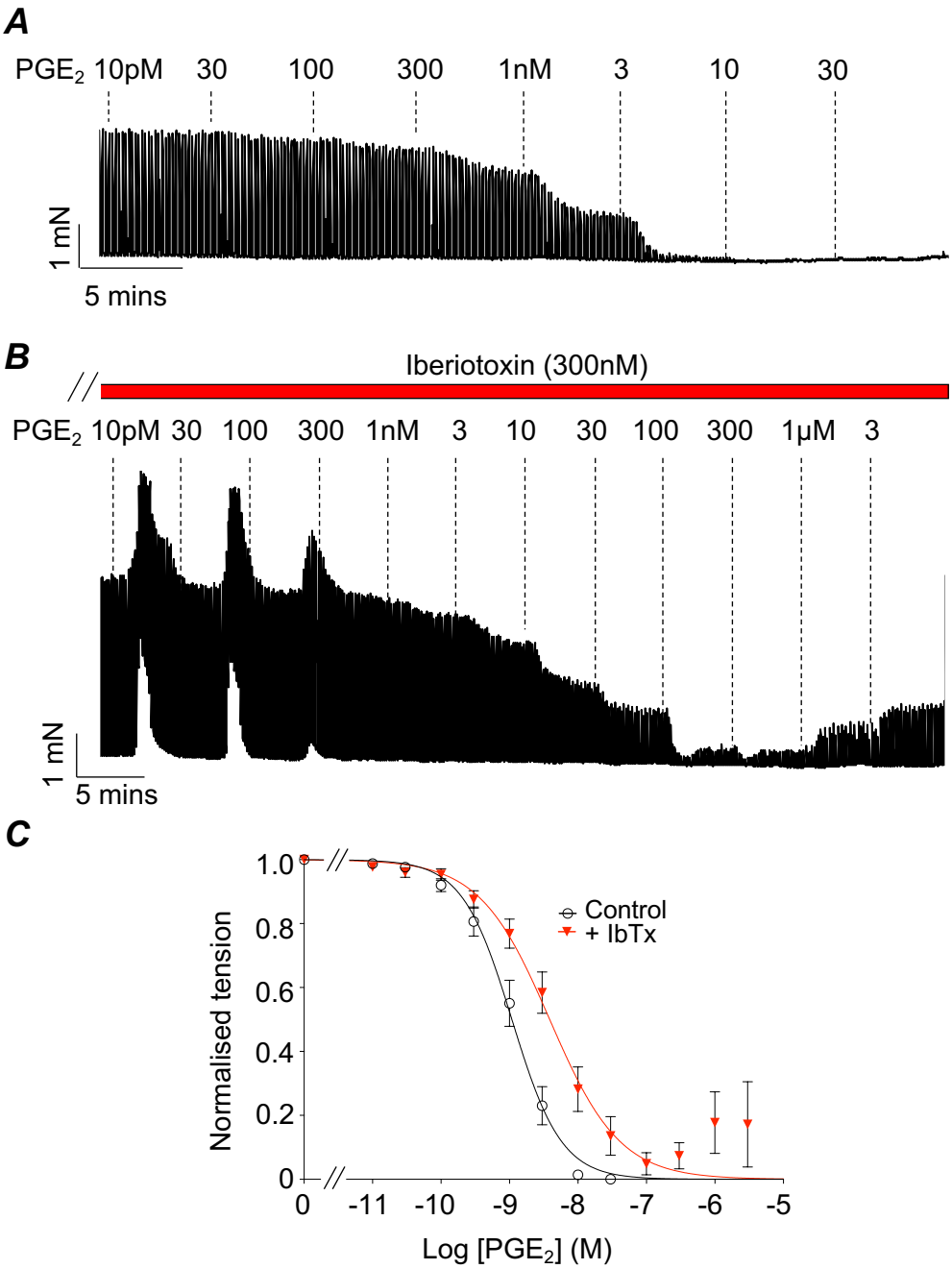

Figure 5.6. ***Effect of the BK channel blocker, iberiotoxin on PGE_2-induced inhibition of nerve-induced contractions of mouse bronchial rings.*** (**A** & **B**) Representative tension recordings exhibiting the effect of PGE_2 (1pM–3μM) on EFS-evoked contractions (2Hz) in the absence (**A**) and presence of iberiotoxin (300nM, **B**). (**C**) Summary concentration-effect curves for PGE_2 (n=8, N=7) before (IC_{50}= 1.3nM) and during incubation with iberiotoxin (IC_{50}= 3.9nM).

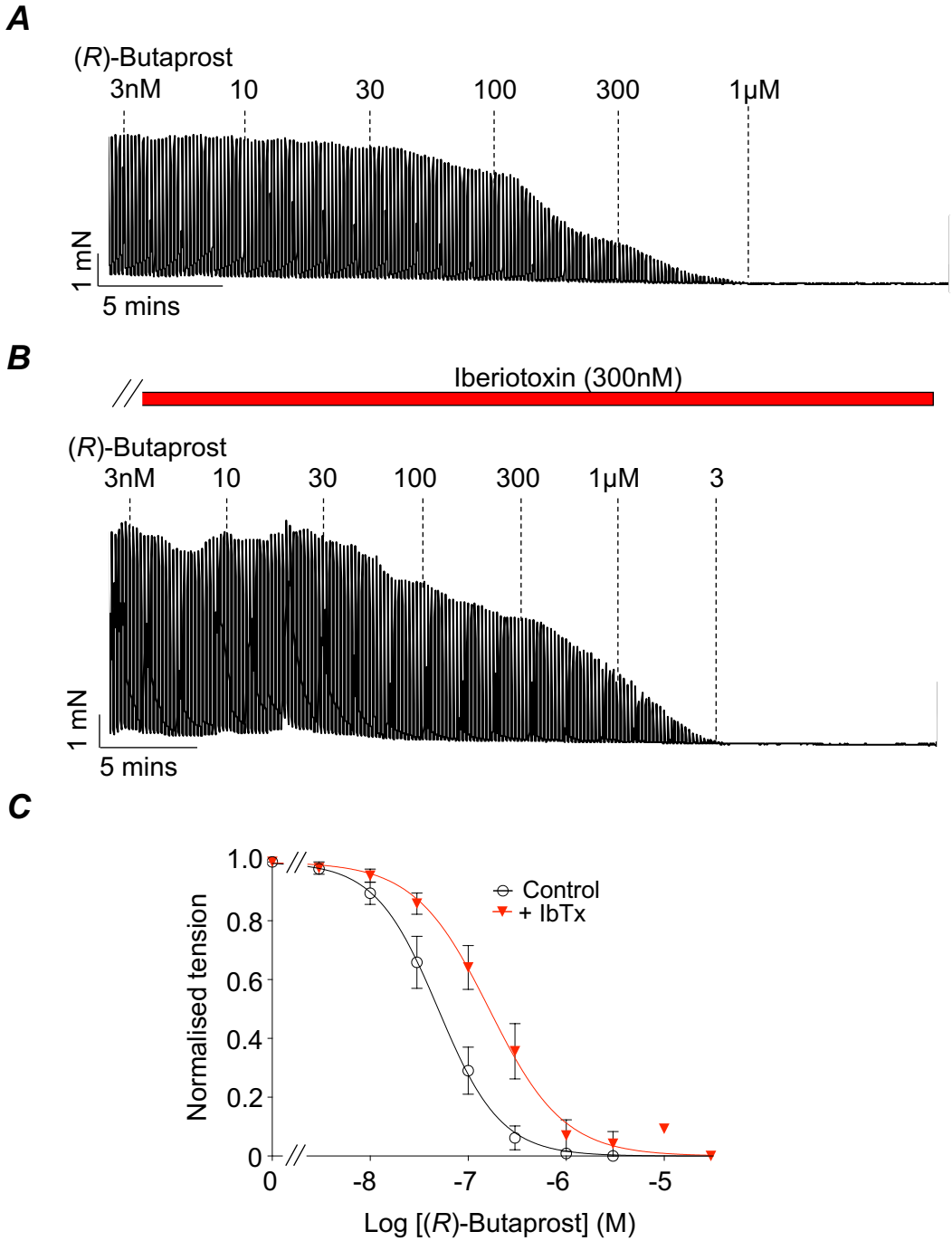

Figure 5.7. ***Effect of the BK channel blocker, iberiotoxin on (R)-Butaprost-induced inhibition of nerve-induced (2Hz) contractions of mouse bronchial rings.*** (**A** & **B**) Representative tension recordings exhibiting the effect of (*R*)-Butaprost (3nM–10μM) on EFS-evoked contractions in the absence (**A**) and presence of iberiotoxin (300nM, **B**). (**C**) Summary concentration-effect curves for (*R*)-Butaprost (n=6, N=5) before (IC_{50}= 49nM) and following incubation with iberiotoxin (IC_{50}= 165nM).

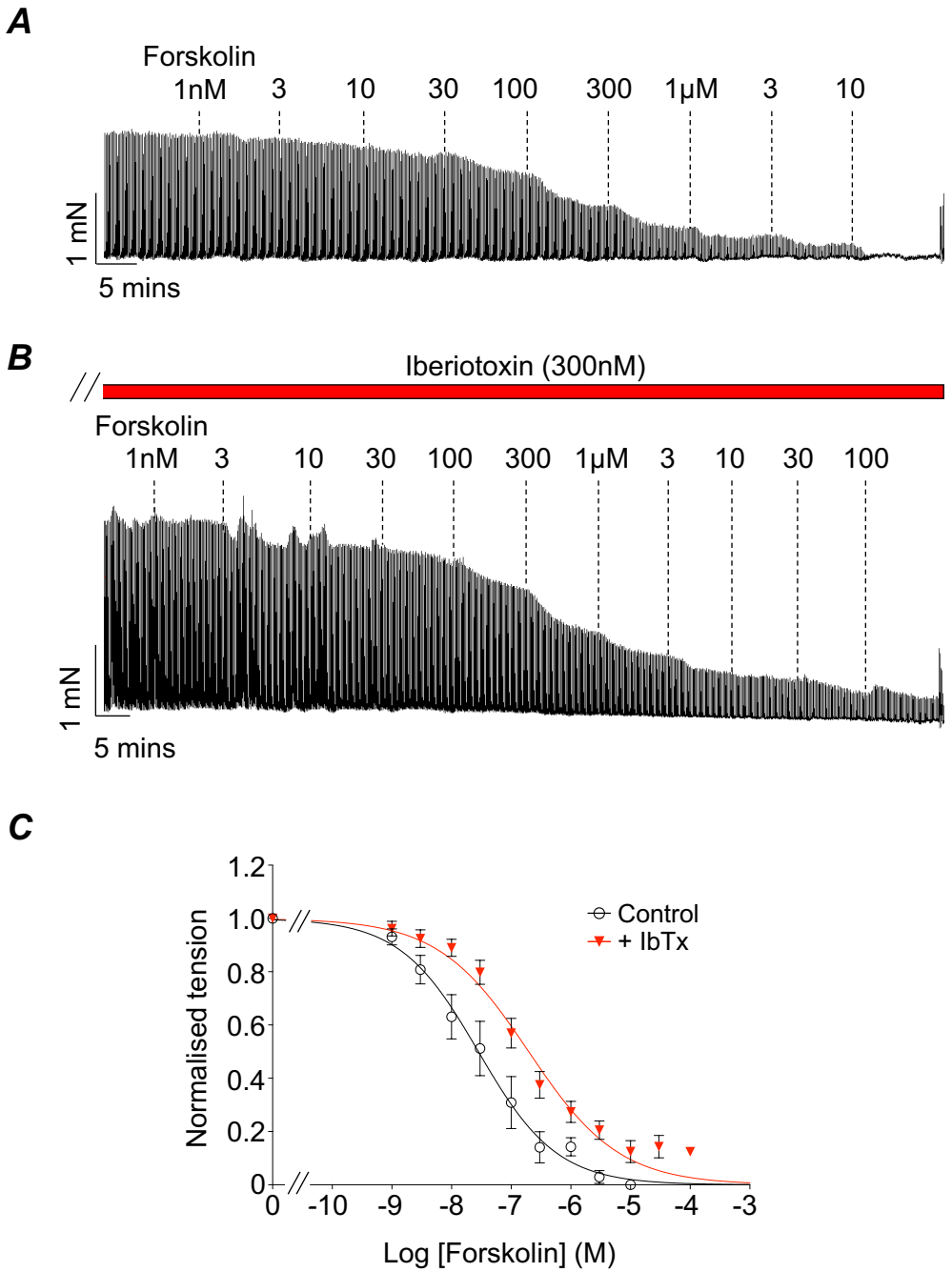

Figure 5.8. ***Effect of the BK channel blocker, iberiotoxin on forskolin-induced inhibition of nerve-stimulated (2Hz) contractions of mouse bronchial rings.*** (**A** & **B**) Representative tension recordings exhibiting the effect of forskolin (1nM–100μM) on EFS-evoked contractions in the absence (**A**) and presence of iberiotoxin (300nM, **B**). (**C**) Summary concentration-effect curves for forskolin (n=9, N=6) before (IC_{50}= 28nM) and following incubation with iberiotoxin (IC_{50}= 196nM).

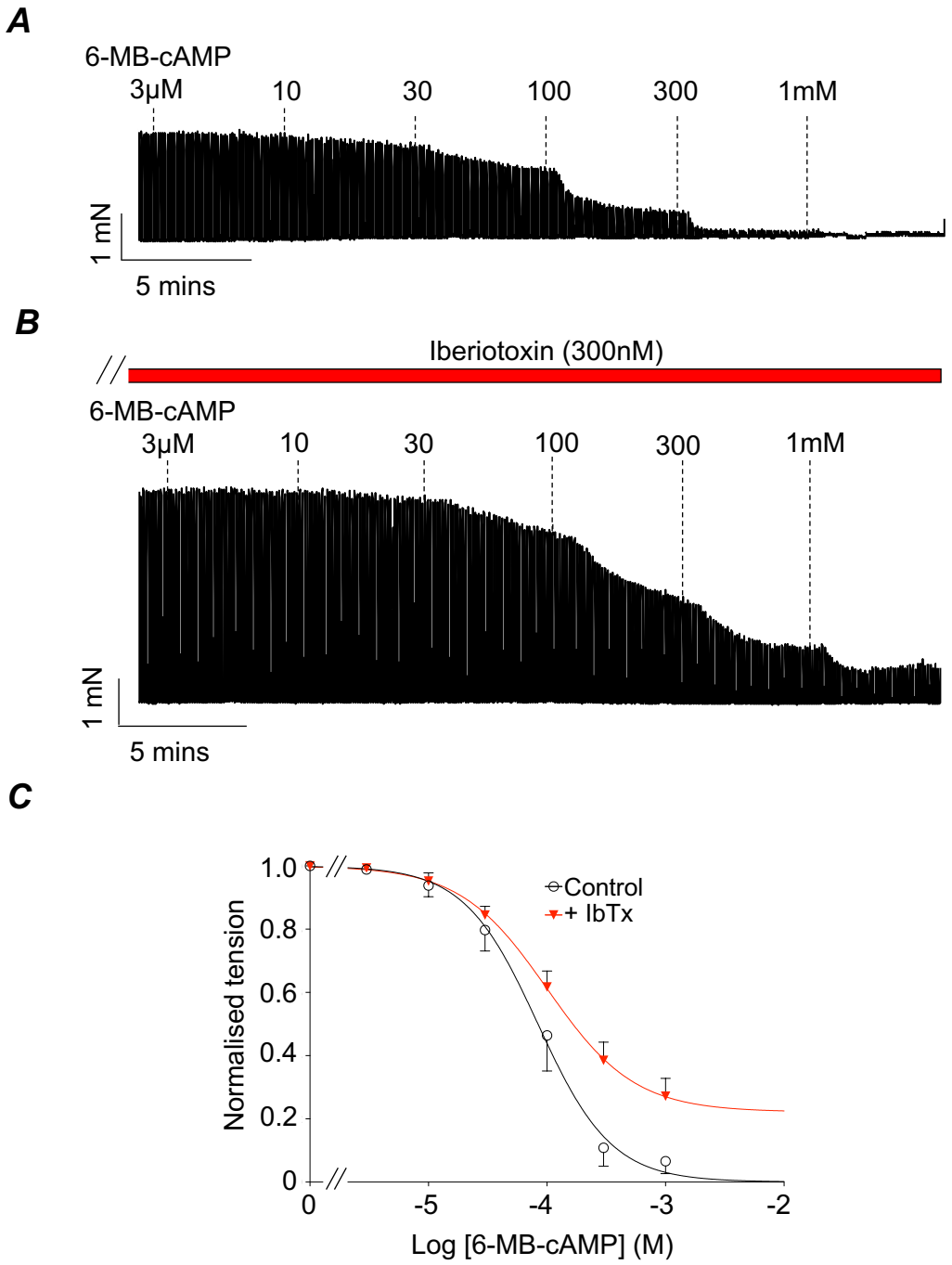

Figure 5.9. ***Effect of the BK channel blocker, iberiotoxin on 6-MB-cAMP-induced inhibition of nerve (2Hz)–evoked contractions of mouse bronchial rings.*** (**A** & **B**) Representative tension recordings showing the effect of 6-MB-cAMP (3μM–1mM) on EFS-evoked contractions in the absence (**A**) and presence of iberiotoxin (300nM, **B**). (**C**) Summary concentration-effect curves for 6-MB-cAMP (n=7, N=7) before (IC_{50}= 84μM) and following incubation with iberiotoxin (IC_{50}= 101μM).

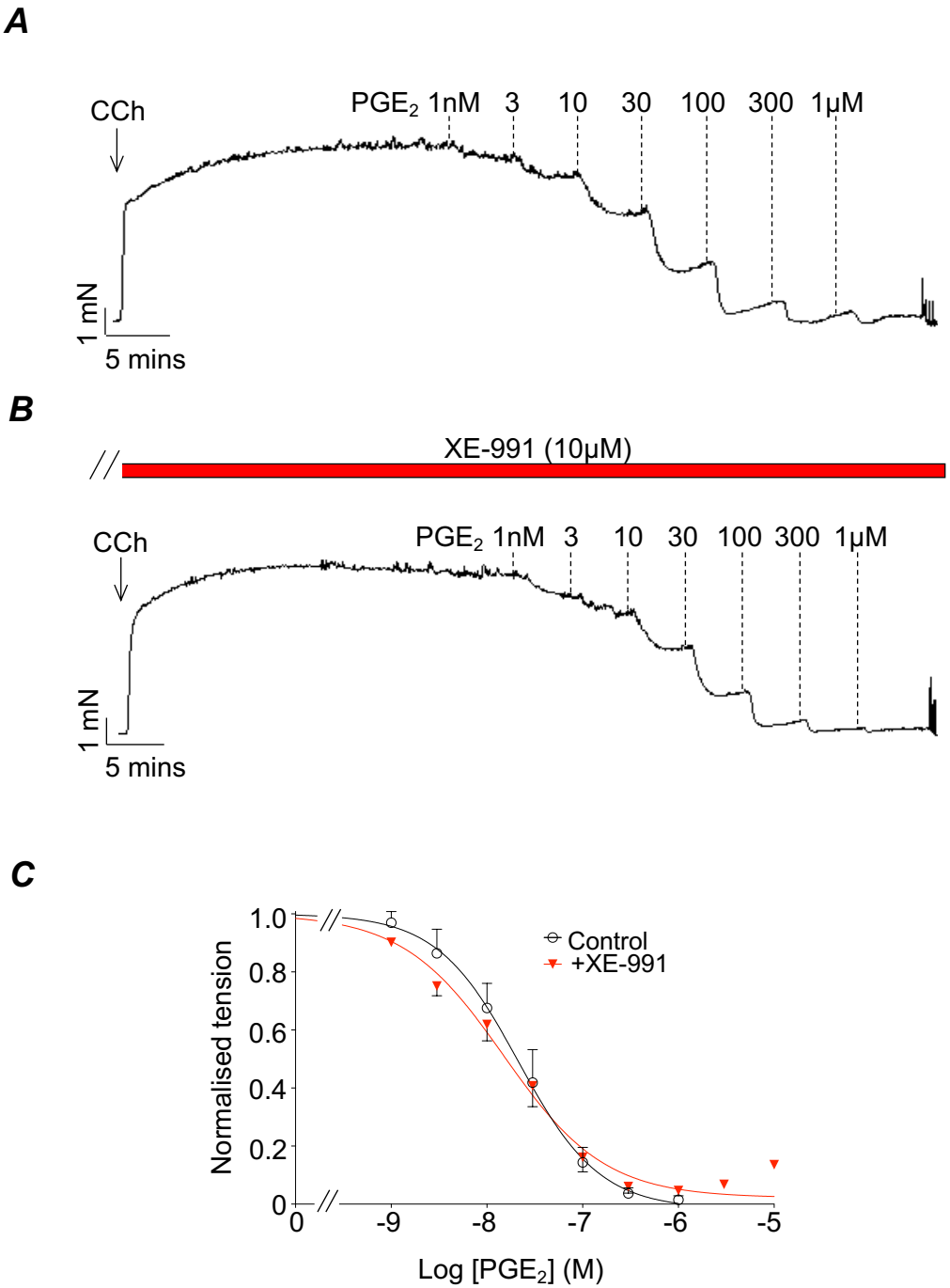

Figure 5.10. ***Effect of K_v7 channel blocker, XE-991 on PGE_2-induced relaxations of mouse bronchial rings.*** (**A** & **B**) Representative tension recordings exhibiting the effect of PGE_2 (1nM–1μM) on CCh-evoked contractions in the absence (**A**) and presence of XE-991 (10μM, **B**). (**C**) Summary concentration-effect curves for PGE_2 (n=7, N=5) before (IC_{50}= 25nM) and after incubation with XE-991 (IC_{50}= 17nM).

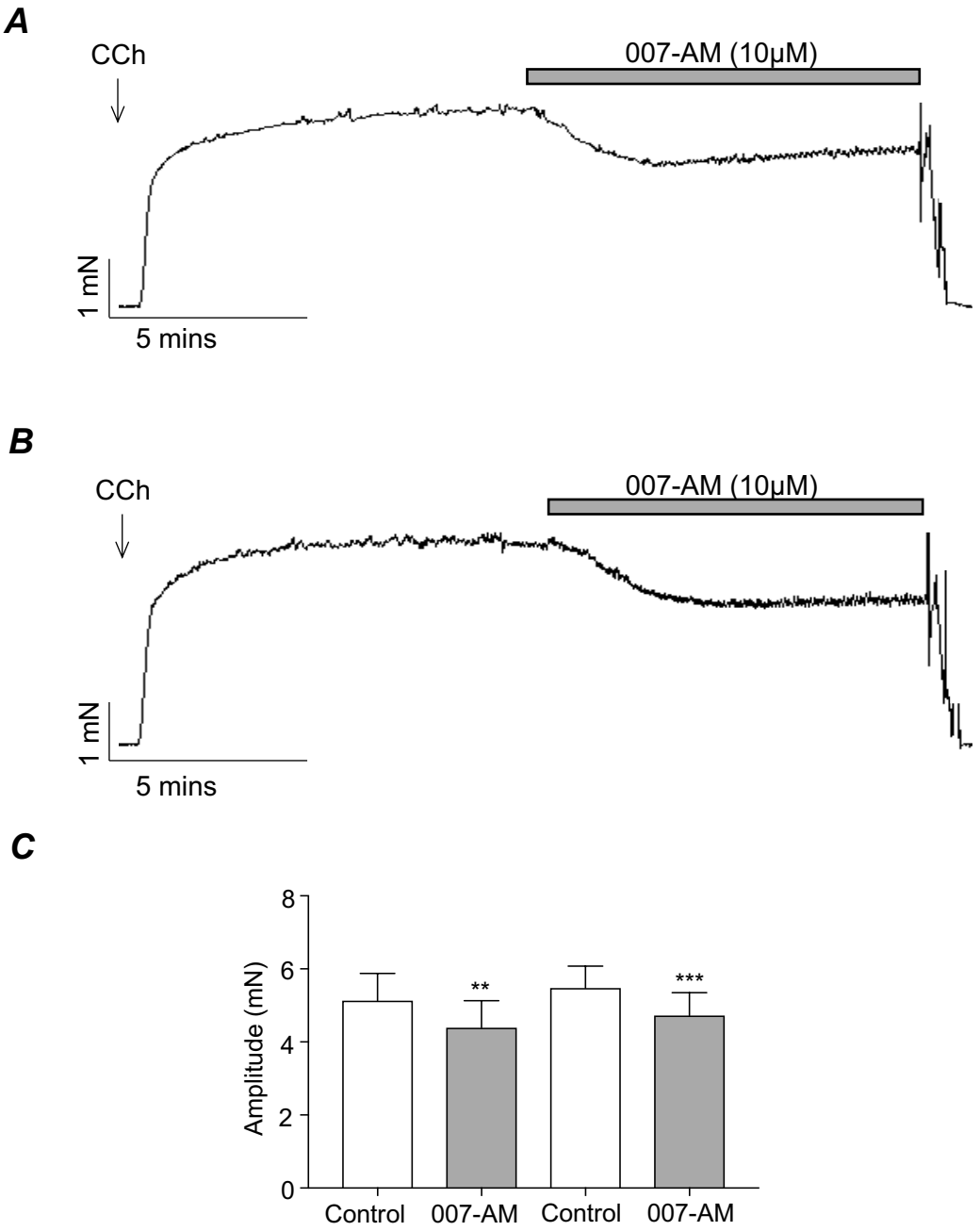

Figure 5.11. ***Effect of of 007-AM on CCh-evoked contractions of mouse bronchial rings.*** (**A** & **B**) Representative tension recordings exhibiting the effect of two 007-AM (10μM) additions on CCh-evoked contractions (1μM). (**C**) Summary bar charts showing the mean amplitude of two consecutive additions of 007-AM compared with control (n=8, N=7, **p<0.01, *** p<0.001, ANOVA).

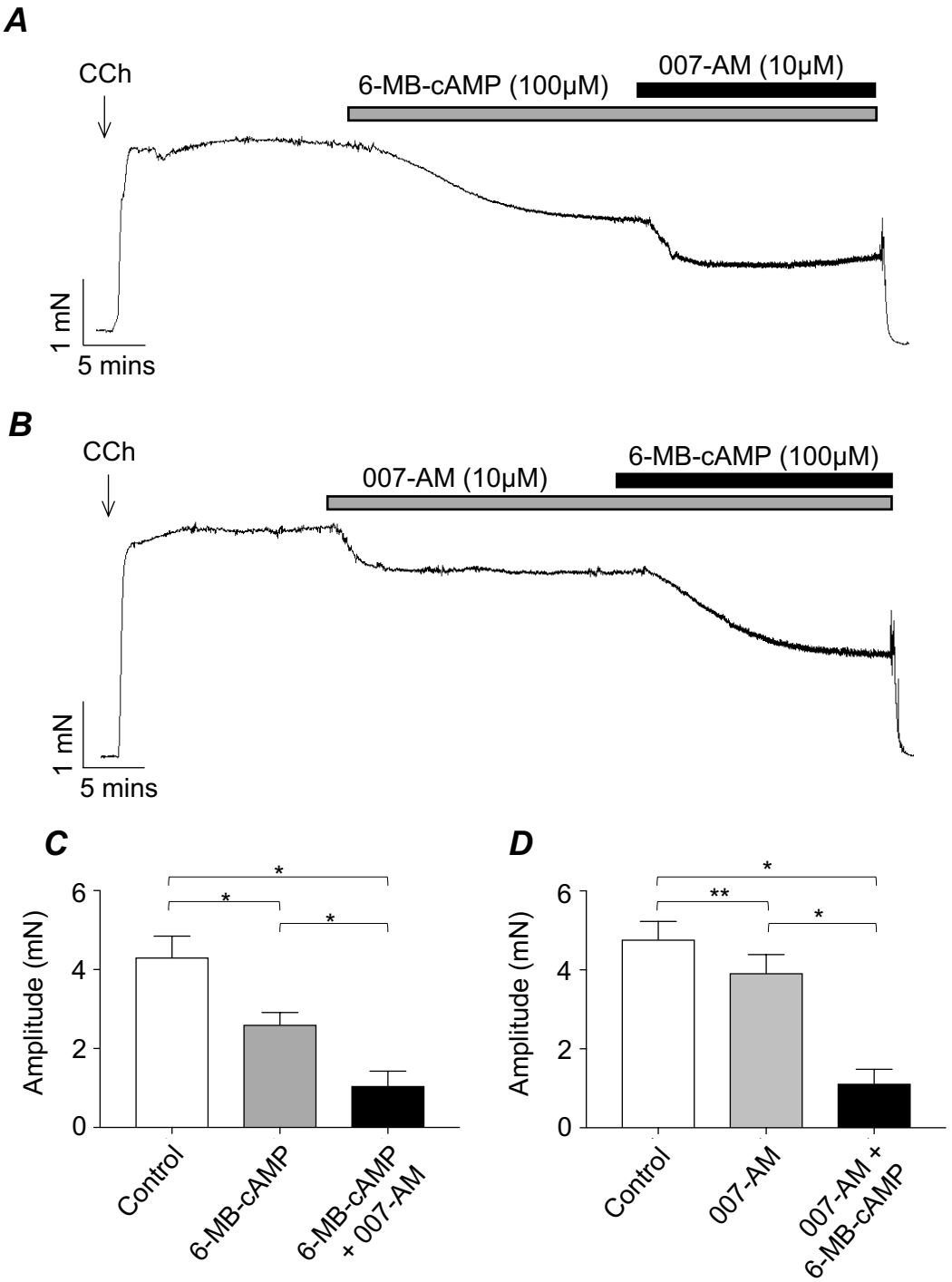

Figure 5.12. ***Effect of 6-MB-cAMP and 007-AM on CCh-evoked contractions of mouse bronchial rings.*** (**A**) Representative tension recording showing the effect of 6-MB-cAMP (100μM), followed by 007-AM (10μM) on CCh-evoked contraction of ASM. (**B**) Representative tension recording exhibiting the effect of 007-AM (10μM), then 6-MB-cAMP (100μM) on the remaining contraction. (**C & D**) Summary bar charts showing the effect of 6-MB-cAMP plus 007-AM on mean contraction amplitude (n=7, N=5, *p<0.05, **p<0.01).

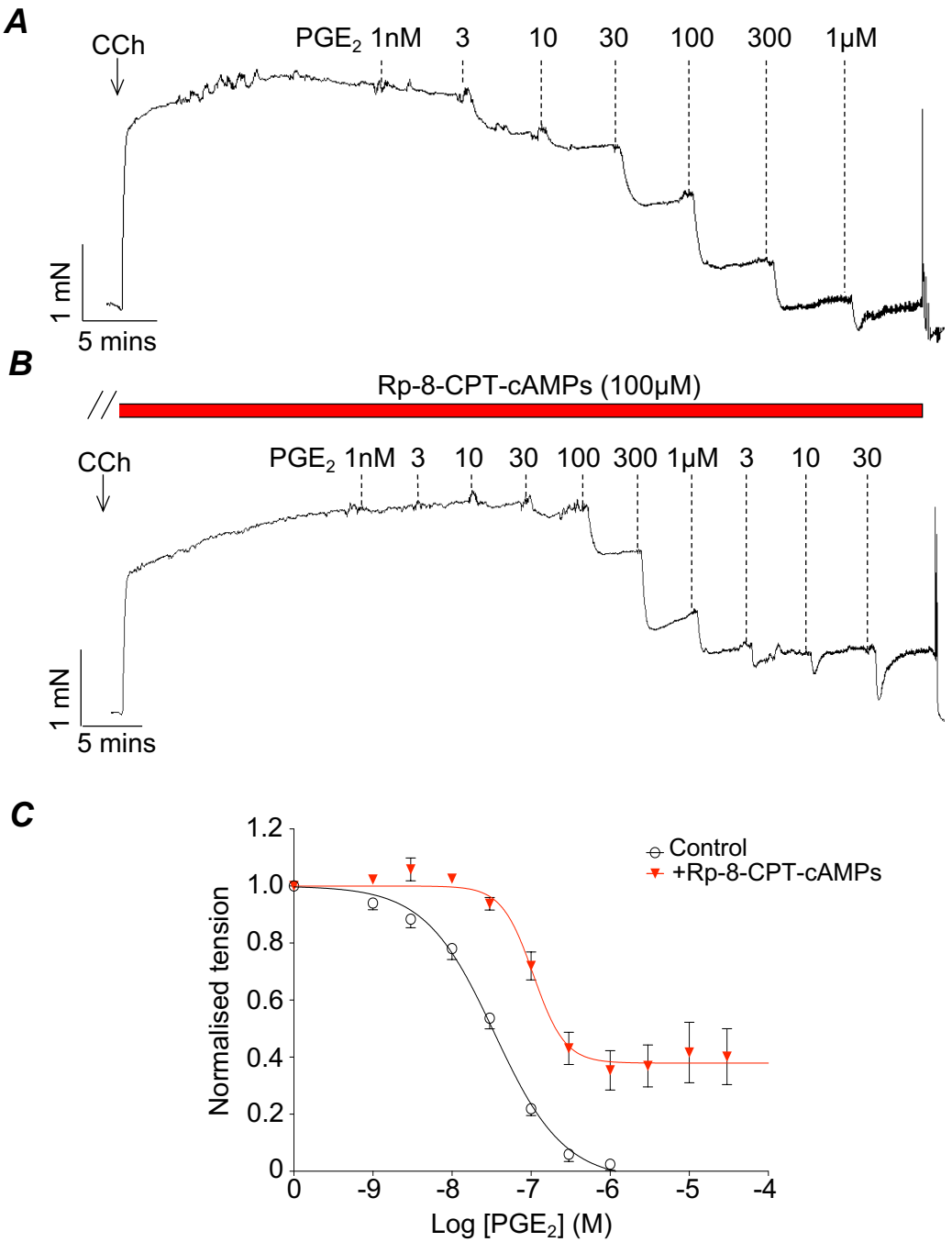

Figure 5.13. ***Effect of the PKA antagonist, Rp-8-CPT-cAMPs on PGE_2-induced relaxations of mouse bronchial rings.*** (**A** & **B**) Representative tension recordings exhibiting the effect of PGE_2 (1nM–30μM) on CCh-evoked contractions in the absence (**A**) and presence of Rp-8-CPT-cAMPs (100μM, **B**). (**C**) Summary concentration-effect curves for PGE_2 (n=7, N=6) before (IC_{50} = 34nM) and after incubation with Rp-8-CPT-cAMPs (IC_{50}= 107nM). The maximum inhibitory effect of PGE_2 in control was 100% compared to 62% in the presence of Rp-8-CPT-cAMPs.

5.3 Discussion

In this chapter we found that the amplitude of PGE_2-induced relaxations of mouse ASM were reduced by the BK channel blocker IbTx, but not the K_v7 channel blocker XE-991. Additionally, we demonstrated that the amplitude of CCh-evoked contractions was reduced by the the PKA and EPAC agonists, 6-MB-cAMP and 007-AM respectively. Furthermore, PGE_2-induced relaxations were diminished in the presence of the PKA inhibitor, Rp-8-CPT-cAMPs, consistent with a role for PKA in PGE_2-mediated relaxations of mouse ASM.

Previous studies have reported that the inhibitory effects of PGE_2 in the airways are mediated via activation of adenylate cyclase, and subsequent increase of intracellular cAMP (Lebender *et al.* 2018; Konya *et al.* 2013; Billington *et al.* 2013; Aso *et al*. 2013; Tilley *et al.* 2003; Spicuzza *et al.* 1998). Upregulation of cAMP activates PKA, and possibly EPAC, to induce relaxation, however the cellular mechanisms underlying the effects of cAMP in mouse ASM are not yet entirely understood (Lebender *et al.* 2018; Konya *et al.* 2013; Zhu *et al*. 2002). In the present study we found that, the inhibitory effects of PGE_2 on mouse ASM were reduced by the BK channel blocker, IbTx. Zhu *et al.* (2002), reported similar findings in human coronary artery smooth muscle cells, reporting that application of PGE_2 to intact human coronary artery myocytes stimulated BK channel activity, via activation of PKG. In the present study we found that the inhibitory effects of PGE_2 were mimicked by the AC and PKA activators, forskolin and 6-MB-cAMP, respectively and that these effects were inhibited by IbTx. Therefore, these data suggest the effects of PGE_2 in ASMC are likely to involve activation of AC and upregulation of PKA. These data agree with findings by Hiramatsu *et al.* (1994), who demonstrated that the inhibitory effects of forskolin and β-adrenoreceptor agonist, isoproterenol on CCh-contracted guinea pig trachea were suppressed by the application of the selective BK channel blocker, charybdotoxin (ChTx). Furthermore, Hiramatsu and colleagues found that application of forskolin stimulated BK channel activity in single channel recordings of porcine tracheal myocytes. Similarly, Kume *et al.* (1994) reported that the catalytic subunit of cAMP dependent PKA also activated BK channels in porcine and ferret ASMCs. Huang *et al.* (1993) found that β_2-adrenoreceptor agonist, salbutamol-induced

relaxations of guinea pig ASM were reduced in the presence of 50nM IbTx. However, it was determined that this effect was not a result of direct interaction between β_2-adrenoreceptor activation and BK channels but rather, because blockade of BK channels produced membrane depolarisation resulting in calcium influx via voltage-gated calcium channels, which functionally antagonised the inhibitory response. Therefore, further investigation would be necessary to determine if PGE_2 activates BK channels in mouse ASM, or if PGE_2 is less effective at relaxing the tissue when BK channels are blocked, and membrane potential is depolarised. Although, not conclusive, the finding that PGE_2 responses were unaffected by XE-991, which has been shown to cause depolarisation of ASM cells (Evseev *et al.* 2013), suggests that PGE_2 may lead to BK channel activation. The role of K_V7 channels in ASM will require further investigation as, in contrast to the results in the present study, Brueggemann *et al.* (2012) reported that K_V7 channels were involved in the bronchodilation of guinea pig and human ASMCs.

In the presence of IbTx, we found that the application of higher concentrations of PGE_2, but not the selective EP2R agonist (*R*)-Butaprost, induced contractions in mouse ASM. Therefore, it seems likely that the contractile effects of PGE_2 resulted from activation of a different EP receptor subtype which is normally masked by the inhibitory effects induced by EP2R activation. PGE_2 can also act on the excitatory prostanoid E receptors EP1 and EP3 (Buckley *et al*. 2011; Sugimoto and Narumiya 2007; McGraw *et al.* 2006; Burgess *et al.* 2004). Buckley *et al.* (2011) reported that application of PGE_2 on guinea pig tracheal strips at rest, elicited contraction that was abolished by an EP1 antagonist, however when the tissue was pre-contracted with CCh application of the same range of concentrations of PGE_2 evoked relaxations. In addition, Tilley *et al.* (2003) demonstrated that airway hyperresponsiveness following exposure to aerosolised PGE_2 was significantly decreased in EP1 $^{-/-}$ and EP3 $^{-/-}$ mice. Therefore, the contractile effects modulated by PGE_2 are likely due to activation of EP1 and/or EP3Rs, however further investigation would be necessary to confirm this idea.

Conventionally, PKA was considered the only downstream effector molecule responsible for cAMP-induced smooth muscle relaxation (Torphy 1994) however, a number of studies have now highlighted an important role of EPAC

in cAMP responses (Humphries *et al.* 2017; Roscioni *et al.* 2011; Zieba *et al.* 2011; Kawasaki *et al.* 1998). We found that application of 6-MB-cAMP and 007-AM elicited synergistic effects in mouse ASM. For example, the inhibitory effect of 007-AM doubled when applied in the presence of 6-MB-cAMP. Li *et al.* (2007), also reported synergistic effects of PKA and EPAC on neurotensin release in endocrine cultured cells expressing the neurotensin N gene. Neurotensin release following incubation with PKA (6-Phe-cAMP) and EPAC (pMeOPT-cAMP) activators were augmented when compared to either incubation with the PKA or EPAC activators alone. Zieba *et al.* (2011) and Roscioni *et al.* (2011), both reported a role for EPAC in relaxation of ASM induced by β-adrenoreceptor agonists. These responses were found to involve downregulation of Rho A, decreasing MLC phosphorylation. Whereas, Roscioni *et al.* (2011) demonstrated that upregulation of PKA by the PKA agonist, 6-Bnz-cAMP and β-adrenoreceptor agonist, isoproterenol led to phosphorylation of the specific PKA substrate vasodilator-stimulated phosphoprotein (VASP) in guinea pig tracheal rings pre-contracted with MCh. This phosphorylation was not observed following activation of EPAC by 007-AM, suggesting that this pathway was exclusively mediated by activation of PKA. Therefore, it is possible that cooperative downstream actions of PKA and EPAC on independent pathways may elicit the potent bronchodilation observed with G_s/cAMP activation in mouse ASM.

It is clear from the present study that activation of PKA and/or EPAC can elicit bronchodilation of mouse ASM, however, it does not necessarily mean that PKA and EPAC were involved in the inhibitory effects induced by PGE_2. Determining a role for EPAC in this effect is difficult due to a lack of selective antagonists (Li *et al.* 2020; Zhu *et al.* 2015; Brown *et al.* 2014; Rehmann 2013). However, Rp-8-CPT-cAMPS is regarded as a selective PKA inhibitor. Roscioni *et al.* (2011) and Morgan *et al.* (2014) demonstrated the selectivity of Rp-8-CPT-cAMPS, as it reduced the inhibitory effects of PKA but not 007-AM on MCh-evoked contractions of guinea pig and human ASM. We found that PGE_2 responses were reduced in the presence of the PKA inhibitor, Rp-8-CPT-cAMPS consistent with a role for PKA in this response. Roscioni *et al.* (2011) reported a similar finding of Rp-8-CPT-cAMPs on the inhibitory effects of PKA and β-

adrenoreceptor activators, 6-Bnz-cAMP and isoproterenol, respectively, on MCh-evoked contractions in guinea pig and human ASM.

In summary, the data from this chapter suggests that PGE_2-mediated relaxations of ASM are likely to involve activation of PKA and BK channels. In contrast, as PGE_2-induced relaxations were unaffected by application of XE-991, it suggests that K_V7 channels were not involved in this response. The contribution of EPAC to PGE_2-mediated relaxations of ASM requires further investigation, but the EPAC activator 007-AM produced a small, but significant, decrease in the amplitude of CCh-evoked contractions, suggesting that it can function as an inhibitory mediator in ASM.

6. Modulation of CCh-evoked calcium oscillations in mouse ASMCs.

6.1 Introduction

Previous chapters have demonstrated that PGE_2 inhibited cholinergic nerve-mediated contractions of mouse ASM. Prakash *et al.* (1997) reported that application of ACh to porcine tracheal SMCs evoked regenerative propagating calcium oscillations. A similar result was observed by Kuo *et al.* (2003) in intact porcine tracheal muscle bundles. Kuo *et al.* (2003) reported that the level of ASM tone directly correlated to the frequency of these oscillations. Dale *et al.* (2018) demonstrated that PGE_2, through activation of EP2&4Rs reduced histamine-evoked calcium oscillations in cultured human bronchial smooth muscle cells (hBSMCs). However, it is not yet known if ACh-evoked calcium oscillations are affected by PGE_2.

The purpose of this study was to investigate if PGE_2 inhibited CCh-induced calcium oscillations in freshly isolated mouse ASMCs and, if so, to investigate the downstream mediators modulating this effect.

6.2 Results

6.2.1 Effect of PGE_2 and the EP2R agonist, (R)-Butaprost on CCh-induced calcium oscillations in mouse ASMCs

Experiments were performed to investigate if CCh could elicit calcium oscillations in freshly isolated mouse ASMCs. *Figure 6.1A* is a representative pseudolinescan demonstrating that application of 1μM CCh evoked an initial calcium transient followed by a series of calcium oscillations that were superimposed on a raised baseline. The corresponding intensity profile plot is displayed in *Figure 6.1B*. For analysis purposes, only calcium oscillations in drug and washout greater than 25% of the mean oscillatory amplitude in control were included in summary data. Measurements of mean frequency and amplitude were made over the time periods 40 to 60 seconds (time period one) and 120 to 140 seconds (time period two). *Figures 6.1C&D* show that the frequency and amplitude of these events were maintained over the 140 seconds time period during which CCh was applied. In 7 cells, mean frequency during the time period one was 15 ± 2.7 versus 13 ± 2.2 per min^{-1} during time period two (*Figure 6.1C*, ANOVA, $p>0.05$). Mean amplitude of responses were $2.0 \pm 0.24 \Delta F/F_0$ in time period one and $1.9 \pm 0.31 \Delta F/F_0$ in time period two (*Figure 6.1D*, ANOVA, $p>0.05$). These data demonstrate that 1μM CCh generated robust calcium oscillations in mouse ASMCs that were well maintained over a 140 second time period.

Bai and Sanderson (2006) reported that the inhibitory effects of several cAMP-elevating agents on mouse lung slices, were mediated through a reduction in calcium oscillation frequency. In light of this, we examined the effect of PGE_2 on CCh-evoked calcium oscillations in freshly isolated mouse ASMCs. *Figure 6.2A* is a representative pseudolinescan showing the effect of PGE_2 (300nM) on CCh-induced calcium oscillations. The corresponding intensity profile plot is displayed in *Figure 6.2B*. Addition of PGE_2 reversibly abolished the CCh-evoked calcium oscillations over a 30 second period. In 13 cells, mean calcium oscillation frequency was significantly reduced by 82%, from 30 ± 4.0 to 5.5 ± 2.8 per min^{-1} (*Figure 6.2C,* paired t test, $p<0.001$). There was also a 72% reduction in oscillation amplitude from 1.4 ± 0.43 to 0.35 ± 0.27 $\Delta F/F_0$ (*Figure 6.2D,* paired t test, $p<0.01$, $n=13$, $N=10$).

Figure 6.2 showed that PGE_2 reduced the CCh-induced calcium responses over a 30 second time frame in isolated mouse ASMCs. We next investigated if this inhibition persisted over an extended time frame. *Figure 6.3A* is a representative pseudolinescan demonstrating the effect of PGE_2 (300nM) over an 80 second time course on CCh-induced calcium oscillations. The associated intensity profile plot is shown in *Figure 6.3B*. It is evident that the inhibitory effects of PGE_2 on CCh-evoked calcium oscillations did not diminish over time. In 6 cells, the mean frequency of calcium oscillations was significantly reduced by 95% from 19 $\pm$ 4.5 to 1 $\pm$ 1 per min^{-1} (*Figure 6.3C,* paired t test, $p<0.001$). There was also a 98% reduction in oscillation amplitude from 1.6 $\pm$ 0.53 to 0.04 $\pm$ 0.04 $\Delta F/F_0$ (*Figure 6.3D,* paired t test, $p<0.05$, n=6, N=5).

The above data suggest that PGE_2 inhibits CCh-evoked calcium oscillations in mouse ASMCs. Experiments were performed to determine if these effects were mimicked by the EP2R agonist, (*R*)-Butaprost. *Figures 6.4A&B* are the representative pseudolinescan and the correlating intensity profile plot, showing the effect of (*R*)-Butaprost (3μM) on 1μM CCh-evoked calcium oscillations in mouse ASMCs. (*R*)-Butaprost significantly reduced the mean frequency of calcium oscillations by 80% from 20 $\pm$ 3.6 to 4 $\pm$ 2.5 per min^{-1} (*Figure 6.4C,* paired t test, $p<0.01$). There was also an 86% reduction in oscillation amplitude from 1.6 $\pm$ 0.35 to 0.23 $\pm$ 0.15 $\Delta F/F_0$ (*Figure 6.4D,* paired t test, $p<0.001$, n=8, N=5). These data suggest that activation of EP2Rs inhibits CCh-induced calcium oscillations in mouse ASMCs.

6.2.2 Effect of cAMP/PKA/EPAC modulators on CCh-evoked calcium oscillations in mouse *ASMCs*

The results thus far, suggest that the inhibitory effects of PGE_2 on CCh-evoked calcium oscillations are mediated via activation of EP2Rs. EP2Rs are G_s protein-coupled receptors that stimulate activation of AC and the cAMP pathway (Aso *et al*. 2013; Sastre and del Pozo 2012; Vancheri *et al*. 2004). Therefore, we next examined if the AC activator, forskolin mimicked the effect of PGE_2 on CCh-evoked calcium oscillations. The representative pseudolinescan shown in *Figure 6.5A* demonstrate that application of 3μM forskolin abolished CCh-evoked calcium oscillations in mouse ASMCs. Forskolin significantly reduced the mean

frequency of calcium oscillations by 96% from 21 ± 2.6 to 0.86 ± 0.86 per min^{-1} (*Figure 6.5C,* paired t test, p<0.001). There was also a 98% reduction in oscillation amplitude from 1.7 ± 0.18 to 0.04 ± 0.04 $\Delta F/F_0$ (*Figure 6.5D,* paired t test, p<0.001, n=7, N=5).

Activation of AC, results in the upregulation of cAMP and cAMP effectors, PKA and EPAC. We next examined if CCh-evoked calcium responses were modulated by EPAC, by examining the effect of the EPAC agonist, 007-AM. *Figure 6.6A&B* are representative pseudolinescan and the correlating intensity plot, showing the effect of 007-AM (10μM) on 1μM CCh-evoked calcium oscillations in mouse ASMCs. 007-AM significantly reduced the mean frequency of calcium oscillations by 59% from 17 ± 1.9 to 7 ± 1.4 per min^{-1} (*Figure 6.6C,* paired t test, p<0.001, n= 8, N= 5), however oscillation amplitude was only modestly reduced, from 2 ± 0.19 to 1.4 ± 0.39 $\Delta F/F_0$ (*Figure 6.6D,* paired t test, p>0.05, n=8, N=5).

To test if activation of PKA affected CCh-evoked calcium oscillations we examined the effects of the PKA activator, 6-MB-cAMP. The representative pseudolinescan and associated intensity plot in *Figure 6.7A&B* show that 6-MB-cAMP (300μM) reduced the frequency of calcium oscillations evoked by 1μM CCh. Mean calcium oscillation frequency was reduced by 33% in 6-MB-cAMP (300μM), from 21 ± 1.7 to 14 ± 2.7 per min^{-1} (*Figure 6.7C,* paired t test, p<0.05). 6-MB-cAMP reduced the mean oscillation amplitude by 40% from 2 ± 0.37 to 1.2 ± 0.23 $\Delta F/F_0$, however this effect did not reach statistical significance (*Figure 6.7D,* paired t test, p>0.05, n=12, N=10).

Based on the above results, we further examined the effect of combined application of 007-AM (10μM) and 6-MB-cAMP (300μM) on CCh-evoked calcium oscillations. The representative pseudolinescan and corresponding intensity profile plot in *Figures 6.8A&B* show addition of both drugs together exerted greater effects than either alone. Mean oscillation frequency was significantly reduced by 83% from 20 ± 2.2 to 3.4 ± 1.8 per min^{-1} (*Figure 6.8C,* paired t test, p<0.01) and mean oscillation amplitude was reduced by 73% from 1.5 ± 0.34 to 0.4 ± 0.23 $\Delta F/F_0$ (*Figure 6.8D,* paired t test, p<0.05, n=7, N=6). These data suggest that combined activation of PKA and EPAC inhibits calcium oscillations in mouse ASMCs.

To confirm a role for PKA, in the inhibitory effects of PGE_2 on CCh-induced calcium oscillations, we examined if the effects of PGE_2 were affected by addition of the PKA inhibitor, Rp-8-CPT-cAMPs (100μM). *Figure 6.9A* is a representative pseudolinescan demonstrating that Rp-8-CPT-cAMPs partially reversed the effects of PGE_2. PGE_2 abolished oscillations in 7 cells (mean oscillation frequency under control conditions was 21 ± 3.7 per min^{-1}). When Rp-8-CPT-cAMPs was added calcium oscillations returned with a mean frequency of 10 ± 2 per min^{-1} (ANOVA, $p<0.05$). The mean amplitude of the events in the presence of PGE_2 and Rp-8-CPT-cAMPs (1.4± 0.39 $\Delta F/F_0$) was not different to control (1.4 ± 0.23 $\Delta F/F_0$; *Figure 6.9D*, ANOVA, $p>0.05$, n=7, N=5). These data further support a role for PKA in the inhibitory effects of PGE_2 on CCh-induced calcium oscillations. *Figure 6.10A* is a representative pseudolinescan demonstrating that the application of Rp-8-CPT-cAMPs (100μM) alone did not affect calcium oscillations evoked by 1μM CCh. *Figure 6.10C* shows that the mean oscillation frequency was 17 ± 2.8 per min^{-1} under control conditions compared to15 ± 5.9 per min^{-1} in Rp-8-CPT-cAMPs (n=7, N=7, $p>0.05$). Mean amplitude was 1.9 ± 0.53 compared to 1.8 ± 0.51 $\Delta F/F_0$ (*Figure 6.10D,* ANOVA, $p>0.05$, n=7, N=7).

6.2.3 Effect of intracellular calcium store modulators and extracellular calcium free solution on CCh-evoked calcium oscillations in mouse ASMCs

Previous studies have shown that calcium oscillations in ASMCs can persist for several cycles in the absence of extracellular calcium or in the presence of calcium channel blockers, suggesting a prominent role for intracellular calcium stores in these responses (Perez and Sanderson 2005; Bergner and Sanderson 2002; Prakash *et al.* 1997; Roux *et al.* 1997). Therefore, we investigated if calcium release from RyRs contributed to CCh-evoked calcium oscillations in mouse ASMCs by examining the effects of the RyR inhibitor, tetracaine (100μM). *Figure 6.11A* is a representative pseudolinescan demonstrating that tetracaine abolished CCh-evoked calcium oscillations. Tetracaine abolished calcium oscillations in all cells tested (n=9) from a mean oscillation frequency and amplitude in control of 25 ± 2.7 per min^{-1} and 1.4 ± 0.44 $\Delta F/F_0$, respectively (*Figures 6.11C&D*, paired t test, $p<0.05$, n=9, N=7). These

data suggest a role for RyR-mediated calcium release in the generation and maintenance of CCh-induced calcium oscillations in mouse ASMCs.

A number of studies have also demonstrated a critical role for IP_3Rs in the generation of calcium oscillations in ASMCs (Sanderson *et al.* 2008; Bai and Sanderson 2006; White *et al.* 2003). Therefore, we next investigated the effects of IP_3R blockade on CCh-evoked calcium oscillations. *Figure 6.12A* is a representative pseudolinescan demonstrating the effect of the IP_3R antagonist, 2-APB (100μM) on CCh-induced calcium oscillations. The corresponding intensity profile plot is displayed in *Figure 6.12B*. In 6 cells, the mean oscillation frequency was significantly reduced by 95% from 20 ± 1.3 to 1 ± 1 per min^{-1} (*Figure 6.12C,* paired t test, $p<0.001$) and mean oscillation amplitude was reduced by 92% from 1.8 ± 0.41 to 0.14 ± 0.14 $\Delta F/F_0$ (*Figure 6.12D,* paired t test, $p<0.05$, n=6, N=3). These data are consistent with a role for IP_3R-mediated calcium release in the development of calcium oscillations in ASMC.

The above data indicate an important role for SR calcium release in the generation of CCh-induced calcium oscillations in ASMC. The contribution of calcium influx across the plasma membrane to this activity was assessed by examining the effect of removal of extracellular calcium on CCh-induced calcium oscillations. The representative pseudolinescan and corresponding intensity profile plot shown in *Figures 6.13A&B* demonstrate that application of EGTA containing calcium free solution did not abolish CCh-evoked calcium oscillations, but caused a reduction in oscillation frequency and amplitude. In 8 cells, mean oscillation frequency was reduced from 13 ± 1.9 to 2.3 ± 1.1 per min^{-1} (*Figure 6.13C,* paired t test, $p<0.001$) and mean oscillation amplitude by 82% from 1.9 ± 0.29 to 0.35 ± 0.2 $\Delta F/F_0$ (*Figure 6.13D,* paired t test, $p<0.01$, n=8, N=6). These data suggest that calcium influx across the plasma membrane is required to sustain CCh-induced calcium oscillations in mouse ASMCs.

6.2.4 Effect of BK channel opener, Compound X on CCh-evoked calcium oscillations in mouse ASMCs

Data in Chapters 3 and 5 indicated a role for BK channels in PGE_2-induced inhibition of CCh-induced contractions in mouse ASM. Therefore, we examined if activation of BK channels affected CCh-evoked calcium oscillations in mouse

ASMCs. *Figure 6.14A* is a representative pseudolinescan demonstrating the effect of the BK channel opener, Compound X (3μM) (Ponte *et al.* 2012) on 1μM CCh-induced calcium oscillations. The corresponding intensity profile plot is displayed in *Figure 6.14B*. Addition of Compound X had no discernible effects on CCh-evoked calcium oscillations. In 8 cells, the mean frequency of calcium oscillations was 14 ± 2.3 per min^{-1} under control conditions compared to 14 ± 2.5 per min^{-1} in Compound X (*Figure 6.14C,* paired t test, p>0.05). Mean oscillation amplitude was also not affected (2.3 ± 0.82 under control conditions versus 2.3 ± 0.71 $\Delta F/F_0$ in Compound x, *Figure 6.14D,* paired t test, p>0.05, n=8, N=6). These data suggest that activation of BK channels did not inhibit CCh-evoked calcium oscillations in mouse ASMCs.

6.2.5 Modulation of caffeine-induced calcium transients in mouse ASMCs

The data above suggest that 1μM CCh can induce calcium oscillations in mouse ASMCs via a combination of calcium release from RyRs and IP_3Rs and calcium influx across the membrane. Therefore, it is possible that PGE_2 could inhibit calcium oscillations by affecting these mechanisms. Caffeine, at high concentrations, is known to induce calcium release from RyRs (Kong *et al.* 2008). Therefore, to examine if PGE_2 affected calcium release from ryanodine-sensitive calcium stores we tested if PGE_2 affected caffeine-induced calcium transients. Control experiments were initially performed to demonstrate that caffeine elicited reproducible responses. *Figure 6.15A* is a representative pseudolinescan demonstrating that application of 10mM caffeine generated reproducible calcium transients in mouse ASMCs when applied for a duration of 10 seconds at 60 second intervals. *Figure 6.15C* displays summary data which demonstrates that the amplitude of caffeine-evoked calcium transients was maintained during three successive applications (mean amplitude in first application 2.2 ± 0.31, second application 2.1 ± 0.31 and third application 1.8 ± 0.26 $\Delta F/F_0$, ANOVA, p>0.05, n=7, N=5). Application of caffeine produced robust and consistent calcium transients.

The data in *Figure 6.16* shows that PGE_2 did not affect the amplitude of caffeine-induced calcium transients. *Figure 6.16A* is a pseudolinescan showing that 10mM caffeine-evoked calcium transients were not affected by the presence

of PGE_2 (300nM). The associated intensity profile plot is shown in *Figure 6.16B*. *Figure 6.16C* displays summary data which demonstrates that the amplitude of caffeine-evoked calcium transients was maintained in the presence of PGE_2 (mean amplitude of 2.3 $\pm$ 0.49 in control to 2.1 $\pm$ 0.45 $\Delta F/F_0$ in PGE_2, paired t test, p>0.05, n=7, N=5). This suggests that PGE_2 does not affect release from, or refilling of ryanodine-sensitive calcium stores and indicates that PGE_2 inhibits carbachol responses via different pathway, such as inhibition of IP_3-mediated calcium release.

Similar results were achieved with the EPAC and PKA modulators, 007-AM and 6-MB-cAMP (*Figure 6.17*). *Figure 6.17A* is a pseudolinescan showing that 10mM caffeine evoked calcium transients before and in the presence of 6-MB-cAMP and 007-AM. The associated intensity profile plot is shown in *Figure 6.17B*. Summary data is displayed in *Figure 6.17C*, it is clear that activation of PKA and EPAC had no discernible effect on caffeine-induced calcium transients (mean amplitude of 3.2 $\pm$ 0.90 in control vs. 3.1 $\pm$ 0.91 $\Delta F/F_0$, paired t test, p>0.05, n=7, N=6). These data demonstrate that the inhibitory effects of these agents on CCh-induced calcium oscillations were also not mediated by inhibition on RyRs.

The data in *Figure 6.12* showed that 2-APB inhibited CCh-induced calcium oscillations in mouse ASMCs, suggesting that calcium release from IP_3Rs was involved in this response. However, 2-APB is known to affect TRP channels and therefore effects of 2-APB should be interpreted with caution (Colton and Zhu 2007). The effects of 2-APB on caffeine-evoked calcium transients was examined to assess if 2-APB affected calcium release from ryanodine-sensitive stores. *Figures 6.18A&B* shows a representative pseudolinescan (*Figure 6.18A*) and corresponding intensity profile plot (*Figure 6.18B*). *Figure 6.18C* displays summary data which demonstrates that the amplitude of caffeine-evoked calcium transients was maintained in the presence of 2-APB (2.7 $\pm$ 0.37 in control versus 2.6 $\pm$ 0.38 $\Delta F/F_0$ in 2-APB, paired t test, p>0.05, n=7, N=5). This indicates that 2-APB does not affect calcium release from RyRs or store refilling pathways.

Finally, experiments were performed to ascertain the effect of removal of external calcium on caffeine responses to gauge whether calcium store content was reduced over the 60 second time period during which calcium removal inhibited the CCh responses. The data in *Figures 6.19* show that the amplitude

of caffeine-evoked calcium transients was preserved over this timescale when calcium was removed from the bathing media. *Figures 6.19A&B* show the representative pseudolinescan (*Figure 6.19A*) and the corresponding intensity profile plot (*Figure 6.19B*). Summary data shown in *Figure 6.19C*, demonstrate that the amplitude of caffeine-evoked calcium transients was not affected by application of EGTA containing calcium free (mean amplitude of 2.7 $\pm$ 0.37 in control versus 2.6 $\pm$ 0.38 $\Delta F/F_0$, paired t test, $p>0.05$, n=6, N=4). This suggests that the effects of calcium removal on CCh-induced calcium oscillations are unlikely to result from depletion of calcium stores and instead support a direct role for calcium influx across the membrane in these responses.

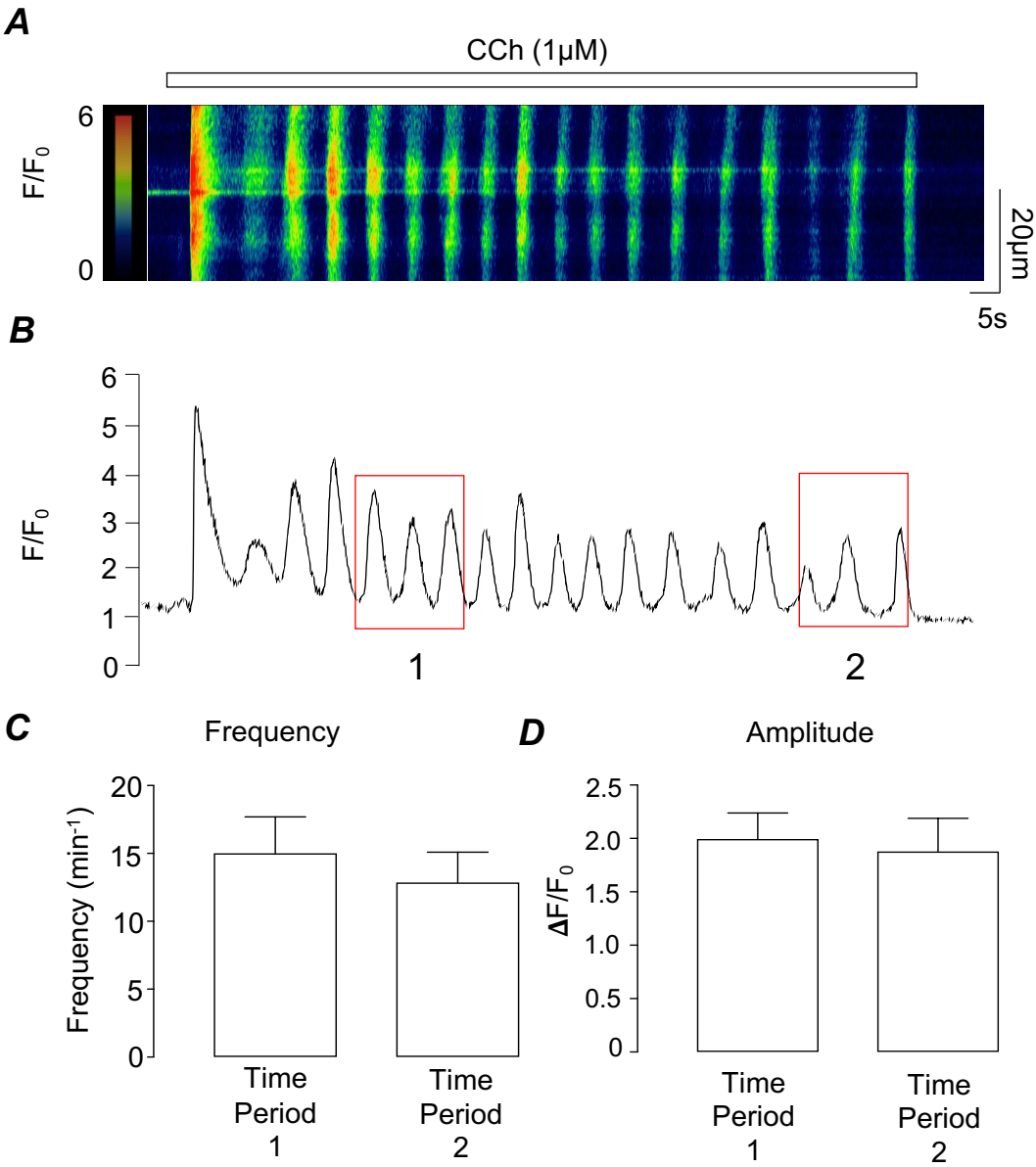

Figure 6.1. ***CCh-induced calcium oscillations in freshly isolated ASMCs.*** (**A**) Representative pseudolinescan illustrating that the addition of CCh (1μM) induced calcium oscillations in ASMCs, and (**B**) the correlating intensity profile plot. Measurements were taken at approx. 40-60 and 120-140 seconds replicating typical drug protocol timings. Summary bar charts plotting mean calcium oscillation frequency (**C**) and amplitude (**D**, n=7, N=7, p>0.05, paired t-test).

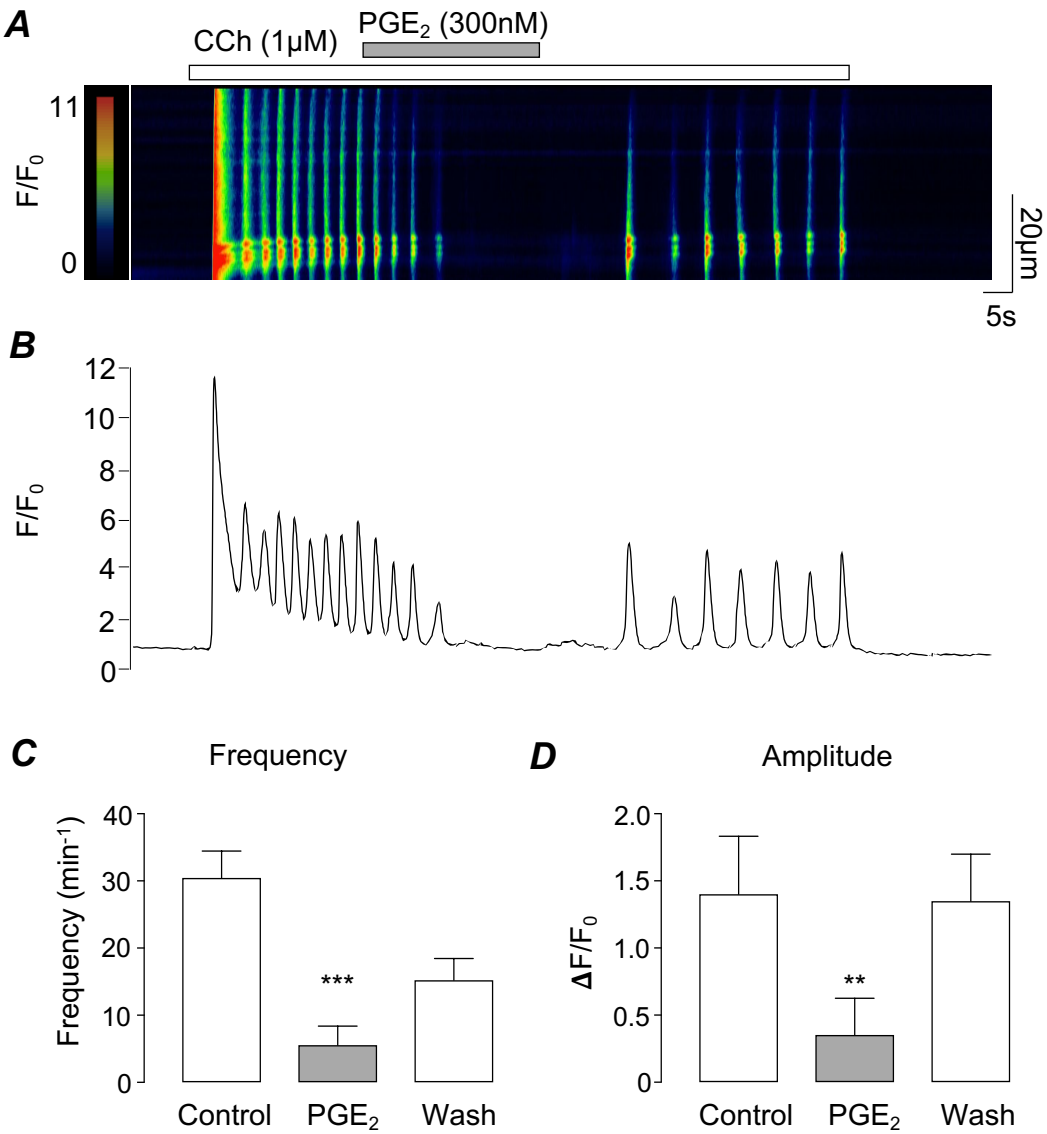

Figure 6.2. ***Effect of PGE_2 on CCh-induced calcium oscillations in freshly isolated ASMCs.*** (**A**) Representative pseudolinescan showing the effects of PGE_2 (300nM) on CCh (1μM)-induced calcium oscillations in ASMCs, and (**B**) the correlating intensity profile plot. Summary bar charts plotting mean calcium oscillation frequency (**C**) and amplitude (**D)** in the absence and presence of PGE_2 **(**n=13, N=10, **p<0.01, ***p<0.001 paired t-test).

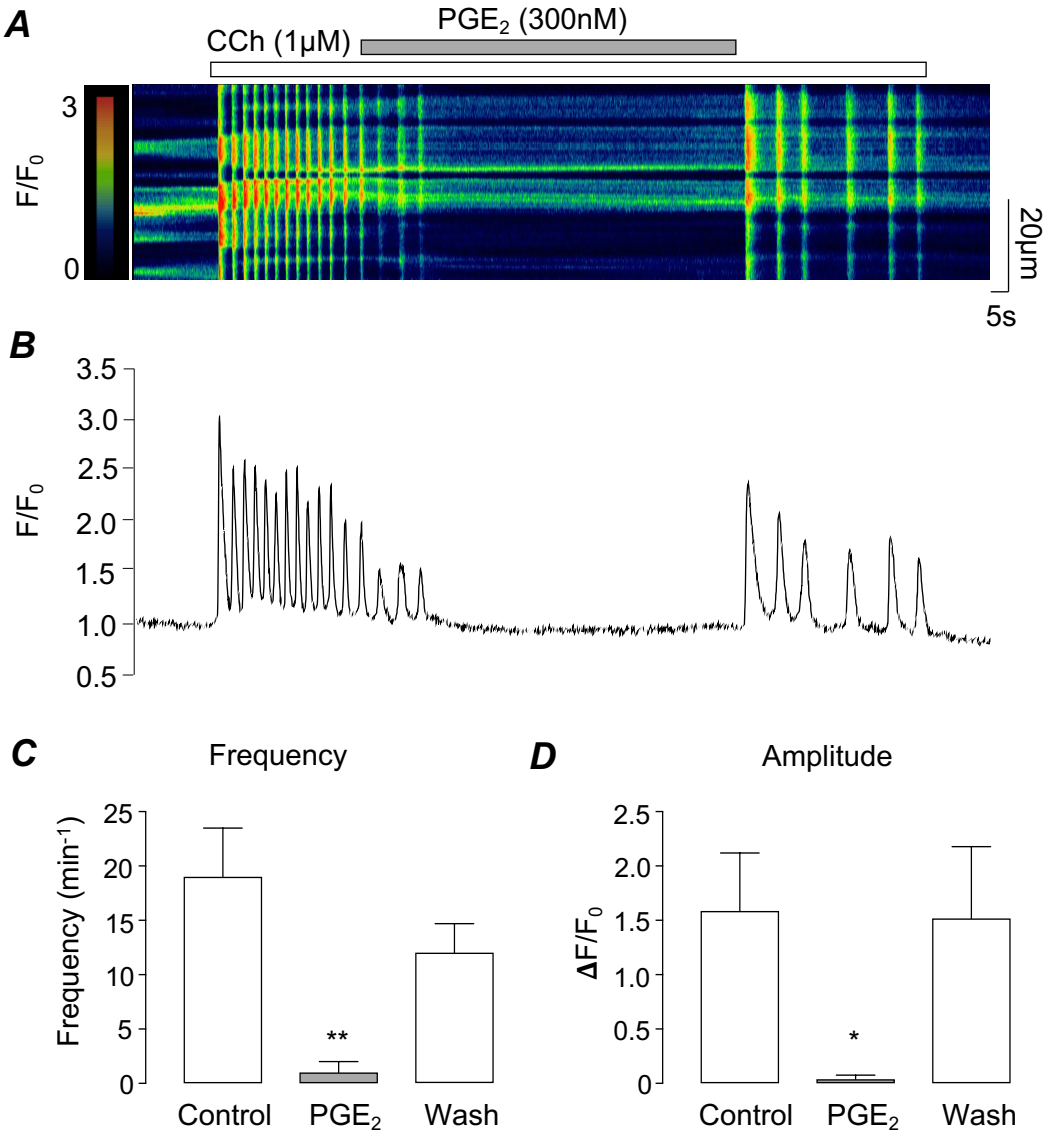

Figure 6.3. ***Addition of PGE_2 for 80 seconds on CCh-induced calcium oscillations in freshly isolated ASMCs***. (**A**) Representative pseudolinescan showing that the inhibitory effects of PGE_2 (300nM) on CCh (1μM)-induced calcium oscillations in ASMCs were maintained over an 80 second period and (**B**) the correlating intensity profile plot. Summary bar charts plotting the effects of PGE_2 on mean calcium oscillation frequency (**C**) and amplitude (**D**, n=6, N=5, *p<0.05, **p<0.01, paired t-test).

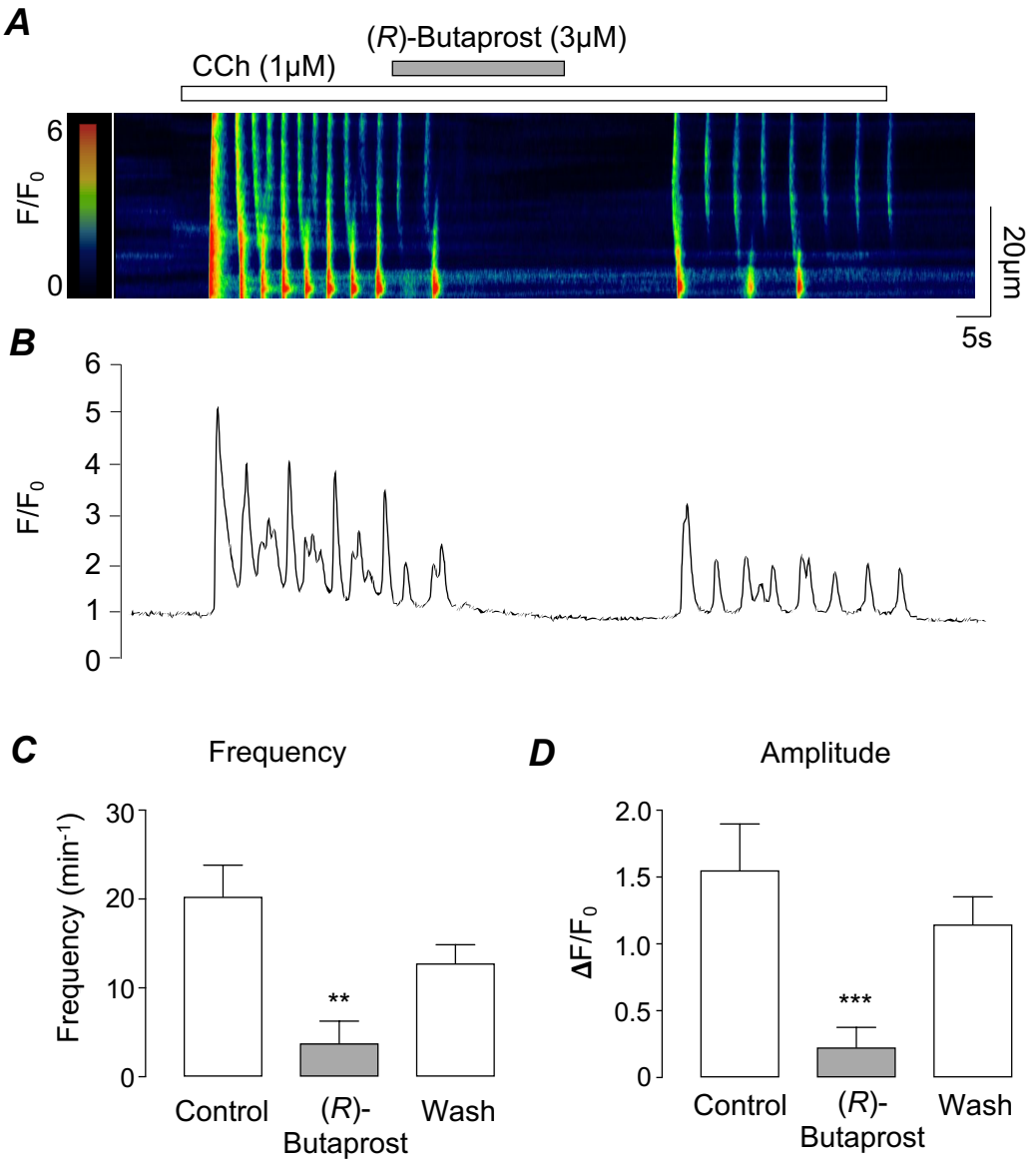

Figure 6.4. ***Effect of the selective EP2R agonist (R)-Butaprost on CCh-induced calcium oscillations in freshly isolated ASMCs***. (**A**) Representative pseudolinescan showing the effects of (*R*)-Butaprost (3μM) on CCh (1μM)-evoked calcium responses in ASMCs, and (**B**) the correlating intensity profile plot. Summary bar charts plotting mean calcium oscillation frequency (**C**) and amplitude (**D**) in the absence and presence of (*R*)-Butaprost (n=8, N=5, **p<0.01, ***p<0.001, paired t-test).

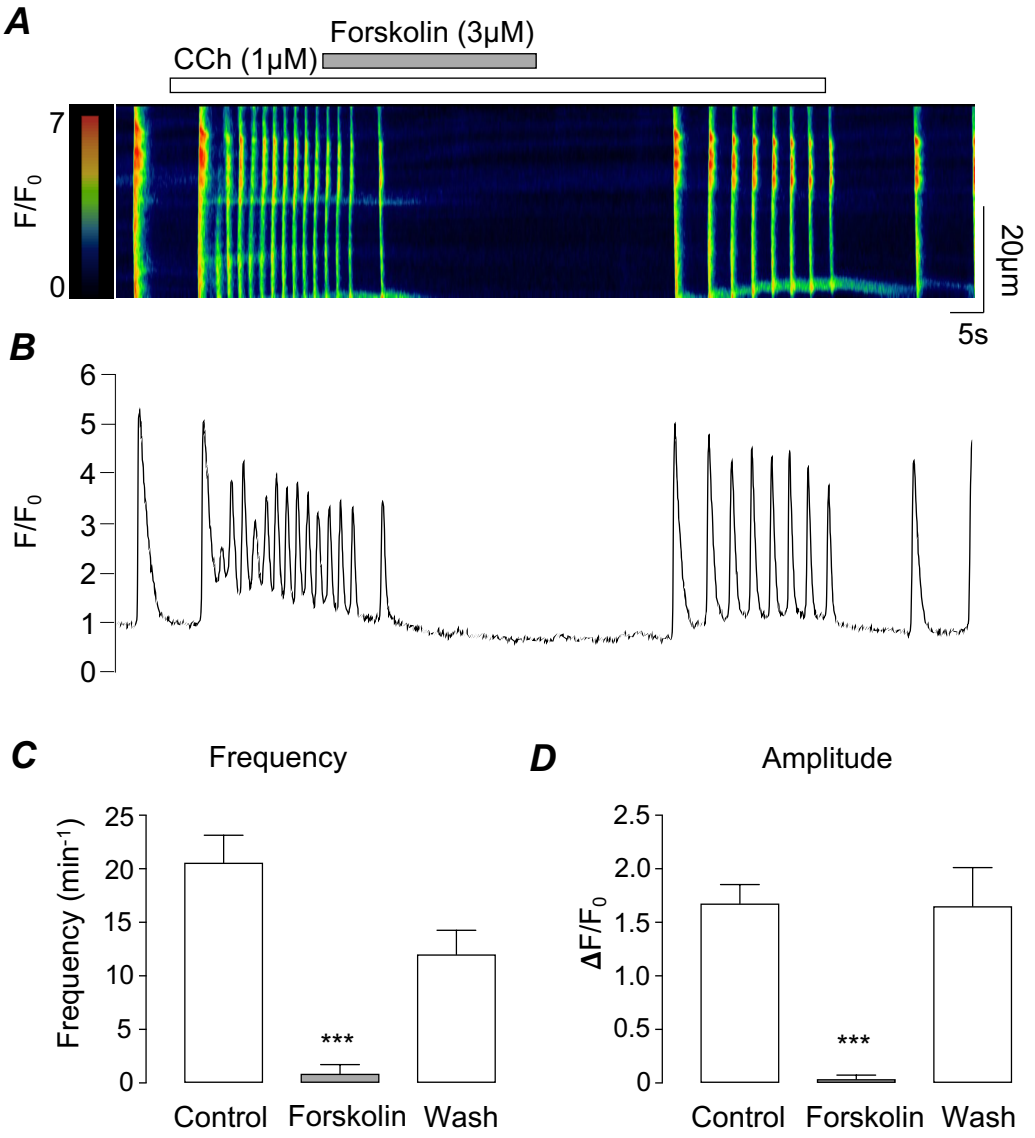

Figure 6.5. ***Effect of forskolin on CCh-induced calcium waves in freshly isolated ASMCs.*** (**A**) Representative pseudolinescan showing the inhibitory effects of forskolin (3μM) on CCh (1μM)-induced calcium oscillations in ASMCs, and (**B**) the correlating intensity profile plot. Summary bar charts plotting mean calcium oscillation frequency (**C**) and amplitude (**D**, n=7, N=5, ***p<0.001, paired t-test).

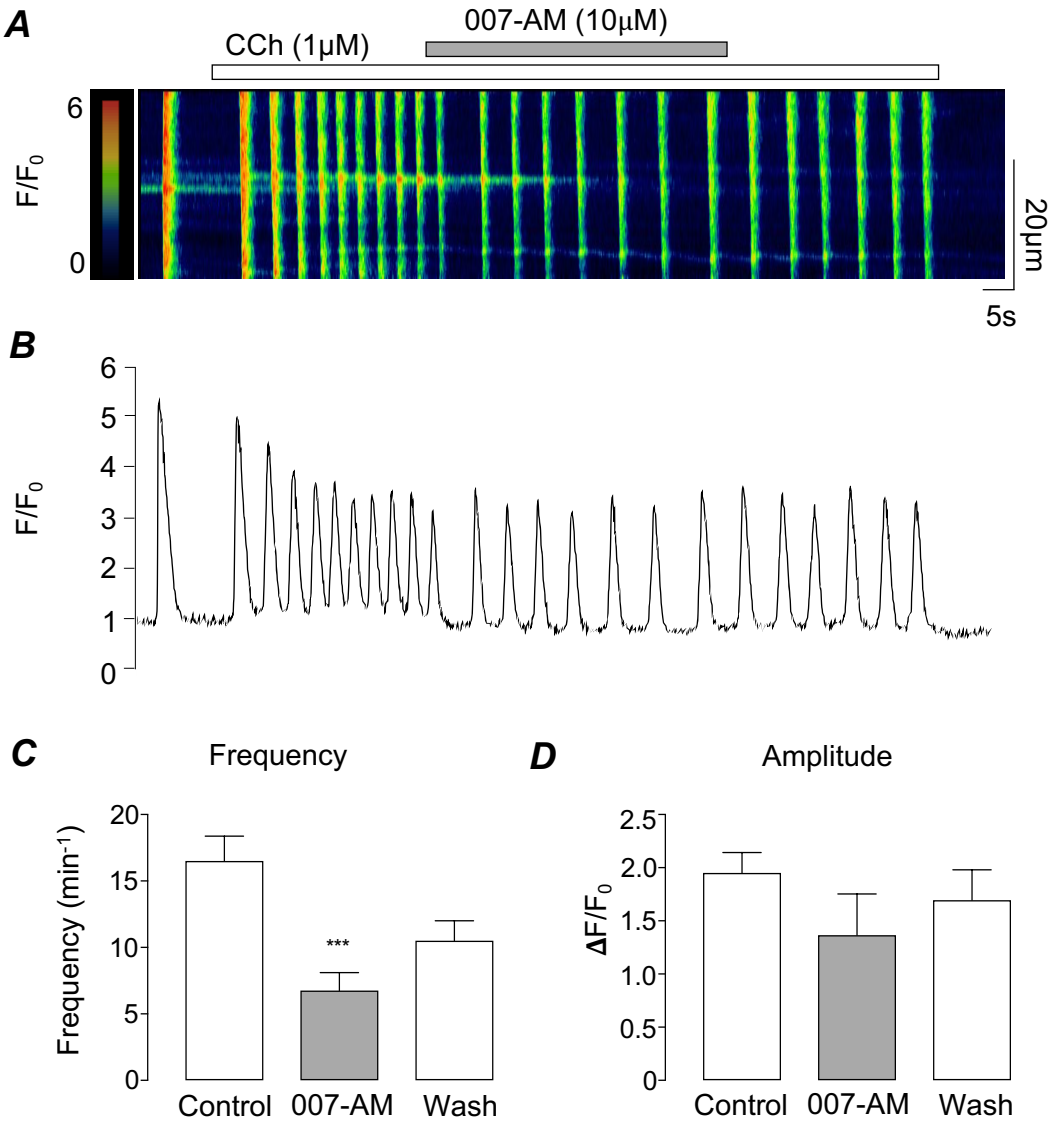

Figure 6.6. ***Effect of the selective EPAC activator, 007-AM on CCh-evoked calcium oscillations in freshly isolated ASMCs.*** (**A**) Representative pseudolinescan illustrating the effects of 007-AM (10µM) on CCh (1µM)-induced calcium oscillations in ASMCs where (**B**) is the corresponding intensity profile plot. Summary bar charts plotting mean calcium oscillation frequency (**C**, n=8, N=5, ***p<0.001, paired t-test) and amplitude (**D**). 007-AM significantly reduced mean calcium oscillation frequency, however, did not significantly reduce mean oscillation amplitude.

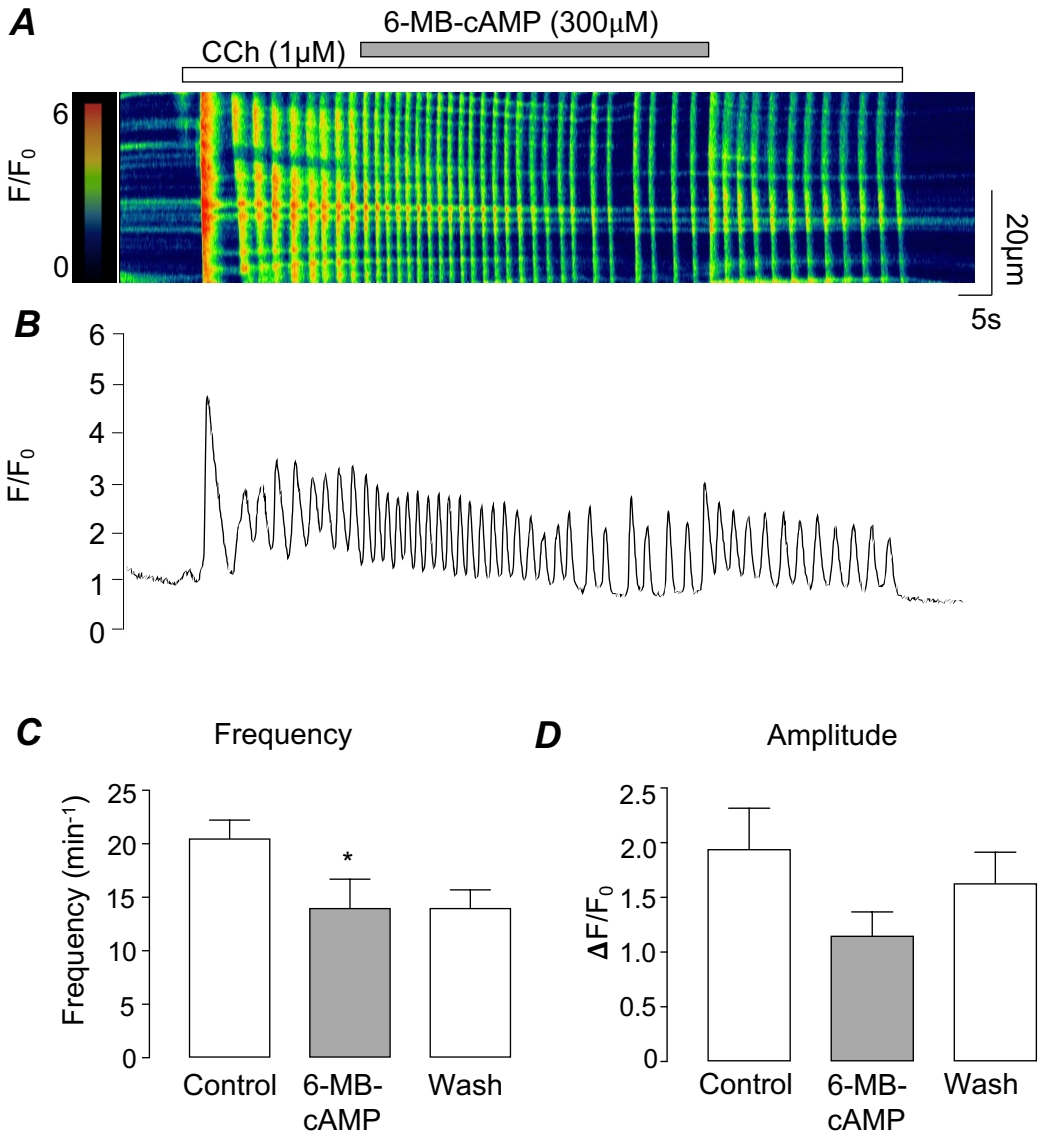

Figure 6.7. ***Effect of the selective PKA activator, 6-MB-cAMP on CCh-induced calcium responses in freshly isolated ASMCs***. (**A**) Representative pseudolinescan showing the effects of 6-MB-cAMP (300µM) on CCh (1µM)-evoked calcium oscillations in ASMCs, and (**B**) the correlating intensity profile plot. Summary bar charts plotting mean calcium oscillation frequency (**C**, n=12, N=10, *p<0.05, paired t-test) and amplitude (**D**). 6-MB-cAMP significantly reduced mean calcium oscillation frequency however, had no discernable effects on mean oscillation amplitude.

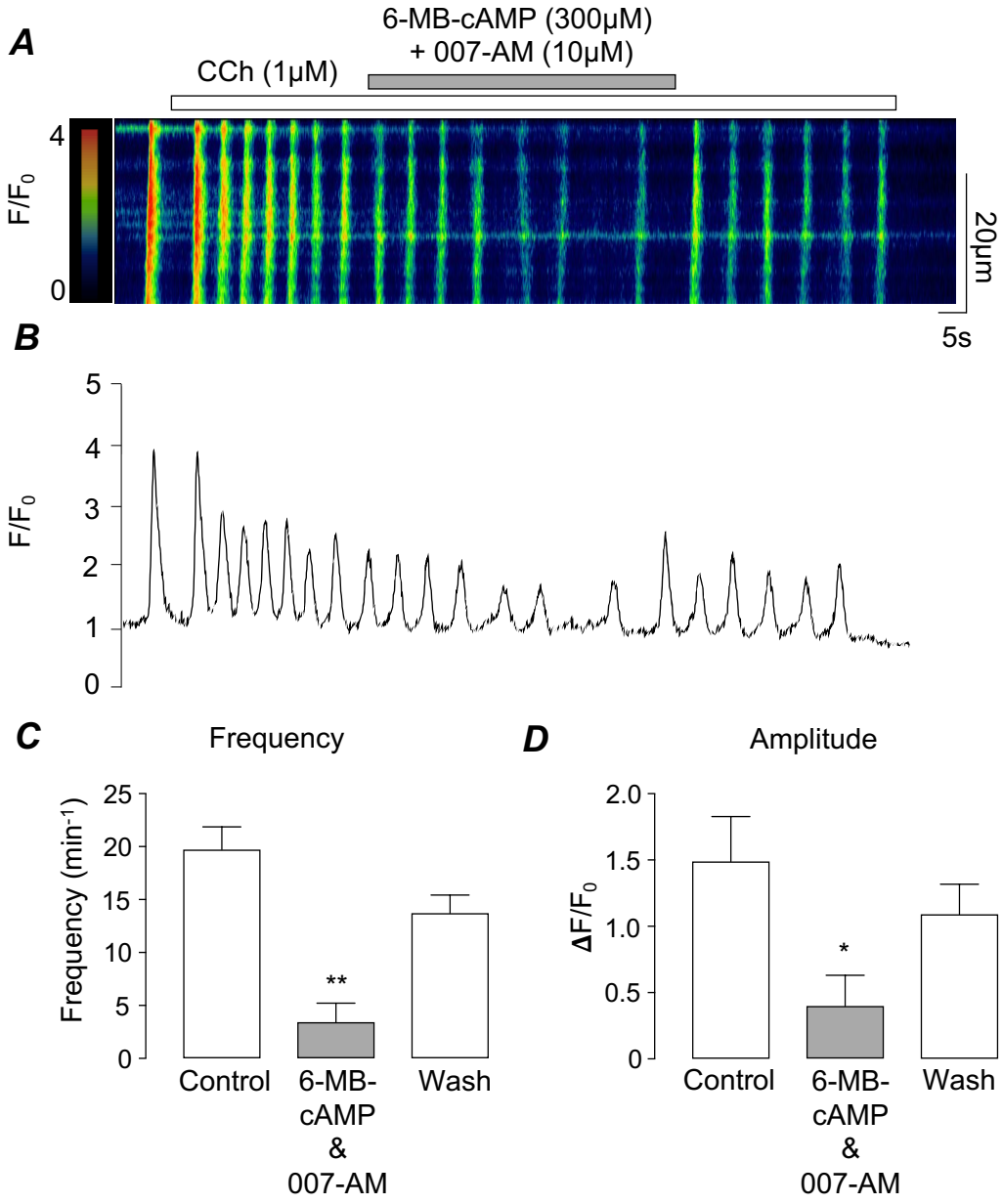

Figure 6.8. ***Effect of 6-MB-cAMP and 007-AM in combination on CCh-induced calcium oscillations in freshly isolated ASMCs.*** (**A**) Representative pseudolinescan showing the effect of dual application of the selective PKA and EPAC activators, 6-MB-cAMP (300μM) and 007-AM (10μM), respectively on CCh (1μM)-evoked calcium oscillations in ASMCs. (**B**) displays the correlating intensity profile plot. Summary bar charts plotting mean calcium oscillation frequency (**C**) and amplitude (**D**, n=7, N=6, *p<0.05, **p<0.01, paired t-test) in the absence and presence of both 6-MB-cAMP and 007-AM.

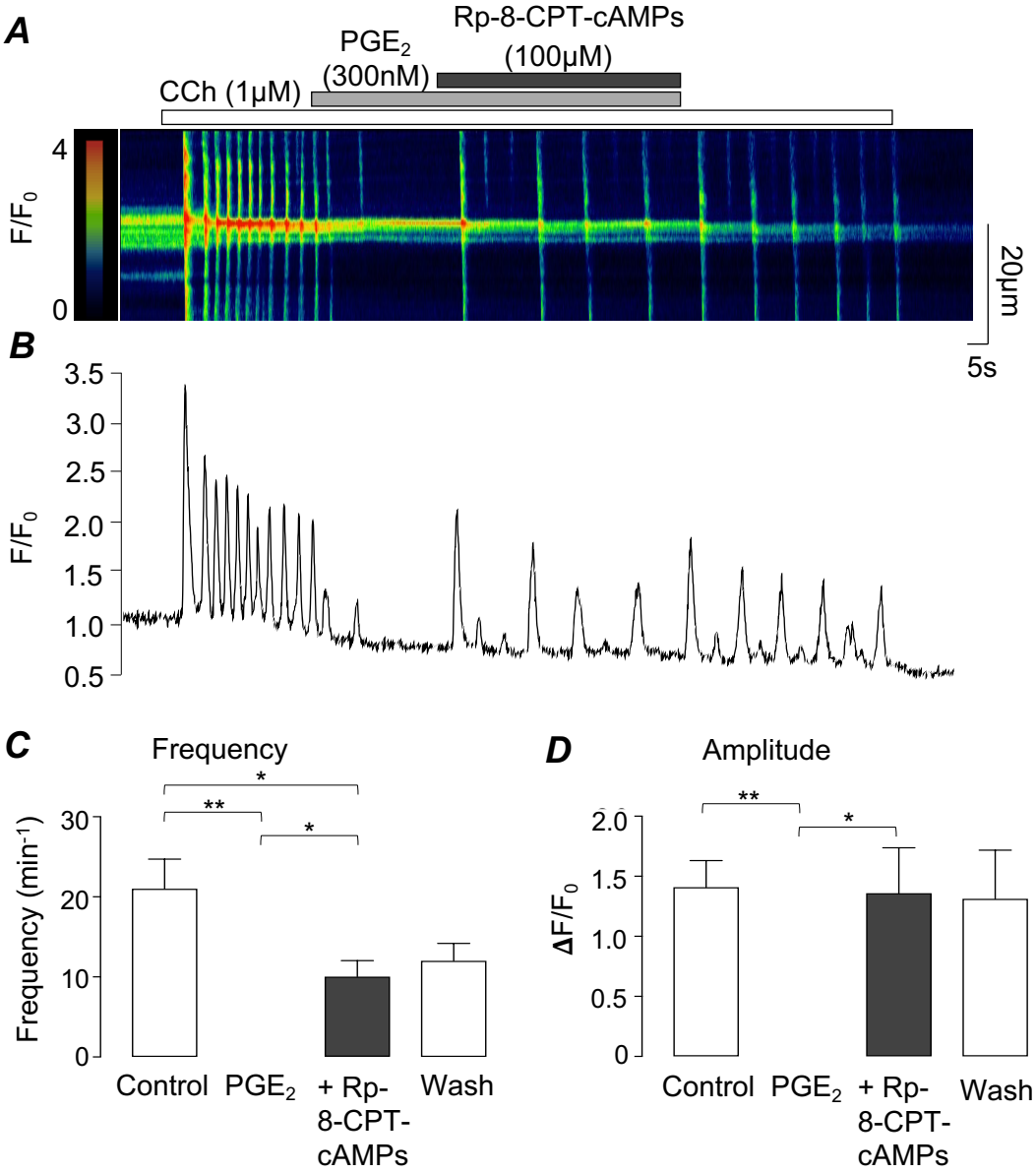

Figure 6.9. ***Effect of the PKA antagonist, Rp-8-CPT-cAMPs on PGE_2-induced inhibition of CCh-evoked calcium oscillations in freshly isolated ASMCs***. (**A**) Representative pseudolinescan showing the effects of PGE_2 (300nM) on CCh (1μM)-evoked calcium oscillations in ASMCs in control conditions and following addition of Rp-8-CPT-cAMPs (100μM). (**B**) displays the corresponding intensity profile plot. Summary bar charts plotting mean calcium oscillation frequency (**C**) and amplitude (**D**, n=7, N=5, *p<0.05, **p<0.01, paired t-test).

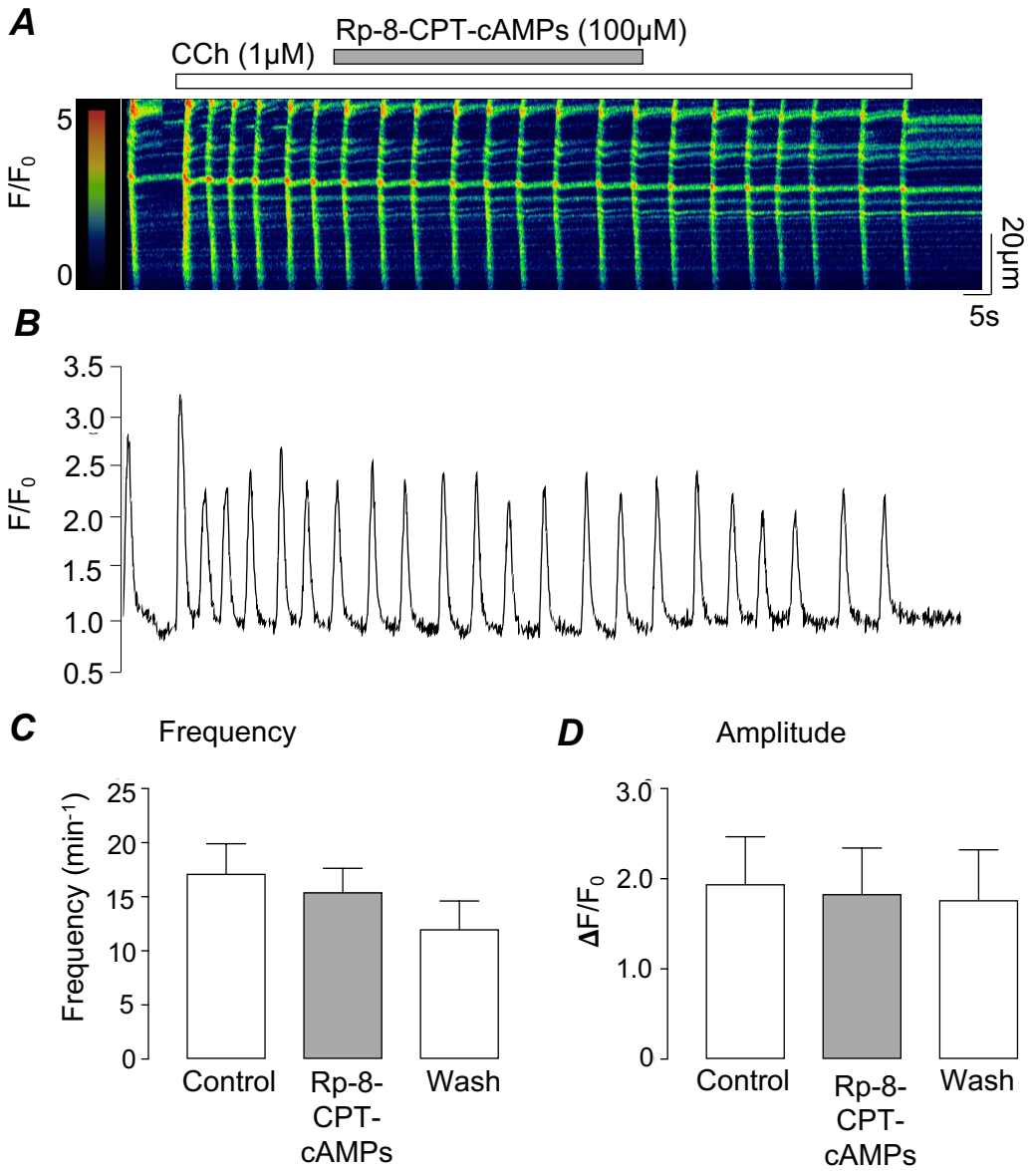

Figure 6.10. ***Effect of the PKA antagonist, Rp-8-CPT-cAMPs on CCh-induced calcium oscillations in freshly isolated ASMCs.*** (**A**) Representative pseudolinescan showing that Rp-8-CPT-cAMPs (100μM) had no discernable effects on CCh (1μM)-induced calcium oscillations in isolated ASMCs, and (**B**) the correlating intensity profile plot. Summary bar charts plotting mean calcium oscillation frequency (**C**) and amplitude (**D**, n=7, N=7, $p>0.05$, paired t-test) in the absence and presence of Rp-8-CPT-cAMPs.

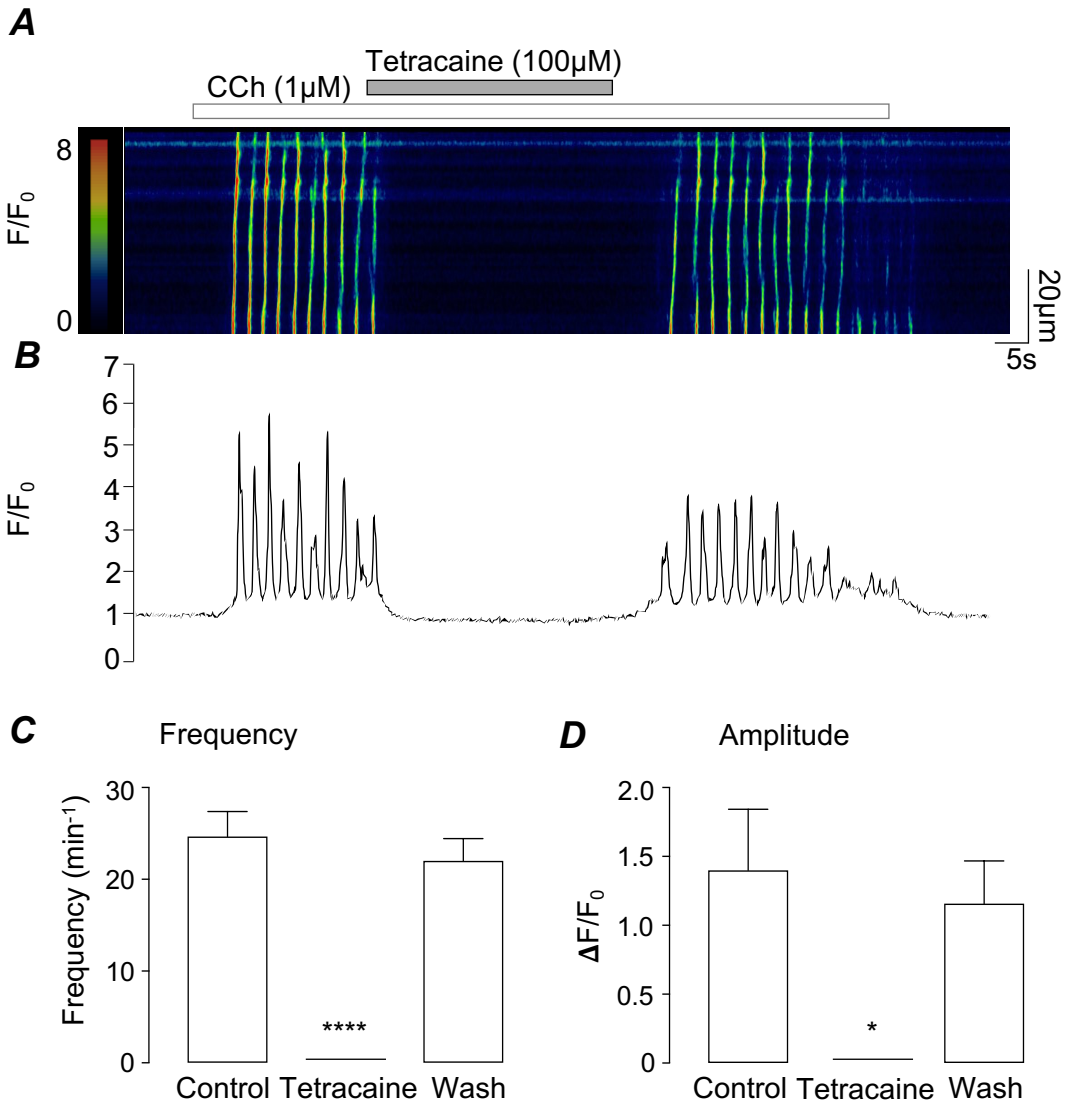

Figure 6.11. ***The RyR blocker, tetracaine abolished CCh-induced calcium oscillations in freshly isolated ASMCs.*** (**A**) Representative pseudolinescan showing the inhibitory effects of the RyR antagonist tetracaine (100μM) on CCh (1μM)-induced calcium oscillations in mouse ASMCs, and (**B**) the correlating intensity profile plot. Summary bar charts plotting mean calcium oscillation frequency (**C**) and amplitude (**D)** in the absence and presence of tetracaine (n=9, N=7, *p<0.05, ****p<0.0001 paired t-test).

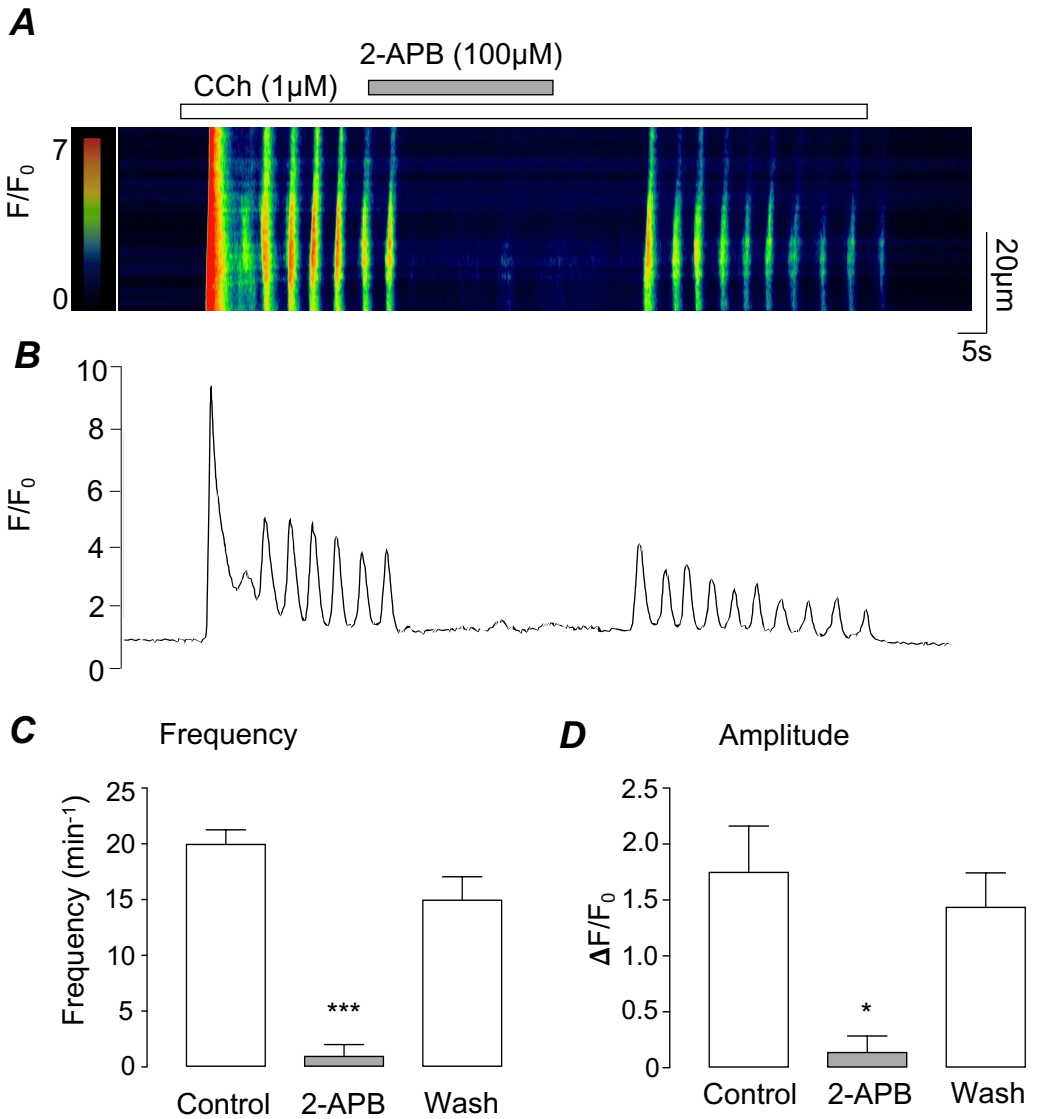

Figure 6.12 ***Effect of the IP_3R antagonist, 2-APB on CCh-induced calcium waves in mouse ASMCs.*** (**A**) Representative pseudolinescan showing the effects of 2-APB (100μM) on CCh (1μM)-induced calcium oscillations in freshly isolated ASMCs where (**B**) is the correlating intensity profile plot. Summary bar charts plotting mean calcium oscillation frequency (**C**) and amplitude (**D**, n=6, N=3, *p<0.05, ***p<0.001, paired t-test).

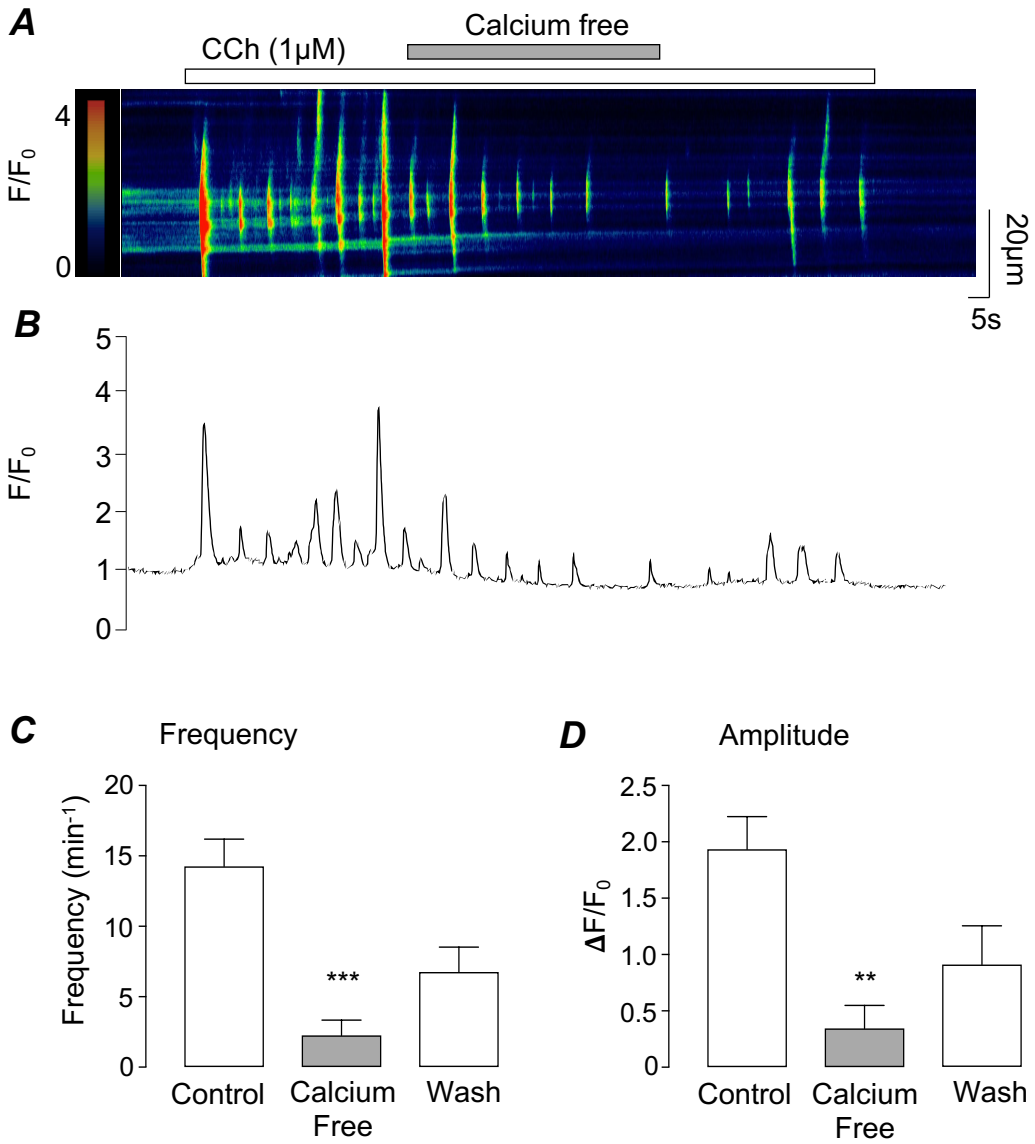

Figure 6.13 ***Effect of extracellular calcium free solution on CCh-induced calcium oscillations in freshly isolated ASMCs.*** (**A**) Representative pseudolinescan showing the effects of calcium-free Hanks' solution on CCh (1μM)-evoked calcium responses in mouse ASMCs, and (**B**) the correlating intensity profile plot. Summary bar charts plotting mean calcium oscillation frequency (**C**) and amplitude (**D**, n=8, N=6, **p<0.01, ***p<0.001, paired t-test) in the presence of a calcium free solution.

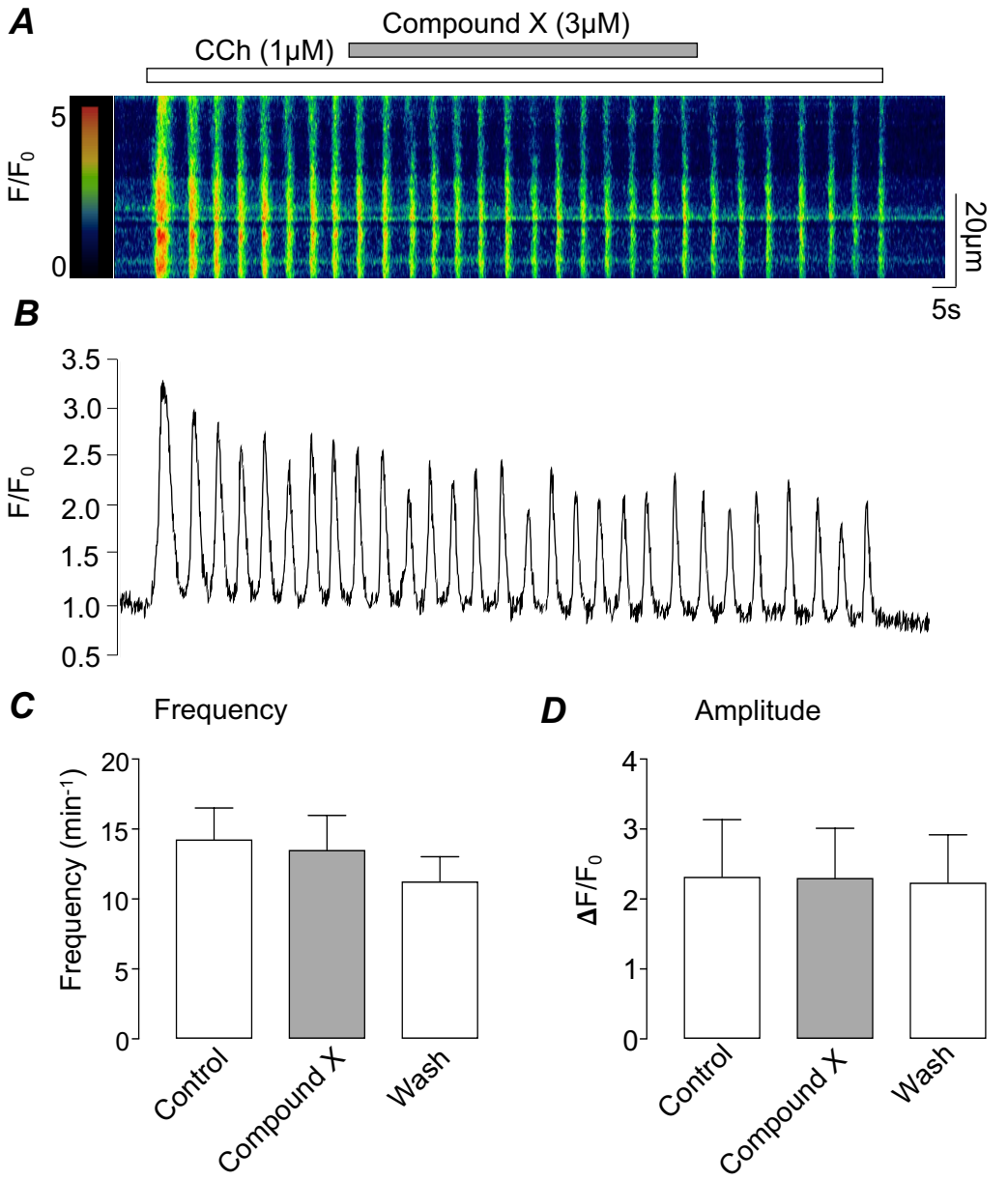

Figure 6.14. ***Effect of the BK channel opener, Compound X on CCh-evoked calcium oscillations in freshly isolated ASMCs.*** Representative pseudolinescan showing the effects of Compound X (3μM) on CCh (1μM)-induced calcium oscillations in mouse ASMCs (**A**), and the correlating intensity profile plot (**B**). Summary bar charts plotting mean calcium oscillation frequency (**C**) and amplitude (**D**, n=8, N=6, $p>0.05$, paired t-test) in the absence and presence of Compound X.

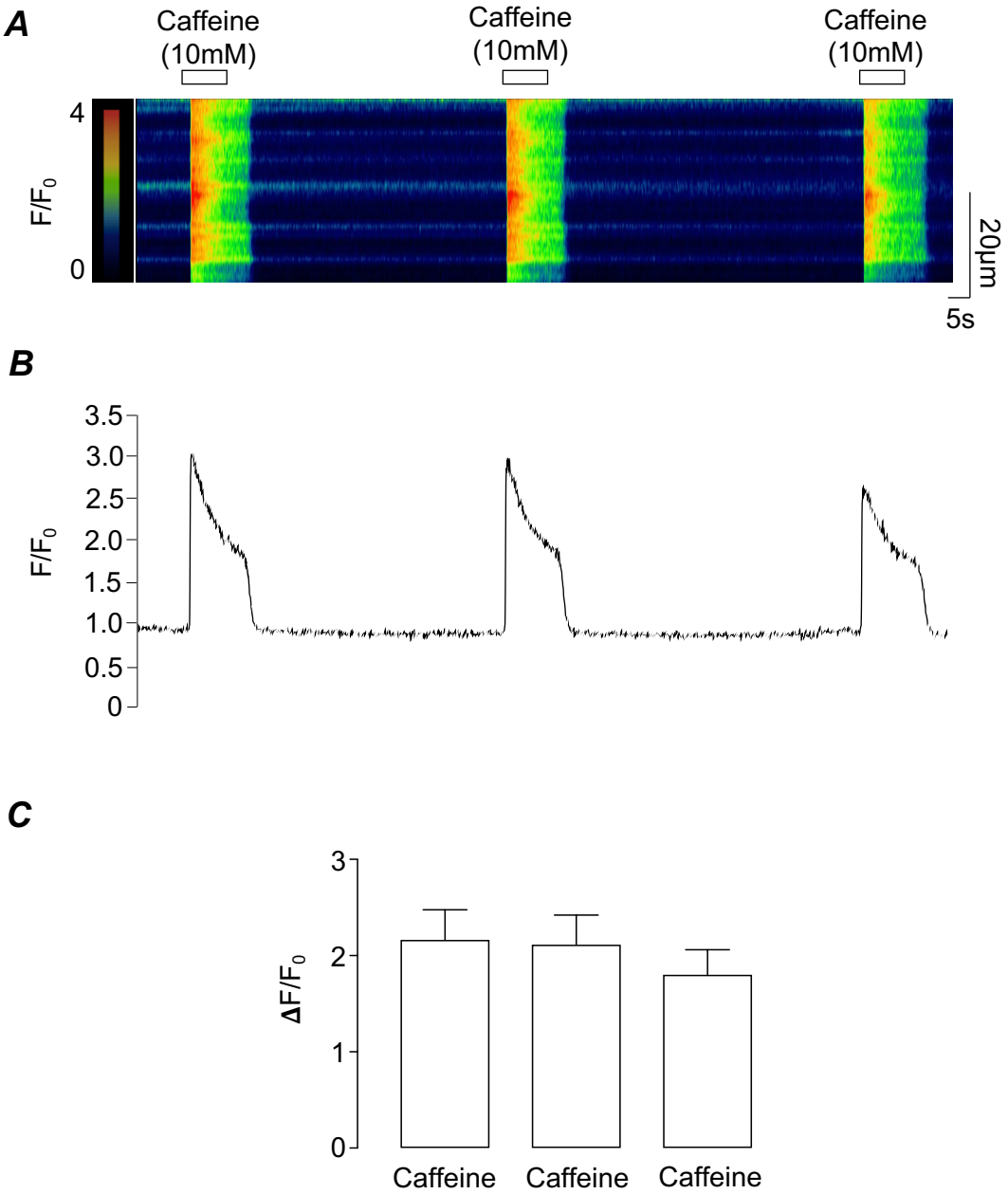

Figure 6.15. ***Successive applications of caffeine induced consistent calcium transients in freshly isolated ASMCs.*** (**A**) Representative pseudolinescan showing that multiple additions of caffeine (10mM) evoked consistent calcium transients in mouse ASMCs, and (**B**) the correlating intensity profile plot. (**C**) Summary bar charts from 7 similar experiments determining the mean amplitude of the initial calcium oscillation in each successive application, with statistical analysis determining no significant difference between transients ($p>0.05$, paired t test, n=7, N=5).

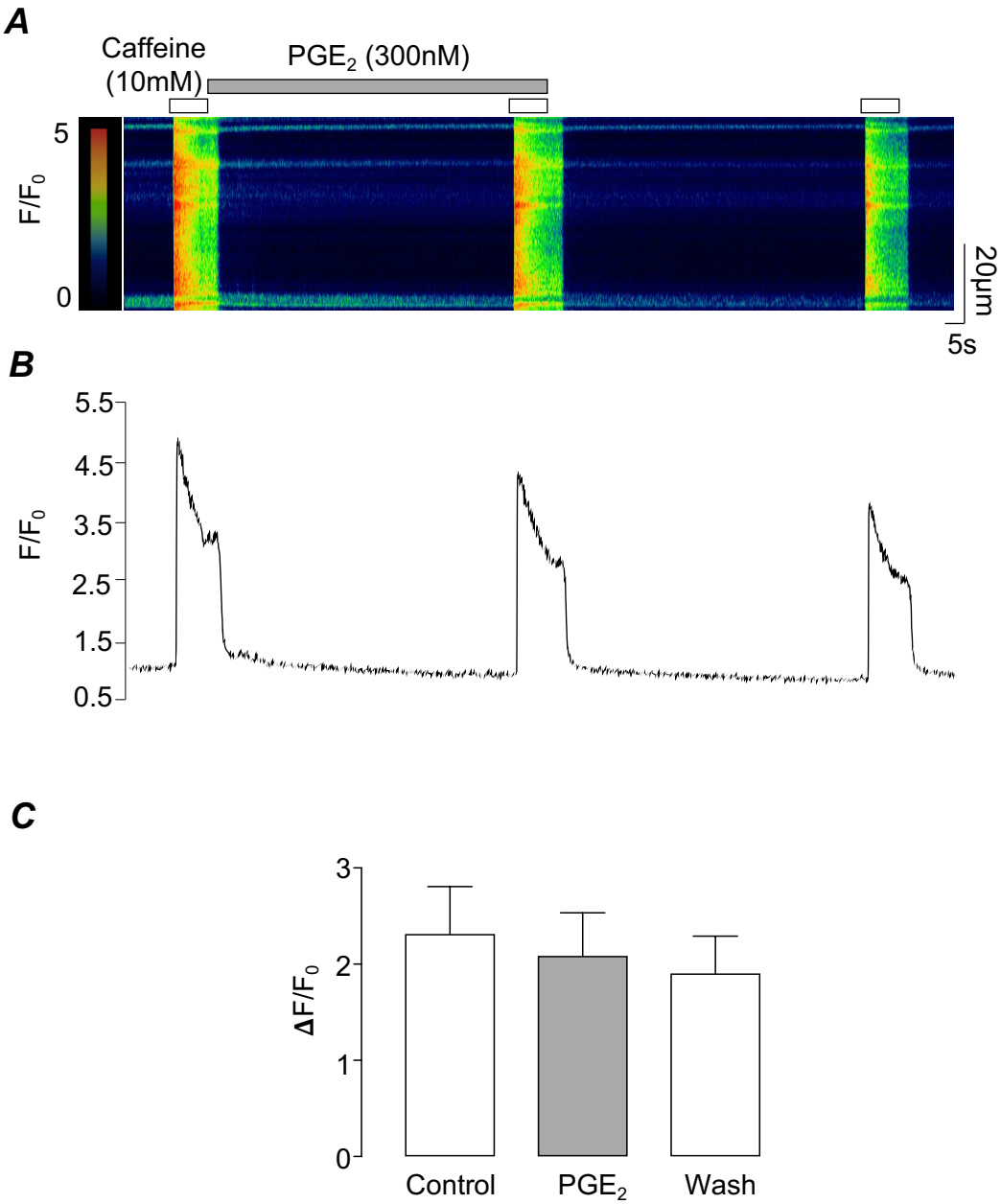

Figure 6.16. ***Effect of PGE_2 on caffeine-induced calcium transients in freshly isolated ASMCs.*** (**A**) Representative pseudolinescan showing the effects of PGE_2 (300nM) on caffeine (10mM)-evoked calcium transients in mouse ASMCs, and (**B**) the correlating intensity profile plot. (**C**) Summary bar charts from 7 similar experiments determining the mean amplitude of the initial calcium oscillation in the presence of PGE_2, with statistical analysis determining no significant difference in the presence of PGE_2 on these oscillations ($p>0.05$, paired t test, $n=7$, $N=5$).

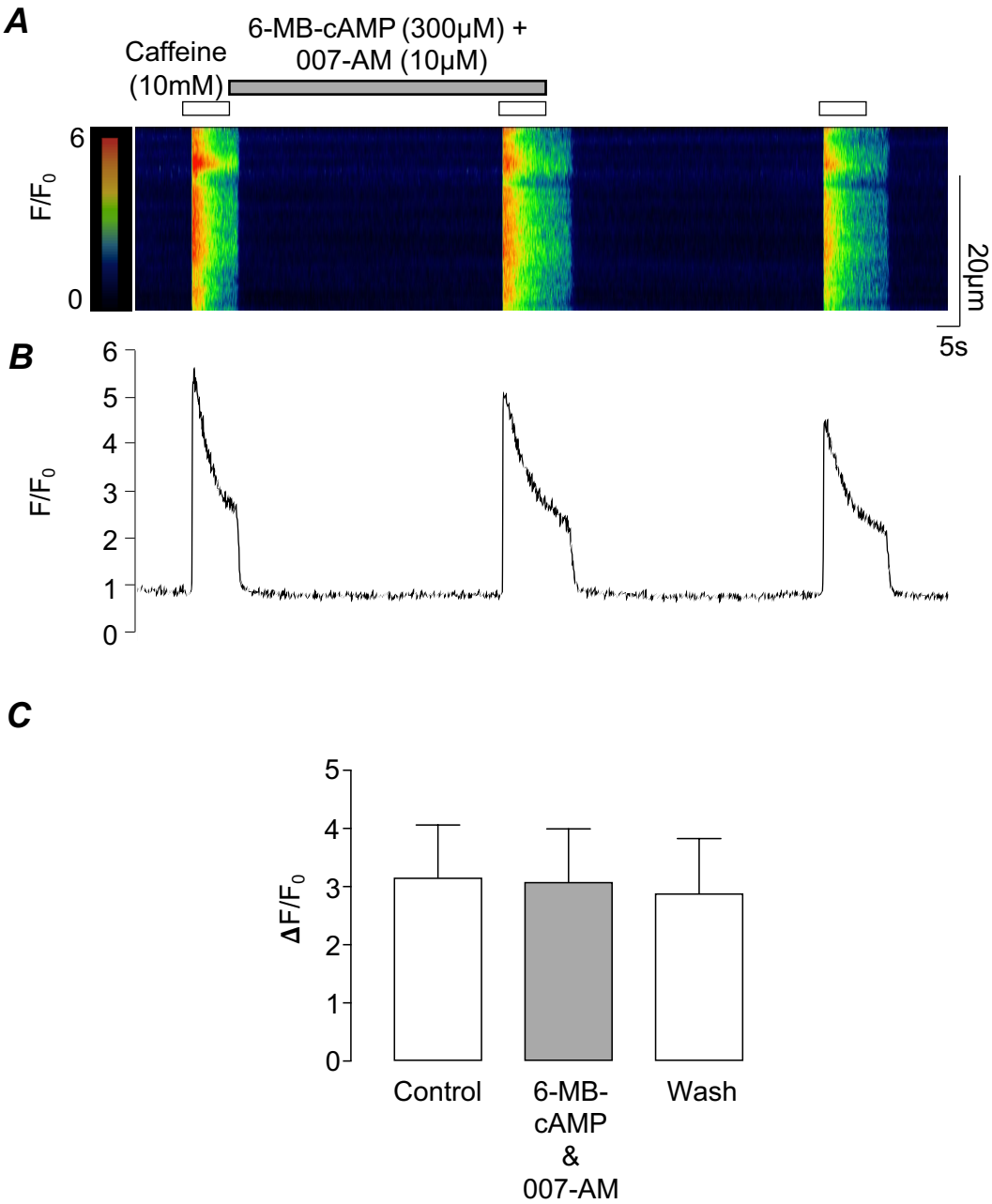

Figure 6.17. ***Effect of 6-MB-cAMP and 007-AM on caffeine-induced calcium transients in freshly isolated ASMCs.*** (**A**) Representative pseudolinescan showing the effects of dual application of the PKA and EPAC agonists, 6-MB-cAMP (300μM) and 007-AM (10μM), respectively on caffeine (10mM)-evoked calcium transients in mouse ASMCs. (**B**) displays the corresponding intensity profile plot. (**C**) Summary bar charts from 7 similar experiments determining the mean amplitude of the initial calcium oscillation in the absence and presence of 6-MB-cAMP and 007-AM, with statistical analysis determining no significant difference in control versus agonists on these oscillations ($p>0.05$, paired t test, n=7, N=6).

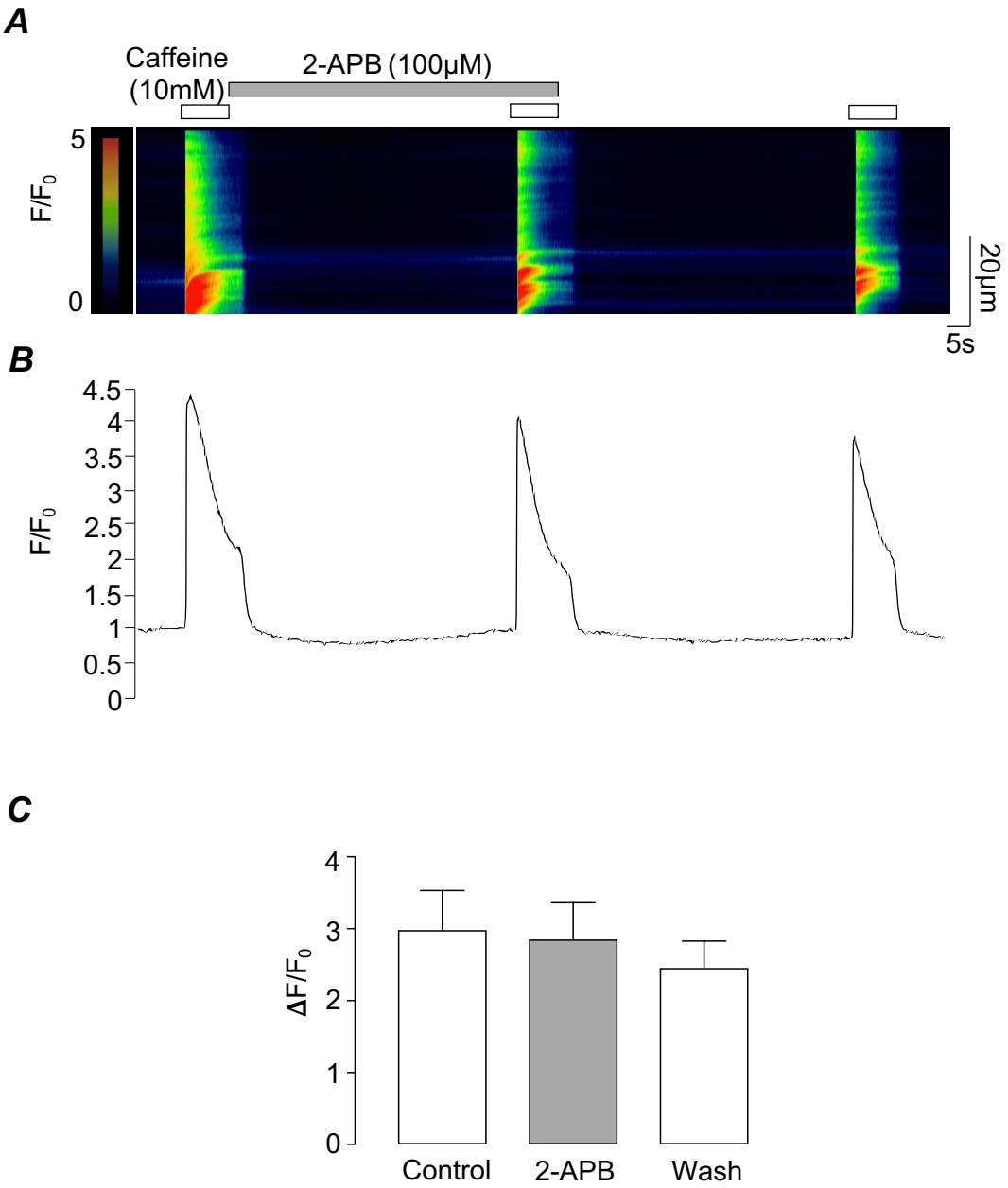

Figure 6.18. ***Effect of the IP_3R antagonist, 2-APB on caffeine-induced calcium transients in freshly isolated ASMCs.*** Representative pseudolinescan showing the effects of 2-APB (100μM) on caffeine (10mM)-evoked calcium transients in mouse ASMCs (**A**) and the correlating intensity profile plot (**B**). (**C**) Summary bar charts from 7 similar experiments determining the mean amplitude of the initial calcium oscillation in the presence of 2-APB, with statistical analysis determining no significant difference in control versus 2-APB ($p>0.05$, paired t test, n=7, N=5).

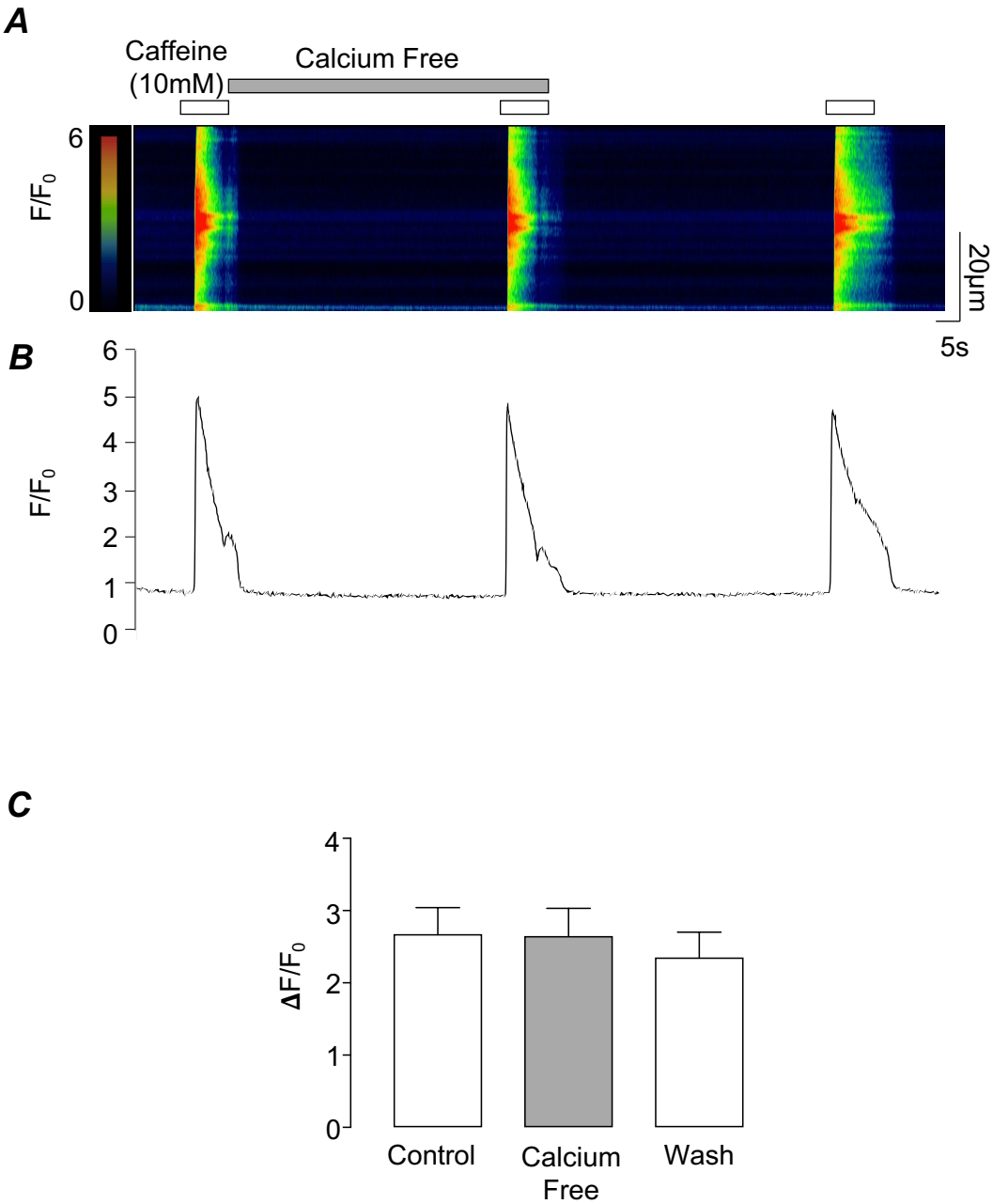

Figure 6.19. ***Effect of extracellular calcium free solution on caffeine-induced calcium transients in freshly isolated ASMCs.*** (**A** & **B**) Representative pseudolinescan showing the effects of removal of calcium from the extracellular solution on caffeine (10mM)-evoked calcium transients in mouse ASMCs (**A**) and the correlating intensity profile plot (**B**). (**C**) Summary bar charts from 6 similar experiments determining that application of a calcium free solution had no discernable effects on the mean amplitude of the initial calcium oscillation ($p>0.05$, paired t test, n=6, N=4).

6.3 Discussion

The main findings of this chapter were as follows: 1) Addition of CCh, induced repetitive calcium oscillations in freshly isolated mouse ASMCs; 2) PGE_2 reduced the frequency and amplitude of these CCh-evoked calcium oscillations; 3) The inhibitory effects of PGE_2 were mimicked by the selective EP2R agonist, (*R*)-Butaprost and by activation of AC with forskolin; 5) Activation of PKA and EPAC with 6-MB-cAMP and 007-AM, respectively reduced the frequency of CCh-induced calcium oscillations but not to the same extent as PGE_2. However, when applied in combination they reduced oscillation frequency and amplitude to a similar degree; 6) CCh-induced calcium responses were abolished by the IP_3R and RyR antagonists, 2-APB and tetracaine and were reduced in frequency by removal of extracellular calcium; 7) Caffeine-evoked calcium transients were not affected by PGE_2 suggesting that PGE_2 does not mediate its effects through the release of calcium from, or refilling of, caffeine-sensitive calcium stores.

In the present study, we found that the addition of 1μM CCh to freshly isolated ASMCs induced an initial calcium transient, followed by a series of calcium oscillations that were superimposed on a raised baseline, similar to that described by Prakash *et al*. (1997) in porcine trachea smooth muscle cells and by Bai and Sanderson (2006) in mouse lung slices. Our findings show that PGE_2 inhibited the frequency and amplitude of CCh-induced calcium oscillations and this effect was mimicked by the selective EP2R agonist, (*R*)-Butaprost, suggesting that these effects were mediated by activation of EP2Rs. Dale *et al*. (2018) reported similar inhibitory effects of PGE_2 on histamine-evoked calcium oscillations in hBSMCs, although they attributed the inhibitory effects of PGE_2 to activation of both EP2 and EP4Rs.

The effects of PGE_2 were comparable to those induced by activation of β-ARs, as Bai and Sanderson (2006) reported that MCh-induced calcium oscillations in mouse ASMCs were inhibited by the β-adrenergic agonist, isoproterenol. Similarly, Prakash *et al*. (1997) found that addition of the β_2-adrenergic agonist, salbutamol reduced the frequency of ACh-evoked calcium oscillations in porcine ASMCs. In both studies, these responses were attributed to activation of the AC/cAMP pathway as they were mimicked by cell permeable

cAMP analog, 8-bromoadenosine-3',5'-cyclic monophosphate (8-Bromo-cAMP). This agrees with the present study as we found that the selective AC agonist, forskolin also inhibited CCh-evoked calcium responses.

Roscioni *et al.* (2009) reported that downstream of β_2-adrenergic activation, PKA and EPAC co-operate to reduce bradykinin-induced IL-8 production in human ASMCs. In contrast, Dale *et al.* (2018) reported that pre-treatment with a selective cAMP-dependent PKA agonist reduced histamine-evoked calcium responses in cultured hBSMCs yet, reported no discernible effects of EPAC activator, 007-AM. We found that individual application of selective PKA and EPAC agonists significantly reduced oscillation frequency but not oscillation amplitude, but, when applied together, exerted greater inhibitory effects, similar to that induced by forskolin. Yu *et al.* (2017) also reported a synergistic effect of PKA and EPAC in the relaxation of coronary artery SMCs following G protein-coupled estrogen receptor 1 activation.

The inhibitory effects of 007-AM suggest that activation of EPAC can inhibit calcium oscillations in ASM but it is not yet clear if EPAC is involved in PGE_2 mediated inhibition of CCh-evoked calcium oscillations. In the present study, application of the PKA inhibitor, Rp-8-CPT-cAMPs abolished the inhibitory effects of PGE_2 on calcium oscillations confirming a role for PKA in this response, however selective inhibitors are not yet available and therefore it was not possible to discern the effect of EPAC inhibition on the inhibitory effects of PGE_2. However, oscillation frequency was still significantly reduced in the presence of Rp-8-CPT-cAMPS in comparison to control suggesting a role for a PKA-independent mechanism in the inhibitory effects of PGE_2 on oscillation frequency. Evidence in support of a role for PKA in inhibition of calcium responses in ASMC comes from Taylor *et al.* (2017), who found that the inhibition of histamine-evoked calcium transients by both PGE_2 and 8-bromo-cAMP were reduced by Rp-8-CPT-cAMPS in bovine tracheal SMCs. In addition, Morgan *et al.* (2014), showed that β_2-adrenoreceptor-induced relaxations were mediated exclusively by PKA using cultured human ASMCs stably expressing the PKA-inhibiting peptides PKI-GFP.

Previous studies have shown that agonist-induced calcium oscillations were induced via calcium release from intracellular calcium stores in ASMCs (Sanderson *et al.* 2008; Pelaia *et al.* 2008; Bergner and Sanderson 2002; Roux

et al. 1997). Data in the present study support this concept as application of the IP_3R and RyR antagonists, 2-APB and tetracaine, respectively, abolished CCh-evoked calcium oscillations. In contrast, Bai *et al.* (2009), reported that MCh-evoked calcium oscillations in mouse ASMCs were abolished by the IP_3R antagonist, 2-APB but not the RyR antagonist, ryanodine. Bai and colleagues applied ryanodine for a maximum of 6.5 minutes however, Nelson *et al.* (1995) demonstrated that it took approximately 8 minutes to achieve the full inhibitory effects of ryanodine on STOCs in arterial SMCs. In addition, Prakash *et al.* (1997) found that 100μM ryanodine significantly reduced the frequency of ACh-evoked calcium oscillations in porcine ASMCs, whereas Bai *et al.* employed ryanodine at a concentration of 50μM. Therefore, this discrepancy may be due to the concentration used and/or the time dependency exhibited by ryanodine.

Our study indicates that both IP_3R and RyRs can mediate calcium release from the SR following the addition of CCh. However, the question remains: if both calcium channels can elicit calcium release, how does individual inhibition of IP_3Rs and RyRs fully abolish CCh-evoked calcium oscillations? Activation of G_q protein-coupled receptors initiates the upregulation of PLC and subsequently increases IP_3 and DAG (Buckley *et al.* 1989; Fukada *et al.* 1989). Therefore, release from IP_3Rs would be expected to be the primary calcium release event which could then induce CICR from RyRs. However, in this scenario it would be expected that inhibition of IP_3Rs would fully abolish CCh-evoked calcium oscillations whereas blockade of RyRs would only partially reduce the calcium response. This discrepancy may be attributable to off-target effects of tetracaine on IP_3Rs, MacMillan *et al.* (2005) reported that application of 100μM tetracaine reduced submaximal levels of caged-IP_3 calcium release by approximately 30%. Therefore, in the present study it is possible that tetracaine blocks RyRs and partially inhibits IP_3Rs, however, this idea requires further investigation.

CCh-evoked calcium oscillations were also reduced, but not abolished, by removal of extracellular calcium, suggesting that calcium release from the SR was the primary source of calcium in these responses. However, as the CCh-evoked calcium oscillations were not affected by the BK channel opener, Compound X, it suggests that calcium entry via VDCCs was not involved in these responses. Similar results were obtained by Roux *et al.* (1997), who found that

the initiation of muscarinic-induced calcium oscillations was not affected by the application of the voltage-dependent calcium channel blocker, verapamil, nor by calcium free solution. Another possibility is that removal of extracellular calcium induced depletion of intracellular stores. However, since caffeine-induced calcium responses remained intact during application of calcium-free media it seems likely that the effects were not mediated by depletion of calcium from intracellular calcium stores. Instead, it appears that calcium influx via a voltage-independent pathway contributes to CCh-induced calcium oscillations in ASMC. One such pathway includes calcium influx via transient receptor potential (TRP) channels, a class of non-selective cation channels. In the airways, TRP channels have been proposed as receptor-operated calcium channels and store-operated calcium channels (Gosling *et al.* 2005). The role of TRP channels in ACh-induced contraction was demonstrated by White *et al.* (2006), who found that increased TRP canonical 1 (TRPC1) expression augmented ACh responses and increased SOCE six-fold in human ASMCs. In addition, Yocum *et al.* (2017) reported that the TRP vanilloid 1 (TRPV1) antagonist, capsazepine reduced MCh-evoked calcium oscillations in mouse ASMCs. Therefore, it is not unreasonable to suggest that TRP channels may contribute to the calcium influx observed in this study, however further investigation would be required to confirm this theory.

In the present study, we found that neither PGE_2, nor 6-MB-cAMP and 007-AM in combination, elicited any effect on caffeine-evoked calcium transients, suggesting that their inhibitory effect on CCh responses did not result from inhibition of RyRs, SERCA or SOCs. Instead, it seems more likely that they affected IP_3 signalling, as has been suggested by Bai and Sanderson (2006), who found that application of the AC agonist, forskolin reduced flash-photolysis of caged-IP_3 in mouse lung slices. A similar result was observed by Dale *et al.* (2018) upon the application of the selective β_2-adrenoreceptor agonist, isoproterenol in cultured human ASMCs.

In summary, the data from this chapter suggests that PGE_2 inhibits CCh-evoked calcium oscillations in ASMCs. These events are dependent upon calcium release from the SR via IP_3Rs and RyRs and are maintained by calcium influx across the membrane. The inhibitory effects of PGE_2 were mimicked by activators of AC, as well as PKA and EPAC and were reduced by the PKA antagonist Rp-8-CPT-cAMPs. In contrast, these agents failed to inhibit caffeine-

evoked calcium transients indicating that PGE_2 does not mediate its inhibitory effects through the inhibition of calcium from or refilling of, caffeine-sensitive calcium stores. Taken together, these data suggest that PGE_2 may mediate its inhibitory actions on CCh-evoked calcium oscillations through activation of PKA, and possibly EPAC, to inhibit IP_3R-dependent calcium signalling.

7. General Discussion

The main objective of this project was to examine the mechanisms underlying the effects of PAR2 activation on mouse ASM contractility. Due to its ability to couple to a number of different G protein-coupled receptors, including $G_{q/11}$, $G_{i/o}$ and $G_{12/13}$, PAR2 can elicit diverse, and often opposing, responses in the airways (Geppetti and Trevisani 2003; Miotto *et al*. 2002; Lan *et al*. 2001). The current study examined the effects of the PAR2 agonist, fLIGRLO on contractions of mouse bronchial rings evoked by CCh and EFS. We found that PAR2 stimulation reduced the amplitude of these responses and that this effect was prevented by the COX 1 and 2 inhibitor, indomethacin, suggesting that endogenously released prostanoids could be involved. Our findings contrast with those of Schmidlin *et al.* (2001) and Chambers *et al.* (2001) which demonstrated that PAR2 stimulating peptides induced contraction, rather than relaxation, of human ASM. However, Chambers and colleagues also reported that, in the same preparation, removal of the epithelium or addition of indomethacin augmented PAR2-induced contractions. When taken together, these data suggest that activation of PAR2 inhibits ASM contraction via release of endogenous prostanoids from the epithelia. A diagram highlighting the proposed mechanism of action of PGE_2 is shown in *Figure 7.1*.

PGE_2 is the most abundantly released prostanoid in the body and is readily produced by a number of airway cell types including epithelia, fibroblasts and ASMCs (Sastre and del Pozo 2012; Huang and Peters-Golden 2008). Previous studies reported that activation of EP2&4Rs were responsible for the relaxant effects of PGE_2 on ASM (Benyahia *et al*. 2012; Tilley *et al.* 2003). We showed that fLIGRLO-induced responses were substantially reduced in the presence of the selective EP2R antagonist, PF-04418948, suggesting that the inhibitory effects of PAR2 were brought about by PGE_2, via activation of EP2Rs. We also found that EFS of bronchial rings pre-contracted with CCh, elicited relaxations that were resistant to TTX and ω-conotoxin, but were inhibited by PF-04418948 indicating that this effect was not mediated by activation of inhibitory nerves, but did involve activation of EP2Rs. CCh-evoked calcium oscillations in freshly isolated ASMCs were not affected by fLIGRLO. This, taken together the short pulse width (0.3ms) used in this study, suggest that the effects of PAR2 activation were unlikely to result from direct stimulation of smooth muscle. Ricciardolo *et al.*

(2000) and Cocks *et al.* (1999) found that removal of the epithelium abolished PAR2-induced relaxations of guinea pig and mouse bronchi. Additionally, Ullman *et al.* (1990) reported an epithelium-dependent inhibitory mediator in response to EFS at 12Hz in isolated ferret trachea. Therefore, it is tempting to speculate that release of PGE_2 from epithelia underlies the inhibitory effects of PAR2 activation in ASM, however, further investigation would be necessary to verify this theory.

PGE_2 exerts its effects via activation of EP1, 2, 3 and 4Rs and my RT-PCR and qPCR experiments demonstrated that all four *Ptger* genes (EPR1-4) were expressed in mouse bronchi, however *Ptger4* (EP4R) transcripts were not detected in isolated ASMCs. We found that exogenously applied PGE_2 inhibited both CCh and EFS-induced contractions of ASM. The EP2R antagonist, PF-04418948 inhibited these responses, however the EP4R antagonist, ONO-AE3-208 did not affect PGE_2-induced inhibition of CCh responses, but produced a small inhibition of EFS responses, when applied in the presence of PF-04418948. In addition, we show that the IC_{50} values for PGE_2 were much lower on EFS responses (1.4nM), compared to those induced by CCh (44nM). My data suggest that PGE_2 may inhibit cholinergic nerve-evoked contractions of ASM via both pre and post-junctional mechanisms. This is consistent with a previous study by Belvisi *et al.* (1996),which reported that PGE_2 inhibited ACh release of guinea pig trachea from cholinergic nerve terminals.

EP2&4Rs are G_s protein-coupled receptors which mediate their inhibitory effects via activation of the AC/cAMP pathway and subsequent upregulation of PKA and possibly EPAC (Lebender *et al.* 2018; Konya *et al.* 2013; Zhu *et al*. 2002). However, the cellular mechanisms underlying the effects of cAMP in mouse ASM are not yet entirely understood (Lebender *et al.* 2018; Konya *et al.* 2013; Zhu *et al*. 2002). We found that the inhibitory responses of PGE_2 were mimicked by the AC and PKA activators, forskolin and 6-MB-cAMP, respectively and that these effects were reduced by the BK channel blocker, IbTx. It is unclear whether the effects of IbTx imply a direct role for activation of BK channels in PGE_2-mediated responses in ASM, or whether PGE_2 was simply less effective under conditions in which BK channels were blocked. Huang *et al.* (1993), suggested that inhibition of salbutamol-induced relaxations of guinea pig ASM produced by IbTx (50nM) were associated with membrane depolarisation and increased calcium influx via voltage-gated calcium channels, which functionally

antagonised the inhibitory response. In the present study we found that PGE_2 responses were unaffected by the K_v7 channel blocker, XE-991, which has been shown to cause depolarisation of ASMCs (Evseev *et al.* 2013). Although not conclusive, this suggests that PGE_2 responses in the present study could involve activation of BK channels.

I conducted a number of experiments to investigate the downstream effector molecules responsible for PGE_2-induced bronchodilation. We found that the PKA activator, 6-MB-cAMP reduced the amplitude of CCh-evoked contractions of ASM and that PGE_2-induced relaxations were inhibited by the PKA blocker, Rp-8-CPT-cAMPs consistent with a role for PKA in this response. The lack of selective EPAC inhibitors available to date, hindered our ability to investigate the potential role of EPAC in this pathway. However, we found that the highly selective EPAC activator, 007-AM reduced the amplitude of CCh responses and Zieba *et al.* (2011) and Roscioni *et al.* (2011) reported a role for EPAC in relaxations of ASM induced by β-adrenoreceptor agonists. Therefore, it is possible that EPAC could also be involved in the inhibitory effects of PGE_2.

It has been suggested that the amplitude of agonist-induced contractions of ASM is correlated with the frequency of underlying calcium oscillations in SMCs (Perez and Sanderson 2005; Kuo *et al.* 2003). We found that CCh-induced calcium oscillations in isolated mouse ASMCs were abolished by PGE_2. In the current study, these effects were mimicked by the EP2R agonist, (*R*)-Butaprost and AC activator, forskolin, and were reduced by the PKA antagonist, Rp-8-CPT-cAMPs, suggesting that the inhibitory effects of PGE_2 on CCh-evoked calcium oscillations were mediated via stimulation of EP2Rs, activation of AC and upregulation of PKA.

Previous studies showed that agonist-induced calcium oscillations in ASMCs were dependent on calcium release from intracellular calcium stores (Sanderson *et al.* 2008; Pelaia *et al.* 2008; Bergner and Sanderson 2002; Roux *et al.* 1997) and we found that CCh-induced calcium oscillations were inhibited by the IP_3R blocker, 2-APB as well as the RyR blocker, tetracaine, consistent with this idea. In addition, the frequency and amplitude of these events was reduced by removal of external calcium suggesting a reliance on both calcium release from intracellular stores and calcium influx across the plasma membrane. However, we demonstrated that PGE_2 failed to inhibit caffeine-evoked calcium

transients suggesting that it did not mediate its inhibitory effects through the inhibition of calcium release from, or refilling of, caffeine-sensitive calcium stores. My data suggest that PGE_2 is more likely to mediate its inhibitory effects on CCh-evoked calcium oscillations through inhibition of IP_3R, rather than RyR-dependent calcium release. Taylor *et al.* (2017), showed that PGE_2 inhibited accumulation of IP_3 in human aortic SMCs stimulated with histamine, suggesting that it inhibited IP_3 production. Such an effect could also account for the effects observed in this study, however, further investigation would be necessary to investigate this issue.

In summary, the present study demonstrates that activation of PAR2 inhibited cholinergic contractions of ASM via production of PGE_2. PGE_2 primarily exerted its inhibitory effects via activation of EP2Rs and subsequent activation of PKA. The effects of PGE_2 appear to be mediated by a combination of activation of BK channels and inhibition of calcium oscillations in ASMCs (*Figure 7.1*), however, further work is required to resolve the mechanism underlying these effects. The data presented in this thesis provide novel insights into the mechanism of action of PGE_2 on mouse ASM and highlight an opportunity for an alternative smooth muscle receptor targeted therapy for bronchodilation via activation of EP2/4Rs.

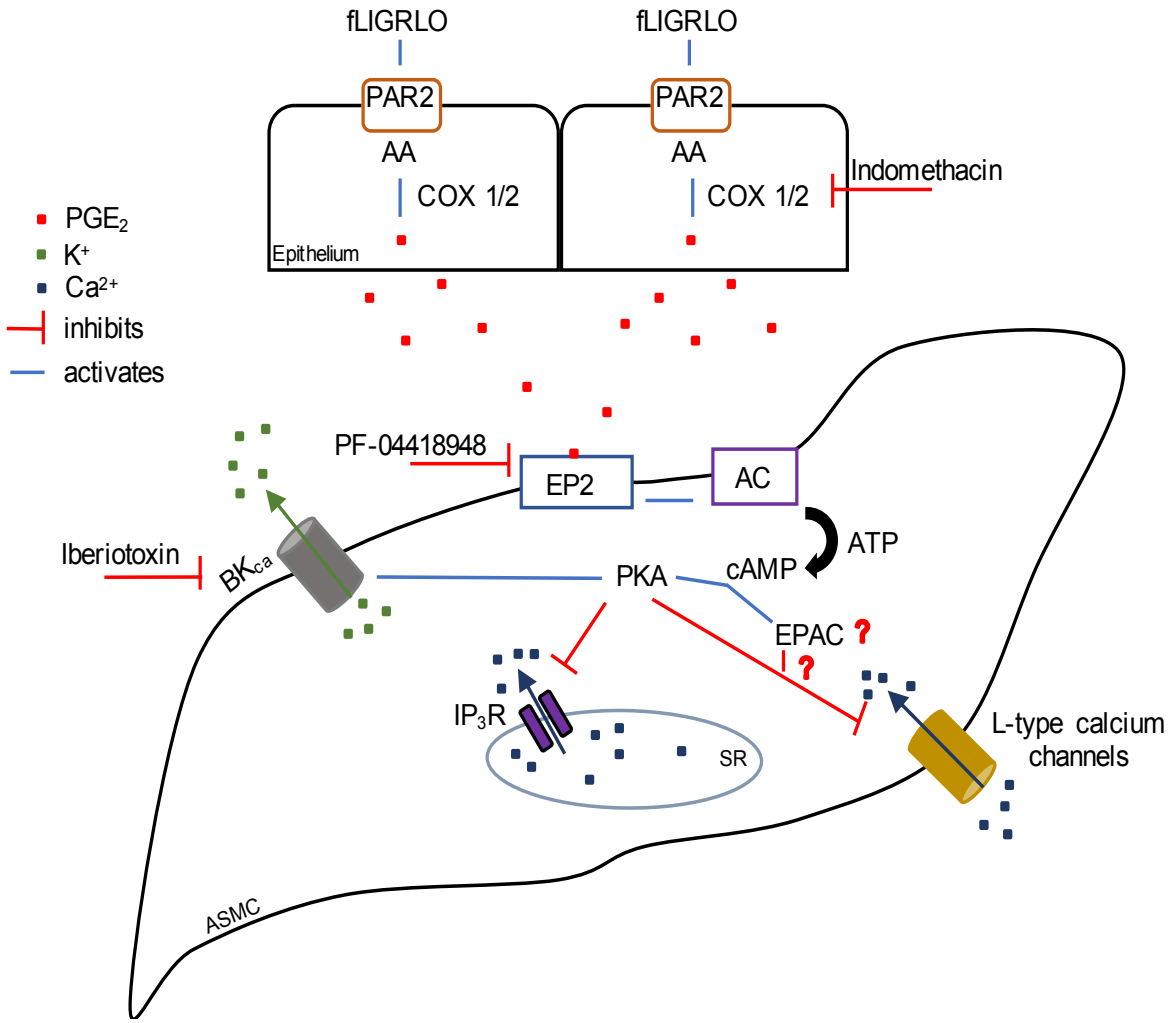

Figure 7.1 Summary of proposed mechanism of action of PGE_2 described in this thesis.

7.1 Future experiments

1. Utilise the patch-clamp technique to investigate the effect of PGE_2 on membrane potential of isolated mouse ASMCs. Does PGE_2 induce activation of BK channels or affect L-type calcium current? If so, are these effects mimicked by the EP2R agonist, (*R*)-Butaprost, and the AC and PKA activators, forskolin and 6-MB-cAMP, respectively?

2. Confirm RT-PCR findings using immunocytochemistry. Do EP2R antibodies label ASMCs? Are EP4R absent on ASMCs? Do EP4R antibodies stain nerves?

3. Examine the expression of PAR2 on whole tissue using immunohistochemistry. Are PAR2 predominately present on the epithelium?

4. Utilise global EPAC $^{-/-}$ mice to investigate the significance of EPAC in PGE_2 mediated responses. Is PGE_2 less effective at inhibiting cholinergic contraction in EPAC deficient mice? Can PGE_2 abolish CCh-evoked calcium oscillations in ASMCs from EPAC $^{-/-}$ mice?

5. Investigate the effect of PGE_2 on caged-IP_3 responses using confocal calcium imaging. Are these responses reduced in the presence of PGE_2? Is the effect reduced in the presence of the PKA inhibitor, Rp-8-CPT-cAMPs? Is this effect mimicked by a PKA activator, 6-MB-cAMP or EPAC activator, 007-AM?

6. Investigate the role of cADPR on CCh-evoked calcium oscillations of mouse ASM. Do cADPR antagonists reduce these oscillations? Do cADPR agonists increase the frequency of CCh-evoked calcium oscillations? Is PGE_2 less effective at inhibiting CCh-evoked calcium oscillations in the presence of a cADPR agonist?

7. Studies on human ASM, in particular ASM from COPD patients. Does activation of EP4Rs in human ASM exhibit similar downstream pathways to

EP2Rs in mouse ASM? Are PGE_2-induced relaxations reduced in ASM from COPD patients? Is the effect of PGE_2 on human ASM reduced by BK channel blockade? Is this effect similar in ASM from control subjects vs COPD patients? Can PGE_2 abolish CCh-evoked calcium oscillations in human ASMCs?

8. References

Abrams, P., Andersson, K.E., Buccafusco, J.J., Chapple, C., Chet de Groat, W., Fryer, A.D., Kay, G., Laties, A., Nathanson, N.M., Pasricha, P.J. and Wein, A.J. (2006). Muscarinic receptors: their distribution and function in body systems, and implications for treating overactive bladder. *British Journal of Pharmacology*, 148(5), pp. 565-578.

Álvarez-Santos, M.D., Álvarez-González, M., Estrada-Soto, S. and Bazán-Perkins, B. (2020). Regulation of Myosin Light-Chain Phosphatase Activity to Generate Airway Smooth Muscle Hypercontractility. *Frontiers in Physiology* [online], 701(11). Available from: https://www.ncbi.nlm.nih.gov/pmc/articles/PMC7333668/ [accessed 5th February 2022].

Alzayady, K.J., Wang, L., Chandrasekhar, R., Wagner, L.E., Petegem., V.F. and Yule, D.I. (2016). Defining the stoichiometry of inositol 1,4,5-trisphosphate binding required to initiate Ca^{2+} release. *Science Signalling* [online], 9(422). Available from: https://pubmed.ncbi.nlm.nih.gov/27048566/ [accessed 19th August 2021].

Andor Oxford Instruments. (2019). *Confocal dual spinning disk* [image online]. Available from: https://andor.oxinst.com/learning/view/article/confocal-dual-spinning-disk [accessed on 8th March 2019].

Angus, J. and Wright, C. (2000). *Organ bath, transducer, and micrometer-controlled support leg for the vessel segments* [image online]. Available from: https://www.researchgate.net/publication/12009884_Techniques_to_study_the_pharmacodynamics_of_isolated_large_and_small_blood_vessels [accessed on 8th March 2019].

Aso, H., Ito, S., Mori, A., Suganuma, N., Morioka, M., Takahara, N., Kondo, M. and Hasegawa, Y. (2013). Differential regulation of airway smooth muscle cell migration by E-prostanoid receptor subtypes. *American Journal of Respiratory Cell and Molecular Biology*, 48(3), pp. 322-329.

Asokananthan, N., Graham, P.T., Fink, J., Knight, D.A., Bakker, A.J., McWilliam, A.S., Thompson, P.J. and Stewart, G.A. (2002). Activation of protease-activated

receptor (PAR)-1, PAR-2, and PAR-4 stimulates IL-6, IL-8, and prostaglandin E_2 release from human respiratory epithelial cells. *The Journal of Immunology*, 168(7), pp.3577-3585.

Ay, B., Prakash, Y.S., Pabelick, C.M. and Sieck, G.C. (2004). Store-operated Ca^{2+} entry in porcine airway smooth muscle. *American Journal of Physiology Lung Cellular and Molecular Physiology*, 286(5), pp. 909-917.

Baba-Aissa, F., Raeymaekers, L., Wuytack, F., De, G.C., Missiaen, L. and Casteels, R. (1996). Distribution of the organeller Ca^{2+} transport ATPase SERCA2 isoforms in the cat brain. *Brain Research*, 743(1-2), pp. 141-153.

Bai, Y. and Sanderson, M.J. (2006). Airway smooth muscle relaxation results from a reduction in the frequency of Ca^{2+} oscillations induced by a cAMP-mediated inhibition of the IP_3 receptor. *Respiratory Research* [online], 7(1). Available from: https://www.ncbi.nlm.nih.gov/pmc/articles/PMC1459146/ [accessed 8th April 2019].

Bai, Y., Edelmann, M. and Sanderson, M.J. (2009). The contribution of inositol 1,4,5-triphosphate and ryanodine receptors to agonist-induced Ca^{2+} signalling of airway smooth muscle cells. *American Journal of Physiology Lung Cellular and Molecular Physiology*, 297 (5), pp. 347-361.

Bao, R., Lifshitz, L.M., Tuft, R.A., Bellve, K., Fogarty, K.E. and ZhuGe, R. (2008). A close association of RyRs with highly dense clusters of Ca^{2+}-activated Cl- channels underlies the activation of STICs by Ca^{2+} sparks in mouse airway smooth muscle. *Journal of General Physiology,* 132(1), pp. 145-160.

Bara, I., Ozier, A., Tunon de Lara, J-M., Marthan, R. and Berger, P. (2010). Pathophysiology of bronchial smooth muscle remodelling in asthma. *European Respiratory Journal*, 36(5), pp. 1174-1184.

Baratelli, F., Lin, Y., Zhu, L., Yang, S.C., Heuzé-Vourc'h, N., Zeng, G., Reckamp, K., Dohadwala, M., Sharma, S. and Dubinett, S.M. (2005). Prostaglandin E_2 induces $FOXP_3$ gene expression and t cell regulatory cell function in human CD_{4+} T cells. *The Journal of Immunology*, 175(3), pp. 1483-1490.

Barnes, P.J., Minette, P. and Maclagan, J. (1988). Muscarinic receptor subtypes in airways. *Trends in Pharmacological Sciences,* 9(11), pp. 412-416.

Belvisi, M.G., Patel, H.J., Takahashi, T., Barnes, P.J. and Giembycz, M.A. (1996). Paradoxial facilitation of acetylcholine release from parasympathetic nerves innervating guinea-pig trachea by isoprenaline. *British Journal of Pharmacology*, 117 (7), pp. 1413-1420.

Benayoun, L., Druilhe, A., Dombret, M-C., Aubier, M. and Pretolani, M. (2003). Airway structural alterations selectively associated with severe asthma. *American Journal of Respiratory and Critical Care Medicine*, 167(10), pp. 1360-1368.

Benyahia, C., Gomez, I., Kanyinda, L., Boukais, K., Danel, C., Leseche, G., Longrois, D. and Norel, X. (2012). PGE_2 receptor (EP_4) agonists: Potent dilators of human bronchi and future asthma therapy?. *Pulmonary Pharmacology and Therapeutics*, 25 (1), pp. 115-118.

Berchtold, M.W., Brinkmeier, H. and Muntener, M. (2000). Calcium ion in skeletal muscle: its crucial role for muscle function, plasticity, and disease. *Physiological Review*, 80(3), pp. 1215-1265.

Bergner, A. and Sanderson, M.J. (2002). Acetylcholine-induced calcium signalling and contraction of airway smooth muscle in lung slices. *Journal of General Physiology*, 119(2), pp. 187-198.

Berridge, M.J. (2008). Smooth muscle cell calcium activation mechanisms. *Journal of Physiology*, 586(21), pp. 5047-5061.

Bezprozvanny, I., Watras, J. and Ehlrich, B.E. (1991). Bell-shaped calcium-response curves of $Ins(1,4,5)P_3$ – and calcium-gated channels from endoplasmic reticulum of cerebellum. *Nature*, 351(6329), pp. 751-754.

Billington, C.K. and Penn, R.B. (2003). Signalling and regulation of G protein-coupled receptors in airway smooth muscle. *Respiratory Research* [online], 4(1). Available from: https://www.ncbi.nlm.nih.gov/pmc/articles/PMC152647/ [accessed 24th April 2019].

Billington, C.K., Ojo, O.O., Penn, R.B. and Ito, S. (2013). cAMP regulation of airway smooth muscle function. *Pulmonary Pharmacology and Therapeutics*, 26(1), pp. 112-120.

Birrell, M, A., Maher, S.A., Buckley, J., Dale, N., Bonvini, S., Raemdonck, K., Pullen, N., Giembycz, M.A. and Belvisi, M.G. (2013). Selectivity profiling of the novel EP2 receptor antagonist, PF-04418948, in functional bioassay systems: atypical affinity at the guinea pig EP2 receptor. *British Journal of Pharmacology*, 168(1), pp. 129-138.

Bohm, S.K., Khitin, L.M., Grady, E.F., Aponte, G., Payan, D.G. and Bunnet, N.W. (1996). Mechanisms of desensitization and resensitization of proteinase-activated receptor 2. *The Journal of Biological Chemistry*, 271(36), pp. 22003-22016.

Bonner, T., Buckley, N., Young, A. and Brann, M. (1987). Identification of a family of muscarinic acetylcholine receptor genes. *Science*, 237(4814), pp. 527-532.

Bootman, M.D. (2012). Calcium signalling. Cold Spring *Harbour Perspectives in Biology* [online], 4(7). Available from: https://www.ncbi.nlm.nih.gov/pmc/articles/PMC3385957/ [accessed 28th June 2021].

Bradley, E., Large, R.J., Bihun, V.V., Mullins, N. D., Hollywood, M.A., Sergeant, G.P. and Thornbury, K.D. (2018). Inhibitory effects of openers of large-conductance Ca^{2+}-activated K^+ channels on agonist-induced phasic contractions in rabbit and mouse bronchial smooth muscle. *American Journal of Physiology-Cell Physiology*, 315(9), pp. 818-829.

Breyer, R.M., Bagdassarian, C.K., Myers, S.A. and Breyer, M.D. (2001). Prostanoid receptors: subtypes and signalling. *Annual Review of Pharmacology and Toxicology*, 41(4), pp. 661-690.

Brown, L.M., Rogers, K.E., Aroonsakool, N.A., McCammon, J.A. and Insel, P.A. (2014). Allosteric inhibition of EPAC. *The Journal of Biological Chemistry*, 289(42), pp. 29148-29157.

Brueggeman, L.I., Haick, J.M., Neuburg, S., Tate, S., Randhawa, D., Cribbs, L.L. and Byron, K.L. (2014). KCNQ (K_V7) potassium channel activators as bronchodilators: combination with a β_2-adrenergic agonist enhances relaxation of rat airways. *American Journal of Physiology Lung Cellular and Molecular Physiology*, 306(6), pp. 476-486.

Brueggemann, L.I., Cribbs, L., Schwartz, J.L., Wang, M., Kouta, A. and Byron, K.L. (2018). Mechanisms of PKA-Dependent Potentiation of $K_V7.5$ Channel Activity in Human Airway Smooth Muscle Cells. *International Journal of Molecular Sciences*, 19(8), pp. 2223.

Brueggemann, L.I., Kakad, P.P., Love, R.B., Solway, J., Dowell, M.L., Crobbs, L.L. and Byron, K.L. (2012). K_V7 potassium channels in airway smooth muscle cells: signal transduction intermediates and pharmacological targets for bronchodilator therapy. *Journal of Physiology Lung Cellular and Molecular Physiology*, 302(1), pp. 120-132.

Buckley, J., Birrel, M., Maher, S., Nials, A., Clarke, D. and Belvisi, M. (2011). EP_4 receptor as a new target for bronchodilator therapy. *British Medical Journal*, 66(12), pp. 1029-1035.

Buckley, N.J., Bonner, T.I., Buckley, C.M. and Brann, M.R. (1989). Antagonist binding properties of five cloned muscarinic receptors expressed in CHO-K1 cells. *Molecular Pharmacology*, 35(4), pp. 469-476.

Buels, K.S. and Fryer, A.D. (2012). Muscarinic Receptor Antagonists: Effects on Pulmonary Function. *Handbook of Experimental Pharmacology*, 208(12), pp. 317-341.

Burford, N.T. and Nahorski, S.R. (1996). Muscarinic M1 receptor- stimulated adenylate cyclase activity in Chinese hamster ovary cells is mediated by $G_s\alpha$ and is not a consequence of phosphoinositidase C activation. *Biochemical Journal*, 315(3), pp. 883-888.

Burgess, J.K., Boustany, S., Black, J.L. and Johnson, P.R.A. (2004). Increased sensitivity of asthmatic airway smooth muscle cells to prostaglandin E_2 might be mediated by increased numbers of E-prostanoid receptors. *Journal of Allergy and Clinical Immunology*, 113(5), pp. 876-881.

Camacho, P. and Lechleiter, J.D. (1995). Calreticulin inhibits repetitive intracellular Ca^{2+} waves. *Cell*, 82(5), pp. 765-771.

Cameron, M.A., Suaning, G.J., Lovell, N.H. and Morley, J.W. (2013). Electrical stimulation of inner retinal neurons in wild-type and retinally degenerate (rd/rd) mice. *PLoS ONE* [online], 8(7). Available from: https://journals.plos.org/plosone/article?id=10.1371/journal.pone.0068882 [accessed on 1st October 2021].

Canning, B.J. (2006). Reflex regulation of airway smooth muscle tone. *Journal of Applied Physiology*, 101(3), pp. 972-985.

Chambers, L.S., Black, J.L., Ge, Q., Carlin, S.M., Au, W.W., Poniris, M., Thompson, J., Johnson, P.R. and Burgess, J.K. (2003). PAR-2 activation, PGE2, and COX-2 in human asthmatic and nonasthmatic airway smooth muscle cells. *American Journal of Physiology: Lung Cellular and Molecular Physiology*, 285(3), pp. 619-627.

Chambers, L.S., Black, J.L., Poronnik, P. and Johnson, P.R.A. (2001). Functional effects of protease-activated receptor-2 stimulation on human airway smooth muscle. *American Journal of Physiology-Lung Cellular and Molecular Physiology*, 281(6), pp.1369-1378.

Chan, W.W. and Mashimo, H. (2013). Lubiprostone Increases Small Intestinal Smooth Muscle Contractions Through a Prostaglandin E Receptor 1 (EP1)-mediated Pathway. *Journal of Neurogastroenterology and Motility*, 19(3), pp. 312-318.

Chung, K.F. (2005). Evaluation of selective prostaglandin E_2 (PGE_2) receptor agonists as therapeutic agents for the treatment of asthma. *Science Signaling*

[online], 9(303). Available from: https://pubmed.ncbi.nlm.nih.gov/16189372/ [Accessed 7th September 2021].

Claar, D., Hartert, T.V. and Stokes-Pebbles, R. (2015). The Role of Prostaglandins in Allergic Lung Inflammation and Asthma. *Expert Review of Respiratory Medicine*, 9(1), pp. 55-72.

Clarke, D.L., Belvisi, M.G., Smith, S.J., Hardaker, E., Yacoub, M.H., Meja, K.K., Newton, R., Slater, D.M. and Giembycz, M.A. (2005). Prostanoid receptor expression by human airway smooth muscle cells and regulation of the secretion of granulocyte colony-stimulating factor. *American Journal of Physiology Lung Cellular and Molecular Physiology,* 288(2), pp. 238-250.

Coburn, R.F. and Baron, C.B. (1990). Coupling mechanisms in airway smooth muscle. *American Journal of Physiology- Lung Cellular and Molecular Physiology*, 284(4), pp. 119-133.

Cocks, T.M. and Moffatt, J.D. (2001). Protease-activated receptor-2 (PAR2) in the airways. *Pulmonary Pharmacology and Therapeutics*, 14(3), pp.183-191.

Cocks, T.M., Fong, B., Chow, J. M., Anderson, G.P., Frauman, A.G., Goldie, R.G., Henry, P.J., Carr, M.J., Hamilton, J.R. and Moffat, J.D. (1999). A protective role for protease-activated receptors in the airways. *Nature*, 398(6723), pp.156-160.

Cohen, D.J., Nelson, W.J. and Maharbiz, M.M. (2014). Galvanotactic control of collective cell migration in epithelial monolayers. *Nature Materials*, 13(3), pp. 409-417.

Coleman, R.A., Smith, W.L. and Narumiya, S. (1994). International Union of Pharmacology Classification of Prostanoid Receptors: Properties, Distribution, and Structure of the Receptors and Their Subtypes. *The American Society for Pharmacology and Experimental Therapeutics,* 46(2), pp. 206-224.

Colton, C.K. and Zhu, M.X. (2007). 2-Aminoethoxydiphenyl borate as a common activator of TRPV1, TRPV2, and TRPV3 channels. *Handbook of Experimental Pharmacology*, 179(2007), pp. 173-187.

Coronado, R., Morrissette, J., Sukhareva, M. and Vaughan, D.M. (1994). Structure and function of ryanodine receptors. *American Journal of Physiology Lung Cellular and Molecular Physiology,* 266(38), pp. 31624-31632.

Corrigan, C.J., Napoli, R.L., Fang, C., Wu, H., Tochiki, K., Reay, V., Lee, T.H. and Ying S. (2012). Reduced expression of the prostaglandin E_2 receptor E-prostanoid 2 on bronchial mucosal leukocytes in patients with aspirin-sensitive asthma. *Journal of Allergy and Clinical Immunology*, 126(6), pp.1636-1645.

Coulson, F.R. and Fryer, A.D. (2003). Muscarinic acetylcholine receptors and airway diseases. *Pharmacology & Therapeutics*, 98(1), pp. 59-69.

Craig, R. and Padrón, R. (2004). Chapter 7 Molecular structure of the sarcomere. In: *Myology* Engel, A.C., and Franzini-Armstrong, C. *Myology*. 3rd ed. New York: McGraw-Hill, pp. 129-166.

Croisier, H., Tan, X., Perez-Zoghbi, J.F., Sanderson, M.J., Sneyd, J. and Brook, B. (2013). Activation of Store-Operated Calcium Entry in Airway Smooth Muscle Cells: Insight from a Mathematical Model. *PLoS ONE* [online], 8(7). Available from: https://journals.plos.org/plosone/article?id=10.1371/journal.pone.0069598 [accessed on 26th October 2021].

D'Andrea, M.R., Derian, C.K., Leturcq, D., Baker, S.M., Brunmark, A., Ling, P., Darrow, A.L., Santulli, R.J., Brass, L.F. and Andrade-Gordon, P. (1998). Characterization of protease-activated receptor-2 immunoreactivity in normal human tissues. *Journal of Histochemistry and Cytochemistry*, 46(2), pp. 157-164.

D'Andrea, M.R., Rogahn, C.J. and Andrade-Gordon, P. (2000). Localization of protease-activated receptors-1 and -2 in human mast cells: indications for mast cell amplification cascade. *Biotechnic and Histochemistry*, 75(2), pp.85-90.

D'Andrea, M.R., Saban, M.R., Nguyen, N.B., Andrade-Gordon, P. and Saban, R. (2003). Expression of protease-activated receptor-1, -2, -3, and -4 in control and experimentally inflamed mouse bladder. *The American Journal of Pathology*, 162(3), pp.907-923.

Dale, P., Head, V., Dowling, M.R. and Taylor, C.W. (2018). Selective inhibition of histamine-evoked Ca^{2+} signals by compartmentalized cAMP in human bronchial airway smooth muscle cells. *Cell Calcium*, 71 (5), pp. 53-64.

Damera, G., Tliba, O. and Panettieri, R.A. (2009). Airway smooth muscle as an immunomodulatory cell. *Pulmonary Pharmacology and Therapeutics*, 22(5), pp. 353-359.

Delamere, F., Holland, E., Patel, S., Bennett, J., Pavord, I. and Knox, A. (1994). Production of PGE_2 by bovine cultured airway smooth muscle cells and its inhibition by cyclo-oxygenase inhibitors. *British Journal of Pharmacology*, 111(12), pp. 983-988.

Dery, O., Thoma, M.S., Wong, H., Grady, E.F. and Bunnett, N.W. (1999). Trafficking of proteinase-activated receptor-2 and β-arrestin-1 tagged with green fluorescent protein. *The Journal of Biological Chemistry*, 274(6), pp.18524-18535.

Desai, S., April, H., Nwaneshiudu, C. and Ashby, B. (2000). Comparison of agonist-induced internalization of the human EP_2 and EP_4 prostaglandin receptors: role of the carboxyl terminus in EP_4 receptor sequestration. *Molecular Pharmacology*, 58(6), pp. 1279-1286.

Dillon, P., Aksoy, M., Driska, S. and Murphy, R. (1981). Myosin phosphorylation and the cross-bridge cycle in arterial smooth muscle. *Science*, 211(4481), pp. 495-497.

Ding, H-L., Ryder, J.W., Stull, J.T. and Kamm, K.E. (2009). Signalling processes for initiating smooth muscle contraction upon neural stimulation. *Journal of Biological Chemistry*, 284(23), pp. 15541-15548.

Drumm, B.T., Large, R.J., Hollywood, M.A., Thornbury, K.D., Baker, S.A., Harvey, B.J., McHale, N.G. and Sergeant, G.P. (2015). The role of Ca^{2+} influx in spontaneous Ca^{2+} wave propagation in interstitial cells of Cajal from the rabbit urethra. *The Journal of Physiology*, 593(15), pp. 3333-3350.

Du, W., McMahon, T.J., Zhang, Z.S., Stiber, J.A., Meissner. G. and Eu, J.P. (2006). Excitation-contraction coupling in airway smooth muscle. *Journal of Biological Chemistry*, 281(40), pp. 30143-30151.

Du, W., Stiber, J.A., Rosenberg, P.B., Meissner, G. and Eu, J.E. (2005). Ryanodine receptors in muscarinic receptor-mediated bronchoconstriction. *Journal of Biological Chemistry*, 280(28), pp. 26287-26294.

Ebina, M., Takahashi, T., Chiba,T. and Motomiya, M. (1993). Cellular hypertrophy and hyperplasia of airway smooth muscles underlying bronchial asthma. A 3-D morphometric study. *The American Review of Respiratory Disease*, 148(3), pp. 720-760.

Engelhardt, S., Hein, L., Dyachenkow, V., Kranias, E.G., Isenberg, G. and Lohse, M.J. (2004). Altered calcium handling is critically involved in the cardiotoxic effects of chronic beta-adremergic stimulation. *Circulation*, 109(9), pp. 1154-1160.

Evseev, A.I., Semenov, I., Archer, C.R., Medina, J.L., Dube, P.H., Shapiro, M.S. and Brenner, R. (2013). Functional effects of KCNQ K^+ channels in airway smooth muscle. *Frontiers in Physiology* [online], 277 (4). Available from: https://www.ncbi.nlm.nih.gov/pmc/articles/PMC3791379/ [accessed 6th May 2019]

Farmer, S.G., Ensor, J.E. and Burch, R.M. (1990). Evidence that cultured airway smooth muscle cells contain Bradykinin B_2 and B_3 receptors. *American Journal of Respiratory Cell and Molecular Biology*, 4(3), pp. 273-277.

FitzPatrick, M., Donovan, C. and Bourke, J.E. (2014). Prostaglandin E_2 elicits greater bronchodilation than salbutamol in mouse intrapulmonary airways in lung slices. *Pulmonary Pharmacology and Therapeutics*, 28 (2014), pp. 68-76.

Foda, H.D., Sharaf, H.H., Absood, A. and Said, S.I. (1995). Pituitary adenylate cyclase-activating peptide (PACAP), a VIP-like peptide, has prolonged airway smooth muscle relaxant activity. *Peptides*, 16(6), pp. 1057-1061.

Fong, Z., Griffin, C.S., Hollywood, M.A., Thornbury, K.D. and Sergeant, G.P. (2019). β_3-Adrenoceptor agonists inhibit purinergic receptor-mediated contractions of the murine detrusor. *The American Journal of Physiology- Cell Physiology*, 317(1), pp. 131-142.

Forskett, J.K., White, C., Cheung, K-H. and Mak, D-O.D. (2007). Inositol triphosphate receptor Ca^{2+} release channels. *Physiological Reviews*, 87(2), pp. 593-658.

Fortner, C.N., Breyer, R.M. and Paul, R.J. (2001). EP_2 receptors mediate airway relaxation to substance P, ATP and PGE_2. *American Journal of Physiology Lung Cellular and Molecular Physiology,* 281(2), pp. 469-474.

Frank, K.F., Bölck, B., Erdmann, E. and Schwinger, R.H.G. (2003). Sarcoplasmic reticulum Ca^{2+}-ATPase modulates cardiac contraction and relaxation. *Cardiovascular Research*, 57(1), pp. 20-27.

Fryer, A.D. and Jacoby, D.B. (1998). Muscarinic Receptors and Control of Airway Smooth Muscle. *American Journal of Respiratory and Critical Care Medicine*, 158(5), pp. 154-160.

Fryer, A.D., Stein, L.H., Nie, Z., Curtis, D.E., Evans, C.M., Hodgson, S.T., Jose, P.J., Belmonte, K.E., Fitch, E. and Jacoby, D.B. (2006). Neuronal eotaxin and the effects of ccr3 antagonist on airway hyperreactivity and M2 receptor dysfunction. *Journal of Clinical Investigation*, 116(1), pp. 228-236.

Fujino, H., West, K.A. and Regan, J.W. (2002). Phosphorylation of glycogen synthase kinase-3 and stimulation of T-cell factor signalling following activation of EP_2 and EP_4 prostanoid receptors by prostaglandin E_2. *The Journal of Biological Chemistry*, 277(4), pp. 2614-2619.

Fujino, H., Xu, W. and Regan, J.W. (2003). Prostaglandin E_2 induced functional expression of early growth response factor-1 by EP_4, but not EP_2, prostanoid receptors via the phosphatidylinositol 3-kinase and extracellular signal-regulated kinases. *The Journal of Biological Chemistry*, 278(14), pp. 12151-12156.

Fukada, K., Kubo, T., Maeda, A., Akiba, I., Bujo, H., Nakai, J., Mishina, M., Higashida, H., Neher, E., Marty, A. and Numa, S. (1989). Selective effector coupling of muscarinic acetylcholine receptor subtypes. *Trends in Pharmacological Sciences*, 10(12), pp. 4-10.

Fukao, M., Mason, H.S., Britton, F.C., Kenyon, J.L., Horowitz, B. and Keef, K.D. (1999). Cyclic GMP-dependent protein kinase activates cloned BKCa channels expressed in mammalian cells by direct phosphorylation at serine 1072. *Journal of Biological Chemistry*, 274(16), pp. 10927-10935.

Gabella, G. (1984). Structural apparatus for force transmission in smooth muscle. *Physiological Reviews*, 64(2), pp.455-477.

Ganesh, T. (2014). Prostanoid Receptor EP2 as a Therapeutic Target. *The Journal of Medical Chemistry*, 57(11), pp. 4454-4465.

Gauvreau, G.M., Watson, R.M. and O'Byrne, P.M. (1999). Protective effects of inhaled PGE2 on allergen-induced airway responses and airway inflammation. *American Journal of Respiratory and Critical Care Medicine*, 159(1), pp. 31-36

Geppetti, P. and Trevisani, M. (2003). Protinease-activated receptors (PARs) and bronchial smooth muscle functions. *Drug Development Research*, 60(1), pp.24-28.

Giannini, G., Conti, A., Mammarella, S., Scrobogna, M. and Sorrentino, V. (1995). The ryanodine receptor/calcium channel genes are widely and differentially expressed in murine brain and peripheral tissues. *Journal of Cell Biology*, 128(5), pp. 893-904.

Goldblatt, M.W. (1933). A depressor substance in seminal fluid. *Journal of the Society of Chemical Industry*, 52(1), pp. 1056-1057.

Goldie, R.G., Fernandes, L.B., Farmer, S.G. and Hay, D.W. (1990). Airway epithelium-derived inhibitory factor. *Trends in Pharmacological Sciences*, 11(2), pp. 67-70.

Gosens, R., Zaagsma, J., Meurs, H. and Halayko, A.J. (2006). Muscarinic receptor signalling in the pathophysiology of asthma and COPD. *Respiratory Research* [online], 73(7). Available from: https://respiratory-research.biomedcentral.com/track/pdf/10.1186/1465-9921-7-73 [accessed on 12th August 2019].

Gosling, M., Poll, C. and Li, S. (2005). TRP channels in airway smooth muscle as therapeutics. *Naunyn-Schmiedeberg's Archives of Pharmacology*, 371(4), pp. 277-284.

Griffin, C.S., Bradley, E., Dudem, S., Hollywood, M.A., McHale, N.G., Thornbury, K.D. and Sergeant, G.P. (2016). Muscarinic Receptor Induced Contractions of the Detrusor are Mediated by Activation of TRPC4 Channels. *Journal of Urology*, 196(6), pp. 1796-1808.

Gunst, S.J. and Tang, D.D. (2000). The contractile apparatus and mechanical properties of airway smooth muscle. *European Respiratory Journal*, 15(3), pp.600-616.

Haddad, E.B., Mak, J.C., Belvisi, M.G., Nishikawa, M., Rousell, J. and Barnes, P.J. (1996). Muscarinic and beta-adrenergic receptor expression in peripheral lungs from normal and asthmatic patients. *American Journal of Physiology*, 270(6), pp. 947-953.

Hafen, B.B. and Burns, B. (2020). *Physiology: smooth muscle* [online]. Florida: StatPearls. Available from: https://www.ncbi.nlm.nih.gov/books/NBK526125/ [accessed on 28th June 2021].

Hagar, R.E., Burgstahler, A.D., Nathanson, M.H and Ehlrich, B.E. (1998). Type III $InsP_3$ receptor channel stays open in the presence of increased calcium. *Nature*, 396(6706), pp. 81-84.

Haick, J.M., Brueggemann, L.I., Schwartz, J.L. and Byron, K.L. (2017). Regulation of endogenous K_V7 potassium channels by histamine in primary cultured human airway smooth muscle cells [online]. *The Federation of American Societies for Experimental Biology Journal*, 31(1). Available from: https://www.fasebj.org/doi/abs/10.1096/fasebj.31.1_supplement.726.6

Hakamata, Y., Nakai, J., Takeshima, H. and Imoto, K. (1992). Primary structure and distribution of a novel ryanodine receptor/ calcium release channel from rabbit brain. *The Federation of European Biochemical Societies,* 312(2-3), pp. 229-235.

Han, J.S., Kim, S.J., Nam, Y., Lee, H.Y., Kim, G.M., Kim, D.M. and Sohn, U.D/ (2019). The Inhibitory Mechanism on Acetylcholine-Induced Contraction of Bladder Smooth Muscle in the Streptozotocin-Induced Diabetic Rat. *Biomolecules and Therapeutics*, 27(1), pp. 101-106.

Hannigan, K.I., Large, R.J., Bradley, E., Hollywood, M.A., Sergeant, G.P., McHale, N.G. and Thornbury, K.D. (2016). Effect of novel BKCa opener on BKCa currents and contractility of the rabbit corpus cavernosum. *The American Journal of Physiology- Cell Physiology,* 310(4), pp. 284-292.

Hartert, T.V., Dworski, R.T., Mellen, B.G., Oates, J.A., Murray, J.J. and Sheller, J.R. (2000). Prostaglandin E_2 decreases allergen-stimulated release of prostaglandin D_2 in airways of subjects with asthma. *American Journal of Respiratory and Critical Care Medicine*, 162(2), pp. 637-640.

Hartney, J.M., Coggins, K.G., Tilley, S.L., Jania, L.A., Lovgren, A.K., Audoly, L.P. and Koller, B.H. (2006). Prostaglandin E_2 protects lower airways against bronchoconstriction. *American Journal of Lung Cellular and Molecular Physiology*, 290 (8), pp. 105-113.

Hatae, N., Sugimoto, Y. and Ichikawa, A. (2002). Prostaglandin Receptors: Advances in the Study of EP3 Receptor Signaling. *Journal of Biochemistry*, 131(6), pp. 781-784.

Hein, L., Ishii, K., Coughlin, S.R. and Kobilka, B.K. (1994). Intracellular targeting and trafficking of thrombin receptors. A novel mechanism for resensitization of a G protein-coupled receptor. *The Journal of Biological Chemistry*, 269(11), pp.27719-27726.

Herrerias, A., Torres, R., Serra, M., Marco, A., Pujols, L., Picado, C. and DeMora, F. (2009). Activity of the cyclooxygenase 2-prostaglandin-E prostanoid receptor pathway in mice exposed to house dust mite aeroallergens, and impact of exogenous prostaglandin E2. *Journal of Inflammation* [online], 6 (30). Available from: https://www.ncbi.nlm.nih.gov/pmc/articles/PMC2776012/#B12 [accessed 24th April 2019].

Hill-Eubanks, D.C., Werner, M.E., Heppner, T.J. and Nelson, M.T. (2011). Calcium signalling in smooth muscle. *Cold Springs Harbour Perspectives in Biology* [online], 3(9), Available from: https://pubmed.ncbi.nlm.nih.gov/21709182/ [accessed 29th July 2021].

Hiramatsu, T., Kume, H., Kotlikoff, M.I. and Takagi, K. (1994). Role of calcium-activated potassium channels in the relaxation of tracheal smooth muscles by forskolin. *Clinical and Experimental Pharmacology and Physiology*, 21(5), pp. 367-375.

Hirota, S., Helli, P. and Janssen, L.J. (2007). Ionic mechanisms and calcium handling in airway smooth muscle. *European Respiratory Journal*, 30(12), pp. 114-133.

Hirota, S., Helli, P.B., Catalli, A., Chew, A. and Janssen, L.J. (2005). Airway smooth muscle excitation-contraction coupling and airway hyperresponsiveness. *Canadian Journal of Physiology and Pharmacology*, 83(8-9), pp. 725-732.

Hisada, T., Kurachi, Y. and Sugimoto, T. (1990). Properties of membrane currents in isolated smooth muscle cells from guinea-pig trachea. *Pflugers Archives*, 416(1-2), pp. 151-161.

Hogg, J.C., Chu, F., Utokaparch, S., Woods, R., Elliott, W.M., Buzatu, L., Cherniack, R.M., Rogers, R.M., Sciurba, F.C., Coxson, H.O. and Pare, P.D.

(2004). The Nature of Small-Airway Obstruction in Chronic Obstructive Pulmonary Disease. *The New England Journal of Medicine,* 350(26), pp.2645-2653.

Holaska, J.M., Black, B.E., Love, D.C., Hanover, J.A., Leszyk, J. and Paschal, B.M. (2001). Calreticulin is a receptor for nuclear export. *The Journal of Cell Biology*, 152(1), pp. 127-140.

Hollenburg, M.D., Renaux, B., Hyun, E., Houle, S., Vergnolle, N., Saifeddine, M. and Ramachandran, R. (2008). Derivatized 2-Furoyl-LIGRLO-amide, a versatile and selective probe for protinease-activated receptor 2: binding and visualization. *The Journal of Pharmacology and Experimental Therapeutics*, 326(2), pp. 453-462.

Horowitz, A., Menice, C.B., Laporte, R. and Morgan, K.G. (1996). Mechanisms of smooth muscle contraction. *Physiological Reviews*, 76(4), pp. 967-1003.

Hoth, M. and Penner, R. (1992). Depletion of intracellular calcium stores activates a calcium current in mast cells. *Nature*, 355(6), pp. 353-356.

Howells, G.L., Macey, M.G., Chinni, C., Hou, L., Fox, M.T., Harriott, P. and Stone, S.R. (1997). Proteinase-activated receptor-2: expression by human neutrophils. *Journal of Cell Science*, 110(7), pp.881-887.

Huang, J.C., Garcia, M.L., Reuben, J.P. and Kacsorowski, G.J. (1993). Inhibition of β-adrenoreceptor agonist relaxation of airway smooth muscle by Ca^{2+}-activated K^+ channel blockers. *European Journal of Pharmacology*, 235(1), pp. 37-43.

Huang, S.K. and Peters-Golden, M. (2008). Eicosanoid lipid mediators in fibrotic lung diseases: ready for prime time?. *Chest*, 133(6), pp. 1442-1450.

Hulme, E.C., Kurtenbach, E. and Curtis, C.A.M. (1991). Muscarinic acetylcholine receptors: structure and function. *Biochemical Society Transactions*, 19(1), pp. 133-138.

Humphries E.S.A., Kamishima T., Quayle J.M. and Dart C. (2017). Calcium/Calmodulin-dependent Kinase 2 Mediates Epac-induced Spontaneous Transient Outward Currents in Rat Vascular Smooth Muscle. *The Journal of Physiology*, 595(18), pp. 6147-6164.

Hwang, S,L., Lee, K,S., Lin, C,L., Lieu, A,S., Cheng, C,Y., Loh, J,K., Hwang, J,F., Su, Y,F. and Howng, S, L. (2004). Effect of aspirin and indomethacin on prostaglandin E2 synthesis in C6 glioma cells. *The Kaohsiung Journal of Medical sciences*, 20(1), pp. 1-5.

Hyvelin, J.M., Martin, C., Roux, E., Marthan, R. and Savineau, J.P. (2000). Human isolated bronchial smooth muscle contains functional ryanodine/caffeine-sensitive Ca^{2+}-release channels. *American Journal of Respiratory and Critical Care Medicine*, 162(2), pp. 687-694.

Iino, M. (2000). Molecular basis of spatio-temporal dynamics in inositol 1,4,5-trisphosphate-mediated Ca^{2+} signalling. *Japanese Journal of Pharmacology*, 82(1), pp. 15-20.

Ikeda, T., Anisuzzaman, A.S.M., Yoshiki, H., Sasaki, M., Koshiji, T., Uwada, J., Nishimune, A., Itoh, H. and Muramatsu, I. (2012). Regional quantification of muscarinic acetylcholine receptors and β-adrenoceptors in human airways. *British Journal of Pharmacology*, 166(6), pp. 1804-1814.

Irie, A., Sugimoto, Y., Namba, T., Harazono, A., Honda, A., Watabe, A., Negishi, M., Narumiya, S. and Ichikawa, A. (1993). Third isoform of the prostaglandin-E-receptor EP_3 subtype with different C-terminal tail coupling to both stimulation and inhibition of adenylate cyclase. *European Journal of Biochemistry*, 217(7), pp. 313-318.

Ishii, K., Chen, K., Ishii, M., Koch, W.J., Freedman, N.J., Lefkowitz, R.J. and Coughlin, S.R. (1994). Inhibition of thrombin receptor signalling by a G-protein coupled receptor kinase. Functional specificity among G-protein coupled receptor kinases. *The Journal of Biological Chemistry*, 269(1), pp.1125-1130.

Israel, DD. and Regan, JW. (2009). EP (3) prostanoid receptor isoforms utilise distinct mechanisms to regulate ERK 1/2 activation. *Biochimica et Biophysica Acta*, 1791(4), pp. 238-245.

Itoh, T. (1991). Pharmacomechanical coupling in vascular smooth muscle cells. *Japanese Journal of Pharmacology*, 55(9), pp. 1-9.

Jackson, M.V., Trout, S.J. and Cunnane, T.C. (2002). Regional variation in electrically-evoked contractions of rabbit isolated pulmonary artery. *British Journal of Pharmacology*, 137(4), pp. 488-496.

Jackson, W.F. (2017). Potassium Channels in Regulation of Vascular Smooth Muscle Contraction and Growth. *Advances in Pharmacology*, 78(8), pp. 89-144.

Jadhav, V., Jabre, A., Chen, M.F. and Lee, T.J.F. (2009). Presynaptic Prostaglandin E_2 EP_1-Receptor Facilitation of Cerebral Nitrergic Neurogenic Vasodilation. *Stroke*, 40(10), pp. 261-269.

Jagger, J.H., Porter, V.A., Lederer, J.W. and Nelson, M.T. (2000). Calcium sparks in smooth muscle. *The American Journal of Physiology*, 278(2), pp. 235-256.

James, A. and Carroll, N. (2000). Airway smooth muscle in health and disease; methods of measurement and relation to function. *European Respiratory Journal*, 15(4), pp. 782-789.

Janssen, L.J. and Sims, S.M. (1994). Spontaneous transient inward currents and rhythmicity in canine and guinea-pig tracheal smooth muscle cells. *Pflugers Archives*, 427(5-6), pp. 473-480.

Janssen, L.J., Tazzeo, T. and Zuo, J. (2004). Enhanced myosin phosphatase and Ca^{2+}-uptake mediate adrenergic relaxation of airway smooth muscle. *American Journal of Respiratory Cell and Molecular Biology*, 30(4), pp. 548-554.

Ji, G., Feldman, M.E., Greene, K.S., Sorrentino, V., Xin, H.B. and Kotlikoff, M.I. (2004). RYR2 proteins contribute to the formation of Ca^{2+} sparks in smooth muscle. *Journal of General Physiology*, 123(4), pp. 377-386.

Jin, M., Yang, H.W., Tao, A.L. and Wei, J.F. (2016). Evolution of the protease-activated receptor family in vertebrates. *International Journal of Molecular Medicine*, 37(3), pp.593-602.

Johnson, S.R. and Knox, A.J. (1997). Synthetic functions of airway smooth muscle in asthma. *Trends in Pharmacological Sciences*, 18(8), pp. 288-292.

Jones, R.L., Noble, P.B., Eilliot, J.G. and James, A.L. (2016). Airway remodelling in COPD: It's not asthma!. *Official Journal of the Asian Pacific Society of Respirology*, 21(4), pp. 1347-1356.

Joo, E.E. and Yamada, K.M. (2014). MYPT1 regulates contractility and microtubule acetylation to modulate integrin adhesions and matrix assembly. *Nature Communications* [online], 5(3). Available from: https://www.ncbi.nlm.nih.gov/pmc/articles/PMC4190669/ [accessed 5th February 2022].

Jude, J.A., Wylam, M.E., Walseth, T.F. and Kannan, M.S. (2008). Calcium signalling in airway smooth muscle. *Proceedings of the American Thoracic Society*, 5(5), pp. 15-22.

Kaftan, E.J., Ehlrich, B.E. and Watras, J. (1997). Inositol 1,4,5-triphosphate ($InsP_3$) and calcium interact to increase the dynamic range of $InsP_3$ receptor-dependent calcium signalling. *The Journal of General Physiology*, 110(5), pp. 529-538.

Kalinski, P. (2012). Regulation of Immune Responses by Prostaglandin E_2. *The Journal of Immunology*, 188(11), pp. 21-28.

Kamm, K.E. and Stull, J.T. (1985). The function of myosin and myosin light chain kinase phosphorylation in smooth muscle. *Annual Review of Pharmacology and Toxicology*, 25(1), pp.593-620.

Katoh, H., Watabe, A., Sugimoto, Y., Ichikawa, A. and Negishi, M. (1995). Characterization of the signal transduction of prostaglandin E receptor EP1

subtype in cDNA-transfected Chinese hamster ovary cells. *Biochimica et Biophysic Acta*, 1244(1), pp. 41-48.

Kawabata, A. and Kawao, N. (2005). Physiology and pathophysiology of proteinase-activated receptors (PARs): PARs in the respiratory system: cellular signalling and physiological/pathological roles. *Journal of Pharmacological Sciences*, 97(11), pp.20-24.

Kawasaki, H., Springett, G.M., Mochizuki, N., Toki, S., Nakaya, M., Matsuda, M., Housman, D.E. and Graybiel, A.M. (1998) A family of cAMP-binding proteins that directly activate Rap1. Science, 282(5397), pp. 2275-2279.

Kellner, J., Tantzscher, J., Oelmez, H., Edelmann, M., Fischer, R., Huber, R.M. and Bergner, A. (2008). Mechanisms altering airway smooth muscle cell Ca^{2+} homeostasis in two asthma models. *Respiration*, 76(2), pp. 205-215.

Kimura, K., Amano, M.I., Chihara, K., Fukata, Y., Nakafuka, M., Yamamori, B., Feng, J., Nakano, T., Okawa, K., Iwamatsu, A. and Kaibuchi, K. (1996). Regulation of myosin phosphatase by Rho and Rho-associated kinase (Rho-kinase). *Science*, 273(5272), pp. 245-248.

Kirschstein, T., Rehberg, M., Bajorat, R., Tokay, T., Porath, K. and Köhling, R. (2009). High K^+-induced contraction requires depolarization-induced Ca_{2+} release from internal stores in rat gut smooth muscle. *Acta Pharmacologica Sinica*, 30(8), pp. 1123-1131.

Kistemaker, L.E.M. and Prakash, Y.S. (2019). Airway Innervation and Plasticity in Asthma. *Physiology*, 34(4), pp. 283-298.

Knight, D.A. and Holgate, S.T. (2003). The airway epithelium: Structural and functional properties in health and disease. *Respirology*, 8(7), pp. 432-446.

Knight, D.A., Lim, S., Scaffidi, A.K., Roche, N., Chung, K.F., Stewart, G.A. and Thompson, P.J. (2001). Protease-activated receptors in human airways: upregulation of PAR-2 in respiratory epithelium from patients with asthma. *Journal of Allergy and Clinical Immunology*, 108(5), pp.797-803.

Komalavilas, P. and Lincoln, T.M. (1996). Phosphorylation of the inositol 1,4,5-trisphosphate receptor: Cyclic GMP-dependent protein kinase mediates cAMP and cGMP dependent phosphorylation in the intact rat aorta. *Journal of Biological Chemistry*, 271(36), pp. 21933-21938.

Komori, S., Kawai, M., Takewaki, T. and Ohashi, H. (1992). GTP-binding protein involvement in membrane currents evoked by carbachol and histamine in guinea-pig ileal muscle. *Journal of Physiology*, 450(1), pp. 105-126.

Kong, H., Jones, P.P., Koop, A., Zhang, L., Duff, H.J. and Chen, W.S.R. (2008). Caffeine induces Ca^{2+} release by reducing the threshold for luminal Ca^{2+} activation of the ryanodine receptor. *Biochemical Journal*, 414(3), pp. 441-452.

Konya, V., Marsche, G., Schuligoi, R. and Heinemann, A. (2013). E-type prostanoid receptor 4 (EP4) in disease and therapy. *Pharmacology and Therapeutics*, 138 (2013), pp. 485-502.

Kotani, M., Tanaka, I., Ogawa, Y., Suganami, T., Matsumoto, T., Muro, S., Yamamoto, Y., Sugawara, A., Yoshimasa, Y., Sagawa, N., Narumiya, S. and Nakao, K. (2000). Multiple signal transduction pathways through two prostaglandin E receptor EP3 subtype isoforms expressed in human uterus. *The Journal of Clinical Endocrinology and Metabolism*, 85(11), pp. 4315-4322.

Kotlikoff, M.I. (1993). Potassium channels in airway smooth muscle: A tale of two channels. *Pharmacology & Therapeutics*, 58(1), pp. 1-12.

Kotlikoff, M.I. and Wang, Y-X. (1998). Calcium Release and Calcium-Activated Chloride Channels in Airway Smooth Muscle Cells. *American Journal of Respiratory and Critical Care Medicine*, 158(1998), pp. 109-114.

Kranias, E.G., Garvery, J.L., Srivastava, R.D. and Solaro, R.J. (1985). Phosphorylation and functional modifications of sarcoplasmic reticulum and myofibrils in isolated rabbit hearts stimulated with isoprenaline. *Biochemical Journal*, 226(1), pp.113-121.

Kume, H., Graziano, M.P. and Kotlikoff, M.I. (1992). Stimulatory and inhibitory regulation of calcium-activated potassium channels by guanine nucleotide-binding proteins. *Proceedings of the National Academy of Sciences*, 89(22), pp. 11051-11055.

Kume, H., Hall, I.P., Washabau, R.J., Takagi, K. and Kotlikoff, M.I. (1994). Beta-adrenergic agonists regulate KCa channels in airway smooth muscle by cAMP-dependent and -independent mechanisms. *The Journal of Clinical Investigation*, 93(1), pp. 371-379.

Kuo, K.H., Dai, J., Seow, C.Y. and van Breeman, C. (2003). Relationship between asynchronous Ca^{2+} waves and force development in intact smooth muscle bundles of the porcine trachea. *American Journal of Physiology Lung Cellular and Molecular Physiology*, 285(6), pp. 1345-1353.

Kuo. I.Y. And Ehrlich, B.E. (2015). Signalling in Muscle Contraction [online]. *Cold Spring Harbour Perspectives in Biology*, 7(2). Available from: https://www.ncbi.nlm.nih.gov/pubmed/25646377

Kyle, B.D. and Braun, A.P. (2014). The Regulation of BK channel activity by pre- and post-translational modifications [online]. *Frontiers in Physiology*, 22(8). Available from: https://www.frontiersin.org/articles/10.3389/fphys.2014.00316/full#B89 [accessed 5th February 2022].

Kyle, B.D., Bradley, E., Large, R., Sergeant, G.P., McHale, N.G., Thornbury, K.D. and Hollywood, M.A. (2013). Mechanisms underlying activation of transient BK current in rabbit urethral smooth muscle cells and its modulation by IP_3-generating agonists. *The American Journal of Physiology- Cell Physiology*, 305(6), pp. 609-622.

Lan, R.S., Knight, D.A., Stewart, G.A. and Henry, P.J. (2001). Role of PGE_2 in protease-activated receptor-1,-2 and -4 mediated relaxation in the mouse isolated trachea. *British Journal of Pharmacology,* 132(1), pp.93-100.

Lanner, JT., Dimitri, K., Georgiou, A.D., Hamilton, J. and Hamilton, S. (2010). Ryanodine receptors: structure, expression, molecular details, and function in calcium release. *Cold Spring Harbor Perspectives in Biology* [online], 2(11). Available from: https://www.ncbi.nlm.nih.gov/pmc/articles/PMC2964179/ [accessed 23rd August 2021].

Lebender, L., Prunte, L., Rumzhum, N. and Ammit, A. (2018). Selectively targeting prostanoid E (EP) receptor-mediated cell signalling pathways: Implications for lung health and disease. *Pulmonary Pharmacology and Therapeutics*, 49, pp. 75-87.

Lechner, S.G., Mayer, M. and Boehm, S. (2003). Activation of M_1 muscarinic receptors triggers transmitter release from rat sympathetic neurons through an inhibition of M-type K^+ channels. *The Journal of Physiology*, 553(3), pp. 789-802.

Li, B., Yu, Q., Wang, R., Gratzke, C., Wang, X., Spek, A., Herlemann, A., Tamalunas, A., Strittmatter, F., Waidelich, R., Stief, C.G. and Hennenberg, M. (2020). Inhibition of Female and Male Human Detrusor Smooth Muscle Contraction by the Rac Inhibitors EHT1864 and NSC23766. *Frontiers in Pharmacology* [online], 409(11). Available from: https://pubmed.ncbi.nlm.nih.gov/32317972/ [accessed on 4th October 2021].

Li, J., O'Connor, K.L., Cheng, X., Mei, F., Uchida, T., Townsend, C. and Evers, M.B. (2007). Cyclic Adenosine 5'-Monophosphate-Stimulated Neurotensin Secretion Is Mediated through Rap1 Downstream of both Epac and Protein Kinase A Signaling Pathways. *Molecular Endocrinology*, 21(1), pp. 159-171.

Li, M., Shang, Y-X., Wei, B. and Yang, Y-G. (2011). The effect of substance P on asthmatic rat airway smooth muscle cell proliferation, migration, and cytoplasmic calcium concentration *in vitro*. *Journal of Inflammation* [online], 8(18). Accessed from: https://journal-inflammation.biomedcentral.com/articles/10.1186/1476-9255-8-18 [accessed on 6th October 2021].

Liao, Y., Erxleben, C., Abramowitz, J., Flockerzi, V., Zhu, M.X., Armstring, D.L. and Birnbaumer, L. (2008). Functional interactions among Orai1, TRPCs, and STIM1 suggest a STIM-regulated heteromeric Orai/TRPC model for SOCE/Icrac

channels. *Proceedings of the National Academy of Sciences*, 105(8), pp. 2895-2900.

Lifshitz, L.M., Carmichael, J.D., Lai, A.F., Sorrentino, V., Bellvé, K., Fogarty, K.E. and ZhuGe, R. (2011). Spatial organization of RyRs and BK channels underlying the activation of STOCs by Ca^{2+} sparks in airway myocytes. *The Journal of General Physiology*, 138(2), pp. 195-209.

Liou, J., Kim, M.L., Heo, W.D., Jones, J.T., Myers, J.W., Ferrell, J.E. and Meyer, T. (2005). STIM is a Ca^{2+} sensor essential for Ca^{2+}-store-depletion-triggered Ca^{2+} influx. *Current Biology*, 15(13), pp. 1235-1241.

Liu, X. and Farley, J.M. (1996). Acetylcholine-induced chloride current oscillations in swine tracheal smooth muscle cells. *Journal of Pharmacology and Experimental Therapeutics*, 276(1), pp.178-186.

Löhn, M., Jessner, W., Furstenau, M., Wellner, M., Sorrentino, V., Haller, H., Luft, F.C. and Gollasch, M. (2001). Regulation of calcium sparks and spontaneous transient outward currents by RyR3 in arterial vascular smooth muscle cells. *Circulation Research*, 89(11), pp. 1051-1057.

MacMillan, D., Chalmers, S., Muir, T.C. and McCarron, J. G. (2005). IP_3-mediated Ca^{2+} increases do not involve the ryanodine receptor, but ryanodine receptor antagonists reduce IP_3-mediated Ca^{2+} increases in guinea-pig colonic smooth muscle cells. *The Journal of Physiology*, 569(2), pp.533-544.

Mader, S. (2007). *Human Biology: Chapter 9 Respiratory System*. 10th ed. Boston: McGraw-Hill.

Magleby, K.L. (2003). Gating Mechanism of BK (Slo1) Channels. *Journal of General Physiology*, 121 (2), pp. 81-96.

Maher, S.A., Birrell, M.A. and Belvisi, M.G. (2009). Prostaglandin E_2 Mediates Cough via the EP_3 Receptor. *American Journal of Respiratory and Critical Care Medicine*, 180(10), pp. 923-928.

Mak, D.O.D., McBride, S. and Forskett, J.K. (1998). Inositol 1,4,5-trisphosphate activation of inositol trisphosphate receptor Ca^{2+} channel by ligand tuning of Ca^{2+} inhibition. *Proceedings of the National Academy of Sciences of the United States of America,* 95(26), pp. 15821-15825.

Mak, J.C. And Barnes, P.J. (1990). Autoradiographic visualization of muscarinic recptor subtypes in human and guinea pig lung. *American Review of Respiratory Disease*, 141(6), pp. 1559-1568.

Mak, J.C., Baraniuk, J.N. and Barnes, P.J. (1992). Localization of muscarinic receptor subtype mRNAs in human lung. *American Journal of Respiratory Cell and Molecular Biology*, 7(3), pp. 344-348.

Mao, C., Kim, S.H., Almenoff, J.S., Rudner, X.L., Kearney, D.M. and Kindman, L.A. (1996). Molecular cloning and characterisation of SCaMPER, a sphingolipid Ca^{2+} release-mediating protein from endoplasmic reticulum. *Proceedings of the National Academy of Sciences,* 93(5), pp. 1993-1996.

Marieb, E. (2001). *Human anatomy & physiology: Chapter 25 The Respiratory System*. 5th ed. San Francisco: Benjamin Cummings.

Marsh, B.J., Fryer, A.D., Jacoby, D.B. and Drake, M.G. (2020). Transient receptor potential ankyrin-1 causes rapid bronchodilation via nonepithelial PGE_2. *American Journal of Physiology Lung Cellular and Molecular Physiology*, 318(5), pp. 934-952.

Maruyama, K., McGuire, J.J. and Kagota, S. (2017). Progression of time-dependent changes to the mechanisms of vasodilation by protease-activated receptor 2 in metabolic syndrome. *Biological and Pharmaceutical Bulletin*, 40(12), pp. 2039-2044.

Mastalerz, L., Sanak, M., Gawlewicz-Mroczka, A., Gielicz, A., Cmiel, A. and Szczeklik, A. (2008). Prostaglandin E_2 systemic production in patients with asthma with and without aspirin hypersensitivity. *Thorax*, 63(1), pp. 27-34.

Matsuzaki, S., Ishizuka, T., Yamada, H., Kamide, Y., Hisada, T., Ichimonji, I., Aoki, H., Yatomi, M., Komachi, M., Tsurumaki, H., Ono, A., Koga, Y., Dobashi, K., Mogi, C., Sato, K., Tomura, H., Mori., M. and Okajima, F. (2011). Extracellular acidification induces connective tissue growth factor production through proton-sensing receptor OGR1 in human airway smooth muscle cells. *Biochemical and Biophysical Research Communications*, 413(4), pp. 499-503.

McFadzean, I. and Gibson, A. (2002). The developing relationship between receptor-operated and store-operated calcium channels in smooth muscle. *The British Journal of Pharmacology*, 135(1), pp. 1-13.

McGraw, D.W., Fogel, K.M., Kong, S., Litonjua, A.A., Kranias, E.G., Aronow, B.J. and Liggett, S.B. (2006). Transcriptional response to persistent β_2-adrenergic receptor signaling reveals regulation of phospholamban, which alters airway contractility. *Physiological Genomics*, 27(2), pp. 171-177.

McGraw, D.W., Mihlbachler, K.A., Schwarb, M.R., Rahman, F.F., Small, K.M., Almoosa, K.F. and Ligget, S.B. (2006). Airway smooth muscle prostaglandin-EP1 receptors directly modulate β_2-adrenergic receptors within a unique heterodimeric complex. *Journal of Clinical Investigation*, 116 (5), pp. 1400-1409.

McGuire, J.J. (2004). 2-Furoyl-LIGRLO-amine: A potent and selective proteinase-activated receptor 2 agonist. *Journal of Pharmacology and Experimental Therapeutics*, 309(3), pp. 1124-1131.

Meissner, G. (2004). Molecular regulation of cardiac ryanodine receptor ion channel. *Cell Calcium*, 35(6), pp. 621-628.

Minette, P.A. and Barnes, P.J. (1988). Prejunctional inhibitory muscarinic recptors on cholinergic nerves in human and guinea pig airways. *Journal of Applied Physiology*, 64(6), pp. 2532-2537.

Miotto, D., Hollenberg, M.D., Bunnett, N.W., Papi, A., Braccioni, F., Boschetto, P., Rea, F., Zuin, A., Geppetti, P., Saetta, M., Maestrelli, P., Fabbri, L.M. and Mapp, C.E. (2002). Expression of protease activated receptor-2 (PAR-2) in central airways of smokers and non-smokers. *Thorax*, 57(2), pp.146-151.

Mitzner, W. (2004). Airway Smooth Muscle: The Appendix of the Lung. *American Journal of Respiratory and Critical Care Medicine,* 169(1), pp. 787-790.

Mizuma, H., Murakami, M. and Mori, M. (2001). Thyroid hormone activation in human vascular smooth muscle cells: expression of type II iodothyronine deiodinase. *Circulation Research*, 88(3), pp. 313-318.

Morel, J.L., Fritz, N., Lavie, J.L. and Mironneau, J. (2003). Crucial role of type 2 inositol 1,4,5-trisphosphate receptors for acetylcholine-induced Ca^{2+} oscillations in vascular myocytes. *Arteriosclerosis, Thrombosis, and Vascular Biology*, 23(9), pp. 1567-1575.

Morgan, J.M., De Smedt, H. and Gillespie, J.I. (1996). Identification of three isoforms of the InsP3 receptor in human myometrial smooth muscle. *Pflügers Archives*, 431(5), pp. 697-705.

Morgan, S.J., Deshpande, D.A., Tiegs, B.C., Misior, A.M., Yan, H., Hershfeld, A.V., Rich, T.C., Panettiera, R.A., An, S.S. and Penn, R.B. (2014). β-agonist-mediated Relaxation of Airway Smooth Muscle Is Protein Kinase A-dependant. *The Journal of Biological Chemistry*, 289(33), pp. 23065-23074.

Mori, A., Ito, A., Morioka, M., Aso, H., Kondo, M., Sokabe, M. and Hasegawa, Y. (2011). Effects of specific prostanoid EP receptor agonists on cell proliferation and intracellular Ca^{2+} concentrations in human airway smooth muscle cells. European Journal of Pharmacology, 659(1), pp. 72-78.

Moss, C.R., Gilbert, C.A., Gabriel, S.A. and Gu, Q. (2015). Protease-activated receptor-2 inhibits BK channel activity in bronchopulmonary sensory neurons. *Neuroscience Letters*, 4(589), pp. 13-19.

Murphy, R.A. and Rembold, C.M. (2005). The latch-bridge hypothesis of smooth muscle contraction. *Canadian Journal of Physiology and Pharmacology*, 83(10), pp. 857-864.

Murray, M.A., Berry, J.L., Cook, S.J., Foster, R.W., Green, K.A. and Small, R.C. (1991). Guinea-pig isolated trachealis: the effects of charybdotoxin on

mechanical activity, membrane potential changes and the activity of plasmalemmal K^+-channels. *British Journal of Pharmacology*, 103(3), pp. 1814-1818.

Nakai, J., Imagawa, T., Hakamata, Y., Shigekawa, M., Takeshima, H. and Numa, S. (1990). Primary structure and functional expression from cDNA of the cardiac ryanodine receptor/calcium release channel. *The Federation of European Biochemical Societies*, 271(1-2), pp. 169-177.

Nakamura, K., Zuppini, A., Arnaudeau, S., Lynch, J., Ahsan, I., Krause, R., Papp, S., De, S.H., Parys, J.B., Muller-Esteryl, W., Lew, D.P., Krause, K.H., Demaurex, N., Opas, M. and Michalak, M. (2001). Functional specialisation of calreticulin domains. Journal of Cell Biology, 154(5), pp. 961-972.

Narumiya, S. (2007). Physiology and pathophysiology of prostanoid receptors. *Proceedings of the Japan Academy*, 83(9-10), pp. 296-319.

Narumiya, S., Sugimoto, Y. and Ushikubi, F. (1999). Prostanoid Receptors: Structures, Properties, and Functions. *American Physiological Society*, 79(4), pp. 1193-1226.

Nelson, M.T., Cheng, H., Rubart, M., Santana, L.F., Bones, A.D., Knot, H.J. and Lederer, W.J. (1995). Relaxation of arterial smooth muscle by calcium sparks. *Science*, 270(5236), pp. 633-637.

Nelson, M.T., Patlack, J.B., Worley, J.F. and Standen, N.B. (1990). Calcium channels, potassium channels, and voltage dependence of arterial smooth muscle tone. *American Journal of Physiology*, 259(1), pp. 3-18.

Nichols, H.L., Saffeddine, M., Theriot, B.S., Hegde, A., Polley, D., El-Mays, T., Vliagoftis,H., Hollenberg, M.D., Wilson, E.H., Walker, J.K.L. and DeFea, K.A. (2012). β-Arrestin-2 mediates the proinflammatory effects of proteinase-activated receptor-2 in the airway. *Proceedings of the National Academy of Sciences of the United States of America*, 109(41), pp. 16660-16665.

Nishigaki, N., Negishi, M. and Ichikawa, A. (1996). Two G_s-coupled prostaglandin E receptor subtypes, EP_2 and EP_4, differ in desensitization and sensitivity to the metabolic inactivation of the agonist. *Molecular Pharmacology*, 50(4), pp. 1031-1037.

Nitsche, J., Josts, J., Heidemann, J., Mertens, H.D., Maric, S., Moulin, M., Haertlein, M., Busch, S., Forsyth, T.V., Svergen, D.T., Uetrecht, C. and Tidow, H. (2018). Structural basis for activation of plasma-membrane calcium-ATPase by calmodulin. *Nature* [online], 206(1). Available from: https://www.nature.com/articles/s42003-018-0203-7.pdf [accessed 28th June 2021].

Nursing Times. (2018). Respiratory rate 2: anatomy and physiology of breathing. [online] Available at: https://www.nursingtimes.net/clinical-archive/respiratory/respiratory-rate-2-anatomy-and-physiology-of-breathing/7024714.article [accessed 25th June 2021].

Nystedt, S., Emilsson, K., Wahlestedt, C. and Sundelin, J. (1994). Molecular cloning of a potential proteinase activated receptor. *Proceedings of the National Academy of Sciences of the United States of America*, 91(20), pp.9208-9212.

Ossovskaya, V.S. and Bunnett, N.W. (2004). Protease-activated receptors: contribution to physiology and disease. *Physiological Reviews*, 84(2), pp.579-621.

Ottini, L., Marziali, G., Conti, A., Charlesworth, A. and Sorrentino, V. (1996). Alpha and beta isoforms of ryanodine receptor from chicken skeletal muscle are the homologues of mammalian RyR1 and RyR3. *Biochemical Journal*, 315(1), pp. 207-216.

Paing, M.M., Stutts, A.B., Kohout, T.A., Lefkowitz, R.J. and Trejo, J. (2002). β-arrestins regulate protease-activated receptor-1 desensitization but not internalization or down-regulation. *The Journal of Biological Chemistry*, 277(1), pp.1292-1300.

Panettieri, R.A., Kotlikoff, M.I., Gertoffer, W.T., Hershenson, M.B., Woodruff, P.G., Hall, I.P. and Banks-Schlegel, S. (2008). Airway smooth muscle in bronchial tone, inflammation, and remodeling: basic knowledge to clinical relevance. *American Journal of Respiratory and Critical Care Medicine*, 177(3), pp. 248-252.

Pantazaka, E., Taylor, E.J.A., Bernard, W.G. and Taylor C.W. (2013). Ca^{2+} signals evoked by histamine H1 receptors are attenuated by activation of prostaglandin EP2 and EP4 receptors in human aortic smooth muscle cells. *British Journal of Pharmacology*, 169(7), pp. 1624-1634.

Pascoe, C.D., Wang, L., Syyong, H.T. and Pare, P.D. (2012). A Brief History of Airway Smooth Muscle's Role in Airway Hyperresponsiveness. *Journal of Allergy* [online], 2012(10), Available from: https://www.hindawi.com/journals/ja/2012/768982/ [accessed 23rd August 2019].

Patel, S., Joseph, S.K. and Thomas, A.P. (1999). Molecular properties of inositol 1,4,5-triphosphate receptors. *Cell Calcium*, 25(3), pp. 247-264.

Paul, R.J., Glück, E. and Rüegg, J.C. (1976). Cross bridge ATP utilisation in arterial smooth muscle. *European Journal of Physiology*, 361(3), pp. 297-299.

Peel, S.E., Liu, B. and Hall, I.P. (2006). A key role for STIM1 in store-operated calcium channel activation in airway smooth muscle. *Respiratory Research* [online], 119(7), Available from: https://respiratory-research.biomedcentral.com/track/pdf/10.1186/1465-9921-7-119.pdf [accessed 23rd August 2021].

Peel, S.E., Liu, B. and Hall, I.P. (2008). ORAI and store-operated calcium influx in human airway smooth muscle cells. *American Journal of Respiratory Cell and Molecular Biology*, 38(6), pp. 744-749.

Pelaia, G., Renda, T., Gallelli, L., Vatrella, A., Busceti, M.T., Agati, S., Caputi, M., Cazzola, M., Maselli, R. and Marsico, S.A. (2008). Molecular mechanisms underlying airway smooth muscle contraction and proliferation: Implications for asthma. *Respiratory Medicine*, 102(8), pp. 1173-1181.

Pera, T. and Penn, R.B. (2016). Bronchoprotection and bronchorelaxation in asthma: New targets, and new ways to target old ones. *Pharmacology and Therapeutics*, 164(8), pp. 82-96.

Perez, J.F. and Sanderson, M.J. (2005). The frequency of calcium oscillations induced by 5-HT, ACh, and KCl determine the contraction of smooth muscle cells of intrapulmonary bronchioles. *Journal of General Physiology*, 125(6), pp. 535-553.

Peutz, S., Lubomirov, L.T. and Pfitzer, G. (2009). Regulation of Smooth Muscle Contraction by Small GTPases. *American Physiology Society*, 24(9), pp. 342-356.

Piper, P.J. and Vane, J.R. (1969). Release of additional factors in anaphylaxis and its antagonism by anti-inflammatory drugs. *Nature*, 223(5201), pp. 29-35.

Ponsioen B., Gloerich M., Ritsma L., Rehmann H., Bos J.L. and Jalink K. (2009). Direct Spatial Control of Epac1 by cyclic AMP. *Molecular and Cellular Biology*, 29(10), pp. 2521-2531.

Ponte, C.G., McManus, O.B., Schmalhofer, W.A., Shen, D-M., Dai, G., Stevenson, A., Sur, S., Shah, T., Kiss, L., Shu, M., Doherty, J.B., Nargund, R., Kaczorowski, G., Suarez-Kurtz, G. and Garcia, M.L. (2012). Selective, direct activation of high-conductance, calcium-activated potassium channels causes smooth muscle relaxation. *Molecular Pharmacology*, 81(4), pp. 567-577.

Prakash, Y.S., Kannan, M.S. and Sieck, G.C. (1997). Regulation of the intracellular calcium oscillations in porcine tracheal smooth muscle cells. *American Journal of Physiology*, 272(3), pp. 966-975.

Prakash, Y.S., Kannan, M.S., Walseth, T.F. and Sieck, G.C. (1998). Role of cyclic ADP-ribose in the regulation of $[Ca^{2+}]i$ in porcine tracheal smooth muscle. *American Journal of Physiology*, 274(6), pp. 1653-1660.

Prakash, Y.S., Pabelick, C.M., Kannan, M.S. and Sieck, G.C. (2000). Spatial and temporal aspects of ACh-induced $[Ca^{2+}]_I$ oscillations in porcine tracheal smooth muscle. Cell Calcium, 27(3), pp. 153-162.

Prakash, Y.S., Van Der Heijden, H.F.M., Kannan, M.S. and Sieck, G.C. (1997). Effects of salbutamol on intracellular calcium oscillations in porcine airway smooth muscle. *American Physiological Society*, 82 (6), pp. 1836-1843.

Putney, J.W. and Bird, G.S. (2008). Cytoplasmic calcium oscillations and store-operated calcium influx. *Journal of Physiology*, 586(13), pp. 3055-3059.

Raeymaekers, L., Verbist, J., Wuytack, F., Plessers, L. and Casteels, R. (1993). Expression of Ca2 binding proteins of the sarcoplasmic reticulum of striated muscle in the endoplasmic reticulum of pig smooth muscles. *Cell Calcium*, 14(8), pp. 581-589.

Raifman, T.K., Kumar, P., Haase, H., Klussmann, E., Dascal, N. and Weiss, S. (2017). Protein Kinase C enhances plasma membrane expression of cardiac L-type calcium channel, $Ca_V1.2$. *Channels*, 11(6), pp. 604-615.

Ramnarine, S.I., Haddad, E.B., Khawaja, A.M., Mak, J.C. and Rogers, D.F. (1996). On muscarinic control of neurogenic mucus secretion in ferret trachea. *Journal of Physiology*, 494(2), pp. 577-586.

Ramos-Franco, J., Bare, D., Caenepeel, S., Nani, A., Fill, M. and Mignery, G. (2000). Single-channel function of recombinant type 2 inositol 1,4, 5-trisphosphate receptor. *Biophysiological Journal*, 79(3), pp. 1388-1399.

Rattay, F. (1999). The basic mechanism for the electrical stimulation of the nervous system. *Neuroscience*, 89(2), pp. 335-346.

Regan, J.W. (2003). EP_2 and EP_4 prostanoid receptor signalling. *Life Sciences*, 74(2-3), pp. 143-153.

Rehmann, H. (2013). Epac-inhibitors: facts and artefacts. Nature: *Scientific Reports* [online], 3(1). Available from: https://pubmed.ncbi.nlm.nih.gov/24149987/ [accessed on 4th October 2021].

Ressmeyer, A.R., Bai, Y., Delmotte, P., Uy, K.F., Thistlethwaite, P., Fraire, A., Sato, O., Ikebe, M. and Sanderson, M.J. (2010). Human airway contraction and formoterol-induced relaxation is determined by Ca^{2+} oscillations and Ca^{2+} sensitivity. *American Journal of Respiratory Cell and Molecular Biology,* 43(2), pp. 179-191.

Ricciardolo, F.L., Steinhoff, M., Amadesi, S., Guerrini, R., Tognetto, M., Trevisani, M., Creminon, C., Bertrand, C., Bunnett, N.W., Fabbri, L.M., Salvadori, S. and Geppetti, P. (2000). Presence and bronchomotor activity of protease-activated receptor-2 in guinea pig airways. American Journal of Respiratory and Critical Care Medicine, 161(5), pp. 1672-1680.

Rice, K.D., Tanaka, R.D., Katz, B.A., Numerof, R.P. and Moore, W.R. (1998). Inhibitors of tryptase for the treatment of mast cell-mediated diseases. *Current Pharmaceutical Design*, 4(5), pp.381-396.

Ricks, T.K. and Trejo, J. (2009). Phosphorylation of protease-activated receptor-2 differentially regulates desensitization and internalization. *Journal of Biological Chemistry*, 284(49), pp.34444-34457.

Robbins, J., Marsh, S.J. and Brown, D.A. (1993). On the mechanism of M-current inhibition by muscarinic m1 receptors in DNA-transfected rodent neuroblastoma x glioma cells. *The Journal of Physiology*, 469(9), pp. 153-178.

Roche, N., Stirling, R.G., Lim, S., Oliver, B.G., Oates, T., Jazrawi, E., Caramori, G. and Chung, F.K. (2003). Effect of acute and chronic inflammatory stimuli on expression of protease-activated receptors 1 and 2 in alveolar macrophages. *The Journal of Allergy and Clinical Immunology*, 111(2), pp. 367-373.

Rodriguez-Roisin, R. (2005). The Airway Pathophysiology of COPD: Implications for Treatment. *Journal of Chronic Obstructive Pulmonary Disease*, 2(6), pp.253-262.

Roffel, A.F., Elzinga, C.R.S. and Zaagsma, J. (1990). Muscarinic M3 receptors mediate contraction of human central and peripheral airway smooth muscle. *Pulmonary Pharmacology*, 3(1), pp.47-51.

Roscioni, S.S., Kristemaker, L.E.M., Menzen, M.H., Elzinga, C.R.S., Gosens, R., Halayko, A.J., Meurs, H. and Schmidt, M. (2009). PKA and Epac cooperate to augment bradykinin-induced interleukin-8 release from human airway smooth muscle cells. *Respiratory Research* [online], 10(1). Available from: https://pubmed.ncbi.nlm.nih.gov/19788733/ [accessed on 31st of August 2021].

Roscioni, S.S., Maarsingh, H., Elzinga, C.R.S., Schuur, J., Menzen, M., Halayko, A.J., Meurs, H. and Schmidt, M. (2011). Epac as a novel effector of airway smooth muscle relaxation. *Journal of Cellular and Molecular Medicine*, 15(7), pp. 1551-1563.

Rossi, D. and Sorrentino, V. (2002). Molecular genetics of ryanodine receptors Ca^{2+}-release channels. *Cell Calcium*, 32(5-6), pp. 307-319.

Roux, E., Guibert, C., Savineau, J.P. and Marthan, R. (1997). $[Ca^{2+}]_i$ oscillations induced by muscarinic stimulation in airway smooth muscle cells: receptors subtypes and correlation with mechanical activity. *British Journal of Pharmacology*, 120(7), pp. 1294-1301.

Säfholm, J., Dahlen, S.E., Delin, I., Maxey, K., Stark, K., Cardell, L.O. and Adner M. (2013). PGE_2 maintains the tone of the guinea pig trachea through a balance between activation of contractile EP_1 receptors and relaxant EP_2 receptors. *British Journal of Pharmacology*, 168(4), pp. 794-806.

Säfholm, J., Manson, M.L., Bood, J., Delin, I., Orre, A.C., Bergman, P., Al-Ameri, M., Dahlén, S.E. and Adner M. (2015). Prostaglandin E_2 inhibits mast cell-dependent bronchoconstriction in human small airways through the E prostanoid subtype 2. *Journal of Allergy and Clinical Immunology*,136(5), pp. 1232-1239.

Salkoff, L., Butler, A., Ferreira, G., Santi, C. and Wei, A. (2006). High-conductance potassium channels of the SLO family. *Nature Reviews Neuroscience*, 7(12), pp. 921-931.

Samsó, M. and Wagenknecht, T. (1998). Contributions of electron microscopy and single-particle techniques to the determination of the ryanodine receptor three-dimensional structure. *Journal of Structural Biology*, 121(2), pp. 172-180.

Sanders, K.M. (2008). Regulation of smooth muscle excitation and contraction. *Neurogastroenterology and Motility*, 20(1), pp. 39-53.

Sanders, K.M., Koh, S.D. and Ward, S.M. (2006). Interstitial cells of cajal as pacemakers in the gastrointestinal tract. Annual review of Physiology, 68(3), pp. 307-343.

Sanderson, M.J., Delmotte,P., Bai, Y. and Perez-Zogbhi, J.F. (2008). Regulation of airway SMC contractility by Ca^{2+} signalling and sensitivity. Proceedings of the American Thoracic Society, 5(1), pp. 23-31.

Sastre, B. and del Pozo, V. (2012). Role of PGE_2 in Asthma and Nonasthmatic Eosinophilic Bronchitis [online]. *Mediators of Inflammation*, 2012(1). Available from: https://www.ncbi.nlm.nih.gov/pmc/articles/PMC3316983/

Sato, Y., Kiriazis, H., Yatani, A., Schmidt, A.G., Hahn, H., Ferguson, D.G., Sako, H., Mitarai, S., Honda, R., Mesnard-Rouiller, L., Frank, K.F., Beyermann, B., Wu, G., Fuijimori, K., Dorn, G.W. and Kranias, E.G. (2001). Rescue of contractile parametes and myocyte hypertrophy in calsequestrin overexpressing myocardium by phospholamban ablation. *The Journal of Biological Chemistry*, 276(12), pp. 9392-9399.

Saunders, H.M. and Farley, J.M. (1991). Spontaneous transient outward currents and Ca^{2+}-activated K^+ channels in swine tracheal smooth muscle cells. *The Journal of Pharmacology and Experimental Therapeutics*, 257(3), pp. 1114-1120.

Schlemper, V., Medeiros, R., Ferreira, J., Campos, M.M. and Calixto, J.B. (2005). Mechanisms underlying the relaxation response induced by bradykinin in epithelium-intact guinea-pig trachea *in vitro*. *British Journal of Pharmacology*, 145(6), pp. 740-750.

Schmidlin, F., Amadesi, S., Dabbagh, K., Lewis, D.E., Knott, P., Bunnett, N.W., Gater, P.R., Geppetti, P., Bertrand, C. and Stevens, M.E. (2002). Protease-activated receptor 2 mediates eosinophil infiltration and hyperreactivity in allergic inflammation of the airway. *The Journal of Immunology*, 169(9), pp. 5315-5321.

Schmidlin, F., Amadesi, S., Vidil, R., Trevisani, M., Martinet, N., Caughey, G., Tognetto, M., Cavallesco, G., Mapp, C., Geppetti, P. and Bunnett, N.W. (2001). Expression and function of proteinase-activated receptor 2 in human bronchial smooth muscle. *American Journal of Respiratory and Critical Care Medicine*, 164(7), pp.1276-1281.

Seo, M.D., Velamakanni, S., Ishiyama, N., Stathopulos, P.B., Rossi, A.M. and Khan, S.A. (2012). Structural and functional conservation of key domains in $InsP_3$ and ryanodine receptors. *Nature*, 483(7387), pp. 108-112.

Seow, C.Y. and Fredberg, J.J. (2001). Historical perspective on airway smooth muscle: the saga of a frustrated cell. *Journal of Applied Physiology*, 91(8), pp. 938-952.

Shabir, S., Borisova, L., Wray, S. and Burdyga, T. (2004). Rho-kinase inhibition and electromechanical coupling in rat and guinea-pig ureter smooth muscle: Ca^{2+}-dependent and -independent mechanisms. *The Journal of Physiology*, 560(3), pp. 839-855.

Sheller, J.R., Mitchell, D., Meyrick. B., Oates, J. and Breyer, R. (2000). EP_2 receptor mediates bronchodilation by PGE_2 in mice. *Journal of Applied Physiology*, 88 (2000) pp. 2214-2218.

Shieh, C.C., Petrini, M.F., Dwyer, T.M. and Farley, J.M. (1991). Concentration-dependence of acetylcholine-induced changes in calcium and tension in swine trachealis. *Journal of Pharmacology and Experimental Therapeutics*, 256(1), pp. 141-148.

Shigemoto, T. and Ohmori, H. (1991). Muscarinic receptor hyperpolarizes cochlear hair cells of chick by activating $Ca(^{2+})$-activated K^+ channels. *The Journal of Physiology*, 442(7), pp. 669-690.

Sieck, G.C., Kannan, M.S. and Prakash, Y.S. (1997). Heterogeneity in dynamic regulation of intracellular calcium in airway smooth muscle cells. *Canadian Journal of Physiology and Pharmacology*, 75(7), pp. 878-888.

Sims, S.M., Jiao, Y. and Zheng, Z.G. (1996). Intracellular calcium stores in isolated tracheal smooth muscle cells. *The American Journal of Physiology*, 271(2), pp. 300-309.

Smyth, E.M., Grosser, T., Wang, M., Yu, Y. and Fitzgerald, G.A. (2009). Prostanoids in health and disease. *Journal of Lipid Research*, 50(4), pp. 423-428.

Smyth, L.M., Bobalova, J., Mendoza, M.G., Lew, C. and Mutafova-Yambolieva, V.N. (2004). Release of β-Nicotinamide Adenine Dinucleotide upon Stimulation of Postganglionic Nerve Terminals in Blood Vessels and Urinary Bladder. *Journal of Biological Chemistry*, 279(47), pp. 48893-48903.

Snetkov, V.A., Hirst, S.J. and Ward, J.P.T. (1996). Ion channels in freshly isolated and cultured human bronchial smooth muscle cells. *Experimental Physiology*, 81(7), pp. 791-804.

Soh, U.J.K, Dores, M.R., Chen, B. and Trejp, J. (2010). Signal transduction by protease-activated receptors. *British Journal of Pharmacology*, 160(2), pp.191-203.

Somlyo, A.P. and Himpens, B. (1989). Cell calcium and its regulation in smooth muscle. *Federation of American Societies for Experimental Biology Journal*, 3(11), pp. 2266-2276.

Somylo, A.P. and Somylo, A.V. (1994). Signal transduction and regulation in smooth muscle. *Nature*, 372(6503), pp. 231-236.

Song, T., Hao, Q., Zheng, Y.M., Liu, Q.A. and Wang, Y.X. (2015). Inositol 1,4,5-trisphosphate activates TRPC3 channels to cause extracellular Ca^{2+} influx in airway smooth muscle cells. *American Journal of Physiology Lung Cellular and Molecular Physiology,* 309(12), pp. 1455-1466.

Song, Y. and Simard, J.M. (1995). Beta-Adrenoreceptor stimulation activates large-conductance Ca^{2+}-activated K^{+} channels in smooth muscle cells from basilar artery of guinea-pig. *Pflügers Archiv: European Journal of Physiology,* 430(6), pp. 984-993.

Spence, A. and Mason, E. (1992). Human anatomy and physiology. 4th ed. St. Paul Minn.: West Publishing Company.

Spicuzza, L., Belvisi, M.G., Birrell, M.A., Barnes, P.J., Hele, D.J. and Giembycz, M.A. (2001). Evidence that the anti-spasmogenic effect of the beta-adrenoceptor agonist, isoprenaline, on guinea-pig trachealis is not mediated by cyclic AMP-dependent protein kinase. *British Journal of Pharmacology*, 133(8), pp. 1201-12.

Spicuzza, L., Giembycz, M.A., Barnes, P.J. and Belvisi, M. (1998). Prostaglandin E_2 suppression of acetylcholine release from parasympathetic nerves innervating guinea-pig trachea by interacting with prostanoid receptors of the EP_3-subtype. *British Journal of Pharmacology*, 123, pp. 1246-1252.

Srivastava, K., Sampson, H.A., Emala, C.W. and Li, X.M. (2013). The anti-asthma herbal medicine ASHMI acutely inhibits airway smooth muscle contraction via prostaglandin E_2 activation of EP_2/EP_4 receptors. *American Journal of Physiology-Lung Cellular and Molecular Physiology*, 305(12). Pp. 1002-1010.

Stalheim, L., Ding, Y., Gullapalli, A., Paing, M.M., Wolfe, B.L., Morris, D.R. and Trejo, J. (2005). Multiple independent functions of arrestins in regulation of protease-activated receptor-2 signaling and trafficking. *Molecular Pharmacology*, 67(1) pp.1-10.

Steinburg, S.F. (2008). Structural basis of protein kinase C isoform function. *Physiological Reviews*, 88(4), pp.1341-1378.

Stern, S., Rotem, A., Burnishev, Y., Weinreb, E. and Moses, E. (2017). External Excitation of Neurons Using Electric and Magnetic Fields in One- and Two-dimensional Cultures. *Journal of Visualized Experiments* [online], 123(5). Available from: https://www.ncbi.nlm.nih.gov/pmc/articles/PMC5607903/ [accessed on 1st October 2021].

Stott J.B., Barrese V. and Greenwood I.A. (2016). Kv7 Channel Activation Underpins EPAC-Dependent Relaxations of Rat Arteries. *Arteriosclerosis, Thrombosis, and Vascular Biology*, 36(12), pp. 2404-2411.

Sturm, E.M., Schratl, P., Schuligoi, R., Konya, V., Sturm, G.J., Lippe, I.T., Peskar, B.A. and Heinemann, A. (2008). Prostaglandin E_2 Inhibits Eosinophil Trafficking through E-Prostanoid 2 Receptors. *The Journal of Immunology*, 181(10), pp. 7273-7283.

Sugimoto, Y. and Narumiya, S. (2007). Prostaglandin E receptors. *The Journal of Biological Chemistry*, 282(16), pp 11613-11617.

Sutko, J.L., Airey, J.A., Welch, W. and Reust, L. (1997). The pharmacology of ryanodine and related compounds. *Pharmacological Reviews*, 49(1), pp. 53-98.

Széll, E.A., Yamamoto, T., de Groat, W.C. and Somogyi, G.T. (2000). Smooth muscle and parasympathetic nerve terminals in the rat urinary bladder have different subtypes of α1 adrenoceptors. *British Journal of Pharmacology*, 130(7), pp. 1685-1691.

Tai, H.H., Ensor, C.M., Tong, M., Zhou, H. and Yan, F. (2002). Prostaglandin catabolizing enzymes. *Prostaglandins & Other Lipid Mediators*, 68-69(8), pp. 483-493.

Takeshima, H., Iino, M., Takekura, H., Nishi, M., Kuno, J., Minowa, O., Takano, H. and Noda, T. (1994). Excitation-contraction uncoupling and muscular degeneration in mice lacking functional skeletal muscle ryanodine-receptor gene. *Nature*, 369(6481), pp. 556-559.

Takeshima, H., Komazaki, S., Hirose, K., Nishi, M., Noda, T. and Iiona, M. (1998). Embryonic lethality and abnormal cardiac myocytes in mice lacking ryanodine receptor type 2. *The European Molecular Biology Organisation Journal*, 17(12), pp. 3309-3316.

Takeshima, Ikemoto, T., Nishi, M., Nishiyama, N., Shimuta, M., Sugitani, Y., Kuno, J., Saito, I., Saito, H., Endo, M., Iino, M. and Noda, T. (1996). Generation and characterization of mutant mice lacking ryanodine receptor type 3. *Journal of Biological Chemistry*, 271(33), pp. 19649-19652.

Tanaka, K., Shibuya, I., Kabashima, N., Ueta, Y. and Yamashita, H. (1998). Inhibition of Voltage-Dependent Calcium Channels by Prostaglandin E_2 in Rat Melanotrophs. *Endocrinology*, 139(12), pp. 4801-4810.

Tanaka, Y., Mochizuki, Y., Tanaka, H. and Shigenobu, K. (1999). Significant role of neuronal non-N-type calcium channels in the sympathetic neurogenic contraction of rat mesenteric artery. *British Journal of Pharmacology,* 128(7), pp. 1602-1608.

Tao, J., Lan, Z., Wang, Y., Hei, H., Tian, L., Pan, W., Zhang, X. and Peng, W. (2016). Large-Conductance Calcium-Activated Potassium Channels in Glomerulus: From Cell Signal Integration to Disease [online]. *Frontiers in Physiology*, 7 (6). Available from: https://www.ncbi.nlm.nih.gov/pmc/articles/PMC4915313/

Taylor, C.W., and Tovey, S.C. (2010). IP_3 receptors: toward understanding their activation. *Cold Spring Harbour Perspectives in Biology* [online], 2(12). Available from: https://www.ncbi.nlm.nih.gov/pmc/articles/PMC2982166/ [accessed 19th August 2021].

Taylor, E.J.A., Pantazaka, E., Shelley, K.L. and Taylor, C.W. (2017). Prostaglandin E_2 inhibits histamine-evoked Ca^{2+} release in human aortic smooth muscle cells through hyperactive cAMP signalling junctions and protein kinase A. *Molecular Pharmacology*, 92(11), pp. 533-545.

Thomas, A.P., Bird, G.S., Hajinoczky, G., Robb-Gaspers, L.D. and Putney, J.W. (1996). Spatial and temporal aspects of cellular calcium signaling. *FASEB*, 10(13), pp. 1505-1517.

Tian, L., Duncan, R.R., Hammond, M.S.L., Coghill, L.S., Wen, H., Rusinova, R., Clark, A.G., Levitan, I.B. and Shipston, M.J. (2001). Alternative splicing switches potassium channel sensitivity to protein phosphorylation. *Journal of Biological Chemistry*, 276(11), pp. 7717-7720.

Tilley, S.L., Hartney, J.M., Erikson, C.J., Jania, C., Nguyen, M., Stock, J., McNeisch, J., Valancius, C., Panettieri, R.A., Penn, R.B. and Koller, B.H. (2003).

Receptors and pathways mediating the effects of prostaglandin E_2 on airway tone. *American Journal of Physiology Lung Cellular and Molecular Physiology*, 284 (12), pp. 599-606.

Tolloczko, B., Jia, Y.L. and Martin, J.G. (1997). Effects of cAMP on serotonin evoked calcium transients in cultured rat airway smooth muscle cells. *American Journal of Physiologyl*, 272(5), pp. 865-871.

Tomita, T. and Kume, H. (1994). Electrophysiology of Potassium Channels in Airway Smooth Muscle. In: Raeburn, D. and Giembycz, MA., eds. *Airway Smooth Muscle: Development, and Regulation of Contractility*. Switzerland: Basel, pp. 163-184.

Torphy, T.J. (1994). Beta-adrenoceptors, cAMP and airway smooth muscle relaxation: challenges to the dogma. *Trends in Pharmacological Sciences*, 15(10), pp. 370-374.

Ullman, A., Ciabattoni, G., Löfdahl, A., Svedmyr, N. and Skoogh, B.E. (1990). Epithelium-derived PGE_2 inhibits the contractile response to cholinergic stimulation in isolated ferret trachea. *Pulmonary Pharmacology*, 3(2), pp. 155-160.

Ullman, A., Ciabattoni, G., Svedmyr, N., Skoogh, B.E. and Löfdahl, A. (1991). Tetrodotoxin does not block the epithelium-dependant release of prostaglandin E_2 induced by electric field stimulation in isolate ferret trachea. *American Journal of Respiratory Cell and Molecular Biology*, 4(7), pp. 243-247.

Ullman, A., Löfdahl, C.G., Svedmyr, M., Bernsten, L. and Skoogh, B.E. (1988). Mucosal inhibition of cholinergic contractions in ferret trachea can be transferred between organ baths. *European Respiratory Journal*, 1(10), pp. 908-912.

Underwood, J. (2004). *General and systematic pathology: Chapter 14 Respiratory Tract.* 4th ed. Edinburgh: Churchill Livingstone/ Elsevier.

Unno, T., Matsuyama, H., Sakamoto, T., Uchiyama, M., Izumi, Y., Okamoto, H., Yamada, M., Wess, J. and Komori, S. (2005). M2 and M3 muscarinic receptor-

mediated contractions in longitudinal smooth muscle of the ileum studied with receptor knockout mice. *British Journal of Pharmacology*, 146 (1), pp. 98-108.

Valverde, M.A., Cantero-Recasens, G., Garcia-Elias, A., Jung, C., Carreras-Sureda, A. and Vicente, R. (2011). Ion Channels in Asthma. *Journal of Biological Chemistry*, 286(38), pp. 32877-32882.

Van der Velden, V.H.J. and Hulsmann, A.R. (1999). Autonomic Innervation of Human Airways: Structure, Function, and pathophysiology in Asthma. *Neuroimmunomodulation*, 6(3), pp. 145-159.

Vancheri, C., Mastruzzo, Sortino, MA. and Crimi, N. (2004). The lung as a privileged site for the beneficial actions of PGE_2. *Trends in Immunology*, 25(1), pp. 40-46.

Villa, A., Podini, P., Panzeri, M.C., Soling, H.D., Volpe, P. and Meldolesi, J. (1993). The endoplasmic-sarcoplasmic reticulum of smooth muscle: immunocytochemistry of vas deferens fibres reveals specialized subcompartments differently equipped for the control of Ca^{2+} homeostasis. *Journal of Cell Biology*, 121(5), pp. 1041-1051.

Volpe, P., Martini, A., Furlan, S. and Mendolesi, J. (1994). Calsequestrin is a component of smooth muscles: the skeletal- and cardiac-muscle isoforms are both present, although in highly variable amounts and ratios. Biochemical Journal, 301(2), pp. 465-469.

Von Euler, U.S. (1936). On the specific vaso-dilating and plain muscle stimulating sibstances from accessory genital glands in man and certain animals (prostaglandin and vesiglandin). *The Journal of Physiology*, 88(2), pp. 213-234.

Vu, T.K.H., Hung, D.T., Wheaton, V.I. and Coughlin, S.R. (1991). Molecular cloning of a functional thrombin receptor reveals a novel proteolytic mechanism of receptor activation. *Cell*, 64(6), pp.1057-1068.

Wang, S., Wang, H., Su, X., Liu, B., Wang, L., Yan, H., Mao, S., Huang, H., Huang, C., Cheng, M. and Wu, G. (2020). β-adrenergic activation may promote

myosin light chain kinase degradation T through calpain in pressure overload-induced cardiac hypertrophy β-adrenergic activation results in MLCK degradation. *Biomedicine and Pharmacotherapy* [online], 129(6). Available from: https://pubmed.ncbi.nlm.nih.gov/32768940/ [accessed on 29th September 2021].

Wang, Y.X. (2014). Calcium Signalling in Airway Smooth Muscle Cells. Switzerland: Springer.

Wang, Y.X., Zheng, Y.M., Mei, Q.B., Wang, Q.S., Collier, M.L., Fleischer, S., Xin, H.B. and Kotlikoff, M.I. (2004). FKBP12.6 and cADPR regulation of Ca^{2+} release in smooth muscle cells. *The American Journal of Cell Physiology*, 286(7), pp. 538-546.

Wang, Z.W. and Kotlikoff, M.I. (1996). Activation of KCa channels in airway smooth cells by endogenous protein kinase A. *American Journal of Physiology*, 271(1), pp. 100-105.

Ward, J.P.T., Ward, J. and Leach, R.M. (2010). *The Respiratory System at a Glance*: *Chapter 1 Structure and Function*, 3rd ed. Chichester: John Wiley & Sons.

Webb, R.C. (2003). Smooth muscle contraction and relaxation. *Advances in Physiology Education*, 27(4), pp. 201-206.

White, R.E., Kryman, J.P., El-Mowafy, A.M., Han, G. and Carrier, G.O. (2000). cAMP-Dependent Vasodilators Cross-Activate the cGMP-Dependent Protein Kinase to Stimulate BK_{ca} Channel Activity in Coronary Artery Smooth Muscle Cells. *Circulation Research*, 86(4), pp. 897-905.

White, T.A., Kannan, M.S. and Walseth, T.F. (2003). Intracellular calcium signalling through cADPR pathway is agonist specific in porcine smooth muscle. *Federation of American Societies for Experimental Biology Journal*, 17(3), pp.482-484

White, T.A., Xue, A., Chini, E.N., Thompson, M., Sieck, G.C. and Wylam, M.E. (2006). Role of transient receptor potential C3 in TNF-alpha-enhanced calcium

influx in human airway myocytes. *American Journal of Respiratory Cell and Molecular Biology*, 35(2), pp. 243-251.

Widdicombe, J.G. (1966). Action potentials in parasympathetic and sympathetic efferent fibres to the trachea and lungs of dogs and cats. *The Journal of Physiology*, 186(1), pp. 56-88.

Widdicombe, J.G. (1998). Autonomic regulation: i-NANC/e-NANC. *American Journal of Respiratory and Critical Care Medicine*, 158(5), pp. 171-175.

Wooldridge, A.A., MacDonald, J.A., Erdodi, F., Ma, C., Borman, M.A., Hartshorne, D.J. and Haystead, T.A.J. (2004). Smooth muscle phosphatase is regulated in vivo by exclusion of phosphorylation of threonine 696 of MYPT1 by phosphorylation of Serine 695 in response to cyclic nucleotides. *Journal of Biological Chemistry*, 279(33), pp. 34496-34504.

Wray, S. and Burdyga, T. (2010). Sarcoplasmic reticulum function in smooth muscle. *American Physiological Society*, 90(1), pp. 113-178.

Xu, H., Zhao, P., Zhang, W.J., Qiu, J.Y., Tan, L., Liu, X.C., Wang, Q., Lou, X., She, Y.S., Zhang, D.A., Liu, B.B., Cao, L., Zhao, X.X., Chen, Y.Y., Li, M.Y., Shen, J., Peng, Y.B., Xue, L., Yu, M.F., Chen, W., Ma, L.Q., Qin, G. and Li, Q.H. (2018). Generation and role of oscillatory contractions in mouse airway smooth muscle. *Cellular Physiology and Biochemistry*, 47(4), pp. 1546-1555.

Xu, W.F., Anderson, H., Whitmore, T.E., Presnell, S.R., Yee, D.P., Ching, A., Gilbert, T., Davie, E.W. and Foster, D.C. (1998). Cloning and characterization of human protease-activated receptor 4. *Proceedings of the National Academy of Sciences*, 95(12), pp.6642-6646.

Yan, F., Gao, H., Zhao, H., Bhatia, M. and Zeng, Y. (2018). Roles of airway smooth muscle dysfunction in chronic obstructive pulmonary disease. *Journal of Translational Medicine* [online], 262 (9), Available from: https://translational-medicine.biomedcentral.com/articles/10.1186/s12967-018-1635-z [accessed 23rd August 2019].

Yanai, M., Sekizawa, K., Ohrui, T., Sasaki, H. and Takishima, T. (1992) Site of airway obstruction in pulmonary disease: direct measurement of intrabronchial pressure. *Journal of Applied Physiology*, 72 (2), pp. 1016-1023.

Yano, T., Zissel, G., Muller-Qernheim, J., Jae Shin, S., Satoh, H. and Ichikawa, T. (2002). Prostaglandin E2 reinforces the activation of Ras signal pathway in lung adenocarcinoma cells via EP3. *Federation of European Biochemical Societies*, 518(1-3), pp. 154-158.

Yocum, G.T., Chen, J., Choi, C.H., Townsend, E.A., Zhang, Y., Xu, D., Fu, X.W., Sanderson, M.J. and Emala, C.W. (2017). Role of transient receptor potential vanilloid 1 in the modulation of airway smooth muscle tone and calcium handling. *American Journal of Physiology Lung Cellular and Molecular Physiology*, 312(6), pp. 812-821.

Yost, C. (1999). Potassium Channels: Basic Aspects, Functional Roles and Medical Significance. *Anaesthesiology*, 90(4), pp. 11861203.

Yu, J.Z. and Rasenick, M.M. (2012). Chapter 2 Receptor signalling and the cell biology of synaptic transmission. In: *Neurobiology of Psychiatric Disorders*, Schlaepfer, T.E. and Nemeroff, C.B., eds. *Handbook of Clinical Neurology*. 3rd ed.

Yu, X., Zhang, Q., Zhao, Y., Schwarz, B.J., Stallone, J.N., Heaps, C.L. and Han, G. (2017). Activation of G protein-coupled estrogen receptor 1 induces coronary artery relaxation via Epac/Rap1-mediated inhibition of RhoA/Rho kinase pathway in parallel with PKA. *PLOS ONE* [online], 12(3). Available from: https://journals.plos.org/plosone/article?id=10.1371/journal.pone.0173085 [accessed on 31st of August 2021].

Zaslona, Z. and Peters-Golden, M. (2015). *Prostanoid synthesis, receptors and signalling*. [image online]. Available from: https://pubmed.ncbi.nlm.nih.gov/26204554/ [accessed 25th August 2021].

Zhang ,Y., Zhou, Y., Chen, S., Hu, Y., Zhu, Z., Wang, Y., Du, N., Song, T., Yang, Y., Guo, A. and Wang, Y. (2019). Macrophage migration inhibitory factor

facilitates prostaglandin E_2 production of astrocytes to tune inflammatory milieu following spinal cord injury. *Journal of Neuroinflammation* [online], 16(85). Available from: https://jneuroinflammation.biomedcentral.com/articles/10.1186/s12974-019-1468-6 [accessed 5th February 2022].

Zhang, Q., Li, W., Ayidaerhan, N., Han, W., Chen, Y., Song, W. and Yue, Y. (2021). IP3R attenuates oxidative stress and inflammation damage in smoking-induced COPD by promoting autophagy. *Journal of Cellular and Molecular Medicine*, 25(13), pp. 6174-6187.

Zhang, S.L., Yu, Y. and Roos, J., Kozak, J.A., Deerinck, T.J., Ellisman, M.H., Stauderman, K.A. and Cahalan, M.D. (2005). STIM1 Is a Ca^{2+} sensor that activates CRAC channels and migrates from the Ca^{2+} store to the plasma membrane. *Nature*, 437(7060), pp. 902-905.

Zhang, W., Du, L. and Gunst, S.J. (2010). The effects of the small GTPase RhoA on the muscarinic contraction of airway smooth muscle result from its role in regulation actin polymerisation. 299(2), pp. 298-306.

Zhao, Z., Zhu, K., Li, Y., Zhu, Z., Pan, L., Pan., T., Borgens, B. and Zhao, M. (2020). Optimization of Electrical Stimulation for Safe and Effective Guidance of Human Cells. *Bioelectricity* [online], 2(4) Available from: https://www.liebertpub.com/doi/full/10.1089/bioe.2020.0019 [accessed on 1st October 2021].

Zhou, X.B., Wulfsen, I., Utku, E., Sausbier, U., Sausbier, M., Wieland, T., Ruth, P. and Korth, M. (2010). Dual role of protein kinase C on BK channel regulation. *Proceedings of the National Academy of Sciences of the United States of America,* 107(17), pp. 8005-8010.

Zhu, S., Han, G. and White, R.E. (2002). PGE_2 action in human coronary artery smooth muscle: role of potassium channels and signalling cross-talk. *Journal of Vascular Research*, 39 (8), pp. 477-488.

Zhu, Y., Chen, H., Boulton, S., Mei, F., Ye, N., Melacini, G., Zhou, J. and Cheng, X. (2015). Biochemical and Pharmacological Characterizations of ESI-09 Based EPAC Inhibitors: Defining the ESI-09 "Therapeutic Window". *Nature: Scientific Reports* [online], 4(9344). Available from: https://www.nature.com/articles/srep09344 [accessed on 4th October 2021].

ZhuGe, R., Fogarty, K.E., Baker, S.P., McCarron, J.G., Tuft, R.A., Lifshitz, L.M and Walsh, J.V. (2004). Ca^{2+} spark sites in smooth muscle cells are numerous and differ in number of ryanodine receptors, large conductance K^+ channels, and coupling ratio between them. *The American Journal of Physiology*, 287(6), pp. 1577-1588.

ZhuGe, R., Sims, S.M., Tuft, R.A., Fogarty, K,E. and Walsh, J.V. (1998). Ca^{2+} sparks activate K^+ and Cl^- channels, resulting in spontaneous transient currents in guinea-pig tracheal myocytes. *The Journal of Physiology*, 513(3), pp. 711-718.

Zieba, B.J., Artamonov, M.V., Jin, L., Momotani, K., Ho, R., Franke, S., Neppl, R.L. Stevenson, A.S., Khromov A.S., Chrzanowska-Wodnicka, M. and Somlyo, A.V. (2011). The cAMP-responsive Rap1 guanine nucleotide exchange factor, Epac, induces smooth muscle relaxation by down-regulation of RhoaA activity. *The Journal of Biological Chemistry*, 286(19), pp. 16681-16692.

Zorzato, F., Fujii, J., Otsu, K., Phillips, M., Green, N.M., Lai, F.A., Meissner, G. and MacLennon, D.H. (1990). Molecular cloning of cDNA encoding human and rabbit forms of the Ca^{2+} release channel (ryanodine receptor) of skeletal muscle sarcoplasmic reticulum. *Journal of Biological Chemistry*, 265(4), pp. 2244-2256.